Antenna Arrays for the Downlink of FDD Wideband CDMA Communication Systems

Antonios Constantinou Koutalos

Αντώνιος Κωνσταντίνου Κουτάλος

A thesis submitted for the degree of Doctor of Philosophy
The University of Edinburgh
November 2002

Abstract

The main subject of this thesis is the investigation of antenna array techniques for improving the performance of the downlink of wideband code division multiple access (WCDMA) mobile communication systems. These communication systems operate in frequency division duplex (FDD) mode and the antenna arrays are employed in the base station. A number of diversity, beamforming and hybrid techniques are analysed and their bit error ratio (BER) versus signal-to-noise ratio (SNR) performance is calculated as a function of the eigenvalues of the mean channel correlation matrix, where this is applicable. Also, their BER versus SNR performance is evaluated by means of computer simulations in various channel environments and using different numbers of transmit antenna elements in the base station. The simulation results of the techniques, along with other characteristics, are compared to examine the relationship among their performance in various channel environments and investigate which technique is most suitable for each channel environment.

Next, a combination of the channel correlation matrix eigenvalue decomposition and space-time processing is proposed as a possible open loop approach to the downlink data signal transmission. It decomposes the channel into M components in the form of eigenvectors (M is the number of transmit antennas in the base station), and attempts to minimise the transmit power that is needed to achieve a target BER at the mobile receiver by employing the optimum number of these eigenvectors. The lower transmit power and the directional transmission by means of eigenvectors are expected to lower interference levels to non-desired users (especially to those users who are not physically close to the direction(s) of transmission). Theoretical and simulation results suggest that this approach performs better than other presented open loop techniques, while the performance gain depends on M and the channel environment.

In simulations it is usually assumed that the base and mobile station have access to perfect estimates of all needed parameters (e.g. channel coefficients). However, in practical systems they make use of pilot and/or feedback signals to obtain estimates of these parameters, which result in noisy estimates. The impact of the noisy estimates on the performance of various techniques is investigated by computer simulations, and the results suggest that there is typically some performance loss. The loss depends on the parameter that is estimated from pilot signals, and may be a function of M, SNR and/or the channel environment.

In certain beamforming techniques the base station operates the transmit antenna array in an open loop fashion by estimating the downlink weight vector from the directional information of the uplink channel. Nevertheless, in FDD systems this results in performance loss due to the separation between the uplink and downlink carrier frequencies ('FDD gap'). This loss is quantified and the results show that it is a function of M and the FDD gap. Also, a very simple technique for compensating this loss is proposed, and results obtained after its application suggest that it eliminates most of the loss. Comparison of the proposed technique with an existing compensation technique suggests that, even though the latter is more complex than the former, it yields very little additional improvement.

Περίληψη διδακτορικής διατριβής

Το κύριο θέμα αυτής της διατριβής είναι η εξέταση τεχνικών στοιχειοκεραίας με στόχο τη βελτίωση της απόδοσης της ευθείας ζεύξης (ζεύξη από το σταθμό βάσης προς τον κινητό σταθμό) σε ευρύπλευρα CDMA (wideband CDMA, WCDMA) συστήματα κινητής ραδιοεπικοινωνίας. Αυτά τα συστήματα κινητής ραδιοεπικοινωνίας λειτουργούν με τη μέθοδο frequency division duplex (FDD), ενώ οι στοιχειοκεραίες χρησιμοποιούνται στο σταθμό βάσης. Ένας αριθμός από diversity, beamforming και υβριδικές μεθόδους στοιχειοκεραίας αναλύονται και η απόδοσή τους υπολογίζεται ως συνάρτηση των ιδιοτιμών του πίνακα αυτοσυσχέτισης του καναλιού, όπου αυτός ο υπολογισμός μπορεί να εφαρμοστεί (η παραπάνω απόδοση εκφράζεται με το λόγο 'λανθασμένα bit πληροφορίας προς σωστά bit πληροφορίας' (bit-error-ratio, BER) ως συνάρτηση του σηματοθορυβικού λόγου (signal-to-noise ratio, SNR)). Επίσης, η απόδοση αυτή υπολογίζεται και με προσομοιώσεις σε υπολογιστή σε διάφορα περιβάλλοντα διάδοσης (κανάλια) και διαφορετικούς αριθμούς στοιχειωδών κεραιών εκπομπής στο σταθμό βάσης. Τα αποτελέσματα των προσομοιώσεων αυτών, καθώς και άλλα χαρακτηριστικά των τεχνικών, συγκρίνονται για να εξεταστεί η μεταξύ τους σχέση σε διάφορα περιβάλλοντα διάδοσης και να ερευνηθεί ποιά τεχνική είναι περισσότερο κατάλληλη για κάθε περιβάλλον.

Έπειτα, μια τεχνική που συνδυάζει τα ιδιοδιανύσματα του πίνακα αυτοσυσχέτισης του καναλιού και την χωρο-χρονική επεξεργασία σήματος (space-time processing) προτείνεται ως μια πιθανή προσέγγιση ανοιχτού βρόχου στην ευθεία εκπομπή. Η τεχνική αναλύει το κανάλι σε M στοιχειώδη συστατικά με τη μορφή ιδιοδιανυσμάτων (M είναι ο αριθμός των στοιχειωδών κεραιών εκπομπής στο σταθμό βάσης), και επιχειρεί να ελαχιστοποιήσει την εκπεμπόμενη ισχύ που χρειάζεται για την επίτευξη μιας επιθυμητής τιμής BER στον κινητό δέκτη χρησιμοποιώντας τον βέλτιστο αριθμό ιδιοδιανυσμάτων. Η χαμηλότερη εκπεμπόμενη ισχύς και η κατευθυντική εκπομπή μέσω των ιδιοδιανυσμάτων αναμένονται να χαμηλώσουν τα επίπεδα παρεμβολής σε μη επιθυμητούς κινητούς χρήστες (ειδικά σε αυτούς τους χρήστες που δε βρίσκονται κοντά στις κατευθύνσεις εκπομπής). Αποτελέσματα θεωρητικής ανάλυσης και προσομοιώσεων δείχνουν ότι η απόδοση αυτής της τεχνικής είναι καλύτερη από αυτή των άλλων παρουσιαζόμενων τεχνικών ανοιχτού βρόχου, ενώ η βελτίωση της απόδοσης εξαρτάται από το M και τα χαρακτηριστικά του περιβάλλοντος διάδοσης.

Σε προσομοιώσεις συστημάτων κινητής ραδιοεπικοινωνίας, συχνά γίνεται η υπόθεση ότι ο σταθμός βάσης και ο κινητός σταθμός έχουν στη διάθεσή τους τις τιμές όλων των παραμέτρων που χρειάζονται (π.χ. καναλικοί παράγοντες). Ωστόσο, στην πράξη οι δύο σταθμοί χρησιμοποιούν πιλοτικά σήματα (pilot signals) και/ή σήματα ανάδρασης (feedback signals) για να αποκτήσουν εκτιμήσεις αυτών των παραμέτρων, τα οποία οδηγούν σε μη τέλειες (θορυβώδεις) εκτιμήσεις. Η επίδραση των θορυβωδών εκτιμήσεων των απαιτούμενων παραμέτρων στην απόδοση διαφόρων τεχνικών στοιχειοκεραίας ερευνάται με τη χρήση προσομοιώσεων σε υπολογιστή, και τα αποτελέσματα δείχνουν ότι συνήθως η απόδοση των τεχνικών χειροτερεύει. Το ποσό κατά το οποίο χειροτερεύει η απόδοση εξαρτάται από την παράμετρο η οποία εκτιμάται από πιλοτικά σήματα, και μπορεί να είναι συνάρτηση του M, του SNR και των χαρακτηριστικών του καναλιού.

Σε κάποιες beamforming τεχνικές ο σταθμός βάσης λειτουργεί τη στοιχειοκεραία εκπομπής με τρόπο ανοιχτού βρόχου, εκτιμώντας το κατευθυντικό διάνυσμα (beamforming vector) που θα χρησιμοποιειθεί στην ευθεία ζεύξη από την κατευθυντική πληροφορία της αντί-

στροφης ζεύξης (ζεύξη από τον κινητό σταθμό προς το σταθμό βάσης). Όμως, σε FDD συστήματα αυτό οδηγεί σε χειρότερη απόδοση, λόγω της διαφοράς μεταξύ της ευθείας και αντίστροφης φέρουσας συχνότητας (‘FDD κενό’). Η χειροτέρεψη της απόδοσης ποσοτικοποιείται, και τα αποτελέσματα δείχνουν ότι είναι συνάρτηση του M και του κενού FDD. Επίσης, μια πολύ απλή τεχνική αντιστάθμισης του χασίματος απόδοσης προτείνεται, και αποτελέσματα αποκτειθέντα μετά την εφαρμογή της δείχνουν ότι αντισταθμίζει το μεγαλύτερο μέρος του χασίματος απόδοσης. Σύγκριση της προτεινόμενης τεχνικής με μια υπάρχουσα τεχνική αντιστάθμισης δείχνει ότι, αν και η τελευταία είναι πιο πολύπλοκη από την πρώτη, αποδίδει (πάρα) πολύ μικρή επιπλέον βελτίωση της απόδοσης.

to my parents, Constantinos and Anastasia
to my sisters, Hara and Vasiliki
and to Maria

στους γονείς μου, Κωνσταντίνο και Αναστασία
στις αδερφές μου, Χαρά και Βασιλική
και στη Μαρία

Declaration of originality

I hereby declare that the research recorded in this thesis and the thesis itself was composed and originated entirely by myself in the School of Engineering and Electronics (formerly known as Department of Electronics and Electrical Engineering) at The University of Edinburgh.

The numerical results included in the thesis were either obtained or processed using software written in C [1] and MATLAB®. The software was written entirely by myself, while in the case of C the functions that generate random numbers and perform the eigenvalue decomposition of matrices were borrowed from [2]. This thesis was written using LaTeX 2_ε [3, 4]. Both the development of the software and the writing up of the thesis was performed on the following UNIX® computer platforms: FreeBSD [5], Linux [6, 7] and Sun Solaris.

November 2002

Antonios Constantinou Koutalos

Acknowledgments

I would like to take this opportunity to express my deepest gratitude to a number of people who have provided me with invaluable help over the course of my studies.

I thank Dr. John Thompson, my supervisor at Edinburgh University, for his priceless help and advice over the course of my research, and for reviewing this thesis. His wise suggestions have always helped me and a great number of them have gone into the thesis.

I thank my parents, Constantinos and Anastasia, for their boundless love and support from the very beginning. Without their continuous encouragement and personal sacrifice nothing would have started in the first place.

I thank my two sisters, Hara and Vasiliki, for their continuous love, help and support, and for cooking those most delicious dishes during my undergraduate studies in Thessaloniki!

I thank Maria Koliatsou for her ceaseless love, support and understanding. I also thank her for giving a special, brighter, meaning to our life and for sharing our dreams.

I thank my good friend Alexandros Astaras for his valuable help when I applied to Edinburgh University for admission as a postgraduate student.

I thank the staff and student members of the Signals and Systems Group for the pleasant working atmosphere. I especially thank Stamatis Georgoulis, Apostolis Georgiadis, Giorgos Vardoulias, José Martin Luna Rivera, Unai Garro Arazola, Kian Pin Ong (Ken) and Nedko Nedev.

I thank the School of Engineering and Electronics (formerly known as Department of Electronics and Electrical Engineering) of the University of Edinburgh for providing the financial support for this work.

I thank the IT support team of the School for their help with computer-related problems and for responding to our requests for new software and utilities that make our work easier.

Lastly, but by no means leastly, I thank the Open Source Software community (especially the Linux, GNU and FreeBSD developers) for providing excellent free software tools that have helped me greatly in my research.

Contents

List of Figures

List of Tables

Acronyms and abbreviations

3GPP	3rd generation partnership project
AOA	Angle of arrival
AOD	Angle of departure
AS	Angular spread
BER	Bit error ratio
BPSK	Binary phase shift keying
BS	Base station
CCI	Co-channel interference
CCM	Channel correlation matrix
CDMA	Code division multiple access
DPCH	Dedicated physical channel
DPDCH	Dedicated physical data channel
DPCCH	Dedicated physical control channel
DS–SS	Direct sequence spread spectrum
EVD	Eigenvalue decomposition
FDD	Frequency division duplex
FDMA	Frequency division multiple access
FH–SS	Frequency hopping spread spectrum
GSM	Global system for mobile communications
ISI	Inter-symbol interference
MAI	Multiple access interference
MC–SS	Multi-carrier spread spectrum
MIMO	Multiple input multiple out
MRC	Maximum ratio combining
MS	Mobile station
OTD	Orthogonal transmit diversity
PN	Pseudo-random (spreading code)
QPSK	Quadrature phase shift keying
RF	Radio frequency

SDMA	Space division multiple access
SNR	Signal to noise (power) ratio
SQNR	Signal to quantisation noise (power) ratio
STS	Space-time spreading
SS	Spread spectrum
TDD	Time division duplex
TDMA	Time division multiple access
TFCI	Transport format combination indicator
TH–SS	Time hopping spread spectrum
TPC	Transmit power control
TXAA	Transmit antenna array
ULA	Uniform linear array
UMTS	Universal mobile telephony system
WCDMA	Wideband code division multiple access
WSSUS	Wide-sense stationary uncorrelated scattering

Nomenclature

$\overline{\bullet}$	Statistical mean of the quantity $\bullet$
$\mathbf{a} \in \mathbb{C}^{M\times 1}$	Array steering vector
α	Forgetting factor
B_s	Bandwidth of a telecommunication system
$b+1$	Number of bits used for quantisation of the real or imaginary part of a complex channel coefficient
$2(b+1)$	Number of bits used for quantisation of a complex channel coefficient
β	Fading factor/amplitude of the channel
C_c	Channel capacity
$\mathbb{C}$	Set of complex numbers
$\mathbb{C}^{M\times N}$	Set of $M \times N$ complex matrices or vectors
$c(t)$	Spreading code (PN code)
γ	Linear SNR (signal power over noise power spectral density, $\gamma = \frac{E_s}{\sigma_n^2}$)
d	Distance in space
D	Antenna element spacing
$\tilde{D}$	Antenna element spacing normalised by wavelength ($\tilde{D} = \frac{D}{\lambda}$)
δ	Angular spread of the channel
E_s	Power of the signal $s(t)$ (linear)
$E_{d,\mathrm{dB}}$	Data signal power in dB
$E_{p,\mathrm{dB}}$	Pilot signal power in dB
$E_{add,\mathrm{dB}}$	Additional pilot signal power with respect to data signal power in dB
$\mathrm{E}\{\bullet\}$	Expectation of the quantity $\bullet$
e_i	i-th eigenvalue of a matrix
ϵ	Ratio of the amplitude of the i-th channel vector sample over the amplitude of the 1st channel vector sampe in the calculation of the mean channel correlation matrix
η	Ratio of number of pilot symbols of a frame over the number of data symbols of the frame ($\eta = \frac{N_p}{N_d}$)
f_c	Carrier frequency

$f_{\mathrm{DL},c}$	Downlink carrier frequency
$f_{\mathrm{UL},c}$	Uplink carrier frequency
$f_{D,\max}$	Maximum Doppler frequency shift
f_q	Doppler frequency shift of the q-th wave of the channel
ϕ_q	Random phase of the q-th wave of the channel
ϕ_z	Phase of the complex number z
g_i	Weight of the i-th Rake finger
$\mathbf{h}(t) \in \mathbb{C}^{M\times 1}$	Time-varying channel vector
h_i	Complex channel coefficient between the i-th transmit antenna at the base station and the single receive antenna at the mobile station
$\mathbf{I} \in \mathbb{C}^{M\times M}$	Complex identity matrix of dimensions $M \times M$
$\Im\{z\}$	Imaginary part of the complex number z
K	Number of eigenvectors used as beamfomers
L	Performance loss (due to various reasons)
L_c	Length of a spreading code in chips
L_{FDD}	Performance loss due to frequency division duplex effects
L_p	Performance loss due to pilot signal effects
λ	Carrier wavelength
M	Number of antenna elements in the base station
N	Number of resolvable temporal taps of the channel
N_d	Number of data symbols in a frame
N_p	Number of pilot symbols in a frame
$n(t)$	White Gaussian stochastic noise process
n	Sample of a white Gaussian stochastic noise process
n_q	Quantisation noise
R_Q	Range of a quantiser
$R_{h_i^{\mathrm{R}}}$	Range of the real part of the i-th channel coefficient
$R_{h_i^{\mathrm{I}}}$	Range of the imaginary part of the i-th channel coefficient
$\mathbb{R}$	Set of real numbers
$\mathbb{R}^{M\times N}$	Set of $M \times N$ real matrices or vectors
$\mathbf{R}$	Mean correlation matrix of the channel ($\mathbf{R} = \mathrm{E}\left[\mathbf{h}(t)\mathbf{h}^{\mathrm{H}}(t)\right]$)
$\mathbf{R}(t)$	Instantaneous correlation matrix of the channel ($\mathbf{R} = \mathbf{h}(t)\mathbf{h}^{\mathrm{H}}(t)$)
$\Re\{z\}$	Real part of the complex number z

ρ_{adj}	Correlation between the signals of two adjacent antenna array elements
$S(\theta, f)$	Azimuthal power spectrum
$s(t)$	Data signal
$\sigma^2_{h_i}$	Variance of the channel coefficient h_i
$\sigma^2_{h_i^{\text{R}}}$	Variance of the real part h_i^{R} of the complex channel coefficient h_i
$\sigma^2_{h_i^{\text{I}}}$	Variance of the imaginary part h_i^{I} of the complex channel coefficient h_i
σ^2_n	Power spectral density of additive white Gaussian noise
T_c	Chip period
T_s	Data symbol period
t	Time variable
θ_q	Angle of arrival/departure of the q-th wave of the channel
$\mathbf{u}_i$	i-th eigenvector of a matrix
v_l	Speed of light ($v_l = 3 \times 10^8$ m/sec)
$\mathbf{v}^{\text{T}}$	Transpose of the complex vector or matrix $\mathbf{v}$
$\mathbf{v}^{\text{H}}$	Complex conjugate transpose of the complex vector or matrix $\mathbf{v}$
W	Processing gain or spreading factor (number of chips in a spreading code)
$\mathbf{w}$	Weight vector (beamformer) used by the antenna array of the base station
z^{R}	Real part of the complex number z
z^{I}	Imaginary part of the complex number z
$\|z\|$	Amplitude of the complex number z
z^*	Complex conjugate of the complex number z

Chapter 1
Introduction

The humble origins of wireless communications can be found toward the late 19th century, when Guglielmo Marconi successfully established the first known man-made radio links, and transmitted information between two points wirelessly (although radio waves had been discovered and first produced in 1888 by Heinrich Herz). These events served as the first demonstrations of what was possible through the use of wireless communication systems, and gave birth to an ever larger number of deployments of these systems, many of which operate widely even today (representative examples include the transmission of speech, music and/or images by radio and television stations). The development of wireless communication systems continued through the years, and their design and implementation was both aided and influenced initially by the invention of the triode cathode tube, and later by the advent of the semiconductor technology in the form of the transistor. Continuous advances in this technology have greatly benefited wireless communication systems, which have been increasingly capable of handling such demanding tasks as video and multimedia transmission, teleconferencing among individuals who are physically thousands of kilometers apart etc.

A modern and very interesting aspect of wireless communications is that of mobile communications (or, equivalently, cellular communications). Although mobile communication systems are relatively recent (current deployments are at their second generation, while third generation ones are anticipated to emerge soon), they offer already a variety of very useful services at reasonable prices, such as relatively cheap and reliable communication with other people. Furthermore, future generation systems promise even more reliable and higher speed communication, which is expected to enable additional services like mobile multimedia, real-time mobile video transmission, mobile access to Internet resources and even shopping, making these systems increasingly indispensable. However, the design of multimedia mobile communication systems is very challenging, and highly robust and efficient signal processing techniques must be employed to make the above promises a reality.

As a result of continuous research efforts all over the world, various efficient signal processing techniques have been developed, including intelligent multi-user detection [140, 143, 224, 233,

234], more efficient spectrum (re)use [55, 60, 116, 126, 127, 170, 198, 199, 229, 236, 257] and antenna array techniques (or smart antennas) [23, 35, 38, 69, 74, 77, 78, 102, 113, 117, 119, 141, 145, 150, 171, 194, 220, 226–228, 254, 255]. In particular, smart antennas in the base and/or the mobile station consist of multiple antenna elements and process the signal of each element so that the performance is improved. Therefore, they add a new spatial dimension to the currently used time, frequency, and code division technologies, emerging as a key capacity enhancement technology for the third generation of mobile communication systems. Smart antenna techniques offer diversity gain [16, 23, 42, 51, 57, 86, 93, 94, 99, 106, 128, 150, 154, 160, 169, 180, 181, 187, 192, 202, 247, 249, 250, 252, 255] and beamforming gain [44, 48, 56, 66, 67, 78, 79, 90, 95, 102, 114, 132, 144, 160, 169, 215, 221, 223, 231, 246]. They also enable deployment of spectrally efficient space-time coding [47, 62, 89, 93, 110, 138, 148, 159–161, 165, 217–219] and multiple input multiple output (MIMO) [43, 69] technologies, and even help in channel measurements and modeling [24, 40, 63, 84, 87, 134, 166, 197]. Also, recent events during the spectrum licensing process for third generation systems in Europe has shown that spectral bandwidth cost may be on the order of billions of euro. In light of this fact, smart antennas offer a robust, elegant and relatively inexpensive means of increasing system capacity in terms of data rates (through signal-to-noise ratio improvement and multiple parallel data links), number of users served (through spatially selective reception and/or transmission and reduction of interference to non-desired users), and quality of service (through improvement of data rates and signal quality).

1.1 Motivation for work

Even though much research effort has been devoted to the area of smart antenna techniques, the majority of the developed techniques apply to the link from mobile station to base station (uplink), resulting in considerable improvement of its performance. However, the link from base station to mobile station (downlink) has received much less attention, resulting in an imbalance between the performance of the two links. Also, the downlink is expected to be more heavily loaded than the uplink due to the nature of the services that are planned to be offered by third and future generations of mobile communication systems (e.g. browsing the Internet or downloading music and/or video files, shopping through the mobile phone etc., all of which require higher data rates on the downlink than the uplink). Consequently, there is a need for further research of the downlink, to alleviate the performance imbalance and address the needs

of the planned services.

In addition, the existing downlink smart antenna techniques have not been systematically compared under the same assumptions and in the same scenarios. Hence, there is a shortage of information as to the relationship among the performance and other technical characteristics of different techniques. Also, there is little information about which techniques are most suitable for practical scenarios of interest. A systematic comparison of the major downlink smart antenna techniques is therefore greatly beneficial, as it will provide information about their relationship, as well as indications about the most suitable techniques for each practical scenario of interest.

Furthermore, theoretical and simulation performance results of downlink smart antenna techniques are usually obtained neglecting the effect of certain phenomena and assuming perfect knowledge of the necessary parameters at both the base and mobile station. In practice, nevertheless, the performance of these techniques typically deteriorates due to phenomena such as frequency division duplex and estimation of the necessary parameters through pilot and/or feedback signals. Since these phenomena are an inseparable part of mobile communication systems where the smart antenna techniques are employed, it is of great interest to study their effects and examine their impact on the performance.

1.2 Contributions of the thesis

This thesis addresses the above points that need further examination. More specifically, a systematic comparison of a number of existing downlink smart antenna techniques in various scenarios of interest and using the same assumptions is first presented. This comparison provides indications about the relationship among the performance as well as other characteristics of the considered techniques, and helps the identification of the most suitable techniques in each scenario. Also, the theoretical performance of the techniques is obtained based on the eigenvalues of the mean channel correlation matrix, where this is applicable.

Next, a combination of the eigenvalue decomposition of the mean channel correlation matrix and space-time coding is examined as a possible open loop approach to the downlink data signal transmission. Its theoretical performance is calculated in terms of the eigenvalues of the above matrix. Also, performance results obtained through simulations are shown to match the theoretical ones. This algorithm is then compared to the above techniques, and it is shown that

its performance is the best among the examined open loop techniques.

The impact of parameter estimation at both the base and mobile station through pilot and/or feedback signals on the performance of the above downlink smart antenna techniques is then examined by means of simulations. It is shown that there is typically some performance loss involved, which usually depends on the number of transmit antennas in the base station, the signal-to-noise ratio and sometimes even on the channel scenario. In addition, the performance loss is plotted as a function of the pilot parameter for different types of pilot signals and in various scenarios.

Moreover, the effect of frequency division duplex on smart antenna techniques that use uplink eigenvectors as downlink beamformers is studied. The correlation between uplink and downlink eigenvectors is expressed as a function of the uplink and downlink carrier frequency separation, and is shown to decrease with this separation and the number of transmit antennas in the base station. The increasingly smaller correlation results in performance loss, which is also expressed as a function of the carrier frequency separation and is shown to be an increasing function of it and the number of transmit antennas in the base station. A simple technique that compensates for the frequency division duplex effects is finally investigated. It is relatively easy to implement as it does not require significant additional computational load, it increases the correlation between uplink and downlink eigenvectors and compensates for most of the performance loss due to frequency division duplex.

1.3 Organisation of the thesis

The work that is presented in this thesis is organised in chapters which are further divided in sections. A short summary of the content of each chapter is as follows.

Chapter 2 contains a brief introduction to wideband code division multiple access (WCDMA) mobile communication systems and to antenna array techniques. The fundamental concepts of CDMA systems are presented and their major advantages and/or limitations are briefly discussed. The basic ideas behind the use of smart antennas in mobile communication systems and the associated benefits are also mentioned. In addition, the chapter introduces the system model and the major assumptions that will be used in the rest of the thesis. In particular, it establishes the configuration and associated parameters of the antenna array in the base station, the propagation environment and the corresponding mathematical model of the channel, the

channel correlation matrix and its eigenvalue decomposition, and finally it contains equation (2.9) which will be important to the calculation of the theoretical performance of a number of algorithms.

Chapter 3 analyses a number of diversity, beamforming and hybrid antenna array techniques which can be employed on the downlink of mobile wireless communication systems. Each technique is introduced and, where applicable, its theoretical performance is calculated based on the combination of the eigenvalue decomposition of the mean channel correlation matrix and equation (2.9) of Chapter 2. The techniques are also simulated in a single user scenario and for different numbers of transmit antennas, and in various representative channel environments including three scenarios with one tap (macro cell, micro cell and pico cell) and one scenario with two taps. The simulation results, along with other technical characteristics of the techniques, are compared to each other, providing indications about which techniques are most suitable for each channel environment. In addition, the techniques are categorised into open loop and closed loop techniques, and comparisons are made within each category so that they are more meaningful.

Chapter 4 examines the eigenvalue decomposition of the mean channel correlation matrix. This examination motivates the investigation of the combination of the channel correlation matrix eigenvalue decomposition and space-time processing as an efficient open loop approach to the downlink data signal transmission. This approach can measure and adapt to varying channel conditions, and will be employed to satisfy a flexible performance criterion that attempts to minimise the transmit power required for the desired signal quality at the mobile receiver. Its theoretical performance will be calculated in terms of the eigenvalues of the mean channel correlation matrix, and it will be shown that its behaviour ranges from pure beamforming to pure diversity, manifesting its adaptability. When it provides purely beamforming gain this gain is in the domain of eigenbeams. When it provides diversity gain, on the other hand, this gain is in the domain of eigenvalues and its order is closely related to the channel conditions as represented by the angle of arrival/departure and angular spread. Also, the algorithm is simulated and the results compared to simulation results of the techniques of Chapter 3. The comparison suggests that this algorithm yields the best performance among all the open loop techniques, when this is measured by the flexible criterion that will be applied.

Chapter 5 discusses the effect of acquiring estimates of the necessary parameters at the base and mobile station using pilot and feedback signals. Various types of pilot signals are first

described, and the procedures of estimating the corresponding parameters at base and mobile station through them are then analysed. Next, the impact of this parameter estimation on the performance of various downlink antenna array algorithms is investigated by means of computer simulations. The results suggest that the noisy estimates of the parameters result in performance loss, and even the same type of pilot signals may have different impact on different algorithms. Also, depending on the type of pilot signals and the parameters that are estimated from them, the performance loss often depends on the number of transmit antennas in the base station and/or the SNR value, and sometimes even on the channel environment.

Chapter 6 investigates the effects of the separation between the carrier frequencies of the uplink and downlink channels due to frequency division duplex (FDD gap) on the performance of open loop downlink beamforming techniques that make use of eigenvectors (eigenbeams). First, the correlation between uplink and downlink eigenbeams is expressed in terms of the FDD gap, and it is shown to decrease as this gap increases. The increasingly smaller correlation between the eigenbeams results in performance loss which is also expressed in terms of the FDD gap, and is shown to be an increasing function of it. Next, a simple approach to compensating for the above frequency division duplex effects is applied, and it is shown that it increases the correlation between uplink and downlink eigenbeams and compensates for most of the performance loss. Finally, comparison of this approach with an existing compensation technique suggests that, even though the latter is more complex and sophisticated than the former, it yields very similar performance improvement.

Chapter 7 contains concluding remarks to the thesis. It provides a summary of the work presented in the thesis, as well as possible directions for future work and/or extensions to this work.

Finally, the thesis contains three appendices. Appendix A contains various auxiliary equations and figures that provide useful information and aid the presentation of the work in the thesis without distracting the reader from the main topic. Appendix B compares theoretical and simulation results of techniques whose theoretical performance was calculated using the combination of the mean channel correlation matrix eigenvalue decomposition and equation (2.9) of Chapter 2. The comparison shows that the two sets of results match very well, confirming that this method of calculating the theoretical performance is correct. Finally, appendix C contains the original publications of the author of this thesis for easy reference.

Chapter 2
Spread spectrum, CDMA/WCDMA, antenna arrays and system model

In this chapter, a brief overview of WCDMA and antenna arrays will be presented. Regarding WCDMA, a number of spread spectrum methods will be briefly discussed, leading gradually to the CDMA and WCDMA concept. Also, the fundamental concept of antenna arrays will be briefly discussed, along with the main gain types and possible drawbacks. Next, the propagation environment, the channel correlation matrix and the system model that will be used throughout this thesis will be introduced. After this introductory chapter, we will move on to the chapters containing the main results of the thesis.

2.1 Overview of spread spectrum, CDMA and WCDMA

This section contains a brief overview of spread spectrum technology and CDMA/WCDMA concepts. It starts with spread spectrum.

2.1.1 Spread spectrum

The spread spectrum technology was initially researched and developed with military applications in mind. This is because it offers a number of attractive advantages, such as a wireless communication means that is resilient to narrow-band jamming and difficult to intercept [200]. Among the first applications of this technology was that of ranging in military radar systems, where it improved accuracy. Applications in wireless communications started to appear after Shannon's classic theory of statistical communication [203]. One of the most important conclusions of this theory is that the maximum possible theoretical capacity C_c of a communication channel is

$$C_c = B_s \log_2(1 + \text{SNR}) \qquad \text{bits/sec}, \tag{2.1}$$

where B_s is the bandwidth of the communication system that uses this channel. Shannon also noted that when the channel is not known to the transmitter, the maximum capacity is achieved

by a noise-like waveform with uniform power spectral density over B_s. This sparked a considerable amount of research, and in a few years many of today's spread spectrum technologies had been developed, including asynchronous CDMA.

The main characteristic of a spread spectrum system is that the transmitted signal has a bandwidth much larger than the bandwidth of the minimum signal-space representation of the corresponding baseband data stream. While there is a number of methods to convert a baseband data stream to a transmit signal with much larger bandwidth, here we will briefly examine only the most common ones:

- **Direct sequence spread spectrum** (**DS–SS**): In this method, the data stream $s(t)$ is modulated by a periodic pseudo-random (pseudo-noise, PN) code $c(t)$, the period of which is equal to the duration of the data stream symbols T_s. Usually the PN code takes the form of a sequence of $+1$ and -1, which are called chips and have a period of T_c (the chips may also be complex). The number of chips W in the PN code is called the processing gain of the code, and can be practically calculated as $W = \frac{T_s}{T_c}$. After the modulation with $c(t)$, the resulting baseband signal $x(t)$ is transmitted at the desired radio frequency (RF) f_c. At the receiver, the received signal $y(t)$ is down-converted to baseband and the obtained signal is multiplied by $c(t)$ to yield a signal that will be used for estimation of the original data stream. Figure 2.1 shows a simple schematic diagram of a DS–SS system.

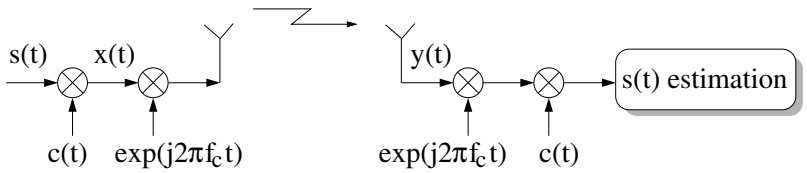

Figure 2.1: *Simple schematic diagram of a direct sequence spread spectrum system.*

- **Frequency hopping spread spectrum** (**FH–SS**): In this method, the transmitter employs a number of different carrier frequencies within a given assigned spectral bandwidth. The carrier frequency that is used for data signal transmission changes over each symbol period T_s, and is determined by a PN code which is known to both the transmitter and the receiver. Figure 2.2 shows a simple schematic representation of the carrier frequency pattern of a FH–SS system.

- **Time hopping spread spectrum** (**TH–SS**): According to this method, time is split into

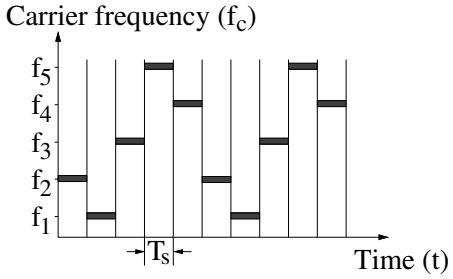

Figure 2.2: *Simple schematic representation of the carrier frequency pattern of a frequency hopping spread spectrum system.*

blocks of time slots. Over each block of time slots, the transmitter transmits only during one time slot, determined by a PN code which is again known to both the transmitter and the receiver. This method is less common than the other methods. Figure 2.3 shows a simple schematic representation of the time slot pattern of a TH–SS system.

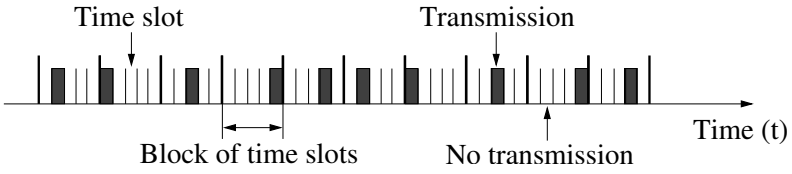

Figure 2.3: *Simple schematic representation of the time slot pattern of a time hopping spread spectrum system.*

- **Multi-carrier spread spectrum** (**MC–SS**): In this method, the transmitter employs a number of carrier frequencies and transmits simultaneously on all of them. While this concept is relatively old, recently there has been interest in using carrier waveforms that are orthogonal in the frequency domain to facilitate multiple simultaneous access to the common channel. In principle, if N_c carrier frequencies are used, N_c symbols are usually spread by different PN codes and are then time-multiplexed. Next, different parts of the resulting time-multiplexed signal are transmitted through the N_c carrier frequencies.

This work will only be concerned with DS–SS, so the other spread spectrum methods will not be examined further. The above short spread spectrum introduction is not meant to be exhaustive, but the reader is referred to [55,60,111,175,198–200,229,236,244] for further information. The next section presents a brief overview of CDMA/WCDMA wireless communication systems.

2.1.2 Wireless communication systems based on CDMA/WCDMA

The DS–SS method is used in CDMA systems, like North America's IS-95 standard. It is also used by third generation mobile communication systems (Universal Mobile Telephony System, UMTS), to enhance their capacity as compared to GSM and DCS-1800 systems. In CDMA-based systems, a number of users of a wireless communication system access the common medium using the same carrier frequency and at the same time, in an asynchronous manner. These users are distinguished from one another because they make use of distinct PN codes to modulate their data streams prior to transmission at the appropriate carrier frequency. There are various types of PN codes that can be used for this purpose, including m-sequence codes, Gold codes and Walsh-Hadamard codes, each having its own characteristics. The interference due to other users who make use of the same carrier frequency appears as background noise, and is mainly determined by the cross-correlation properties of the PN codes.

Consider a simple CDMA mobile communication system with a single (non-sectored) cell, served by a base station with an antenna which is omnidirectional over the azimuth. The capacity, in terms of number of simultaneous served users U, of this system is [76]

$$U = 1 + \frac{W}{E_b/N_o} - \frac{I_o}{E_s}, \tag{2.2}$$

where W is the processing gain, E_b is the transmit power per bit and N_o the noise power spectral density, I_o denotes the background noise and E_s the power at which the base station receives each mobile user (which is the same for all U users due to the power control mechanism to be discussed shortly). This means that the system capacity is inversely proportional to each user's transmit power. Consequently, decreasing each user's transmit power, directly increases the system capacity. Therefore, CDMA systems are called interference-limited (i.e. their capacity is limited by the interference that users cause to each other), in contrast to (single-cell) TDMA/FDMA systems which are primarily bandwidth-limited (i.e. their capacity is mainly limited by the amount of the available bandwidth). Although this conclusion is drawn for the uplink capacity of the above single-cell CDMA system, in [76] it is shown that it also holds for both the uplink and downlink capacities of CDMA systems with multiple sectored cells, which are the cell types that we will consider.

Wireless communication systems based on CDMA usually operate in FDD mode, using different carrier frequencies for the uplink and downlink. Also, the nature of the uplink and downlink

is different and will be analysed separately. Figure 2.4 shows a simple schematic diagram of the CDMA uplink. A number of mobile users use distinct PN codes to modulate their data stream, and they transmit the resulting signal into the common medium using the same carrier frequency. The base station receives the superposition of their transmit signals, plus noise and interference from users of other cells of the system. Then, it correlates the received signal with each user's PN code to obtain an estimate of the U users' data streams.

Because of the asynchronous operation of the uplink, the level of interference from users of the same or other cells (due to non-zero cross-correlation among the U PN codes) is unpredictable [76, 238]. Also, a major problem occurs when a user close to the base station transmits at the same power as a user that is far away from it, as the signal of the former will be stronger than that of the latter and will swamp it [236]. This is called the near-far effect and can have a detrimental effect on the performance. A possible solution to this problem is a power control system, which operates in the base station and specifies each mobile user's transmit power, so that all users are received with the same power at the base station [236, 238, 239, 243].

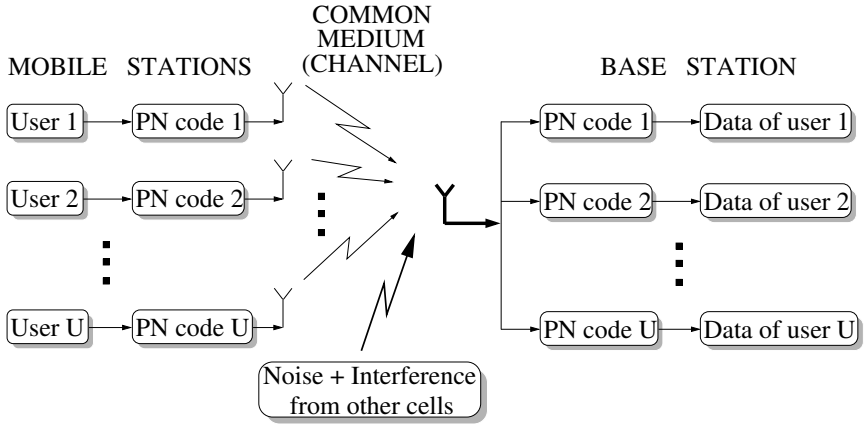

Figure 2.4: *Simple schematic diagram of the CDMA uplink with U users.*

Next, Figure 2.5 shows a simple schematic diagram of the CDMA downlink. The data signal transmission from base station to mobile stations is done in the same way as on the uplink, but the transmission is now synchronous. This means that interference levels may now be controlled more easily, and there is no near-far effect. However, mobile users close to the cell borders may experience high interference levels from users of neighboring cells. This problem may be solved by increasing the transmit power to these users, but this may produce more interference to users close to the base station.

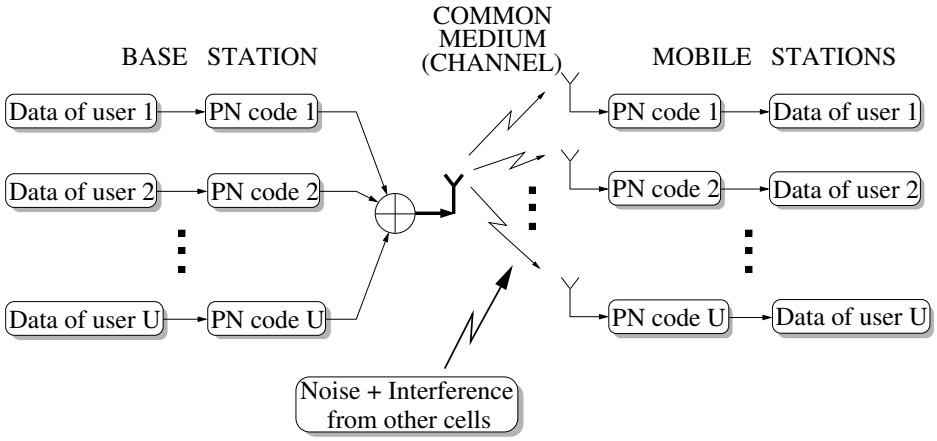

Figure 2.5: *Simple schematic diagram of the CDMA downlink with U users.*

An important characteristic of CDMA is that it offers high resolution over time, as the auto-correlation function of the PN codes takes on significant values only during a chip period T_c, which is very small. This means that signals (also called 'taps', see section 2.3.2 below) arriving at the receiver with relative delays equal to or larger than T_c can be resolved. These signals were first considered as interference that degraded the desired signal (which is usually the first tap to arrive at the receiver). However, it has been shown in [229] that they can actually be used

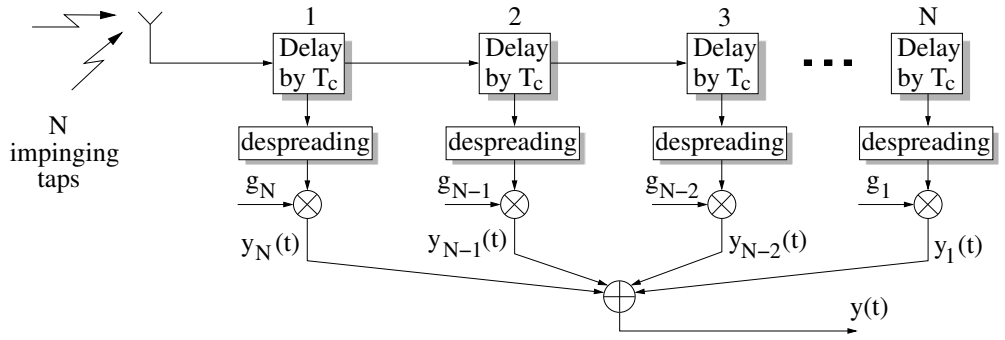

Figure 2.6: *Simple schematic diagram of the basic concept of a Rake receiver.*

to improve the desired signal, since they are themselves delayed copies of the desired signal. This is possible using the 'Rake' technique, which was originally developed in [174] and whose basic principle is schematically shown in Figure 2.6. Assuming that there are N taps temporally separated from each other by T_c, a Rake receiver stores the signals $y_i(t)$, $i = 1..N-1$, due to the $N-1$ first taps, until the N-th tap has been received. Then, it sums all the N taps (after despreading and weighting them with appropriate weights g_n, $n = 1..N$) to obtain an improved

version $y(t)$ of the received signal. This structure is a standard component of CDMA receivers.

Now we move on to WCDMA mobile communication systems which are based on CDMA, so everything that has been presented so far in this section is still valid for them. Here we will present a short description of the air interface (Layer 1) of WCDMA systems, but for more information the reader is referred to [8–11]. Layer 1 of WCDMA uses physical channels which are characterised by a specific carrier frequency, scrambling code, channelisation code (optional), start and stop instant (determining duration), and (on the uplink) relative phase (0 or $\frac{\pi}{2}$). It also uses transport channels which can be thought of as low-level services offered to higher layers, and are categorised into dedicated channels (using inherent mobile station addressing) and common channels (using explicit mobile station addressing, if addressing is needed). Transport channels are described as being capable of being mapped to physical channels. Let us examine the uplink and downlink channels separately, starting with the former.

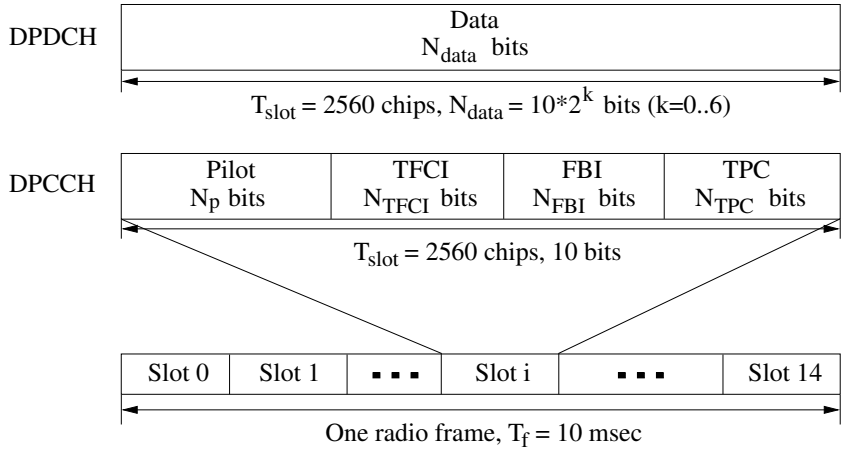

Figure 2.7: *Frame structure of uplink DPDCH and DPCCH.*

The two main uplink dedicated physical channels are the dedicated physical data channel (uplink DPDCH) and the dedicated physical control channel (uplink DPCCH), which are I/Q code multiplexed. The uplink DPDCH carries data symbols, and there may be zero, one or several such channels on each radio link. The uplink DPCCH carries control information, consisting of known pilot bits to support channel estimation for coherent detection, transmit power control commands (TPC), feedback information (FBI) and an optional transport-format combination indicator (TFCI). There can be only one uplink DPCCH on each radio link. The structure of the uplink DPDCH and DPCCH is shown in Figure 2.7. A radio frame is a processing unit consisting of 15 slots (which contain fields with bits), which has a duration of $T_f = 10$ msec and a

length of $15 \times 2560 = 38400$ chips, to make up a total chip rate of 3.84×10^6 chips/sec. Each slot contains $T_{slot} = 2560$ chips, corresponding to one power-control period. The DPDCH and DPCCH are frame-aligned with one another. The parameter k determines the number of bits per uplink DPDCH slot as $N_{data} = 10 \times 2^k$, and is related to the spreading factor (or processing gain, W) as $W = \frac{256}{2^k}$. The DPDCH spreading factor W ranges from 4 to 256. On the other hand, the number of bits per uplink DPCCH slot is always 10 and its spreading factor is always 256. The exact number of bits in the uplink DPDCH (N_{data}) and in the various uplink DPCCH fields (N_p, N_{TFCI}, N_{FBI} and N_{TPC}) are specified in tables [9], while the slot format to be used is determined by higher layers (and can also be re-configured by higher layers, if necessary). There are also a number of uplink common channels described in [9].

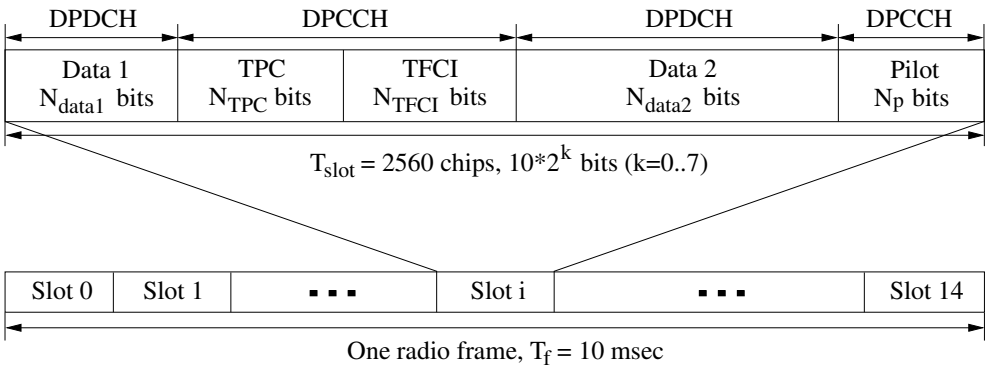

Figure 2.8: *Frame structure of downlink DPCH.*

In contrast to the uplink, there is only one downlink dedicated physical channel (downlink DPCH). In addition, the single downlink DPCH contains the downlink DPDCH (which carries data symbols) and DPCCH (which carries control information—known pilot bits, transmit power control commands (TPC) and transport-format combination indicator (TFCI)). These are time multiplexed within the downlink DPCH, as depicted in Figure 2.8 which shows the structure of the downlink DPCH. Again each frame has a duration of $T_f = 10$ msec and is split into 15 slots, each of $T_{slot} = 2560$ chips corresponding to one power control period. The parameter k determines the total number of bits per downlink DPCH slot as 10×2^k, and is related to the spreading factor as $W = \frac{512}{2^k}$. The spreading factor may thus range from 4 to 512. The exact number of bits of the various downlink DPCH fields (N_{data1}, N_{TPC}, N_{TFCI}, N_{data2} and N_p) are specified in tables [9], while the slot format to be used is determined by higher layers (and can also be re-configured by higher layers, if necessary). There are also a number of downlink common channels described in [9], including the common pilot channel.

Regarding the use of multiple antennas for improved performance in WCDMA, two kinds of transmit diversity are specified: open loop and closed loop transmit diversity. For open loop transmit diversity, the method of space-time block coding [16, 160] is employed [9] (the basic concept of this method is analysed in section 3.1.1 of Chapter 3). For closed loop transmit diversity, the base station applies different complex weight factors to the transmit signals of different antennas [11]. The weight factors are determined at the mobile station so that the received power is maximised, and are then transmitted to the base station (the basic concept of this method is analysed in section 3.1.2 of Chapter 3). There are two possible modes: mode 1 and mode 2. In mode 1, only the phases of the complex weights are adjusted, while in mode 2 both the phases and the amplitudes of the complex weights are adjusted. For more detailed information on the specified transmit diversity techniques, the reader is referred to [9, 11].

The next section contains a brief introduction to the concept of antenna arrays, as well as the associated characteristics and achievable gains.

2.2 Antenna arrays

This section first considers a number of reasons for using antenna arrays in mobile communication systems. Probably the most obvious reason is the **directional reception and transmission (beamforming)**. When an antenna array with multiple antenna elements is used for reception, the received signals of the individual elements can be weighted and then combined. The weights can be chosen so that the SNR of the signal coming from the direction of the desired mobile user is maximised. Similarly, if the antenna array is used for transmission, the transmit signals of the individual antenna elements can be weighted prior to transmission. Again, the weights can be chosen so that the individual signals combine coherently in the direction of the desired mobile user. In both cases, the antenna array can be thought of as forming a beam in the desired user direction [56, 67, 78, 102, 114, 145, 221]. Beamforming also directly improves received signal quality. It has been found that narrow azimuthal beamwidth in elevated base station transmit antenna arrays reduces multipath fading at the mobile station, while narrow beamwidth on the vertical plane increases the received power at the mobile station [104]. Another direct benefit of beamforming is **interference suppression**. When an antenna array forms a beam as described above, the signals received from or transmitted in the direction of non-desired users have (very) small amplitude. This effectively suppresses interference from/to other co-channel users [142, 251], improving the overall system performance. This basic concept is

often called space division multiple access (SDMA) [18, 66, 80]. Another reason for using antenna arrays is the offered **spatial diversity** which results in **multipath fading reduction**. Typically, the individual elements of an antenna array are spatially separated, so they sample or probe different locations of the three dimensional space. When the distance between these elements is sufficiently large, there is small correlation among their signals, providing spatial diversity [42,99,106,128,180,192,247,250,252,253,255]. The immediate benefit is a reduction of the probability of deep multipath fades in the received signal amplitude [104, 194].

The immediate benefit of the above points is improved received signal quality in the form of fading reduction and SNR enhancement, which can be traded off in various ways. For instance, it can be used to increase the cell size, reducing the number of base stations required to serve a given area, and ultimately the total cost of the system (this is especially desired at the initial stages of a mobile communication system deployment where cost minimization is of paramount importance). At later stages where the initial cost is no longer a major issue and the user demand for mobile communication is (usually) greater, the gain of antenna arrays can be used to increase the system capacity by serving more users. Also, this gain can be used for better quality of service, by improving the quality of the already existing services (e.g. through higher data rates and reduced outage probability) and offering the possibility for new ones. Furthermore, the spatial processing gain from antenna arrays can be used to reduce the performance overhead of power control, since interference from high power users can be spatially suppressed.

Having discussed some of the major advantages of using antenna arrays, now we move on to their main characteristics. Figure 2.9 shows the schematic diagram of an antenna array with M elements which are omnidirectional over the azimuth. Even though there is a number of possible geometrical configurations of the M elements (such as circular, rectangular, zig zag etc. [214]), the most common one is the linear configuration, as it is very simple. Assuming the carrier frequency is f_c and the corresponding carrier wavelength is λ ($\lambda = \frac{v_l}{f_c}$, where $v_l = 3\times10^8$ m/sec is the speed of light), the physical distance D between adjacent elements is fixed and usually equal to $\frac{\lambda}{2}$, to avoid grating lobes (which are equivalent to spatial aliasing phenomena). Such an array is called the uniform linear array (ULA), and will be used throughout this thesis.

Each element carries its own signal $y_i(t)$, $i = 1..M$, while the M signals are often placed in a vector as

$$\mathbf{y}(t) = \left[y_1(t)\ \ y_2(t)\ \ y_3(t)\ \ \cdots\ \ y_M(t)\right]^{\mathrm{T}}, \tag{2.3}$$

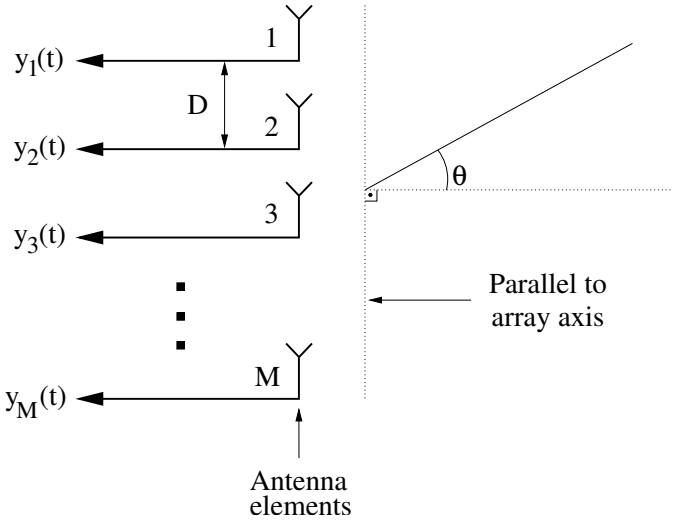

Figure 2.9: *Simple schematic diagram of a uniform linear array (ULA) with M elements.*

where the T superscript denotes the vector transpose operation[1]. When the array is used for reception, the receiver is provided with M signals which are properly processed to obtain an estimate of the original transmitted signal. There is a large number of signal processing techniques available for processing the received signals with various goals (such as maximisation of received signal SNR, extraction of directional information etc.). On the other hand, when the array is used for transmission, the transmitter transmits M signals which have been first properly processed according to a specific goal (such as forming a beam, provision of spatial diversity to the receiver etc.). Processing the signal prior to transmission is generally more difficult than processing it after reception, as various parameters (such as information about the propagation environment) may not be known at the transmitter prior to transmission. Also, some signal processing techniques process the signal in the form of the vector $\mathbf{y}(t)$ (this is usually done in beamforming techniques), while others process the individual signals $y_i(t)$, $i = 1..M$, one by one (this is often true of diversity techniques). A number of both types of techniques will be examined in this thesis.

A very important parameter of an M-element array is its steering vector $\mathbf{a}(D, \theta) \in \mathbb{C}^{M\times 1}$, which represents the array impulse response to a source transmitting from the azimuthal direction of θ. In order to write the array steering vector, we use the assumptions of the narrow-band

[1]The signals $y_i(t)$, $i = 1..M$, are treated as complex, as this allows for easier mathematical manipulation of them. In practice, $\cos(t)$ and $\sin(t)$ basis functions of the same period are used for transmission of the real and imaginary part respectively (the transmitted signal is the summation of these two signals). The receiver is able to distinguish between them as the $\cos(t)$ and $\sin(t)$ functions are orthogonal when integrated over integer multiples of their period.

antenna array model. The two main assumptions of this model are: **a**) All the transmissions are narrow-band, in the sense that the bandwidth of the transmitted signal is much smaller than the carrier frequency f_c (this effectively means that the array response can be assumed frequency-independent over the bandwidth of the transmitted signal), and **b**) The received signal of each array element is corrupted by spatially and temporally white Gaussian noise of zero mean and variance σ_n^2 (the 'spatially white noise' assumption effectively means that the noise affects all the antenna array elements in a similar manner). Assumption **a**) holds even for WCDMA, where the transmitted signal bandwidth is approximately 4 MHz and the carrier frequency is about 2 GHz. The narrow-band model will be used throughout the thesis. After its assumptions, the array steering vector can be written as follows

$$\mathbf{a}(D,\theta) = \begin{bmatrix} 1 \\ e^{J\{\frac{2\pi D}{\lambda}\sin(\theta)\}} \\ \vdots \\ e^{J\{\frac{2\pi D}{\lambda}(M-1)\sin(\theta)\}} \end{bmatrix} = \begin{bmatrix} 1 \\ e^{J\{2\pi \tilde{D}\sin(\theta)\}} \\ \vdots \\ e^{J\{2\pi \tilde{D}(M-1)\sin(\theta)\}} \end{bmatrix}, \tag{2.4}$$

where $\tilde{D} = \frac{D}{\lambda}$ is the array element spacing normalised by the carrier wavelength. Equation (2.4) shows that $\mathbf{a}(D,\theta) = \mathbf{a}(D, 180^{\text{o}} - \theta)$ (since $\sin(\theta) = \sin(180^{\text{o}} - \theta)$), so the response of a uniform linear array to signals coming from opposite sides of the array is the same and the signals cannot be distinguished. Also, uniform linear arrays suffer from end-fire effects, as transmissions coming from directions at or close to $\theta = 90^{\text{o}}$ or $\theta = -90^{\text{o}}$ are very sensitive to noise. However, these arrays are widely used in practice because of their simplicity, while the communication system designer ensures that signals do not come from opposite sides of the array or from directions at or close to $\theta = 90^{\text{o}}$ or $\theta = -90^{\text{o}}$.

After this brief discussion of the main advantages and characteristics of antenna arrays, we move on to the description of the system model that will be used throughout.

2.3 System model

Throughout this work we assume that the area served by a mobile communication system is divided into smaller hexagonal parts, called cells, as shown in Figure 2.10 [15, 58, 72, 123, 130, 131]. Each cell is in turn split into three sectors, each of 120^{o} to cover the 360^{o} azimuth.

2.3.1 Base station

Each base station serves one cell but employs a different antenna for each sector of the cell [23, 77, 114, 117, 194, 220, 254, 255]. Each base station antenna is a uniform linear array (ULA) containing M omnidirectional antenna elements, and is used for signal transmission to mobile stations. On the other hand, mobile stations use a single omnidirectional antenna for signal reception. The simple schematic diagram of such a base station is shown in Figure 2.11. The distance between adjacent array elements is denoted by D. The parameter θ is the central angle of departure (AOD), while δ is the angular spread (AS) which arises from the fact that the signal is reflected and/or scattered by physical objects in the channel propagation environment before being received [24, 45, 104, 124, 164, 176, 190, 210, 230]. Although the base station transmits

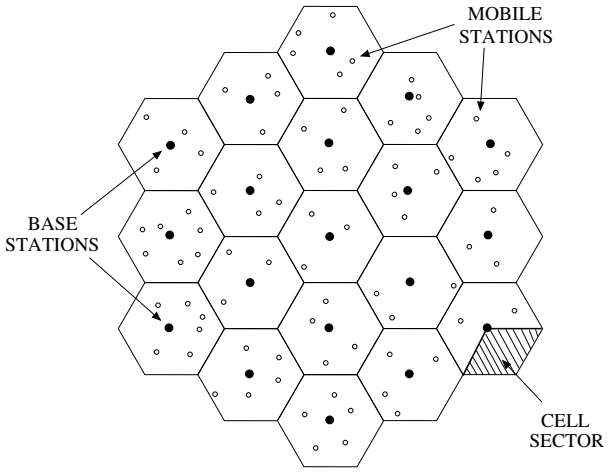

Figure 2.10: *The area served by a mobile communication system is divided into hexagonal cells. Each cell contains three sectors of* 120^o *each.*

waves in all directions over $[-60^{\text{o}}, 60^{\text{o}}]$ according to its array radiation pattern, only waves whose angle of departure lies in $\left[\theta - \frac{\delta}{2}, \theta + \frac{\delta}{2}\right]$ contribute to the signal received at the mobile station, due to the location of the mobile station and the location of physical reflectors and scatterers. The distribution of the angle of departure is assumed uniform over $\left[\theta - \frac{\delta}{2}, \theta + \frac{\delta}{2}\right]$. A number of other AOD distributions have been assumed in various studies, such as Gaussian [17] and $\cos^n()$ [124], but the uniform distribution allows for the derivation of a closed form expression for the mean channel correlation matrix (CCM) and the results are shown in [190] to agree well with measured data in [124]. The base station controls each array element adaptively by means of a signal processor (SP). Each signal processor can be as simple as a mixer or more sophisticated such as a Rake [174, 229] tapped delay line (in the latter case the set of the M

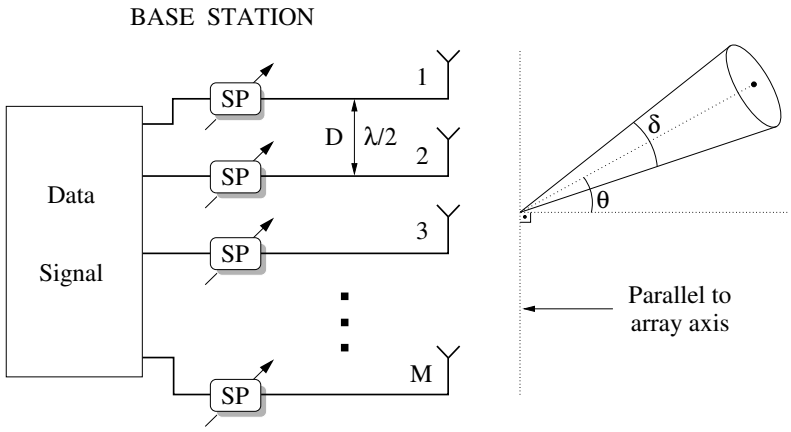

Figure 2.11: *Simple schematic diagram of a base station equipped with a uniform linear array with M omnidirectional elements.*

signal processors constitutes a 2-dimensional filter which processes signals over both space and time [72, 81, 117, 220]).

2.3.2 Channel propagation environment

The channel is assumed to be frequency selective with N resolvable temporal taps. A simple schematic representation of the channel propagation environment is shown in Figure 2.12 [19, 24, 36, 45, 63, 75, 83, 87, 104, 123, 124, 130, 131, 164, 190, 210, 211, 229, 230]. When the base station transmits waves over $[-60^o, 60^o]$, if there is visual contact between it and the mobile station, the waves that are in the direction of the mobile station are received by its single antenna without any further reaction with the propagation environment. This is called the direct path in Figure 2.12. On the other hand, waves that are in other directions are usually reflected and/or scattered by objects in the propagation environment (such as hills, buildings, cars, foliage etc). Some of them are reflected/scattered in the direction of the mobile station, and are eventually received by it. For instance, Figure 2.12 shows a group of waves reflected by a cluster of local reflectors/scatterers (blue waves), another group of waves reflected by a cluster of remote reflectors/scatterers (red waves) and one wave reflected by hills (green wave). Each wave within a group of waves generates a corresponding signal on the mobile station antenna. Also, the waves of a given group usually arrive at the mobile station with delays such that the signals that they generate on its antenna cannot be resolved in time. Therefore, the signals of all the waves within each group are seen by the mobile receiver as one signal, which is referred to as a channel tap. The relative power values and delays of the signals created on the mobile receiver

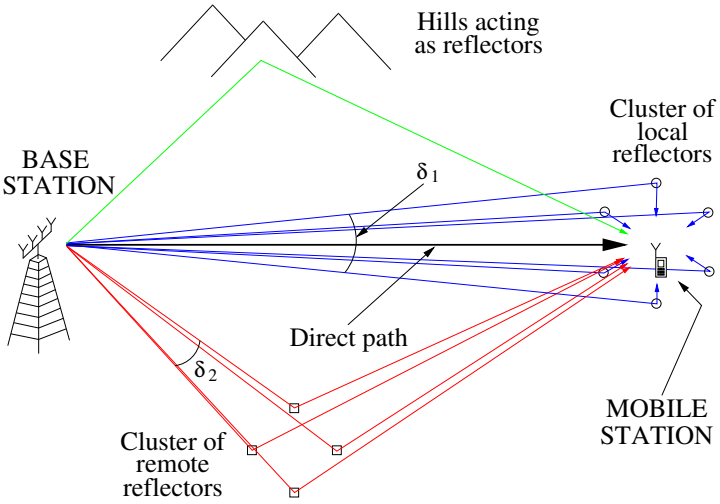

Figure 2.12: *Simple schematic representation of the channel propagation environment with various types of reflectors and scatterers.*

antenna by the taps of Figure 2.12 are shown schematically in Figure 2.13. The power profile usually decays exponentially [104]. The paths that the waves within each group follow and the electromagnetic properties of the objects that reflect and scatter them are usually different, resulting in uncorrelated signals within each tap. Consequently, the signal that the mobile receiver receives from each tap is the superposition of a (large) number of uncorrelated signals. This model is called wide sense stationary uncorrelated scattering (WSSUS) [63, 210, 230]. Thus, we model the channel vector of the n-th tap $\mathbf{h}_n(t) \in \mathbb{C}^{M\times 1}$ as the superposition of a number of uncorrelated plane waves (also called rays or components) as follows:

$$\mathbf{h}_n(t) = \begin{bmatrix} h_{n,1}(t) \\ h_{n,2}(t) \\ \vdots \\ h_{n,M}(t) \end{bmatrix} = \sqrt{\frac{P_n}{Q_n}} \sum_{q=1}^{Q_n} \underbrace{e^{\jmath(\phi_q + 2\pi f_q t)}}_{\beta_q(\phi_q, f_q, t)} \underbrace{\begin{bmatrix} 1 \\ e^{\jmath\{\frac{2\pi D}{\lambda}\sin(\theta_q)\}} \\ \vdots \\ e^{\jmath\{\frac{2\pi D}{\lambda}(M-1)\sin(\theta_q)\}} \end{bmatrix}}_{\mathbf{a}_q(\tilde{D},\theta_q)}$$

$$= \sqrt{\frac{P_n}{Q_n}} \sum_{q=1}^{Q_n} \beta_q(\phi_q, f_q, t)\mathbf{a}_q(\tilde{D}, \theta_q), \tag{2.5}$$

where $h_{n,i}(t)$, $i = 1..M$, is the complex coefficient of the n-th channel tap between the i-th antenna element of the base station and the single antenna of the mobile station, P_n is the tap power, Q_n the number of uncorrelated plane waves contributing to the tap and ϕ_q the random

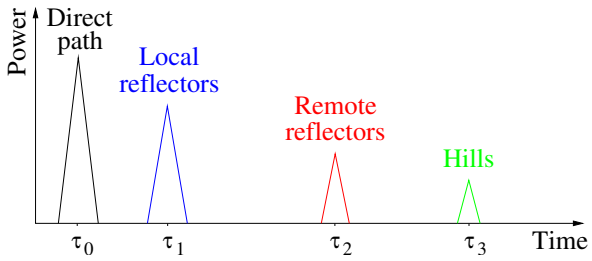

Figure 2.13: *Simple schematic representation of the received signal power profile at the mobile station in the channel propagation environment of Figure 2.12.*

phase of the q-th wave, which is uniformly distributed over $[0, 2\pi)$. Also, f_q is the Doppler frequency shift of the q-th wave, θ_q the angle of departure of the q-th wave and λ is the wavelength of the carrier frequency f_c. The complex number $\beta_q(\phi_q, f_q, t)$ is called the fading factor of the q-th wave, $\mathbf{a}_q(\tilde{D}, \theta_q) \in \mathbb{C}^{M\times 1}$ is the array steering vector of the q-th wave and $\tilde{D} = \frac{D}{\lambda}$ denotes the normalised antenna element spacing. The number of waves Q_n included in the n-th tap must be large so that the real and imaginary parts of the channel coefficients approximate very closely the behaviour of Gaussian random variables, according to the central limit theorem [162]. Then, if there is no direct path between the base station and the mobile station, the amplitude of each channel coefficient is a random number which follows Rayleigh distribution [72, 104, 176, 210], and the channel is characterised as Rayleigh fading. If there is a direct path between base and mobile station, however, the amplitude of each channel coefficient follows Rician distribution.

Figure 2.14 shows the variation of the amplitude of a given channel coefficient over one thousand symbol periods T_s, where $T_s = 104.2$ μsec (the maximum Doppler frequency shift is $f_{D,\max} = 110$ Hz). The amplitude is not constant but varies randomly with time, because the relative phases of the waves change with time in a random way. Also, when the relative phases are such that the Q_n waves add up incoherently, the amplitude of the channel coefficient experiences a deep fade whose magnitude can be 20 dB as shown in Figure 2.14, or even larger. This fading phenomenon causes sudden and severe signal loss at the mobile receiver, and is one of the factors that have the most detrimental effect on the performance of mobile communication systems. The frequency of the fades (i.e. the rate at which the fades cross a given negative threshold) is proportional to the maximum Doppler frequency shift, which in turn is proportional to the speed at which the mobile station is moving [45, 63, 104, 210] (that is, the faster the mobile is moving the more frequent the fades become).

Figure 2.15(a) shows the variation of the amplitude of the channel over both space and time,

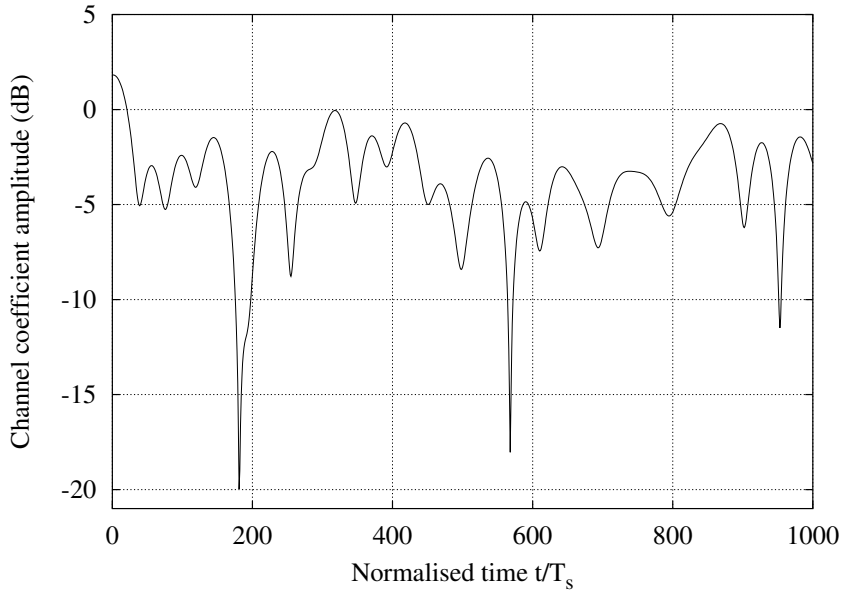

Figure 2.14: *Variation of the amplitude of a given coefficient of a channel tap over time (time fading). The plot was generated by implementing equation (2.5) on a computer.*

when the angular spread is zero. Although there is fading over time, there is no fading over space (i.e. the channel coefficients of all M array elements fade simultaneously). This is due to zero angular spread, and can be explained as follows. First, let us observe from equation (2.5) that the difference between the phases of the signals of the i-th and the k-th antenna elements ($i, k = 1..M, i \neq k$) due to the q-th plane wave is given by

$$\Delta p_q = \left[\frac{2\pi D}{\lambda}(i-1)\sin(\theta_q)\right] - \left[\frac{2\pi D}{\lambda}(k-1)\sin(\theta_q)\right] = \left[\frac{2\pi D}{\lambda}\sin(\theta_q)\right](i-k). \qquad (2.6)$$

That is, for given i and k, Δp_q depends only on θ_q. Also from Figure 2.11 we observe that when the angular spread is zero ($\delta = 0$), the angles of departure θ_q of all Q_n waves in equation (2.5) are the same and equal to the central angle of departure $\theta_q = \theta$, $q = 1..Q_n$. Consequently, all differences Δp_q, $q = 1..Q_n$, are the same, resulting in no difference between the channel coefficients of the i-th and the k-th antenna element. Therefore, with zero angular spread all M channel coefficients fade simultaneously over time, as shown in Figure 2.15(a). However, when the angular spread is not zero the angles of departure θ_q will be different for different values of q, and the phase differences Δp_q will also be different for different values of q. Therefore, while the Q_n plane waves of the i-th channel coefficient may add up coherently, the same Q_n plane waves of the k-th channel coefficient may add up incoherently, resulting in two different

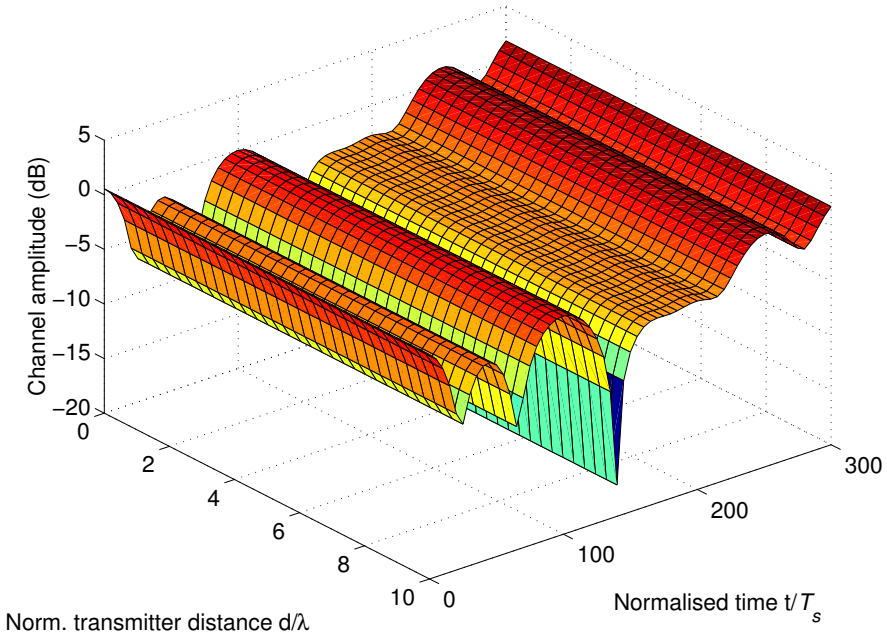

(a) Angular spread is 0°. There is fading over time but not over space.

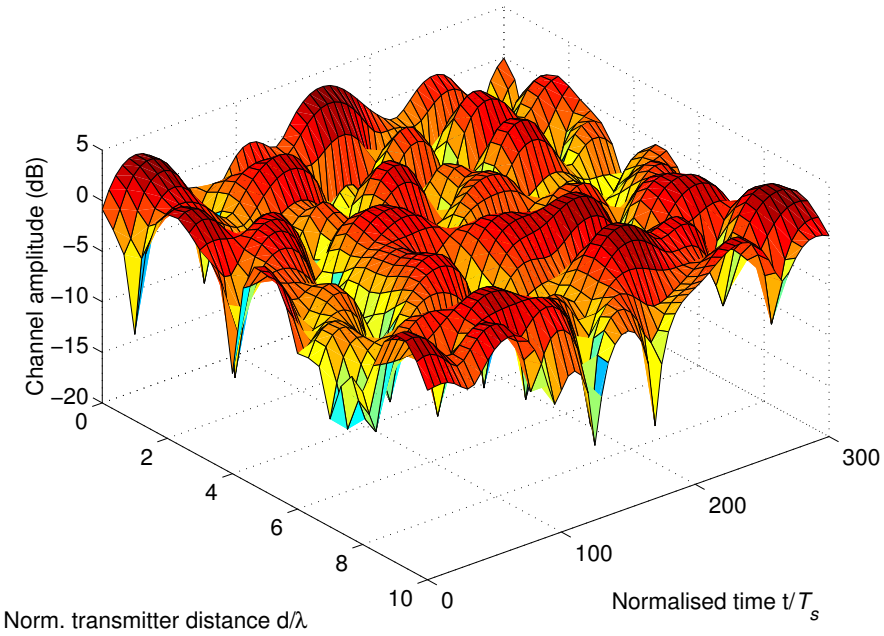

(b) Angular spread is 50°. There is fading over both time and space.

Figure 2.15: *Channel amplitude variation over space and time for angular spread* 0^o *and* 50^o*. The plot was generated by implementing equation (2.5) on a computer.*

channel coefficients. Thus, now the two channel coefficients do not fade simultaneously, giving rise to fading over space. In this case there is fading over both space and time, as shown in Figure 2.15(b) where the angular spread is 50°.

2.3.3 Mean correlation matrix of the channel

The mean channel correlation matrix is of particular importance, and it is useful to both beamforming and diversity antenna array techniques. For beamforming techniques, it provides information about the direction of the intended mobile station, and helps steering the main beam in the correct direction. For diversity techniques, it provides information about the correlation between the signals of different antenna elements and, thus, about potential limitations to the diversity gain imposed by the channel environment, since the diversity gain decreases as this correlation increases [104, 122, 176, 190]. Also, the eigenvalue decomposition of this matrix is important in the theoretical performance analysis of many algorithms. In particular, we will show that its eigenvalues can be used to calculate the theoretical performance of most antenna array algorithms to be analysed in Chapters 3 and 4.

The mean correlation matrix $\mathbf{R}_n \in \mathbb{C}^{M\times M}$ of the n-th tap of the channel is obtained from its channel vector $\mathbf{h}_n(t)$ as follows

$$\mathbf{R}_n = \mathrm{E}\left\{\mathbf{h}_n(t)\mathbf{h}_n^{\mathrm{H}}(t)\right\} = \mathrm{E}\left\{\begin{bmatrix} h_{n,1}(t) \\ h_{n,2}(t) \\ \vdots \\ h_{n,M}(t) \end{bmatrix}\begin{bmatrix} h_{n,1}^*(t) & h_{n,2}^*(t) & \cdots & h_{n,M}^*(t) \end{bmatrix}\right\}$$

$$= \begin{bmatrix} r_{n,11} & r_{n,12} & \cdots & r_{n,1M} \\ r_{n,21} & r_{n,22} & \cdots & r_{n,2M} \\ \vdots & \vdots & \ddots & \vdots \\ r_{n,M1} & r_{n,M2} & \cdots & r_{n,MM} \end{bmatrix}, \tag{2.7}$$

where $r_{n,ij} = \mathrm{E}\left\{h_{n,i}(t)h_{n,j}^*(t)\right\}$ and $\mathrm{E}\{\bullet\}$ denotes expectation. The correlation matrix has been calculated theoretically in [190] and the results are included in section A.1 of appendix A for easy reference. The correlation matrix has Hermitian symmetry, as $r_{n,ij} = r_{n,ji}^*$. Strictly speaking, the correlation matrix depends on the normalised spacing $\tilde{D}$, angular spread δ and angle of arrival/departure θ through the channel vector of equation (2.5), but in equation (2.7) we omit

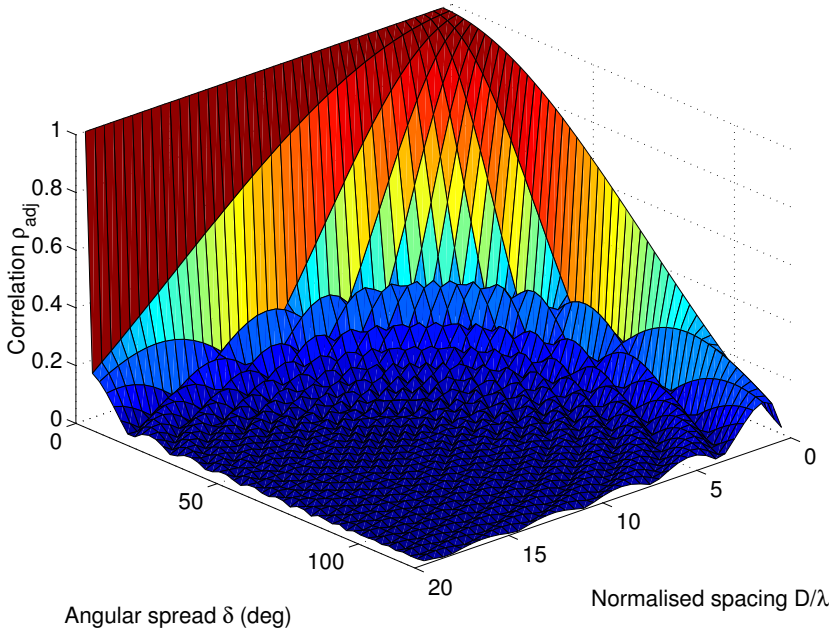

Figure 2.16: *Correlation between the channel coefficients of any two adjacent antenna elements as a function of spacing and angular spread.*

this dependence for notation simplicity. The entry $r_{n,ij}$ represents the complex correlation coefficient between the i-th and j-th channel coefficients of the n-th tap. If the i-th and j-th array elements are adjacent, let $\rho_{\text{adj}} = |r_{n,ij}|$ denote the correlation between their channel coefficients ($|r_{n,ij}|$ is the magnitude of $r_{n,ij}$, and $0 \leq \rho_{\text{adj}} \leq 1$). The correlation matrix has been calculated using equations (A.2) and (A.3) of appendix A (page 157), and the correlation $\rho_{\text{adj}} = |r_{n,12}|$ has been plotted as a function of normalised spacing and angular spread in Figure 2.16. Although $|r_{n,12}|$ is the correlation between the channel coefficients of the first and second array elements, it also represents the correlation between the channel coefficients of any two adjacent array elements because the array is uniform. The correlation ρ_{adj} for very small values of normalised spacing and angular spread is very close to one. This means that adjacent channel coefficients are highly correlated and fade simultaneously over time, as shown in Figure 2.17(a) for $M = 4$. These conditions favour beamforming antenna array techniques. However, as the value of normalised spacing and angular spread increases, the correlation ρ_{adj} decreases and approaches zero. This means that adjacent channel coefficients are less correlated and fade almost independently, as shown in Figure 2.17(b) for $M = 4$. These conditions favour diversity antenna array techniques. It is interesting to note that when δ is close to zero, the correlation ρ_{adj} is very close to one for all $\tilde{D}$ values shown in Figure 2.16, and even large $\tilde{D}$ values (e.g. $\tilde{D} = 20$)

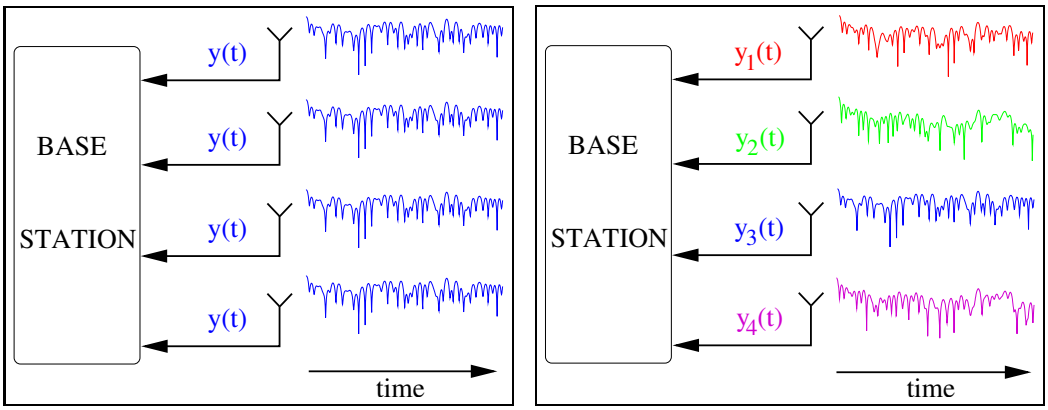

(a) High correlation, fading of antennas over time is similar, beamforming gain is favoured.

(b) Low correlation, fading of antennas over time is different, diversity gain is favoured.

Figure 2.17: *Fading of the signals of different antennas over time for high and low correlation among them. The plot was generated by implementing equation (2.5) on a computer.*

can result in highly correlated channel coefficients. Increasing the array element spacing is often used in practice to decrease the correlation and increase the diversity gain. Nevertheless, this should be done with great care in environments with (very) small angular spread, as the correlation may not be decreased sufficiently, resulting in reduced diversity gain.

The eigenvalue decomposition (EVD) of the correlation matrix will play an important role in the theoretical analysis of many algorithms to be analysed in the following chapters. By performing the EVD of $\mathbf{R}_n$ we express it as a function of its eigenvalues and eigenvectors. More specifically, if e_i, $i = 1..M$, is its i-th eigenvalue and $\mathbf{u}_i \in \mathbb{C}^{M\times 1}$, $i = 1..M$, the corresponding eigenvector, $\mathbf{R}_n$ can be written as

$$\mathbf{R}_n = \mathbf{U}\mathbf{E}\mathbf{U}^{\mathrm{H}} = \begin{bmatrix} \mathbf{u}_1 & \mathbf{u}_2 & \cdots & \mathbf{u}_M \end{bmatrix} \begin{bmatrix} e_1 & 0 & \cdots & 0 \\ 0 & e_2 & \cdots & 0 \\ \vdots & \vdots & \ddots & \vdots \\ 0 & 0 & \cdots & e_M \end{bmatrix} \begin{bmatrix} \mathbf{u}_1^{\mathrm{H}} \\ \mathbf{u}_2^{\mathrm{H}} \\ \vdots \\ \mathbf{u}_M^{\mathrm{H}} \end{bmatrix}$$

$$= \sum_{i=1}^{M} e_i \left(\mathbf{u}_i \mathbf{u}_i^{\mathrm{H}} \right), \tag{2.8}$$

where $\mathbf{E}$ is a diagonal matrix with diagonal entries equal to the eigenvalues $e_1, e_2, \cdots, e_M$ and

$\mathbf{U}$ is a matrix whose columns are equal to the corresponding eigenvectors $\mathbf{u}_1, \mathbf{u}_2, \cdots, \mathbf{u}_M$. The eigenvectors have unit norm, they are orthogonal to each other and constitute an orthonormal basis in the M-dimensional space [92]. Hence, the channel is decomposed into M independent components, each with power equal to its corresponding eigenvalue. Also, formula (14-5-28) of [176] gives the performance of a receiver with M statistically independent diversity paths of unequal strength. Therefore, the independence of the eigenvectors and the fact that the eigenvalues are in general unequal, enables the use of this formula for the calculation of the theoretical performance of many algorithms. According to the formula, the average bit error ratio (BER) for BPSK modulation is given as

$$P_b = \frac{1}{2} \sum_{k=1}^{M} \pi_k \left(1 - \sqrt{\frac{\bar{\gamma}_k}{1 + \bar{\gamma}_k}} \right), \tag{2.9}$$

where

$$\pi_k = \prod_{\substack{i=1 \\ i \neq k}}^{M} \frac{\bar{\gamma}_k}{\bar{\gamma}_k - \bar{\gamma}_i} \tag{2.10}$$

and $\bar{\gamma}_i$ is the average SNR of the i-th component.

In this chapter, a brief overview of spread spectrum and CDMA/WCDMA technologies was presented. Also, the fundamental concept of antenna arrays was briefly discussed, along with the main gain types and possible drawbacks. Next, the propagation environment, the channel correlation matrix and the system model that will be used throughout this thesis were introduced. Following this brief introductory chapter, is the first chapter containing the main results of the thesis.

Chapter 3
Analysis and comparison of downlink antenna array techniques

In this chapter we will analyse a number of diversity, beamforming and hybrid antenna array techniques which can be employed on the downlink of mobile wireless communication systems. Each technique will be introduced and, where applicable, its theoretical performance will be calculated based on the combination of the eigenvalue decomposition of the mean channel correlation matrix and equation (2.9). The techniques will also be simulated in a single user scenario and in various channel environments. The simulation results, along with other characteristics of the techniques, will be compared to each other, providing indications about which techniques are suitable for each channel environment. The techniques will be split into two categories: open loop and closed loop. Open loop techniques are those in which the base station does not receive any kind of information (about the downlink channel and/or other parameters) by means of feedback signals from the mobile station. Closed loop techniques are those in which the base station receives and uses some kind of information by means of feedback signals from the mobile station.

3.1 Open loop antenna array techniques

The open loop techniques that will be analysed in this section are space-time spreading and maximum SNR.

3.1.1 Space-time spreading

Space-time spreading (STS) [160, 161] is an open loop diversity technique, and its schematic diagram for $M = 2$ is shown in Figure 3.1 (useful diversity references include [23, 30, 34, 42, 51–53, 57, 65, 85, 86, 93, 99, 106, 128, 133, 150, 163, 180, 181, 192, 202, 246, 247, 249, 250, 252, 253, 255]). If M antenna elements are used in the base station, the data stream $s(t)$ of a user

is divided into M 'substreams' $s_i(t)$, $i = 1..M$, and their (complex) spreading code $c(t)$[1] of length L_c chips is used to construct M new spreading codes $c_i(t)$, $i = 1..M$, each of length ML_c chips (more information about how this is done in practice can be found in [160]). Then, each antenna element transmits a function of all M data substreams and spreading codes. The received signal y at the single-antenna mobile receiver is a linear superposition of the M data substreams and spreading codes, which have been distorted by the channel and perturbed by additive noise. The receiver decouples the M transmitted data substreams by cross-correlating y with each $c_i(t)^*$. Finally, it estimates the downlink channel coefficients and uses this knowledge to obtain an estimate $\hat{s}_i(t)$, $i = 1..M$, of all the data substreams.

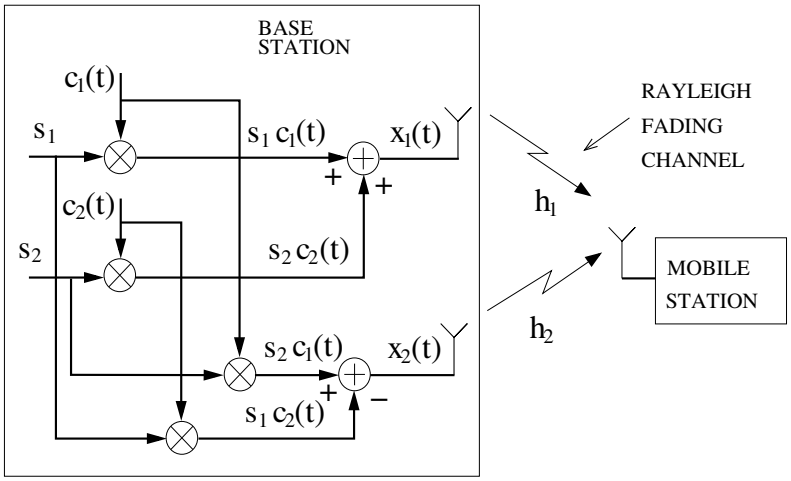

Figure 3.1: *Simple schematic diagram of space-time spreading with $M = 2$ array elements.*

Space time spreading is based on the theory of orthogonal designs, which had been known for $M = 2$, $M = 4$ and $M = 8$ antenna elements, and later was extended to any M for real signal constellations in [217]. Space time spreading schemes using real signal constellations achieve full transmission rate for any M (that is, they use one symbol period per transmitted data symbol). However, for complex signal constellations, it is shown in [217] that a full transmission rate scheme exists only for $M = 2$, which is presented in [16].

Calculation of the theoretical BER versus SNR performance of STS has been performed in [160]. When M antenna elements are used in the base station the expected SNR of the decision

[1]Note that although both the data signal $s(t)$ and the spreading code $c(t)$ vary over time, the spreading code varies much more rapidly than the data signal and determines the bandwidth of the transmitted signal.

signal at the mobile receiver is given as follows

$$\mathrm{SNR}_{\mathrm{STS}} = E_s \frac{1}{M} \frac{\mathrm{E}\left[\sum_{i=1}^{M} |h_i|^2\right]}{\sigma_n^2}, \tag{3.1}$$

where E_s is the power of the transmitted signal across all M antennas, σ_n^2 is the power spectral density of additive white Gaussian noise and E[•] denotes expectation. Equation (3.1) shows that STS yields order M diversity gain.

Also, given that the trace of a square matrix equals the sum of its eigenvalues [98], equation (3.1) can be written as follows

$$\mathrm{SNR}_{\mathrm{STS}} = \frac{E_s}{M} \frac{\mathrm{E}\left[\sum_{i=1}^{M} |h_i|^2\right]}{\sigma_n^2} = \frac{E_s}{M} \frac{\sum_{i=1}^{M} \mathrm{E}\left[|h_i|^2\right]}{\sigma_n^2} = \frac{E_s}{M} \frac{\mathrm{trace}\left(\mathbf{R}_{\mathrm{DL}}\right)}{\sigma_n^2}$$

$$= \frac{E_s}{M} \frac{\sum_{i=1}^{M} e_i}{\sigma_n^2} = E_s \frac{\sum_{i=1}^{M} \left(\frac{e_i}{M}\right)}{\sigma_n^2}, \tag{3.2}$$

where $\mathbf{R}_{\mathrm{DL}}$ is the mean correlation matrix of the downlink channel and e_i its i-th eigenvalue. This means that STS uses M independent diversity paths each with power equal to the corresponding eigenvalue of $\mathbf{R}_{\mathrm{DL}}$ scaled by M. Therefore, equation (2.9) can be used to calculate its bit error ratio versus signal to noise ratio performance with $\bar{\gamma}_i = \frac{e_i}{M}$, $i = 1..M$.

3.1.2 Maximum SNR

Maximum SNR (MAX SNR) [182] is a beamforming technique, and its schematic diagram is depicted in Figure 3.2 (useful beamforming references include [41, 46–48, 56, 66, 67, 78, 79, 89, 95, 100–103, 110, 114, 119, 120, 132, 144, 169, 206, 207, 215, 216, 221–223, 231, 246]). It maximises the expected SNR of the decision signal at the mobile receiver by using an appropriate weight vector $\mathbf{w}^{\mathrm{H}} \in \mathbb{C}^{1\times M}$ to transmit the data signal to the intended mobile station. The expected SNR of the decision signal at the mobile receiver for a 1-tap channel scenario is

$$\mathrm{SNR}_{\mathrm{MAXSNR}} = E_s \frac{\mathbf{w}^{\mathrm{H}} \mathrm{E}\left[\mathbf{h}_{\mathrm{DL}} \mathbf{h}_{\mathrm{DL}}^{\mathrm{H}}\right] \mathbf{w}}{\sigma_n^2} = E_s \frac{\mathbf{w}^{\mathrm{H}} \mathbf{R}_{\mathrm{DL}} \mathbf{w}}{\sigma_n^2}, \tag{3.3}$$

where $\mathbf{h}_{\mathrm{DL}}$ is a sample of the downlink channel vector at the moment of reception and $\mathbf{R}_{\mathrm{DL}}$ its mean correlation matrix. Thus, the weight vector $\mathbf{w}^{\mathrm{H}}$ that maximises the expected SNR of the decision signal while keeping the transmit power equal to that of a single-antenna base station,

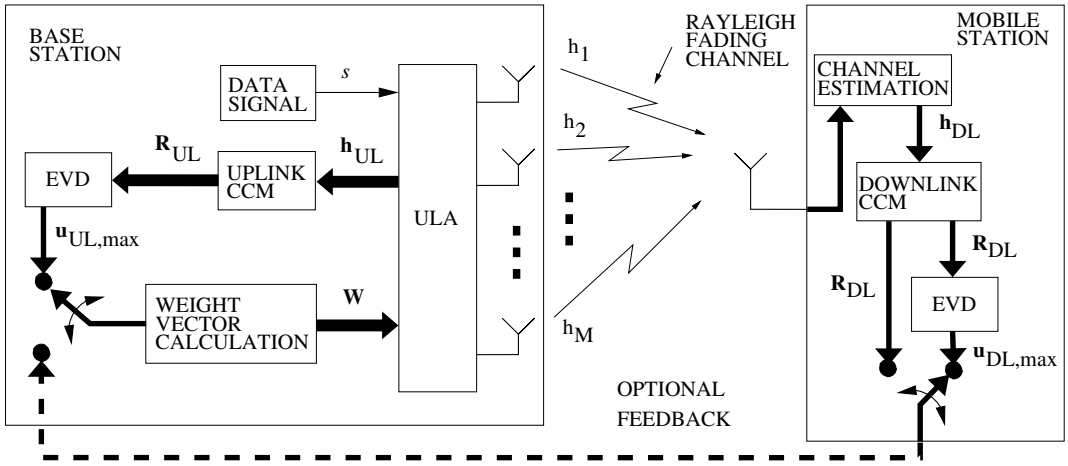

Figure 3.2: *Simple schematic diagram of maximum SNR with M antenna elements.*

is the solution to the following mathematical problem

$$\mathbf{w}^{\mathrm{H}} = \arg\left[\max_{\substack{\mathbf{w} \\ \text{TX power=const}}} \left(\frac{\mathbf{w}^{\mathrm{H}}\mathbf{R}_{\mathrm{DL}}\mathbf{w}}{\sigma_n^2}\right)\right]. \tag{3.4}$$

It is known that the solution is the principal eigenvector $\mathbf{u}_{\mathrm{DL,max}}$ of $\mathbf{R}_{\mathrm{DL}}$ (the principal eigenvector is the eigenvector that corresponds to the maximum eigenvalue $e_{\mathrm{DL,max}}$ of $\mathbf{R}_{\mathrm{DL}}$). Replacing $\mathbf{R}_{\mathrm{DL}}$ from equation (2.8) and $\mathbf{w}^{\mathrm{H}} = \mathbf{u}_{\mathrm{DL,max}}^{\mathrm{H}}$, to equation (3.3) we obtain

$$\mathrm{SNR}_{\mathrm{MAXSNR}} = E_s \frac{\mathbf{u}_{\mathrm{DL,max}}^{\mathrm{H}}\left[\sum_{i=1}^{M} e_{\mathrm{DL},i}\left(\mathbf{u}_{\mathrm{DL},i}\mathbf{u}_{\mathrm{DL},i}^{\mathrm{H}}\right)\right]\mathbf{u}_{\mathrm{DL,max}}}{\sigma_n^2} = E_s \frac{e_{\mathrm{DL,max}}}{\sigma_n^2}, \tag{3.5}$$

that is, the mean SNR of the decision signal is proportional to the maximum eigenvalue of $\mathbf{R}_{\mathrm{DL}}$. The theoretical performance of MAX SNR can thus be obtained by using equation (2.9) with only one branch with average SNR equal to $e_{\mathrm{DL,max}}$. By using the principal eigenvector as the weight vector, the base station forms a beam with a maximum in the direction that maximises the mean SNR of the decision signal, and the weight vector is often called beamformer. This is depicted in Figure 3.3 where the maximum of the beam that corresponds to the principal eigenvector is in the direction of the mobile receiver, while the maximum of the beams corresponding to the other eigenvectors are in other directions[2]. Thus, the gain in equation (3.5) is

[2]We point out that Figure 3.3 is just a simple schematic representation of the radiation patterns of the eigenvectors and is not meant to describe them in every detail. For instance, in practice the radiation pattern of an eigenvector may have more than one maximum (due to more than one angle of departure contributing to the signal received by the mobile), which is not depicted in Figure 3.3.

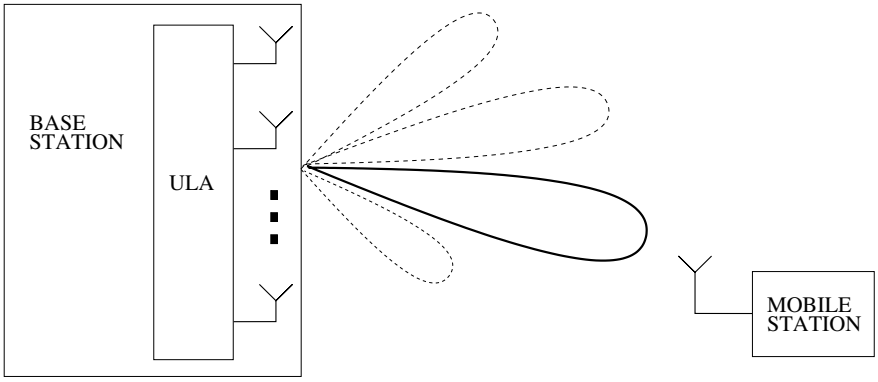

Figure 3.3: *Schematic representation of the beams formed by the M eigenvectors with the principal eigenbeam pointing in the direction that maximises the mean SNR.*

called beamforming gain. In case of a channel propagation environment with N taps, the mean correlation matrices of all downlink taps are summed

$$\mathbf{R}_{\mathrm{DL,sum}} = \sum_{n=1}^{N} \mathrm{E}\left[\mathbf{h}_{\mathrm{DL},n}(t)\mathbf{h}_{\mathrm{DL},n}^{\mathrm{H}}(t)\right], \tag{3.6}$$

and the principal eigenvector of $\mathbf{R}_{\mathrm{DL,sum}}$ is then used as weight vector by the base station.

In this technique, the base station needs to know the mean correlation matrix of the downlink channel, $\mathbf{R}_{\mathrm{DL}}$, in order to be able to calculate its principal eigenvector and use it as beamformer. We have seen in Chapter 2 that the mean correlation matrix of the channel depends on the carrier frequency, the antenna element spacing, the angle of departure or arrival and the angular spread of the channel environment [190]. The antenna element spacing is the same for both channels. Also, when the carrier frequencies of the two channels do not differ too much, the wavelengths of the electromagnetic waves of the two channels are similar, and we expect the same physical objects to act as reflectors and scatterers on the waves of *both* channels. Then, we can assume that the uplink angle of arrival is almost the same as the downlink angle of departure, and that the angular spread values of the two channels are similar [166]. Furthermore, in time division duplex (TDD) systems the uplink and downlink carrier frequencies are the same, causing the two correlation matrices to be the same. Then, the base station can calculate the uplink correlation matrix $\mathbf{R}_{\mathrm{UL}}$ from the signals that it receives on the uplink and use it as the downlink correlation matrix $\mathbf{R}_{\mathrm{DL}}$. In this case the optional feedback path of Figure 3.2 is not used. However, in frequency division duplex (FDD) systems the two carrier frequencies are different and the correlation matrices of the two channels are in general not

the same. Nevertheless, making the assumption that the two carrier frequencies do not differ by a large amount and that the two channels have similar long term statistical properties, we can say that the two correlation matrices do not differ too much. Then, the base station can still use the uplink correlation matrix as the downlink correlation matrix. The performance in this case deteriorates as compared to the case where the exact downlink correlation matrix is known at the base station. The performance loss depends on the carrier frequency separation and the correlation between the two channels (initial indications about the correlation of the two channels can be found in [166]). Again the optional feedback path of Figure 3.2 is not used. Alternatively, the base station can transform the uplink correlation matrix from the uplink carrier frequency to the downlink carrier frequency [100, 101, 103]. Also, the downlink correlation matrix can be calculated at the mobile station from pilot signals that the base station transmits from each antenna element. Then, the mobile station can feed back to the base station either the correlation matrix or its principal eigenvector, depending on the chosen trade off between the computational complexity that can be afforded by the mobile station (the larger the M the more complex the calculation of the principal eigenvector) and the feedback rate that can be afforded by the entire system (feeding back the whole matrix needs higher rate feedback than the principal eigenvector). In the actual 3GPP specifications for closed loop transmit diversity with $M = 2$ transmit antennas, the mobile station feeds back to base station the phase (and possibly amplitude) adjustment of the second antenna with respect to the first antenna [11]. In this case the optional feedback path of Figure 3.2 is used. With this approach the base station obtains a better estimate of the principal eigenvector of the downlink correlation matrix (subject to calculation and quantisation errors at the mobile station, and noise in the feedback signals), but a feedback path is now required. In the simulations MAX SNR is operated in an open loop fashion (i.e. the principal eigenvector of the uplink correlation matrix is used as beamformer), and that is why it is included in this section.

3.2 Closed loop antenna array techniques

The closed loop techniques that will be analysed in this section are transmit antenna array, selection diversity, fixed beams and eigenbeamforming.

3.2.1 Transmit antenna array

While MAX SNR of section 3.1.2 maximises the mean SNR of the decision signal, the technique that is called transmit antenna array (TXAA) maximises the instantaneous SNR of the decision signal [137, 187]. Its schematic diagram is depicted in Figure 3.4. The weight vector $\mathbf{w}^{\mathrm{H}}$ is now different and is chosen so that the instantaneous SNR of the decision signal is maximised. For an M-element antenna array and a channel propagation environment with one tap, the weight vector of TXAA is calculated as

$$\mathbf{w}^{\mathrm{H}} = \frac{1}{\sqrt{\mathbf{h}_{\mathrm{DL}}^{\mathrm{H}}\mathbf{h}_{\mathrm{DL}}}}\mathbf{h}_{\mathrm{DL}}^{\mathrm{H}} = \frac{1}{\sqrt{\sum_{i=1}^{M}|h_{\mathrm{DL},i}|^2}}\mathbf{h}_{\mathrm{DL}}^{\mathrm{H}}, \tag{3.7}$$

where $\mathbf{h}_{\mathrm{DL}}$ is a sample of the channel vector of the single downlink tap and $h_{\mathrm{DL},i}$, $i = 1..M$, its i-th coefficient. Hence, the weight vector is equal to the complex conjugate transpose (Hermitian) of the normalised channel vector, which forms such a radiation pattern that maximises the instantaneous SNR of the decision signal. The mean SNR of the decision signal is now

$$\mathrm{SNR}_{\mathrm{TXAA}} = E_s\frac{\mathrm{E}\left[\sum_{i=1}^{M}|h_{\mathrm{DL},i}|^2\right]}{\sigma_n^2}, \tag{3.8}$$

which shows that transmit antenna array with M antennas yields both M-order diversity gain and beamforming gain. Also, equation (3.8) can be written as

$$\mathrm{SNR}_{\mathrm{TXAA}} = E_s\frac{\sum_{i=1}^{M}\mathrm{E}\left[|h_{\mathrm{DL},i}|^2\right]}{\sigma_n^2} = E_s\frac{\mathrm{trace}(\mathbf{R}_{\mathrm{DL}})}{\sigma_n^2} = E_s\frac{\sum_{i=1}^{M}e_{\mathrm{DL},i}}{\sigma_n^2}. \tag{3.9}$$

Thus, the theoretical bit error ratio versus signal to noise ratio performance of transmit antenna array can be calculated using equation (2.9) with M components and $\bar{\gamma}_i = e_{\mathrm{DL},i}$, $i = 1..M$. In the case of a channel propagation environment with N taps, the instantaneous correlation matrices of all N downlink taps are summed as follows

$$\mathbf{R}(t)_{\mathrm{DL,sum}} = \sum_{i=1}^{N}\mathbf{h}_{\mathrm{DL},i}(t)\mathbf{h}_{\mathrm{DL},i}^{\mathrm{H}}(t), \tag{3.10}$$

and the principal eigenvector of $\mathbf{R}(t)_{\mathrm{DL,sum}}$ is then used as weight vector. Note that in this case the instantaneous SNR of the decision signal is *not* maximised. This would require the use of a tapped delay line with N taps on each branch of the M antenna elements, and that the n-th, $n = 1..N$, tap weight of the m-th, $m = 1..M$, delay line be equal to the complex conjugate of the

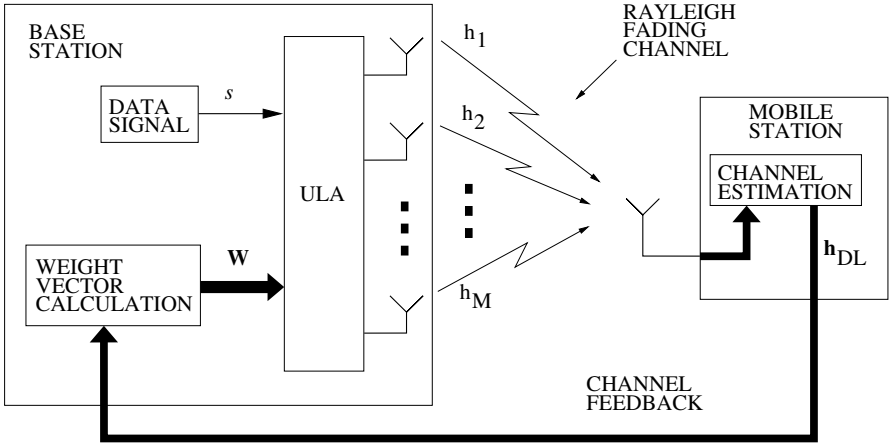

Figure 3.4: *Simple schematic diagram of transmit antenna array with M antenna elements.*

n-th tap of the time-inverted tap coefficients of the m-th channel coefficient.

Transmit antenna array needs, prior to transmission to the intended mobile station, the value of the downlink channel vector that the mobile station will measure at the moment of reception. Nevertheless, in FDD systems, before the actual reception of the transmitted signal by the mobile station, the channel has not happened yet and the base station cannot know its value. In practice the downlink channel vector is first estimated at the mobile station and then fed back to the base station. The downlink channel vector that the base station obtains this way is not exactly equal to the actual channel vector because of estimation and quantisation errors at the mobile station and noise in the feedback signals. Also, if the maximum Doppler frequency shift $f_{D,\max}$ is not zero, the channel changes over time and the feedback delay will cause additional discrepancy between the actual and the estimated channel vector. Consequently, in practice the weight vector is not exactly equal to the Hermitian of the actual channel vector as equation (3.7) requires, and this affects the overall performance. However, in computer simulations of TXAA the weight vector can be set exactly equal to the Hermitian of the actual channel vector (assuming that $f_{D,\max} = 0$ Hz), to obtain the lower bound on the performance of downlink antenna array techniques in channel propagation environments with one tap.

3.2.2 Selection diversity

The techniques that have been analysed so far use all M antenna elements for data signal transmission to the intended mobile station, and essentially transmit a different version of the same

signal from each element. The technique that is called selection diversity, however, uses only one antenna element for data signal transmission [99], according to the following rule. The base station transmits pilot signals from each element of the array, and the mobile receiver measures which element yields the highest SNR ('best' element identification). This information is fed back to the base station, which then uses *only* this element to transmit data signals to this mobile receiver (this technique is used in HIPERLAN/2 [49]). The schematic diagram of selection diversity is depicted in Figure 3.5. In case of channel propagation environments with N taps, the power of each antenna element over all N taps is taken into account in the calculation of its SNR.

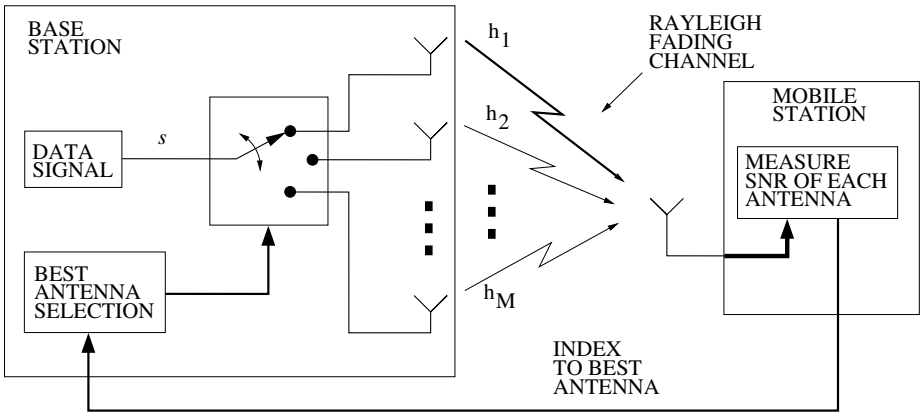

Figure 3.5: *Simple schematic diagram of selection diversity with M antenna elements.*

The mean SNR of the decision signal is

$$\mathrm{SNR}_{\mathrm{SELDIV}} = E_s \frac{\mathrm{E}\left[\max\left\{|h_{\mathrm{DL},1}|^2, |h_{\mathrm{DL},2}|^2, \cdots, |h_{\mathrm{DL},M}|^2\right\}\right]}{\sigma_n^2}, \tag{3.11}$$

where $h_{\mathrm{DL},i}$ is a sample of the i-th coefficient of the downlink channel at the moment of reception.

Selection diversity yields diversity gain but lacks beamforming gain as it uses only one antenna element. It avoids the deep fades that occur in the amplitude of the received signal by choosing out of the M available signals the one that yields the highest SNR. We have seen in Chapter 2 that when the array element spacing or the angular spread of the channel is large, the correlation between the signals of any two adjacent antenna elements ρ_{adj} is small (Figure 2.16). This means that the signals of the M elements are loosely correlated and fade almost independently over time (Figure 2.15(b)); then the probability that there is at least one signal that is not in a

deep fade which can yield a high SNR value is increased, improving the performance. On the other hand, when the spacing or the angular spread is small the correlation ρ_{adj} is high (Figure 2.16). This means that the M signals are highly correlated and fade simultaneously over time (Figure 2.15(a)). In this case when a deep fade occurs, all M signals will be affected by this fade and there will be no signal that can yield a high SNR value, deteriorating the performance.

Theoretical analysis of the performance of a CDMA system using selection diversity has been developed in [27]. The average probability of error for uncorrelated signals (i.e. $\rho_{\text{adj}} = 0$) and binary phase shift keying (BPSK) modulation is given as

$$P_b = M \sum_{k=0}^{M-1} \binom{M-1}{k} \frac{(-1)^k}{k+1} p\left(\frac{\gamma_o}{k+1}\right), \tag{3.12}$$

where γ_o is the expected SNR of each antenna element and $p(\gamma_o)$ is defined as

$$p(\gamma_o) = \frac{1}{2}\left(1 - \sqrt{\frac{\gamma_o}{1+\gamma_o}}\right). \tag{3.13}$$

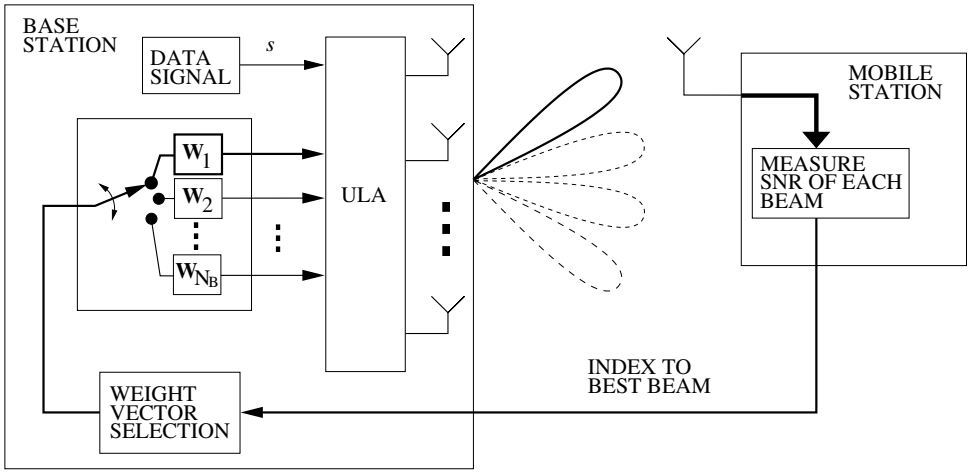

Figure 3.6: *Simple schematic diagram of fixed beams with M antenna elements.*

3.2.3 Fixed beams

Fixed beams is a technique that uses all M antenna elements of the base station to form beam patterns [144]. It forms these beam patterns in a way that is different from those of MAX SNR and TXAA, and selects the pattern that will be used for data signal transmission similarly to the selection of the best antenna element in selection diversity. More specifically, the base

station uses its array to form a fixed number of beam patterns, N_B, to cover the 120º of a sector. Then, it transmits pilot signals through each beam pattern and the intended mobile receiver measures which beam pattern yields the highest SNR. This information is fed back to the base station, which then uses *only* this beam pattern to transmit data signals to this mobile receiver. The schematic diagram of fixed beams is shown in Figure 3.6. In case of channel propagation environments with N taps, the power of each beam pattern over all N taps is taken into account in the calculation of its SNR. In this work we use a number of beam patterns equal to the number of antenna elements in the base station, $N_B = M$, uniformly distributed over the 120º of the sector, as shown in Figure 3.7 for $N_B = M = 4$. The spatial beam pattern configuration for $M = 2$ and $M = 8$ is shown in Figures A.3 and A.4 of appendix A, respectively (pages 166 and 167 respectively).

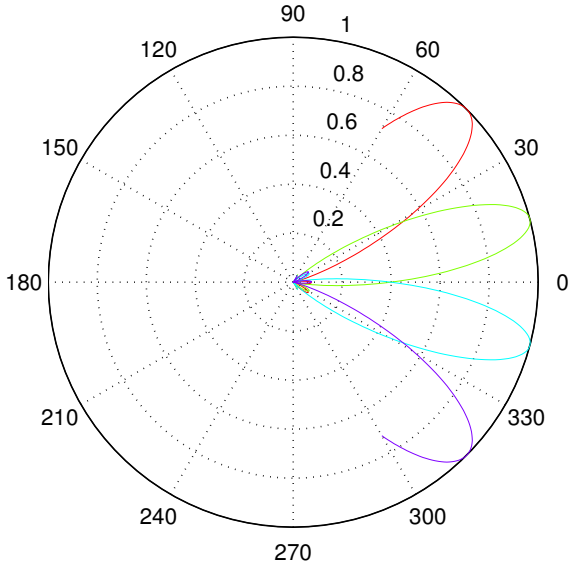

Figure 3.7: *Uniform spatial beam configuration in fixed beams for $N_B = M = 4$.*

The mean SNR of the decision signal is given by

$$\mathrm{SNR}_{\mathrm{FB}} = E_s \frac{\mathrm{E}\left[\max\left\{\mathbf{w}_1^{\mathrm{H}}\mathbf{h}_{\mathrm{DL}}\mathbf{h}_{\mathrm{DL}}^{\mathrm{H}}\mathbf{w}_1, \mathbf{w}_2^{\mathrm{H}}\mathbf{h}_{\mathrm{DL}}\mathbf{h}_{\mathrm{DL}}^{\mathrm{H}}\mathbf{w}_2, \ldots, \mathbf{w}_{N_B}^{\mathrm{H}}\mathbf{h}_{\mathrm{DL}}\mathbf{h}_{\mathrm{DL}}^{\mathrm{H}}\mathbf{w}_{N_B}\right\}\right]}{\sigma_n^2} \tag{3.14}$$

where $\mathbf{w}_i$, $i = 1..N_B$, is the weight vector corresponding to the i-th beam pattern and $\mathbf{h}_{\mathrm{DL}}$ is a sample of the downlink channel vector at the moment of reception.

The main gain type of fixed beams is beamforming gain. Let us call 'active angle' the angle that contains the plane waves that contribute to the signal received by the mobile station, and

is essentially equal to the angular spread of the channel propagation environment. We expect the beamforming gain to be maximised when the active angle is covered completely by any one beam. This can happen when the mobile station lies exactly in the direction of the maximum radiation of a beam and the angular spread is smaller than the beamwidth of the beam pattern. This is shown by the orange active angle of Figure 3.8 which has AOD = -15^{o} and AS = 10^{o}. Analogously, we expect the beamforming gain to be minimised when the smallest possible part of the active angle is covered by the beam patterns. This can happen when the mobile station lies exactly between any two beams and the angular spread is very small, as shown by the pink active angle of Figure 3.8 which has AOD = 0^{o} and AS = 2^{o}. Also, in case of rich scattering propagation environments with large angular spread (large active angle), different beam patterns may be chosen for the transmission of consecutive data symbols even if the mobile receiver does not move significantly. This is shown by the brown active angle of Figure 3.8 which has AOD = 25^{o} and AS = 30^{o}. The beam pattern that covers most of the active angle is the green one, and this is the pattern that is expected to be chosen and used most of the time. However, the red pattern also covers a significant part of the active angle and is expected to be chosen for transmission a number of times, even if the mobile station does not move significantly (that is, even if the angle of departure and the angular spread do not change significantly). This provides additional diversity gain to the mobile receiver improving the overall performance.

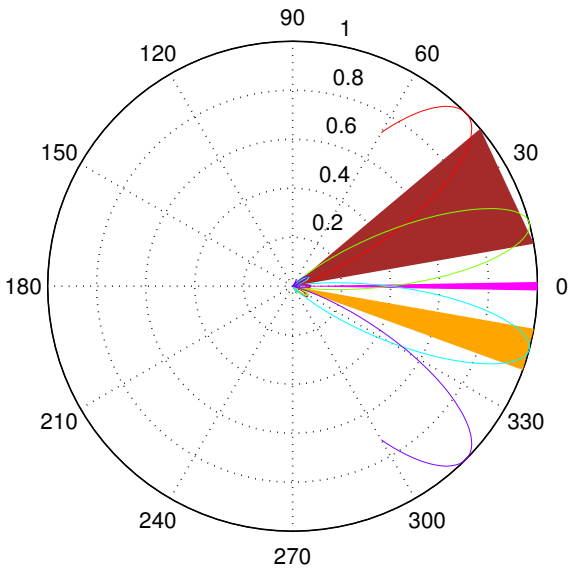

Figure 3.8: *Example of three different active angles in fixed beams.*

3.2.4 Eigenbeamforming

Eigenbeamforming is a technique that combines beamforming and diversity gain, and whose fundamental concept is very similar to fixed beams, but uses eigenbeams instead of conventional beams [46, 206]. Its schematic diagram is shown in Figure 3.9. More specifically, the base station transmits pilot signals from all M antenna elements which are used by the mobile station to estimate the downlink channel vector and calculate its mean correlation matrix $\mathbf{R}_{\mathrm{DL}}$. Then, the mobile station performs the eigenvalue decomposition of $\mathbf{R}_{\mathrm{DL}}$ and feeds the eigenvectors that correspond to the K largest eigenvalues back to the base station ($K \leq M$). Finally, it measures which of the K eigenvector beam patterns (or 'eigenbeams') yields the highest SNR at its receiver and feeds this information back to the base station which uses *only* this eigenvector for data signal transmission to this mobile station. If the channel consists of N temporal taps, the mobile station sums the N correlation matrices as follows

$$\mathbf{R}_{\mathrm{DL,sum}} = \sum_{i=1}^{N} \mathrm{E}[\mathbf{h}_{\mathrm{DL},i}\mathbf{h}_{\mathrm{DL},i}^{\mathrm{H}}], \tag{3.15}$$

and performs the eigenvalue decomposition of the summed matrix $\mathbf{R}_{\mathrm{DL,sum}}$. The main gain type of this technique is beamforming gain, as (eigen)beam patterns are used for data signal transmission. However, if the channel conditions are such that more than one (eigen)beam is chosen by the mobile station over consecutive data symbols (as we have seen in fixed beams in section 3.2.3), the mobile station will also be provided with diversity gain.

Out of a number of available signals provided by the K eigenbeams, the one with the highest SNR is picked. In channel propagation environments with one tap the K signals are mutually uncorrelated because the eigenvectors are mutually orthogonal, while their mean SNR is equal to the eigenvalues of the single correlation matrix $\mathbf{R}_{\mathrm{DL}}$, which are generally unequal. Therefore, the performance of eigenbeamforming in these channel propagation environments is the same as the performance of a selection diversity system with K uncorrelated diversity branches of unequal power. The theoretical analysis of such a system has been performed in [28]. The bit error ratio is given by equation (3) of [28], which for Rayleigh fading simplifies to

$$P_b = \int_0^{\infty} Q(\sqrt{\gamma}) \sum_{j=1}^{K} \frac{e^{-\frac{\gamma}{\bar{\gamma}_j}}}{\bar{\gamma}_j} \prod_{\substack{i=1 \\ i\neq j}}^{K} \left(1 - \frac{\gamma e^{-\frac{\gamma}{\bar{\gamma}_i}}}{\bar{\gamma}_i}\right) \mathrm{d}\gamma, \tag{3.16}$$

where $\bar{\gamma}_i$ is the expected mean SNR of the i-th diversity branch (which in eigenbeamforming is

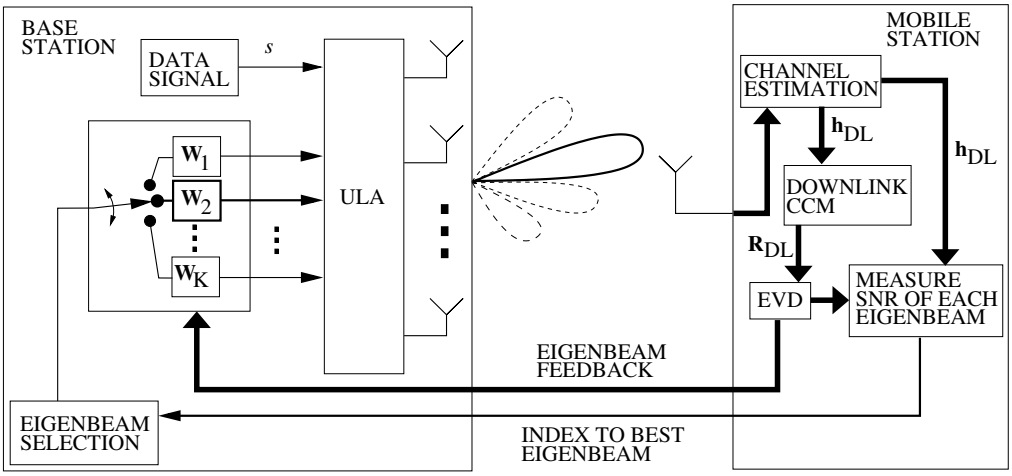

Figure 3.9: *Simple schematic diagram of eigenbeamforming with M antenna elements.*

equal to the i-th eigenvalue of the correlation matrix) and

$$Q(x) = \frac{1}{\sqrt{2\pi}} \int_x^\infty e^{-\frac{u^2}{2}} \mathrm{d}u = \frac{1}{2}\mathrm{erfc}\left(\frac{x}{\sqrt{2}}\right). \tag{3.17}$$

From the above description of eigenbeamforming, we can see that it bears a strong similarity to fixed beams, but it has a number of fundamental differences as well. The most important of these are: **a**) eigenbeamforming uses eigenbeams while fixed beams uses conventional beams, **b**) an eigenbeam can have several (local) maxima pointing in different directions, while a conventional beam like those used in fixed beams has a maximum in one particular direction, **c**) the radiation pattern of an eigenbeam can vary over time as the channel conditions change, while the radiation pattern of a conventional beam is fixed, and **d**) eigenbeamforming requires higher feedback rate as it needs to feed back the K dominant eigenbeams plus an index to the highest SNR eigenbeam, while fixed beams needs to feed back only an index to the highest SNR beam. These differences can result in eigenbeamforming yielding better performance than fixed beams under certain channel conditions. For instance, if the active angle lies between two conventional beams and the angular spread is small as shown by the pink active angle of Figure 3.8, fixed beams will yield its worst performance and can do nothing to improve it. In eigenbeamforming, on the other hand, most likely there will be an eigenbeam with direction of maximum radiation equal to the angle of departure, enabling it to perform better. Nevertheless, if the active angle is covered completely by a conventional beam as shown by the orange active angle of Figure 3.8, the two techniques will yield similar performance.

3.3 Simulation results

All the downlink antenna array techniques that have been analysed so far have been simulated by Monte Carlo simulation and the results are presented in this section. The techniques are again split into open loop and closed loop categories. The carrier frequency of the downlink channel is equal to 2 GHz and the transmit antenna array spacing is equal to $\lambda/2$, unless otherwise stated. The modulation of the data signals is binary phase shift keying. All simulations

Type of cell	**AOD** (degrees)	**AS** (degrees)	ρ_{adj} (when $D = \frac{\lambda}{2}$)
Macro cell	15	10	0.988
Micro cell	30	45	0.825
Pico cell	0	120	0.035

Table 3.1: *Cell types used in the simulations with one channel tap.*

are performed in a one-user scenario, where the base station communicates with one user and there is no co-channel interference (CCI) from other users. In each simulation the bit error ratio is calculated over 10^6 data symbols which are transmitted from base station to mobile station. These data symbols are not coded in any way. Noiseless estimates of the M downlink channel coefficients h_i, $i = 1..M$, are available to the mobile receiver. The downlink channel vectors of consecutive data symbols are uncorrelated, to minimise simulation time. This is achieved by

Tap	**Tap power** (dB)	**AOD** (degrees)	**AS** (degrees)	ρ_{adj} (when $D = \frac{\lambda}{2}$)
# 1	0	2	10	0.987
# 2	-3	30	25	0.943

Table 3.2: *Tap characteristics used in the simulations with two channel taps.*

generating a different set of the Q scattered signals of equation (2.5) and re-calculating the M channel coefficients over each data symbol. Simulations of channel propagation environments with one tap are performed in three different types of cells: macro cell, micro cell and pico cell. The characteristics (AOD and AS) of each cell type are shown in Table 3.1 [204, 205] (the sectorisation angle of 120^{o} is used for 'very large' AS in the pico cell [204, 205]). Also shown in Table 3.1 is the correlation between the signals of two adjacent antenna elements ρ_{adj} in each cell type when the transmit array spacing is $D = \frac{\lambda}{2}$. In addition, due to the plethora of possible multi-tap channel propagation environments, the simulations are performed in one

such environment with two taps, which are shown in Table 3.2. The power of the second tap is 3 dB smaller than the power of the first tap, to account for the fact that the taps that arrive after the first one usually travel over longer distances and are generally subject to larger attenuation [104, 176]. The two taps are assumed to be resolved by the Rake receiver at the mobile station, and are combined as shown in Figure 2.6 (page 12). Also, the mutual interference between them is assumed to be negligible. The impact of neglecting the mutual interference is (very) small, as this interference causes an irreducible BER at very high SNR values which are out of practical interest. An exception occurs when the processing gain of the spreading codes is very low (e.g. 4 or 8), which may cause an irreducible BER at SNR values of interest.

3.3.1 Open loop techniques

In this section we will present bit error ratio versus signal to noise ratio simulation results for the two open loop techniques: space time spreading and maximum SNR.

3.3.1.1 Space-time spreading

The STS technique has been simulated for $M = 2$, $M = 4$ and $M = 8$ transmit antenna elements in the base station, and the results are shown in Figure 3.10. Figures 3.10(a), 3.10(b) and 3.10(c) show simulation results in the three 1-tap cells for $M = 2$, $M = 4$ and $M = 8$ respectively. The SNR value of the x-axis is the expected SNR of the decision signal at the mobile receiver. Also shown in these three figures, is the case where the base station uses a single transmit antenna ($M = 1$), which we call the conventional base station/transmitter and is useful in determining the gain that STS with $M > 1$ yields. Figure 3.10(d) depicts simulation results for $M = 2, 4, 8$ and the single-antenna transmitter in the 2-tap scenario and will be discussed below.

In Figure 3.10(a) we see that STS provides the smallest gain over the conventional transmitter in the macro cell. This happens because STS is a diversity technique, and the diversity gain of the macro cell is low due to large correlation coefficient ($\rho_{\text{adj}} = 0.988$). If STS is exploited in a macro cell in practice, the correlation coefficient may be decreased by using a larger transmit antenna spacing. However, the STS gain becomes larger in the micro cell and is maximised in the pico cell where the diversity gain is maximum due to small correlation coefficient ($\rho_{\text{adj}} = 0.035$). Also, when the channel conditions change from macro to micro cell the correlation coefficient decreases from $\rho_{\text{adj}} = 0.988$ to $\rho_{\text{adj}} = 0.825$ and the performance is improved by

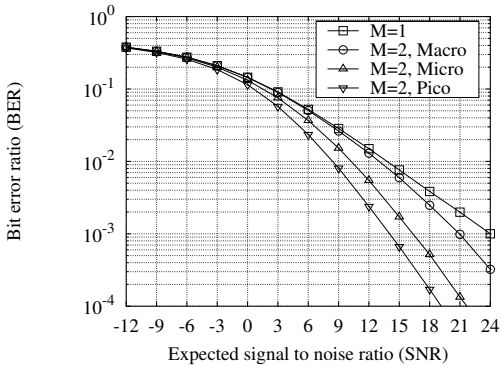

(a) $M = 2$ in the macro, micro and pico cell

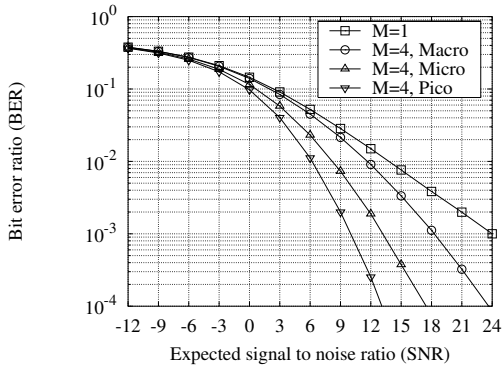

(b) $M = 4$ in the macro, micro and pico cell

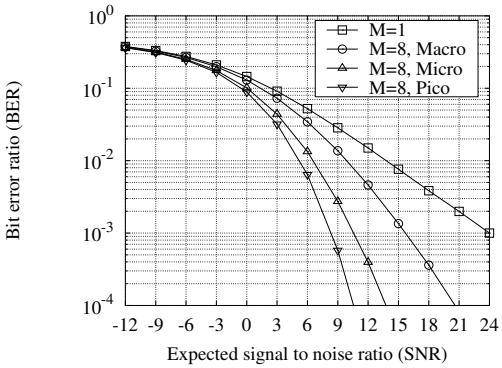

(c) $M = 8$ in the macro, micro and pico cell

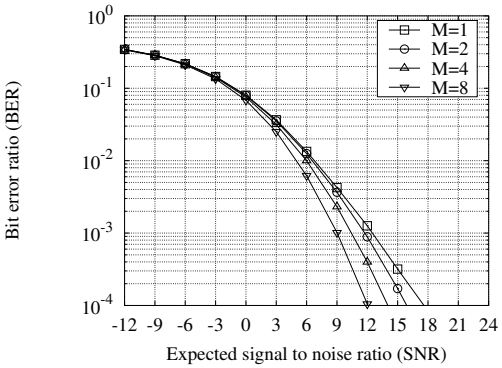

(d) $M = 1, 2, 4, 8$ in the 2-tap scenario

Figure 3.10: *Simulation results of space-time spreading in all cell types.*

about 4.7 dB at BER = 10^{-3}, while when the channel conditions change from micro to pico cell the correlation coefficient decreases from $\rho_{\text{adj}} = 0.825$ to $\rho_{\text{adj}} = 0.035$ and the performance is improved by about 2.3 dB at the same BER. This means that when the correlation coefficient is close to one, relatively small decreases in its value can result in large performance improvement, while if it is not close to one (e.g. $\rho_{\text{adj}} \lessapprox 0.7$), even large decreases in its value yield relatively small performance improvement [124, 128, 190]. Therefore, when the correlation coefficient is below a given threshold, e.g. 0.7, it could be considered to yield satisfactory diversity gain, as decreasing its value further yields diminishing returns. Furthermore, the performance in the macro cell is worse than the performance in the pico cell by about 7 dB at BER = 10^{-3}, which shows the detrimental effect that a high correlation coefficient can have on the performance of STS in particular, and techniques that rely only on diversity gain in general.

Figures 3.10(b) and 3.10(c) show the same trends as Figure 3.10(a), resulting in the same conclusions. Also, comparison among Figures 3.10(a), 3.10(b) and 3.10(c) shows that the STS gain over the single-antenna transmitter for a given cell type increases with the number of antennas M. For instance, the gain over the single-antenna transmitter at BER = 10^{-3} in the micro cell is about 7.6 dB when $M = 2$, 10.8 dB when $M = 4$ and 13.9 dB when $M = 8$. Thus, the STS gain increases as M increases and as ρ_{adj} decreases.

Figure 3.10(d) shows simulation results for $M = 2, 4, 8$ in the 2-tap scenario with the two taps of Table 3.2. When $M = 2$, the performance in this scenario is better than the performance in all the 1-tap cells. When $M = 4, 8$, the performance in the 2-tap scenario is better than that of both macro and micro cell, and very similar to that of the pico cell. Also, when $M = 8$ the performance in the 2-tap scenario is (slightly) worse than that of the pico cell for SNR ≥ 8 dB. Additionally, increasing M in the scenario with the two taps improves the performance over the single-antenna transmitter, but not by a large amount. This may be due to low diversity gain provided by the two taps, as their correlation coefficient ρ_{adj} is quite high (0.987 and 0.943 respectively).

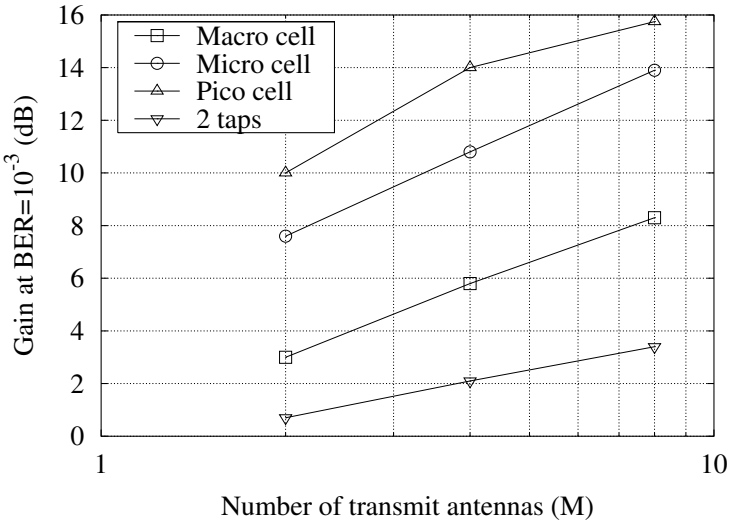

Figure 3.11: *Gain of space-time spreading over the single antenna transmitter at BER* = 10^{-3}.

Figure 3.11 contains a summary of the results in Figure 3.10, and depicts the STS gain over the single-antenna transmitter at BER = 10^{-3} as a function of M in both the 1-tap and 2-tap channel propagation scenarios. It shows that in both macro and micro cell the gain in dB increases almost linearly with $\log(M)$, while in pico cell it does not increase linearly. Also, under the

2-tap scenario increasing M improves the performance by a relatively small amount—but in this scenario there is already multipath diversity. Therefore, when the correlation coefficient is large (e.g. macro and micro cell), increasing the diversity order in the form of M increases the diversity gain almost linearly. Nevertheless, when the correlation coefficient is small (e.g. pico cell), increasing the diversity order above 4 gives diminishing returns in terms of diversity gain, as this gain is already high.

3.3.1.2 Maximum SNR

In the simulation of MAX SNR the uplink and downlink carrier frequencies are $f_{\mathrm{UL},c} = 2.14$ GHz and $f_{\mathrm{DL},c} = 1.95$ GHz respectively, while the spacing is $D = \frac{\lambda_{\mathrm{MID}}}{2}$, where λ_{MID} is the wavelength of the carrier frequency $f_{\mathrm{MID},c} = \frac{f_{\mathrm{UL},c}+f_{\mathrm{DL},c}}{2}$. Since the difference between the two carrier frequencies is not large ($\simeq 9.5\%$ of $f_{\mathrm{MID},c}$), we can assume that the physical objects that act as reflectors and scatterers on the uplink signals will also act as reflectors and scatterers on the downlink signals. For this reason, the uplink angle of arrival and angular spread can be considered the same as the downlink angle of departure and angular spread respectively. Thus, the base station can estimate the uplink channel correlation matrix from the uplink signals that it receives from the mobile station and use its principal eigenvector as beamformer on the downlink (that is, the technique is operated in an open loop fashion). Instead of simulating the uplink channel and estimating its correlation matrix from the uplink signals, in the actual simulation we calculate the uplink correlation matrix at the base station using equations A.2 and A.3 of appendix A. The uplink correlation matrix will be estimated from pilot signals transmitted on the uplink from mobile to base station in Chapter 5. The technique has been simulated for $M = 2$, $M = 4$ and $M = 8$ transmit antenna elements, and the results are shown in Figure 3.12. Figures 3.12(a), 3.12(b) and 3.12(c) show simulation results in the three 1-tap cells for $M = 2$, $M = 4$ and $M = 8$ respectively. Also shown in these three figures, is the case of the conventional transmitter which will be useful in determining the gain that MAX SNR with $M > 1$ yields. In addition, Figure 3.12(d) depicts simulation results for $M = 2, 4, 8$ and the single-antenna transmitter in the channel propagation environment with two taps.

Figure 3.12(a) shows that MAX SNR yields the maximum gain over the single-antenna transmitter in the macro cell. This is because the angular spread is small and the entire power that reaches the mobile receiver is concentrated in a small angle which is illuminated by the beam formed by the base station. On the other hand, MAX SNR does not yield any gain at all in the

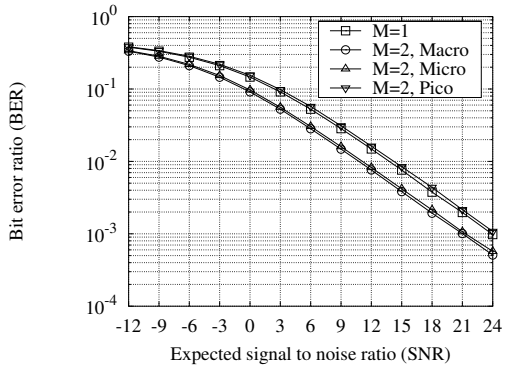

(a) $M = 2$ in the macro, micro and pico cell

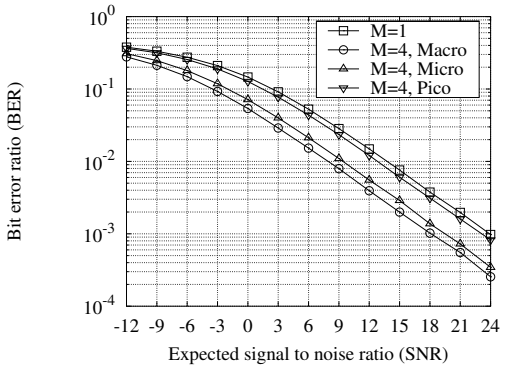

(b) $M = 4$ in the macro, micro and pico cell

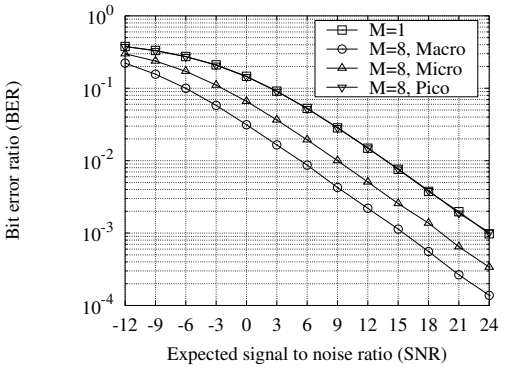

(c) $M = 8$ in the macro, micro and pico cell

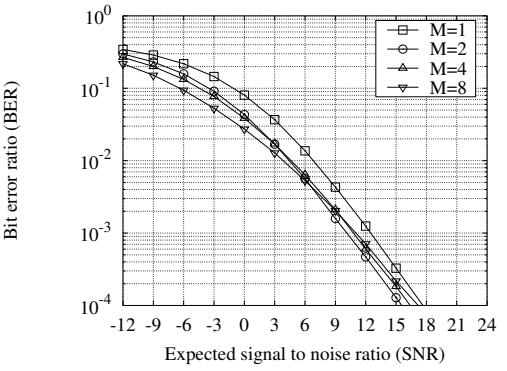

(d) $M = 1, 2, 4, 8$ in the 2-tap scenario

Figure 3.12: *Simulation results of maximum SNR in all cell types.*

pico cell. In this case the angular spread is large and there is no preferred direction of transmission, so forming a directional beam pattern cannot improve the performance. Moreover, the gain yielded in the micro cell is almost the same as that yielded in the macro cell, because, although the angular spread is larger in the micro cell, the beam formed by the two antenna elements is wide enough to illuminate most of it.

Figures 3.12(b) and 3.12(c) show similar results to Figure 3.12(a). However, in these figures the performance in the micro cell is significantly worse than the performance in the macro cell. This is because as M increases, the main beam becomes narrower (Figure A.2 on page 165) and illuminates only a small part of the angular spread. Also, Figure 3.12(d) shows that MAX SNR yields a good gain over the single-antenna transmitter in the 2-tap scenario when $M = 2$,

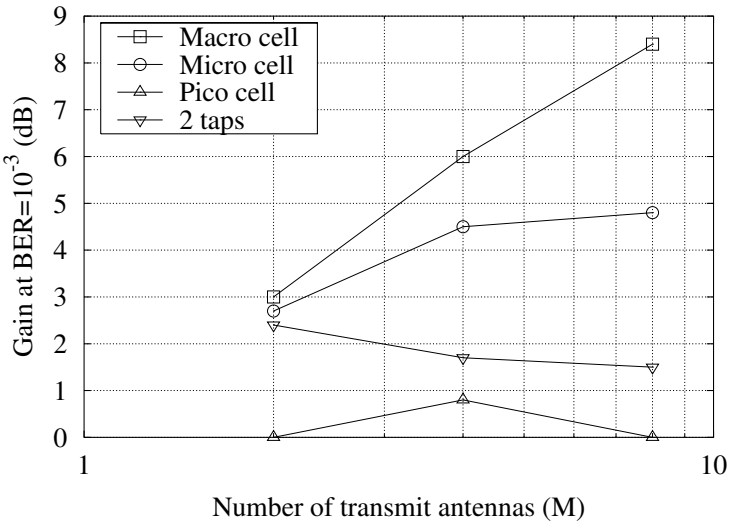

Figure 3.13: *Gain of maximum SNR over the single antenna transmitter at BER* = 10^{-3}.

but as M increases it does not provide much gain. This may be attributed to the fact that the two taps cannot be exploited at the same time as M increases, because the beamwidth of the main beam becomes narrower, and both taps can no longer be illuminated simultaneously. Rather, they are spatially configured so that they behave as though they were a single tap with angular spread (approximately) equal to the combined angular spread of the two taps. Given that the combined angular spread is relatively large, the increasingly narrow beam of MAX SNR is not able to yield much gain. Finally, comparison among Figures 3.12(a), 3.12(b) and 3.12(c) shows that increasing M does not always improve the performance of MAX SNR. This is more clearly shown in Figure 3.13 which depicts the MAX SNR gain over the conventional transmitter at BER = 10^{-3} as a function of M in all the simulated scenarios. In the macro cell the gain in dB increases almost linearly with $\log(M)$. In the micro cell increasing M above 4 yields little gain. In the pico cell using an $M > 1$ hardly provides any gain. Also, in the 2-tap scenario the gain actually decreases as M increases due to large angular spread of the two taps.

3.3.2 Closed loop techniques

In this section we will present bit error ratio versus signal to noise ratio simulation results for the closed loop techniques: transmit antenna array, selection diversity, fixed beams and eigenbeamforming.

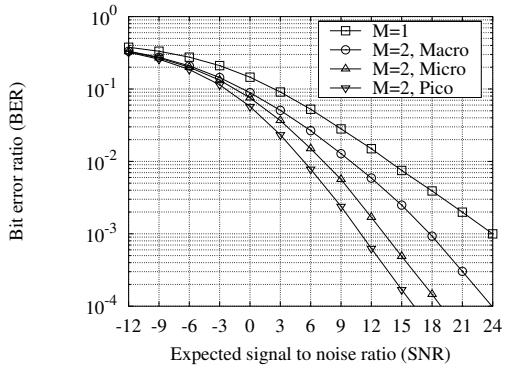

(a) $M = 2$ in the macro, micro and pico cell

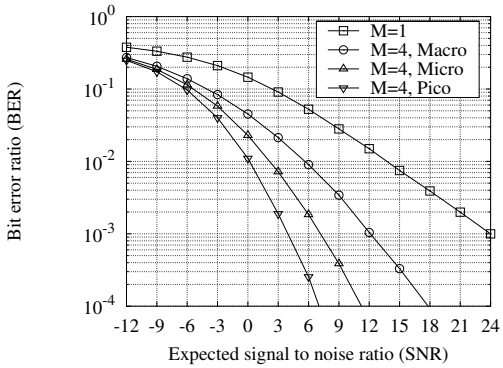

(b) $M = 4$ in the macro, micro and pico cell

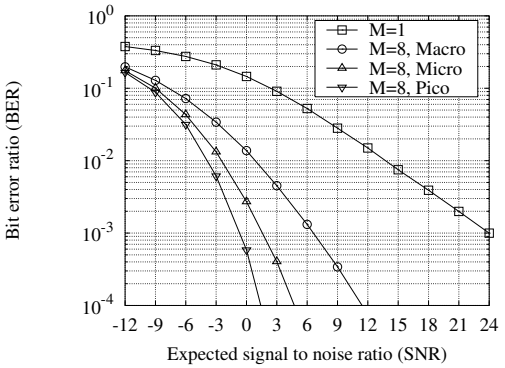

(c) $M = 8$ in the macro, micro and pico cell

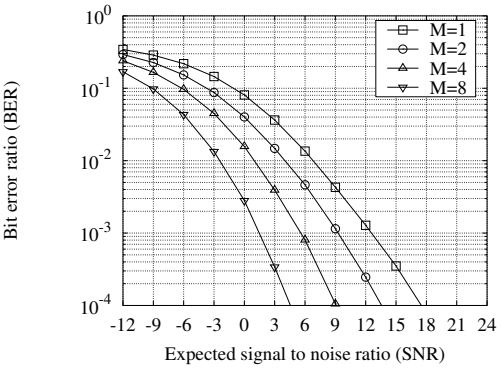

(d) $M = 1, 2, 4, 8$ in the 2-tap scenario

Figure 3.14: *Simulation results of transmit antenna array in all cell types.*

3.3.2.1 Transmit antenna array

In the simulation of TXAA the base station is assumed to know the M downlink channel coefficients h_i, $i = 1..M$, that it needs to calculate the weight vector perfectly. As we have noted earlier, this is difficult to achieve in practice (especially for large Doppler frequency shift), but we can use it in the simulations to obtain the lower bound on the performance of all downlink techniques in channel propagation environments with 1 tap. The technique has been simulated in the three 1-tap cells for $M = 2$, $M = 4$ and $M = 8$, and the results are shown in Figures 3.14(a), 3.14(b) and 3.14(c) respectively. Each figure contains also simulation results for the single-antenna transmitter case. Furthermore, Figure 3.14(d) depicts simulation results for $M = 2, 4, 8$ and the single-antenna transmitter in the 2-tap scenario.

The same trends observed in the discussion of the STS simulation results can also be seen here, because both techniques contain diversity gain (of course, TXAA contains additional beamforming gain). For example, Figure 3.14(a) shows that as the channel conditions change from macro to pico cell the performance of TXAA improves due to higher diversity gain. Also, the performance improvement provided by changing from macro to micro cell is larger than the improvement provided by changing from micro to pico cell. Furthermore, Figures 3.14(b) and 3.14(c) show results similar to Figure 3.14(a), and comparison among all three figures shows that TXAA performance improves as M increases.

Figure 3.14(d) shows that, as M increases, transmit antenna array yields significant gain over the single-antenna transmitter in the 2-tap scenario. This is expected as the antenna element weights at the base station are updated over *each* data symbol to take into account changes in the instantaneous values of the channel coefficients. This enables the technique to exploit both taps and improve the performance.

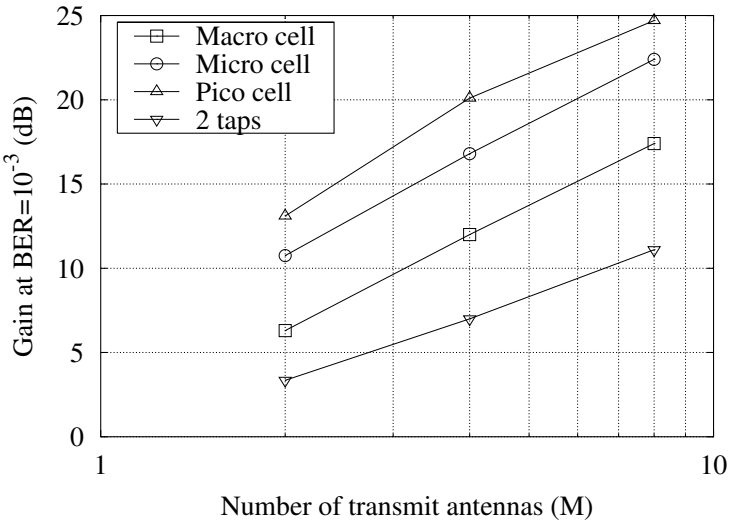

Figure 3.15: *Gain of transmit antenna array over the single antenna transmitter at BER* = 10^{-3}.

Finally, Figure 3.15 summarises the results of Figure 3.14, and depicts the TXAA gain over the single-antenna transmitter at BER = 10^{-3} as a function of M in all the simulated scenarios. The gain in dB increases almost linearly with $\log(M)$ in both macro and micro cell. In the pico cell, however, increasing M above 4 starts to provide diminishing returns as the diversity gain is already high. Moreover, even in the 2-tap scenario the gain scales well with $\log(M)$ for the reason mentioned above. However, in this scenario the gain is smaller than that of the 1-tap

scenarios, probably because there is already multipath diversity and the margin for additional improvement through increase of M is small.

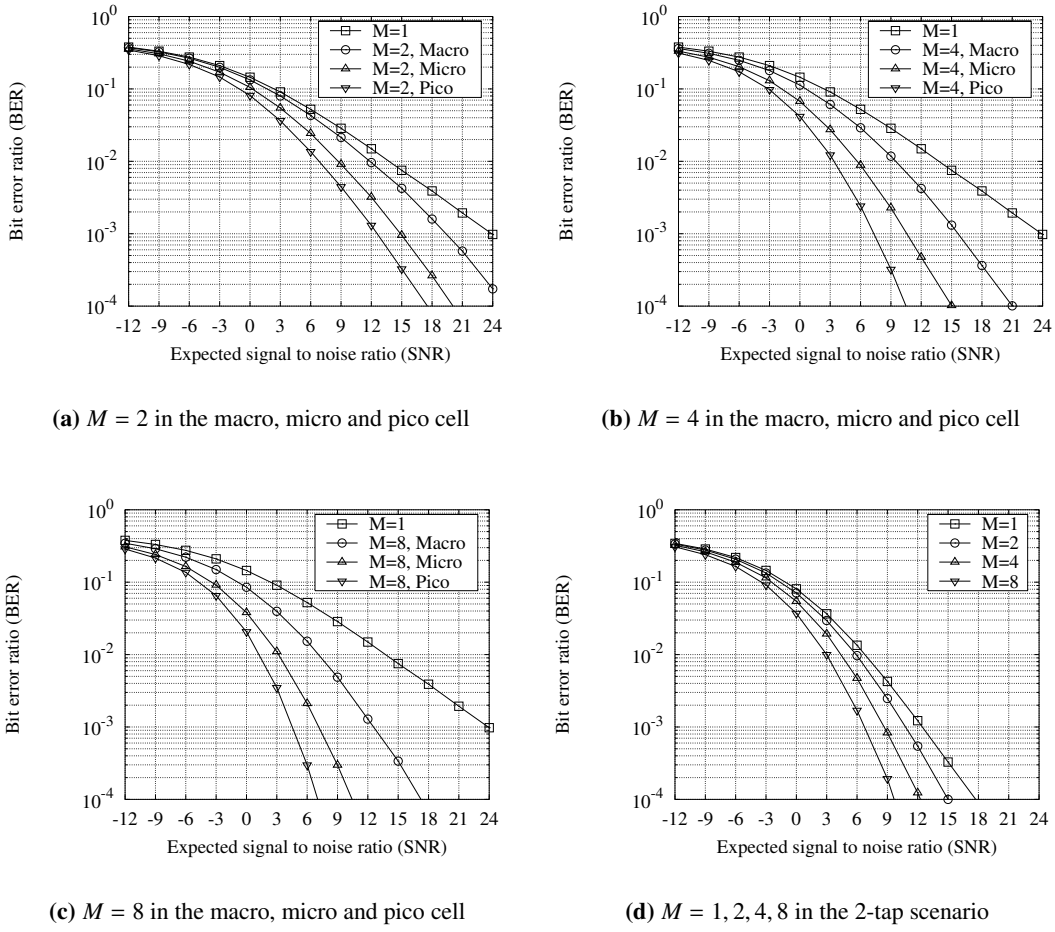

(a) $M = 2$ in the macro, micro and pico cell

(b) $M = 4$ in the macro, micro and pico cell

(c) $M = 8$ in the macro, micro and pico cell

(d) $M = 1, 2, 4, 8$ in the 2-tap scenario

Figure 3.16: *Simulation results of selection diversity in all cell types.*

3.3.2.2 Selection diversity

In the simulation of selection diversity the base station is assumed to know which antenna element yields the highest SNR at the mobile receiver over each data symbol, and uses this element for transmission. The technique has been simulated in the three 1-tap cells for $M = 2$, $M = 4$ and $M = 8$, and the results are shown in Figures 3.16(a), 3.16(b) and 3.16(c) respectively. Each figure contains also simulation results for the conventional base station. Moreover, Figure 3.16(d) depicts simulation results for $M = 2, 4, 8$ and the single-antenna transmitter in the 2-tap scenario.

Selection diversity uses only one antenna element for signal transmission and, thus, contains only diversity gain and no beamforming gain. Therefore, again the basic observations made in the discussion of the STS simulation results can also be made here. For instance, Figure 3.16(a) shows that as the channel conditions change from macro to pico cell the selection diversity performance improves due to higher diversity gain. Moreover, the transition from macro to micro cell yields larger performance improvement than the transition from micro to pico cell. Also, Figures 3.16(b) and 3.16(c) show results similar to Figure 3.16(a), and comparison among the three figures shows that the performance of selection diversity improves with M.

Figure 3.16(d) shows that the selection diversity gain over the single-antenna transmitter increases with M in the 2-tap scenario. However, this gain is not too high, as selection diversity contains only diversity gain. Also, it is a bit larger than the corresponding gain of space-time spreading (Figure 3.10(d)) which is also a diversity technique. This may be because selection diversity uses the highest SNR antenna over *each* data symbol and is able to exploit the combined angular spread of the two taps better than space-time spreading, yielding more diversity gain.

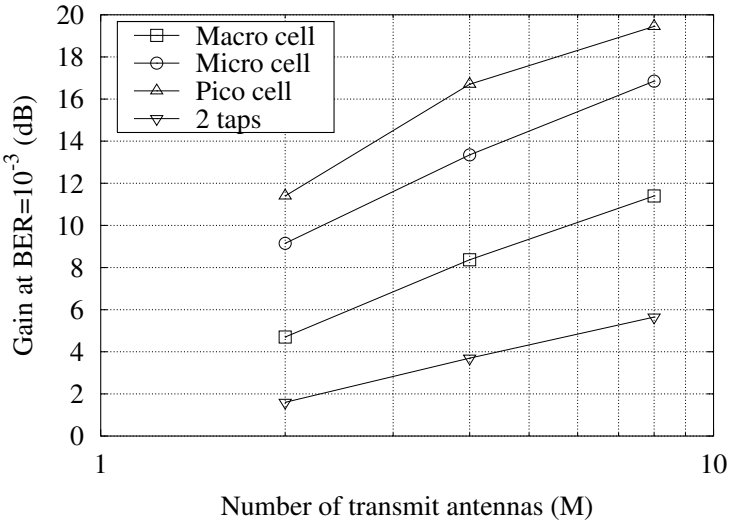

Figure 3.17: *Gain of selection diversity over the single antenna transmitter at BER* = 10^{-3}.

Finally, Figure 3.17 again summarises the results of Figure 3.16, and depicts the selection diversity gain over the conventional transmitter at BER = 10^{-3} as a function of M in all the simulated scenarios. The gain in dB increases almost linearly with $\log(M)$ in both macro and micro cell, but in the pico cell increasing M above 4 starts to provide diminishing returns. Also,

the gain scales linearly with $\log(M)$ in the 2-tap scenario. However, the slope is less steep and the overall gain smaller than the corresponding slope and overall gain of the 1-tap cells probably because there is already multipath diversity.

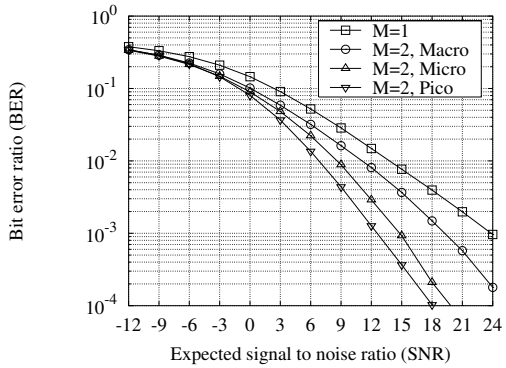

(a) $M = 2$ in the macro, micro and pico cell

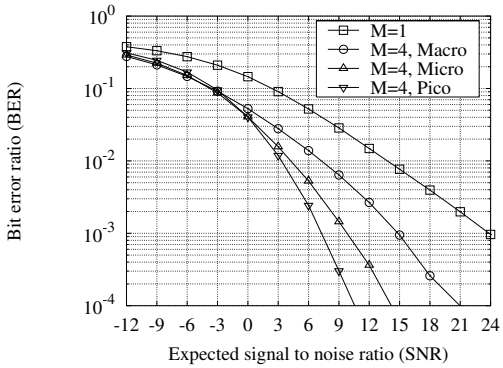

(b) $M = 4$ in the macro, micro and pico cell

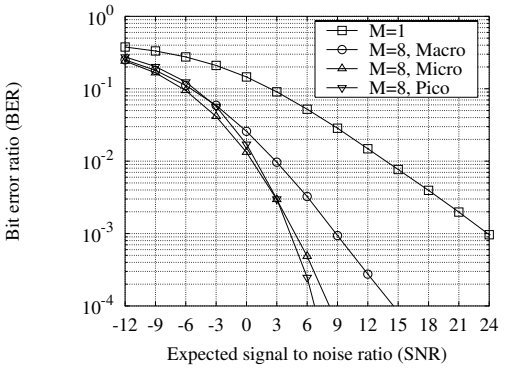

(c) $M = 8$ in the macro, micro and pico cell

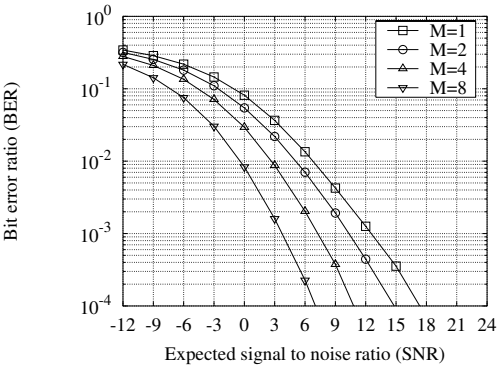

(d) $M = 1, 2, 4, 8$ in the 2-tap scenario

Figure 3.18: *Simulation results of fixed beams in all cell types.*

3.3.2.3 Fixed beams

In the simulation of fixed beams the base station is assumed to know which beam yields the highest SNR at the mobile receiver over each data symbol and uses this beam for transmission. The technique has been simulated in the three 1-tap cells for $M = 2$, $M = 4$ and $M = 8$ transmit antenna elements in the base station, and the results are shown in Figures 3.18(a), 3.18(b) and 3.18(c) respectively. Each figure also contains simulation results for the conventional base station. Also, Figure 3.18(d) depicts simulation results for $M = 2, 4, 8$ and the single-antenna

transmitter in the 2-tap scenario.

Figure 3.18(a) shows that for $M = 2$ the performance at all shown SNR values improves as the angular spread increases (i.e. transition from macro to pico cell). This is because the diversity gain of using different beams over different symbol periods improves as the angular spread increases. However, Figures 3.18(b) and 3.18(c) show that, for small SNR values, the performance worsens with increasing angular spread. When SNR is small, the benefit from diversity gain is also small and the beamforming gain prevails. But when the angular spread increases the beamforming gain deteriorates as there is no preferred direction of transmission, affecting the performance (especially for large M where the main beam becomes narrow). This behaviour has also been seen in the results of MAX SNR in Figure 3.12. On the other hand, when the SNR is larger the benefit from diversity gain is also larger, compensating for the beamforming gain loss and improving the overall performance. Comparison among the three figures shows that increasing M in the same cell type improves the performance of fixed beams.

Figure 3.18(d) shows that the fixed beams gain over the single-antenna transmitter in the 2-tap scenario increases with M. Also, this gain is larger than that of the two diversity techniques, space-time spreading and selection diversity, which is naturally due to additional beamforming gain in fixed beams.

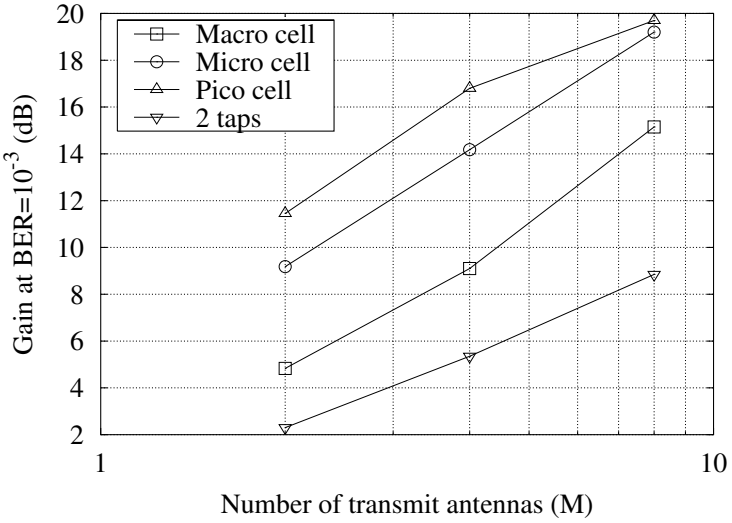

Figure 3.19: *Gain of fixed beams over the single antenna transmitter at BER* = 10^{-3}.

Figure 3.19 summarises the results of Figure 3.18, and depicts the fixed beams gain over the single-antenna transmitter at BER = 10^{-3} as a function of M in all the simulated scenarios. In

the macro cell, increasing M yields increasing beamforming gain as the angular spread is small and can be fully exploited. Also, in the micro cell the gain scales almost linearly with $\log(M)$, while in the pico cell using an M larger than 4 starts to provide diminishing returns. In the 2-tap scenario the gain scales well with $\log(M)$, due to the combination of beamforming gain and improved diversity gain. As in previous techniques, the gain in this scenario is smaller than that of the 1-tap scenarios, which may be because there is already multipath diversity.

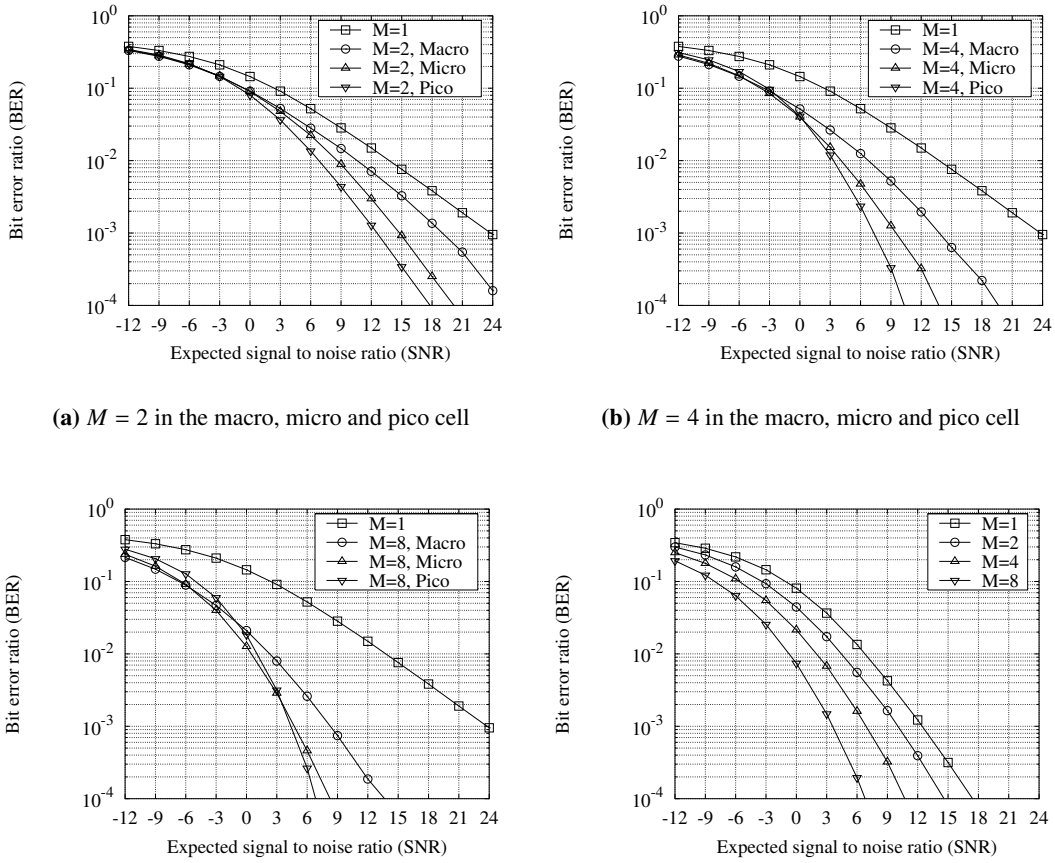

(a) $M = 2$ in the macro, micro and pico cell

(b) $M = 4$ in the macro, micro and pico cell

(c) $M = 8$ in the macro, micro and pico cell

(d) $M = 1, 2, 4, 8$ in the 2-tap scenario

Figure 3.20: *Simulation results of eigenbeamforming in all cell types.*

3.3.2.4 Eigenbeamforming

In the simulation of eigenbeamforming the base station is assumed to know which eigenvector of the mean downlink correlation matrix $\mathbf{R}_{\mathrm{DL}}$ yields the highest SNR at the mobile receiver over each data symbol and uses this eigenvector for transmission. The technique has been simulated

in the three 1-tap cells for $M = 2$, $M = 4$ and $M = 8$, and the results are shown in Figures 3.20(a), 3.20(b) and 3.20(c) respectively. Also, Figure 3.20(d) depicts simulation results for $M = 2, 4, 8$ and the single-antenna transmitter in the 2-tap scenario.

Because eigenbeamforming is very similar to fixed beams, the results in Figure 3.20 are similar to the results of fixed beams in Figure 3.18. More specifically, Figure 3.20(a) shows that for $M = 2$ the performance at all shown SNR values improves as the angular spread increases (i.e. transition from macro to pico cell). However, Figures 3.20(b) and 3.20(c) show that for small SNR values the performance worsens with increasing angular spread, due to small benefit from diversity gain and the small beamforming gain. Furthermore, when SNR is larger the overall performance improves in these two figures as the benefit from diversity gain is also larger and compensates for the beamforming gain loss. Finally, comparison among the three figures shows that increasing M under the same cell type improves the performance of eigenbeamforming.

Figure 3.20(d) shows that the eigenbeamforming gain in the 2-tap scenario increases with M. Also, the results of this figure are very similar to the corresponding results of fixed beams (Figure 3.18(b)), presumably because of the similarities between the two techniques.

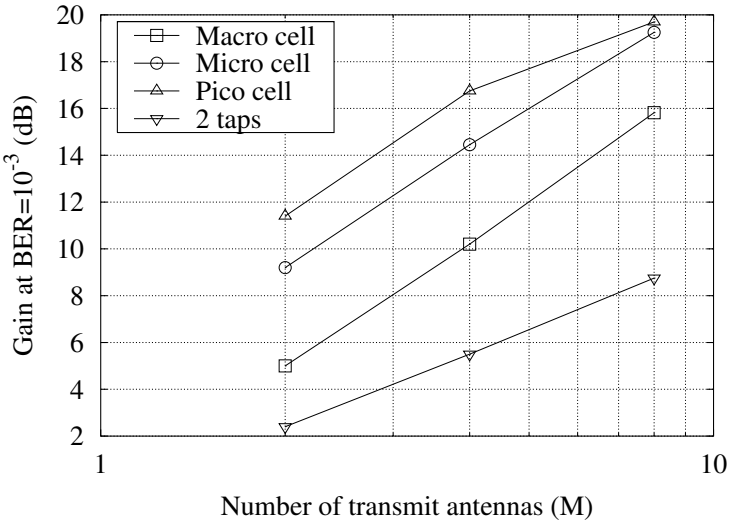

Figure 3.21: *Gain of eigenbeamforming over the single antenna transmitter at BER* $= 10^{-3}$.

Figure 3.21 summarises the results of Figure 3.20, and depicts the eigenbeamforming gain over the single-antenna transmitter at BER $= 10^{-3}$ as a function of M in the three cell types. The gain in dB scales almost linearly with $\log(M)$ in both macro and micro cell. In the pico cell,

however, using an M larger than 4 starts to yield diminishing returns. In the 2-tap scenario the gain scales well with $\log(M)$, as the fixed beams gain did (Figure 3.19). Finally, the gain in this scenario is again smaller than that of the 2-tap scenarios as there is already multipath diversity.

3.4 Comparison of simulation results

The simulation results of all the presented techniques will be compared to each other in this section. From the description of TXAA we see that, in channel propagation environments with one tap, it is the transmission equivalent of maximum ratio combining (MRC) reception. Hence, it maximises the SNR of the decision signal under white Gaussian noise conditions [176], thus providing the optimum performance. This can also be confirmed by the results of Figure 3.14, which show that TXAA yields the highest gain over the single-antenna transmitter and provides the lower bound on the BER performance of all the presented techniques. Therefore, we can treat TXAA as a reference and calculate the performance loss that results from using a particular technique instead of TXAA at a specific BER value, for a given M and under a particular cell type. For instance, to calculate the loss at BER = 10^{-3} of STS for $M = 2$ in the macro cell, we subtract the STS gain of the macro cell curve for $M = 2$ of Figure 3.11 (about 3 dB) from the TXAA gain of the macro cell curve for $M = 2$ of Figure 3.15 (about 6.2 dB), and the loss is about 3.2 dB. Then, we can compare this performance loss among all techniques and determine how the techniques compare to each other: the smaller the performance loss of a particular technique the better the technique performs.

Figure 3.22 shows the performance loss of each technique with respect to TXAA at BER = 10^{-3}, as a function of the number of transmit antennas in the macro cell. Solid curves correspond to open loop techniques while dashed curves correspond to closed loop techniques. As expected, the worst performance is yielded by the two open loop techniques. The performance loss of STS increases by about 3 dB every time M is doubled. This can be explained by comparison of equations (3.1) and (3.8), which shows that the STS SNR is worse than the TXAA SNR by $10\log_{10}(M)$ dB. Also, the MAX SNR loss is very similar to that of STS. This can be explained by comparison of Figures 3.10 and 3.12, which shows that, when $M = 2$, STS and MAX SNR yield very similar performance at BER = 10^{-3} in all cell types. However, this does not hold for other M and/or BER values. The selection diversity loss scales almost linearly with $\log(M)$, producing the highest performance loss among the closed loop techniques. This is expected, because selection diversity lacks beamforming gain and relies only on diversity gain.

The performance loss of fixed beams increases when M is increased from 2 to 4, but decreases when M is increased from 4 to 8. Figure 3.7 shows that, when $M = 4$, the active angle of the macro cell (AOD = 15°, AS = 10°) is covered completely by one beam (the green one). Thus, fixed beams contains only beamforming gain and no diversity gain. Nevertheless, Figure A.4 of appendix A (page 167) shows that, when $M = 8$, the active angle of the macro cell is not covered by one beam only but lies between two beams. Thus, in this case fixed beams contains additional diversity gain which makes the performance loss smaller. Eigenbeamforming suffers the smallest performance loss of all techniques (between about 1.3 and 1.8 dB) and yields the best performance. However, this is achieved at the cost of relatively high feedback rate from mobile to base station. Finally, it is noteworthy that the fixed beams performance is in general close to that of eigenbeamforming, even though there is a large difference between the feedback rate requirement of the two techniques.

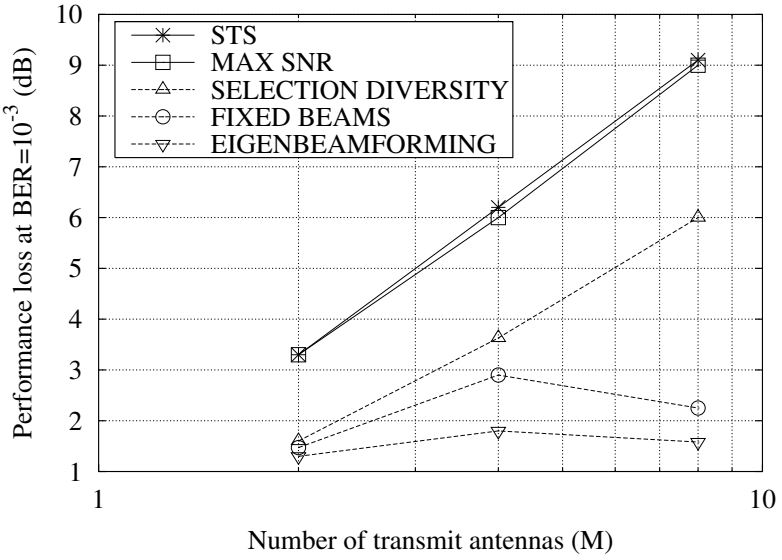

Figure 3.22: *Performance loss of the techniques at BER* $= 10^{-3}$ *compared to TXAA in the macro cell.*

When a BER of 10^{-3} needs to be achieved at the mobile station without feedback (i.e. using an open loop algorithm) in a macro cell, MAX SNR may be preferred over STS. This is because, although STS and MAX SNR yield very similar performance at BER $= 10^{-3}$, MAX SNR is advantageous as it requires less complexity at the mobile receiver. However, as we have noted above, the STS performance may be improved easily in practice by increasing the transmit antenna spacing, and in this case STS may be preferred to MAX SNR. Regarding the case

where feedback is afforded and a closed loop algorithm can be used, if $M = 2$, selection diversity appears to be a good choice. This is because it yields almost the same performance as the other closed loop algorithms, it is very simple and its required feedback rate is low. However, if $M > 2$ fixed beams may be preferred as it requires feedback rate similar to selection diversity and yields better performance (of course, fixed beams requires a more complex base station than selection diversity, but the additional complexity is relatively small). Finally, if a relatively high feedback rate can be afforded, then eigenbeamforming can be used and it will provide performance close to the lower bound (TXAA).

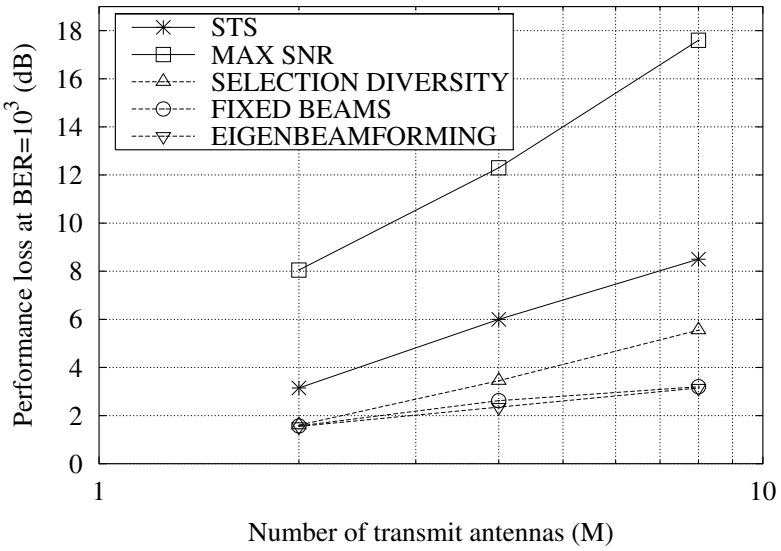

Figure 3.23: *Performance loss of the techniques at BER* $= 10^{-3}$ *compared to TXAA in the micro cell.*

Figure 3.23 shows the performance loss of each technique with respect to TXAA at BER $= 10^{-3}$ as a function of the number of transmit antennas in the micro cell. The MAX SNR loss is now larger, as the active angle of the micro cell is wider (larger angular spread) and cannot be fully exploited by means of beams. However, a wider active angle means that the correlation coefficient ρ_{adj} is now smaller (as can be seen in Figure 2.16 on page 26) and the diversity gain larger, favoring diversity techniques. The STS loss is the same as in the macro cell (starting from 3 dB and increasing by 3 dB each time M doubles), which is expected because the STS SNR is smaller than the TXAA SNR by $10\log_{10}(M)$ dB regardless of the channel environment. Also, the fact that STS contains diversity gain and can benefit from the richer scattering environment of the micro cell, enables it to perform closer to the closed loop

techniques than MAX SNR. The selection diversity loss again scales linearly with $\log(M)$, but its performance is now closer to that of the other two closed loop techniques (especially that of eigenbeamforming and for larger M values), due to increased diversity gain. In addition, Figure 3.23 shows that there is little difference between the performance of fixed beams and eigenbeamforming in the micro cell. On page 42 we noted that these two techniques have both similarities and differences. The former are basically due to the diversity gain being similar in the two techniques, as both make use of the selection diversity concept to choose which (eigen)beam to use for transmission. The latter are essentially due to the beamforming gain not being similar in the two techniques, because of the differences between steering vector beams (used in fixed beams) and eigenbeams (used in eigenbeamforming), as noted on page 42. Therefore, any difference between the performance of the two techniques is expected to be due to the different beamforming gain in the two techniques. However, because of relatively large angular spread, the beamforming gain of the micro cell is (relatively) small, so the differences are not pointed out. Also, the diversity gain is (relatively) large, enhancing the similarity. Thus, the differences between the two techniques are 'suppressed' while the similarities are emphasised, causing them to perform similarly. Finally, we note that the beamforming gain of the micro cell is very small but *not* equal to zero. This appears to be the reason why fixed beams and eigenbeamforming perform better than selection diversity, even though all of them contain similar diversity gain, since they make use of the selection diversity concept.

When a BER of 10^{-3} needs to be achieved at the mobile station without feedback in the micro cell, STS is now preferred over MAX SNR as it clearly yields a better performance. In addition, a simple increase of the array element spacing can enhance the STS performance further. Also, when feedback is afforded and a closed loop algorithm can be used, selection diversity appears again to be a good choice, as it yields similar performance to the other two closed loop algorithms (especially for small M), it needs low feedback rate and is very simple. Finally, fixed beams yields a performance almost identical to that of the more complex eigenbeamforming, and may be preferred over selection diversity when a better performance is required (especially for large M) and a (slightly) more complex base station can be afforded.

Figure 3.24 shows the performance loss of each technique with respect to TXAA at BER = 10^{-3} as a function of the number of transmit antennas in the pico cell. The angular spread of the pico cell is very large and the power is not concentrated in a particular spatial direction, making the beamforming gain minimal (very close to zero). Under these conditions the directional

transmission of MAX SNR cannot improve the performance, and MAX SNR with $M > 1$ does not provide any gain with respect to the single antenna transmitter (this can also be seen in Figures 3.12 and 3.13 on pages 48 and 49 respectively). Consequently, the MAX SNR performance loss is maximised. Also, the STS performance loss is the same as in the previous two cell types, which is expected as explained above. Finally, all three closed loop techniques now yield effectively the same performance. This may be attributed to the fact that all of them contain the same type of diversity gain, which results from their use of the selection diversity concept. Also, the beamforming gain of the pico cell is virtually zero, so fixed beams and eigenbeamforming which contain beamforming gain cannot perform better than selection diversity which does not contain beamforming gain.

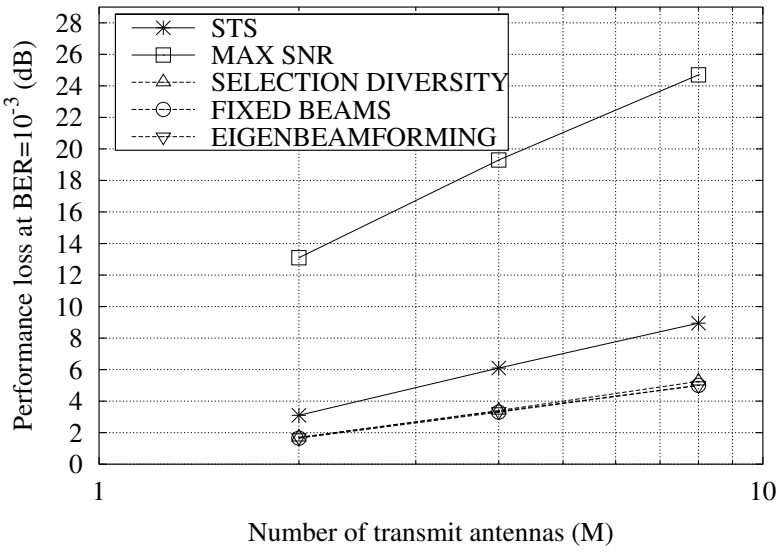

Figure 3.24: *Performance loss of the techniques at BER* $= 10^{-3}$ *compared to TXAA in the pico cell.*

When a BER of 10^{-3} needs to be achieved at the mobile station without feedback in the pico cell, STS is again preferred over MAX SNR, as it is able to exploit the improved diversity and yield a much better performance. In addition, if a closed loop technique can be used, selection diversity is preferred over the others, as it yields virtually the same performance as the other two closed loop techniques, and possesses the important advantage of needing low feedback rate and being very simple.

In addition, we note that if performance equal to the lower bound is required and the channel

fading is relatively slow (small Doppler frequency shift), transmit antenna array can be used in all three cell types (but it needs very high feedback rate). This is especially true for large M, as transmit antenna array provides little gain over the other closed loop techniques for small M, as can be seen in Figures 3.22, 3.23 and 3.24.

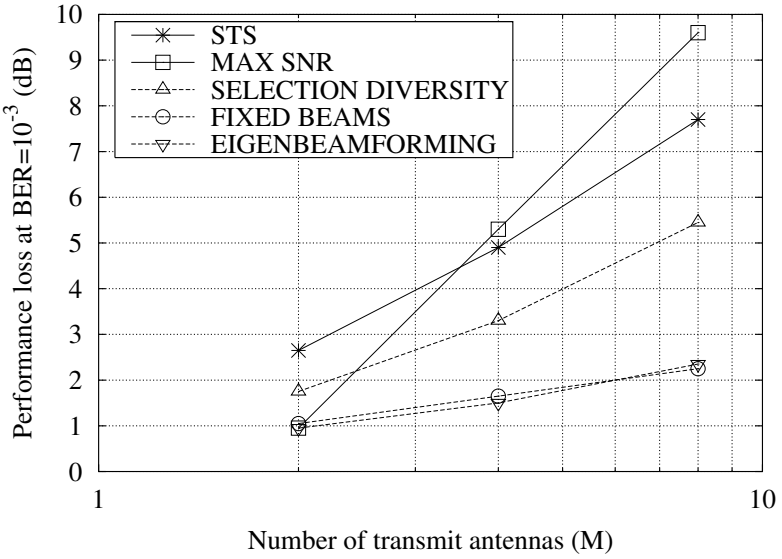

Figure 3.25: *Performance loss of the techniques at BER* $= 10^{-3}$ *compared to TXAA in the channel propagation environment with two taps.*

Comparison among Figures 3.10(d) (page 45), 3.12(d) (page 48), 3.14(d) (page 50), 3.16(d) (page 52), 3.18(d) (page 54) and 3.20(d) (page 56) shows that transmit antenna array provides the best performance among all the presented techniques in the frequency selective scenario (although it does not maximise the instantaneous SNR of the received signal in this scenario). Therefore, we will use it again as a reference and compare all the other techniques to it, exactly as we did for the comparison of the techniques in the 1-tap cells above. To this end, Figure 3.25 shows the performance loss of each technique with respect to TXAA at BER $= 10^{-3}$ as a function of the number of transmit antennas in the 2-tap scenario. Again solid curves correspond to open loop techniques while dashed curves correspond to closed loop techniques. The results show that for $M = 2$ MAX SNR yields very good performance and is better than all other techniques (with the exception of eigenbeamforming). This may be because the main beam is wide enough to exploit the most part of the two taps. However, as M increases, the MAX SNR performance worsens rapidly and even for $M = 4$ it is already worse than that of space-time spreading. The space-time spreading performance loss increases with M. The rate

of this increase is about 2 dB when M increases from 2 to 4 and about 3 dB when M increases from 4 to 8. Among the three closed loop techniques, selection diversity provides the worst performance which is consistent with the results of the 1-tap cells, and may be again due to its lack of beamforming gain. Furthermore, fixed beams and eigenbeamforming yield very similar performance in the 2-tap scenario, which has also been noted in the results of the 1-tap cells.

3.5 Summary

In this chapter we analysed a number of diversity, beamforming and hybrid antenna array algorithms which are candidates for employment on the downlink of WCDMA mobile communication systems. The basic operation of each algorithm was briefly introduced, and the theoretical BER versus SNR performance of some of the algorithms was calculated based on the combination of the eigenvalue decomposition of the mean channel correlation matrix and equation (2.9) (page 28). The algorithms were also simulated in various representative 1-tap and one 2-tap channel propagation environment. The simulation results along with other characteristics of the algorithms were compared, and indications about which algorithm(s) are suitable for each channel environment were provided.

More specifically, it was shown that pure diversity algorithms, such as space-time spreading, do not perform well in environments where the correlation coefficient ρ_{adj} is large, because the benefit from the diversity gain is small. Beamforming algorithms like maximum SNR perform in general better in such environments. However, the performance of the diversity algorithms may be improved in practice by increasing the transmit antenna array spacing, which effectively makes ρ_{adj} smaller and the diversity benefit larger. Hybrid algorithms that combine diversity and beamforming gain, such as fixed beams and eigenbeamforming, appear to perform well in a variety of different channel environments, but usually require some form of information feedback from mobile to base station, which may have a negative impact on the overall system capacity. When such information feedback can be used, these algorithms can be employed to improve the performance. In general, the higher the feedback rate and the more complex the base station, the larger the performance improvement. Nevertheless, in certain channel environments such as the pico cell, even simple algorithms such as selection diversity yield performance equal to that of the more complex algorithms like eigenbeamforming. An interesting result is that fixed beams yields performance very similar to that of eigenbeamforming, even though it uses (much) lower feedback rate. An explanation is possible through closer examination of

the differences and similarities of the two techniques, as noted on page 61. In addition, it was shown that, depending on the channel environment, increasing the number of transmit antennas M in the base station does not always yield a better performance. A characteristic example of this behaviour is the maximum SNR technique in the pico cell.

Chapter 4
Efficient use of eigenbeams for downlink transmission

In this chapter the eigenvalue decomposition of the mean channel correlation matrix will be examined further. This examination will motivate the investigation of the combination of this decomposition and space-time processing as a possible open loop approach to the downlink data signal transmission. The open loop mode of this technique is similar to that of maximum SNR. The technique can also measure and adapt to channel conditions and will be employed to satisfy a flexible performance criterion. Its theoretical BER versus SNR performance will be calculated in terms of the eigenvalues of the mean correlation matrix, and it will be shown that its behaviour ranges from pure beamforming to pure diversity, illustrating its adaptability. When it provides diversity gain, this gain is in the domain of eigenvalues and its order depends on the channel conditions (as represented by angle of arrival/departure and angular spread). Also, the technique will be simulated and the results will be compared to simulation results of the techniques analysed in Chapter 3. This comparison will illustrate that the technique yields the best performance among all the open loop techniques, when this is measured by the flexible performance criterion that will be applied.

4.1 Introduction

When the eigenvalue decomposition of the $M \times M$ mean channel correlation matrix is performed, the matrix is decomposed into M eigenvalues and M eigenvectors, which are independent components in the M-dimensional space [92]. The correlation matrix is a function of all M eigenvalues and eigenvectors, as shown in equation (2.8), and, thus, spans the M-dimensional space. Also, each eigenvector or set of eigenvectors spans a subspace of the M-dimensional space. When a technique uses an eigenvector or a set of eigenvectors for signal transmission, it essentially exploits the corresponding subspace to transfer the signal power from base station to mobile station. For instance, maximum SNR uses the principal eigenvector as beamformer and exploits the subspace spanned by this eigenvector for power transfer to the mobile station,

while space-time spreading uses all M eigenvectors, exploiting the M-dimensional space. It is shown below that the value(s) of the eigenvalue(s) are indicative of how efficiently a particular subspace can transfer the signal power from base station to mobile station. Exploiting this fact, the technique that will be investigated in this chapter will use the M eigenvalues to adaptively determine which subspace to employ. This decision will be based on a flexible performance criterion that attempts to minimise the SNR (i.e. transmit power) that is needed to yield a specific target BER at the mobile receiver. As the channel conditions in the form of angle of departure and angular spread change so do the eigenvalues, and the technique can switch to another subspace to optimise the performance according to the above criterion in the new conditions.

The basic idea of this technique (without the adaptive optimisation of the performance as the channel conditions change over time) was mentioned briefly in [46], but was not analysed further in that paper. Moreover, the idea of applying the aforementioned flexible performance criterion was not mentioned or explored in [46].

4.2 Motivation

Equation (3.5) shows that when the principal eigenvector of the mean downlink channel correlation matrix $\mathbf{R}_{\mathrm{DL}}$ is used as beamformer, the mean SNR of the MAX SNR algorithm is proportional to its maximum eigenvalue $e_{\mathrm{DL,max}}$. It can also be shown that the same holds for the i-th eigenvector and eigenvalue. That is, replacing the mean downlink channel correlation matrix from equation (2.8) to equation (3.3) and using the i-th eigenvector as beamformer (i.e. $\mathbf{w} = \mathbf{u}_i$ in equation (3.3)), it is shown that the SNR is proportional to the i-th eigenvalue e_i

$$\mathrm{SNR} = E_s \frac{\mathbf{u}_i^{\mathrm{H}} \left[\sum_{j=1}^{M} e_j \left(\mathbf{u}_j \mathbf{u}_j^{\mathrm{H}} \right) \right] \mathbf{u}_i}{\sigma_n^2} = E_s \frac{e_i}{\sigma_n^2}. \tag{4.1}$$

This means that the value of the i-th eigenvalue is an indication of how efficiently the power is transferred from the base station across the downlink channel to the intended mobile station, if the i-th eigenvector is used as beamformer. Therefore, by examining the amplitudes of the eigenvalues we can make this power transfer more efficient.

Figure 4.1 shows the value of the 4 eigenvalues of the mean downlink channel correlation matrix as a function of angular spread δ, when a 4-element antenna array is used by the base station (the carrier frequency is $f_c = 2$ GHz, the transmit antenna spacing is $D = \frac{\lambda}{2}$ and the

angle-of-departure is AOD = 1°). We observe that for small values of δ there is clearly a dominant eigenvalue and all other eigenvalues have much smaller values. In this case, only the subspace spanned by the dominant eigenvector can transfer the power efficiently to the mobile station. However, as the angular spread increases, the value of the smaller eigenvalues increases, too, and becomes comparable to that of the dominant one (especially for angular spread values close to 120°, all M eigenvalues have very similar value). This means that the subspaces spanned by the eigenvectors corresponding to these smaller eigenvalues become also efficient in terms of power transfer. Therefore, when δ increases, using only the dominant eigenvector as beamformer does not exploit fully the underlying structure of the channel.

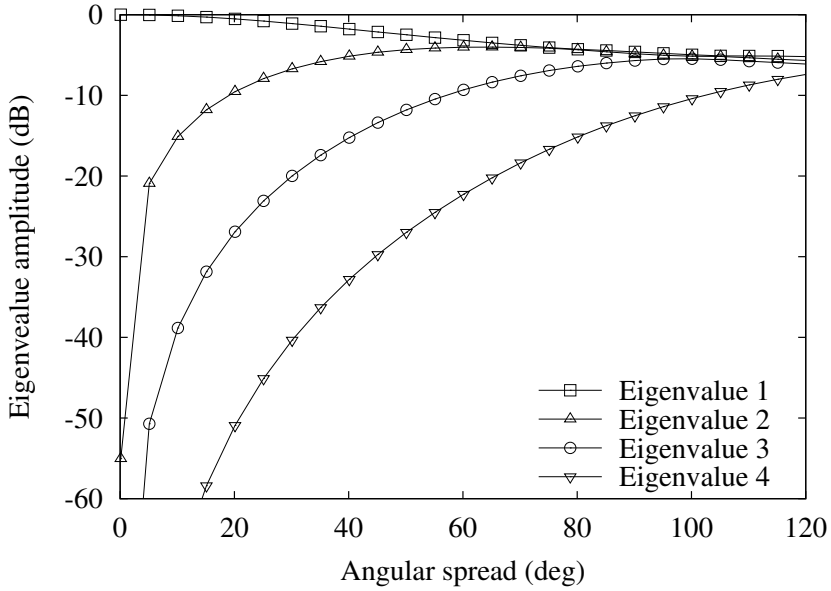

Figure 4.1: *Amplitude of the eigenvalues of the mean correlation matrix as a function of angular spread (f_c = 2 GHz, $D = \frac{\lambda}{2}$, AOD = 1°).*

To investigate and quantify the potential diversity gain of using more than one eigenvector as beamformer, we will plot the required SNR for a target BER = 10^{-3}, when various numbers of eigenvectors are used as beamformers. Using the principal eigenvector provides a mean SNR proportional to the largest eigenvalue, so using the K eigenvectors that correspond to the K largest eigenvalues will yield K diversity paths with mean SNR values proportional to the corresponding K largest eigenvalues. Since these eigenvectors are mutually orthogonal, the K diversity paths are mutually uncorrelated. This, combined with the fact that the eigenvalues are in general unequal, means that equation (2.9) can be used for the calculation of the required

SNR, according to the following procedure. We calculate the mean downlink channel correlation matrix for a particular value of M, D, AOD and δ as described in [190], and perform its eigenvalue decomposition. Assuming that the K eigenvectors corresponding to the K largest eigenvalues are used as beamformers and the (linear) SNR value is γ, we then multiply the K largest eigenvalues by the quantity $\gamma\frac{1}{K}$ and use them in equation (2.9) to obtain the BER yielded by this K and SNR value. This way we are able to search the SNR needed by this K to yield the target BER. Varying the value of K from 1 to M and the angular spread from 0^o to 120^o, and using $M = 4$, $f_c = 2$ GHz, $D = \frac{\lambda}{2}$ and AOD = 1^o, we obtain the results of Figure 4.2. We note that the $K = 1$ curve (1 eigenvector) corresponds to the performance of maximum SNR while the $K = M$ curve (M eigenvectors) corresponds to the performance of space-time spreading, as we have seen in Chapter 3. Also, we have plotted a dotted line which indicates that the lowest required SNR over all shown angular spread values is about 10.1 dB.

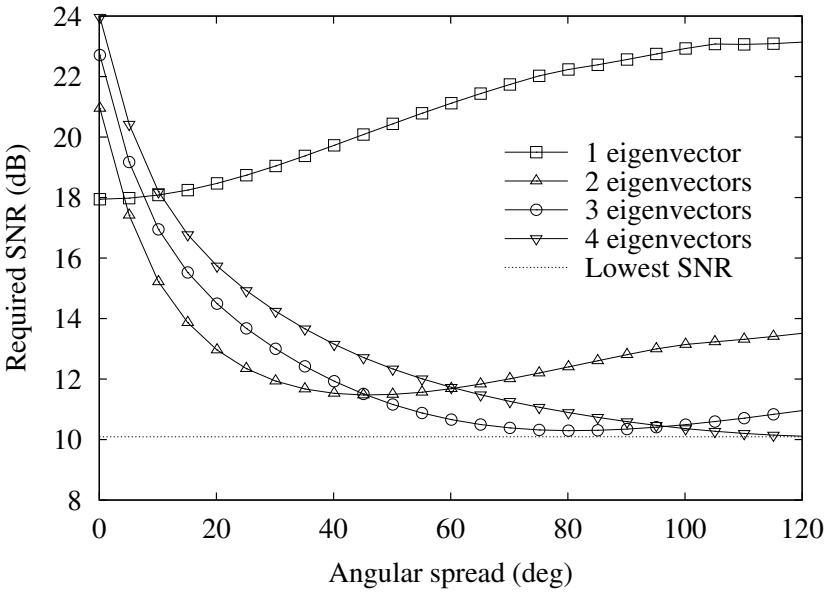

Figure 4.2: *Required SNR for a target BER=10^{-3} as a function of angular spread ($M = 4$, $f_c = 2$ GHz, $D = \frac{\lambda}{2}$, AOD = 1^o).*

The results of Figure 4.2 show that $K = 1$ provides the lowest required SNR only if the angular spread is small (smaller than about 4^o). For larger angular spread values (e.g. $\delta \gtrapprox 4^o$) a value of $K > 1$ provides the lowest required SNR to yield the specified target BER. For instance, if $4^o \lessapprox \delta \lessapprox 45^o$, a value of $K = 2$ provides the lowest required SNR, while if $\delta \gtrapprox 97^o$ a value of $K = M$ (space-time spreading) provides the lowest required SNR. Also, the lowest required SNR over all shown angular spread values is about 10.1 dB and is provided by $K = M$ (space-

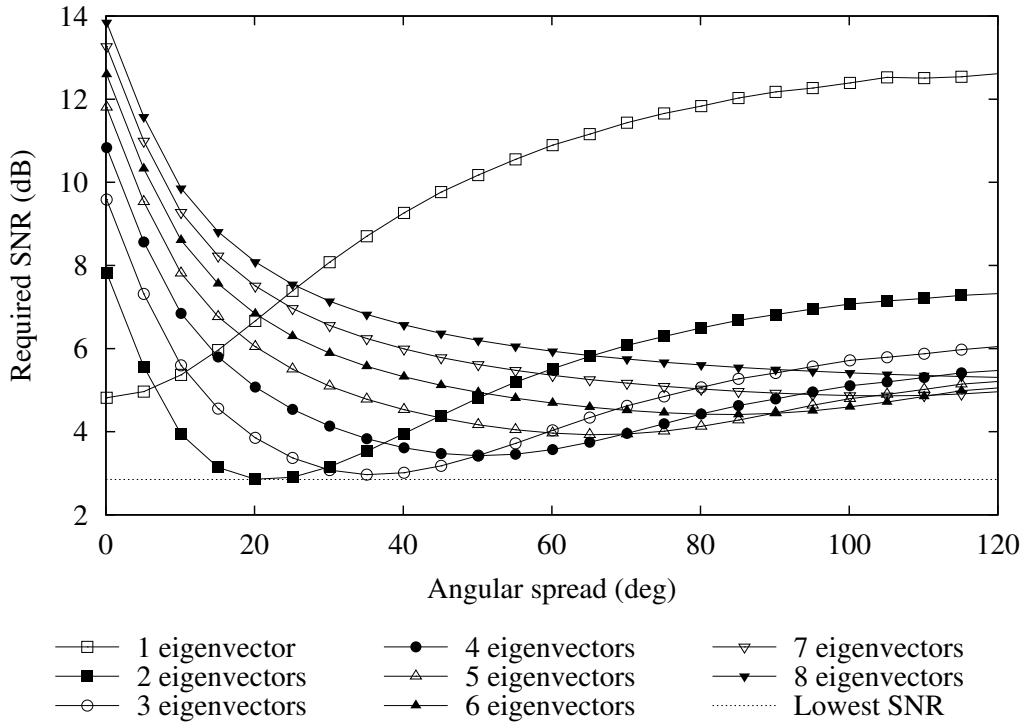

Figure 4.3: *Required SNR for a target BER=10^{-2} as a function of angular spread ($M = 8$, $f_c = 2$ GHz, $D = \frac{\lambda}{2}$, AOD = 1^o).*

time spreading) at very large angular spread values ($\delta \simeq 120^{\text{o}}$). In addition, Figure 4.3 shows the required SNR for $M = 8$ and a target BER $= 10^{-2}$ as a function of angular spread when different numbers of eigenvectors are used as beamformers by the base station (again the carrier frequency is $f_c = 2$ GHz, the transmit antenna spacing is $D = \frac{\lambda}{2}$ and the angle-of-departure is AOD $= 1^{\text{o}}$). The results of Figure 4.3 show the same trends as those of Figure 4.2. That is, again when the angular spread is small ($\delta \lessapprox 4.5^{\text{o}}$) a value of $K = 1$ provides the lowest required SNR, while as δ increases a value of $K > 1$ provides the lowest required SNR for the specified target BER. For example, when $29.5^{\text{o}} \lessapprox \delta \lessapprox 50^{\text{o}}$ a value of $K = 3$ provides the lowest required SNR, while when $70^{\text{o}} \lessapprox \delta \lessapprox 89.5^{\text{o}}$ a value of $K = 5$ provides the lowest required SNR. Also, now the lowest required SNR over all shown angular spread values (which occurs at $\delta \simeq 20^{\text{o}}$ and is about 2.85 dB) is not provided by one of the existing techniques (i.e. maximum SNR with $K = 1$ or space-time spreading with $K = M = 8$), but by $K = 2$. That is, none of the existing techniques can take full advantage of the underlying structure of this channel scenario. In the next section we examine a technique that uses the number of eigenvectors K which minimises the SNR that is needed to achieve a particular target BER.

4.3 Algorithm description

When $K > 1$ eigenvectors are used as beamformers by the base station, they are combined with a diversity technique to yield diversity gain in addition to the beamforming gain that they provide anyway. In this chapter we will examine the combination of the K eigenbeams with space-time spreading [160], which belongs to the category of space-time coding schemes [217]. The authors of [110] applied space-time coding to 'normal' beams[1] for a base station with $M = 4$ transmit antennas and $K = 2$ beams, for complex signal constellations (quadrature phase shift keying, QPSK). However, the known space-time coding schemes for complex signals do not achieve full transmission rate for $M > 2$ [217] (i.e. they use more than one symbol period per data symbol transmitted). Therefore, here we explore the combination of space-time spreading and eigenbeams for real signal constellation (binary phase shift keying, BPSK), which achieves full transmission rate for any M [217] and, in the case of eigenbeams, any K (i.e. it uses one symbol period per data symbol transmitted). When complex signals have to be used (e.g. QPSK in wideband CDMA), the K eigenbeams can be combined with orthogonal transmit diversity (OTD) [57, 181, 187] instead of space-time coding. Orthogonal transmit diversity yields full transmission rate but its diversity gain is smaller than that of space-time coding because not every data symbol is transmitted through all the available diversity branches as in space-time coding. However, when it is combined with coding it is able to yield most of the diversity gain that space-time coding provides [57, 106]. Also, as we pointed out in the introduction of this chapter, the authors in reference [46] mention briefly the application of space-time coding techniques to eigenbeams, but do not analyse it further. Here, we will explicitly present the combination of space-time spreading and eigenbeams and analyse its performance (the previous section describing our motivation has already provided initial performance hints). In the next section we describe this combination.

First the base station determines the target BER that it should use. This can be done in accordance with other system requirements, such as desired voice or service quality at the mobile receiver. Then, it obtains an estimate of the mean downlink correlation matrix $\mathbf{R}_{\mathrm{DL}}$ as we have described in the MAX SNR algorithm (last paragraph of section 3.1.2 which starts on page 33). After that, it follows the procedure used to obtain the required SNR for a specific target BER described in the previous section, to calculate the K (where $1 \leq K \leq M$) that provides the lowest required SNR for the specified target BER. Once the value of K is determined, the

[1] 'Normal' beams are beam patterns generated by steering vectors, as opposed to those generated by eigenvectors.

base station combines the K eigenbeams according to space-time spreading and uses them to transmit the data signal to the intended mobile station. We call this scheme 'Minimum BER', or 'MIN BER' for short.

For instance, if the base station calculates that $K = 2$ eigenbeams provide the lowest required SNR, the intended mobile user's data symbol stream $s(t)$ is divided into two symbol substreams $s_1(t)$ and $s_2(t)$, as in space-time spreading [160] (e.g. $s_1(t)$ can contain the odd data symbols of $s(t)$ and $s_2(t)$ can contain the even data symbols of $s(t)$). The base station then uses two consecutive symbol periods, T_1 and T_2, to transmit the vector signals $\mathbf{x}_1^H(t) \in \mathbb{C}^{1\times M}$ and $\mathbf{x}_2^H(t) \in \mathbb{C}^{1\times M}$, respectively, where

$$\mathbf{x}_1^H(t) = \sqrt{\frac{E_s}{2}}\left[s_1(t)c(t)\mathbf{u}_1^H + s_2(t)c(t)\mathbf{u}_2^H\right] \qquad \text{(over } T_1\text{)} \tag{4.2}$$

$$\mathbf{x}_2^H(t) = \sqrt{\frac{E_s}{2}}\left[s_2(t)c(t)\mathbf{u}_1^H - s_1(t)c(t)\mathbf{u}_2^H\right], \qquad \text{(over } T_2\text{)} \tag{4.3}$$

and E_s is the power of each data substream across the $K = 2$ eigenbeams, $c(t)$[2] is the intended mobile user's spreading code (which may be real or complex) and $\mathbf{u}_1 \in \mathbb{C}^{M\times 1}$ and $\mathbf{u}_2 \in \mathbb{C}^{M\times 1}$ denote the two eigenvectors of $\mathbf{R}_{DL}$ that correspond to its two largest eigenvalues e_1 and e_2, respectively. Assuming a 1-tap channel propagation environment, the intended mobile station receives the signal $y_1(t)$ due to transmission of $\mathbf{x}_1^H(t)$ and the signal $y_2(t)$ due to transmission of $\mathbf{x}_2^H(t)$, which after despreading with the spreading code $c(t)$ (or $c^*(t)$ in case of complex codes, where the asterisk denotes complex conjugate) are written as

$$y_1(t) = \sqrt{\frac{E_s}{2}}\left[s_1(t)\mathbf{u}_1^H + s_2(t)\mathbf{u}_2^H\right]\mathbf{h} + n_1 \tag{4.4}$$

$$y_2(t) = \sqrt{\frac{E_s}{2}}\left[s_2(t)\mathbf{u}_1^H - s_1(t)\mathbf{u}_2^H\right]\mathbf{h} + n_2, \tag{4.5}$$

where $\mathbf{h} \in \mathbb{C}^{M\times 1}$ denotes a sample of the instantaneous vector of the single channel tap, while n_1 and n_2 denote samples of a white Gaussian stochastic process and appear as additive noise terms. In the calculation of $y_1(t)$ and $y_2(t)$ we have assumed that the channel vector $\mathbf{h}$ does not change significantly over the two consecutive symbol periods T_1 and T_2 (this is the default assumption in space-time spreading, too). The mobile station receiver uses the received signals $y_1(t)$ and $y_2(t)$ to obtain an estimate $\hat{s}_1(t)$ and $\hat{s}_2(t)$ of the data signals $s_1(t)$ and $s_2(t)$, respectively,

[2] Although both the data signal $s(t)$ and the spreading code $c(t)$ vary over time, the spreading code varies much more rapidly and essentially determines the bandwidth of the spread signal that is transmitted by the base station.

as follows

$$\hat{s}_1(t) = \Re\left\{\left(\mathbf{u}_1^{\mathrm{H}}\mathbf{h}\right)^* y_1(t) - \left(\mathbf{u}_2^{\mathrm{H}}\mathbf{h}\right)^* y_2(t)\right\} \Rightarrow \ldots$$

$$\Rightarrow \hat{s}_1(t) = \left[\sqrt{\frac{E_s}{2}}\left(\mathbf{u}_1^{\mathrm{H}}\mathbf{h}\mathbf{h}^{\mathrm{H}}\mathbf{u}_1 + \mathbf{u}_2^{\mathrm{H}}\mathbf{h}\mathbf{h}^{\mathrm{H}}\mathbf{u}_2\right)\right] s_1(t) + \Re\left\{n_{11} - n_{12}\right\} \tag{4.6}$$

$$\hat{s}_2(t) = \Re\left\{\left(\mathbf{u}_2^{\mathrm{H}}\mathbf{h}\right)^* y_1(t) + \left(\mathbf{u}_1^{\mathrm{H}}\mathbf{h}\right)^* y_2(t)\right\} \Rightarrow \ldots$$

$$\Rightarrow \hat{s}_2(t) = \left[\sqrt{\frac{E_s}{2}}\left(\mathbf{u}_1^{\mathrm{H}}\mathbf{h}\mathbf{h}^{\mathrm{H}}\mathbf{u}_1 + \mathbf{u}_2^{\mathrm{H}}\mathbf{h}\mathbf{h}^{\mathrm{H}}\mathbf{u}_2\right)\right] s_2(t) + \Re\left\{n_{21} - n_{22}\right\}, \tag{4.7}$$

where $\Re$ denotes the real part of a complex number, and $n_{11} = n_1(\mathbf{h}^{\mathrm{H}}\mathbf{u}_1)$, $n_{12} = n_2(\mathbf{h}^{\mathrm{H}}\mathbf{u}_2)$, $n_{21} = n_1(\mathbf{h}^{\mathrm{H}}\mathbf{u}_2)$ and $n_{22} = n_2(\mathbf{h}^{\mathrm{H}}\mathbf{u}_1)$. The mobile station estimates the complex quantities $\mathbf{u}_1^{\mathrm{H}}\mathbf{h}$ and $\mathbf{u}_2^{\mathrm{H}}\mathbf{h}$ that it needs to obtain the estimates of the data signals from orthogonal pilot signals that are transmitted through each eigenbeam by the base station. Since there is a space-time spreading scheme for real signals and any M [217], the same approach can be applied to any number of eigenvectors K. Analysis of minimum BER for $K = 4$ is presented in section A.2 of appendix A, while analysis for $K = 8$ is presented in section A.3 of the same appendix.

Calculation of the mean SNR from $\hat{s}_1(t)$ yields the following result

$$\begin{aligned}
\mathrm{SNR}_{\mathrm{MINBER}} &= \frac{E_s}{2}\mathrm{E}\left[\frac{\left(\mathbf{u}_1^{\mathrm{H}}\mathbf{h}\mathbf{h}^{\mathrm{H}}\mathbf{u}_1 + \mathbf{u}_2^{\mathrm{H}}\mathbf{h}\mathbf{h}^{\mathrm{H}}\mathbf{u}_2\right)^2}{(n_{11} - n_{12})(n_{11} - n_{12})^*}\right] \\
&= \frac{E_s}{2}\frac{\mathbf{u}_1^{\mathrm{H}}\mathrm{E}\left[\mathbf{h}\mathbf{h}^{\mathrm{H}}\right]\mathbf{u}_1 + \mathbf{u}_2^{\mathrm{H}}\mathrm{E}\left[\mathbf{h}\mathbf{h}^{\mathrm{H}}\right]\mathbf{u}_2}{\sigma_n^2} \\
&= \frac{E_s}{2}\frac{\mathbf{u}_1^{\mathrm{H}}\mathbf{R}_{\mathrm{DL}}\mathbf{u}_1 + \mathbf{u}_2^{\mathrm{H}}\mathbf{R}_{\mathrm{DL}}\mathbf{u}_2}{\sigma_n^2} \\
\Rightarrow \mathrm{SNR}_{\mathrm{MINBER}} &= \frac{E_s}{2}\frac{e_1 + e_2}{\sigma_n^2},
\end{aligned} \tag{4.8}$$

where e_1 and e_2 are the two largest eigenvalues of $\mathbf{R}_{\mathrm{DL}}$, and σ_n^2 denotes the noise power spectral density. Also, calculation of the mean SNR from $\hat{s}_2(t)$ yields the same result. Equations (4.6), (4.7) and (4.8) show that minimum BER achieves the expected order 2 diversity gain by using two eigenvectors as beamformers. The contribution of each diversity path is proportional to the corresponding eigenvalue of the eigenvector that has created the diversity path. In the general case of K eigenvectors the mean SNR is

$$\mathrm{SNR}_{\mathrm{MINBER}} = \frac{E_s}{K}\frac{\sum_{i=1}^{K} e_i}{\sigma_n^2}, \tag{4.9}$$

which shows that diversity of order K in the domain of eigenvalues is achieved with K eigenvectors.

The above analysis was done for the case of a 1-tap channel scenario. If the channel consists of N temporal taps, the procedure of determining the number of eigenvectors to be used must be modified. In order to take into account the information of all temporal taps in the correlation matrix that will be subject to eigenvalue decomposition, the mean correlation matrices of all N temporal taps are summed as follows

$$\mathbf{R}_{\mathrm{SUM}} = \sum_{n=1}^{N} \mathrm{E}\left[\mathbf{h}_n(t)\mathbf{h}_n^{\mathrm{H}}(t)\right] = \sum_{n=1}^{N} \mathbf{R}_n, \tag{4.10}$$

and the eigenvalue decomposition of the resulting summed matrix $\mathbf{R}_{\mathrm{SUM}}$ is performed. In the case of a 1-tap scenario, the eigenvalues of the eigenvalue-decomposed matrix were multiplied by $\gamma\frac{1}{K}$ and then used in equation (2.9) in the process of calculating the optimum K, because they represent the expected contribution of the diversity path provided by each eigenvector. However, now that the channel consists of N temporal taps the eigenvalues of $\mathbf{R}_{\mathrm{SUM}}$ do not represent the expected contribution of each eigenvector any more and cannot be used in equation (2.9). Also, since now there are a total of N channel taps, each eigenvector does not provide only one contribution but a total of N contributions across these N taps, which for the k-th eigenvector are noted as $e_{k1}, e_{k2}, \cdots, e_{kN}$. The expected contribution of the k-th, $k = 1..K$, eigenvector $\mathbf{u}_k$ of $\mathbf{R}_{\mathrm{SUM}}$ due to the n-th, $n = 1..N$, channel tap is given by the following expression[3]

$$e_{kn} = \frac{\mathbf{u}_k^{\mathrm{H}}\mathbf{R}_n\mathbf{u}_k}{\sigma_n^2}. \tag{4.11}$$

Therefore, in order to calculate the SNR that is needed by the K 'largest' eigenvectors of $\mathbf{R}_{\mathrm{SUM}}$ to yield the specified target BER, the base station now multiplies the KN contributions e_{kn}, $k = 1..K$ $n = 1..N$, by $\gamma\frac{1}{K}$ and then uses them in equation (2.9). Once the optimum K has been calculated, the base station combines the K 'largest' eigenvectors of $\mathbf{R}_{\mathrm{SUM}}$ with space-time spreading as in the case of the 1-tap channel propagation environment and transmits the data signal to the intended mobile station as normal.

As the mobile station moves within the physical environment, the channel conditions in the

[3]This expression does not take into account the interference among the taps that results from the loss of orthogonality among their spreading codes. This is not expected to be significant unless the processing gain is very small (e.g. 4 or 8).

form of angle of departure and angular spread change. This is reflected on the channel correlation matrix which is permanently monitored by the base station. Therefore, the base station is able to change the number of eigenbeams K that it uses for data signal transmission, to adapt to the new channel conditions and attempt to achieve the target BER at the intended mobile station with the lowest possible transmit power. Also, non-intended mobile stations are subject to less interference because of the lower transmit power and the directional transmission. A further advantage of minimum BER is that it can be operated in an open loop fashion (using the eigenvectors of the uplink correlation matrix, as in maximum SNR), thus avoiding the need for feedback of channel or correlation matrix information from mobile to base station.

The behaviour of minimum BER can vary from pure beamforming ($K = 1$) all the way to pure diversity ($K = M$). Therefore, it is expected to be especially beneficial in cases where neither beamforming nor diversity techniques can fully exploit the channel environment to yield the maximum gain. Such an example is an environment with small to moderate angular spread that can result in an adjacent element correlation coefficient in the approximate range $0.7 \lessapprox \rho_{\text{adj}} \lessapprox 0.99$[4].

In minimum BER, the performance is optimised according to the target BER, which is a *flexible* criterion as it can be changed to meet other system requirements, such as voice or service quality at mobile receiver. However, changing the target BER may result in the selection of a different number of eigenbeams K. Also, the number of eigenbeams may change whenever the channel conditions change, as we have noted above, and both transmission and reception should change accordingly. In this case the mobile station receiver must be notified of the new K, so that it is able to receive and demodulate the transmitted signals correctly.

4.4 Simulation results

Minimum BER has been simulated by Monte Carlo simulation and the results are presented in this section. The technique has been optimised for a target BER = 10^{-3}. This means that

[4]It is pointed out that these limits are approximate rather than exact, and are based on the fact that beamforming techniques need in general small angular spread (i.e. high ρ_{adj}, for instance $\rho_{\text{adj}} \gtrapprox 0.99$) to perform efficiently, while diversity techniques need in general large angular spread (i.e. small ρ_{adj}, for instance $\rho_{\text{adj}} \lessapprox 0.7$) to perform efficiently. The former claim (about the beamforming techniques) can be confirmed by the simulation results of the next section, where it will be shown, for example, that even in environments with ρ_{adj} as high as 0.988, the beamforming technique called maximum SNR does not yield the lowest required SNR for a specific target BER. The latter claim (about the diversity techniques) can be confirmed by the simulation results of the diversity techniques of Chapter 3 (for instance sections 3.3.1.1 and 3.3.2.2), and by the results of studies such as [190] and [124].

the number of eigenvectors K has been chosen so that it minimises the required SNR for a BER = 10^{-3} at the mobile station receiver. The uplink and downlink carrier frequencies are $f_{\mathrm{UL},c}$ = 2.14 GHz and $f_{\mathrm{DL},c}$ = 1.95 GHz respectively. The transmit antenna array spacing is $D = \frac{\lambda_{\mathrm{MID}}}{2}$, where λ_{MID} is the wavelength of the carrier frequency $f_{\mathrm{MID},c} = \frac{f_{\mathrm{UL},c}+f_{\mathrm{DL},c}}{2}$. As in maximum SNR, the base station uses the eigenvectors and eigenvalues of the uplink correlation matrix (that is, the technique is operated in an open loop fashion). In the actual simulation we calculate the uplink correlation matrix at the base station using equations A.2 and A.3 of appendix A. The uplink correlation matrix will be estimated from pilot signals transmitted on the uplink from mobile to base station in Chapter 5. The modulation of the data signals is binary phase shift keying. The simulations are performed in a one-user scenario, where the base station communicates with one user and there is no co-channel interference from other users. In each simulation the bit error ratio is calculated over 10^6 data symbols which are transmitted from base station to mobile station. These data symbols are not coded in any way. We assume that the mobile receiver has access to noiseless estimates of the M downlink channel coefficients h_i, $i = 1..M$. Also, the downlink channel vectors of consecutive data symbols are uncorrelated, to minimise simulation time. Simulations for 1-tap channel propagation environments are performed in the macro cell, micro cell and pico cell of Table 3.1. The simulations are also performed in a 2-tap scenario with the two temporal taps of Table 3.2. In this case the two taps are assumed to be resolved by the mobile receiver and there is no mutual interference between them[5].

The technique has been simulated for $M = 2$, $M = 4$ and $M = 8$ transmit antenna elements in the base station. Figures 4.4, 4.5 and 4.6 show simulation results in the three 1-tap cells for $M = 2$, $M = 4$ and $M = 8$ respectively. Also shown in these three figures, is the case of the single-antenna transmitter which is useful in determining the gain that minimum BER with $M > 1$ yields in various scenarios. Every figure depicts also the number of eigenvectors K that were used for data signal transmission in each cell and for each M. In addition, Tables 4.1, 4.2 and 4.3 show the SNR that all possible values of K need in order to achieve the target BER (10^{-3}) in all three cells for $M = 2$, $M = 4$ and $M = 8$ respectively. In each case, the K that needs the lowest SNR was used by the base station. Finally, Figure 4.7 depicts simulation results for $M = 2, 4, 8$ and the single-antenna transmitter in the 2-tap scenario.

[5]Again we point out that the impact of neglecting the mutual interference on the results is (very) small, as this interference causes an irreducible BER at very high SNR values which are out of the range of interest. An exception occurs when the processing gain of the spreading codes is very low (e.g. 4 or 8), which may cause an irreducible BER at SNR values of interest.

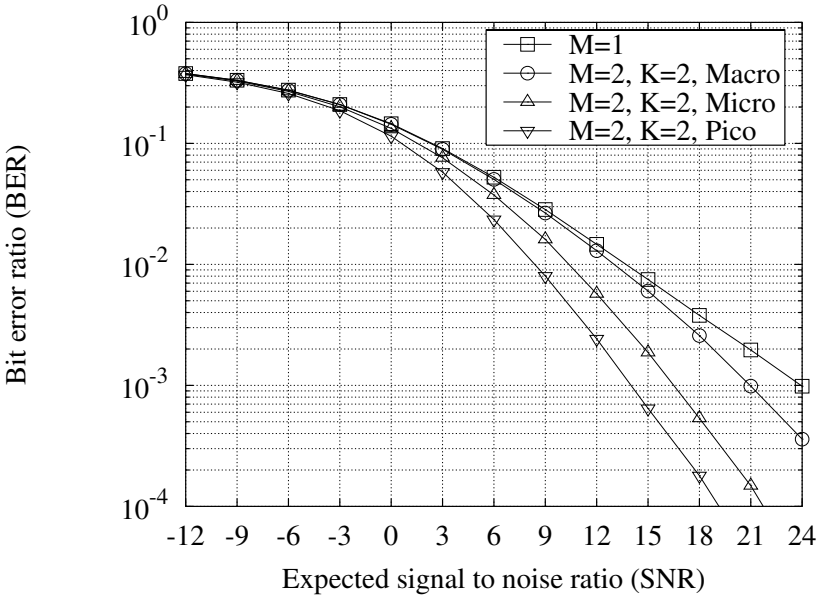

Figure 4.4: *Simulation results of minimum BER for $M = 2$ in the macro, micro and pico cell.*

K ($M = 2$)	**Macro cell** ($\rho_{\text{adj}} = 0.988$ when $D = \frac{\lambda}{2}$)	**Micro cell** ($\rho_{\text{adj}} = 0.825$ when $D = \frac{\lambda}{2}$)	**Pico cell** ($\rho_{\text{adj}} = 0.035$ when $D = \frac{\lambda}{2}$)
1	20.984	21.391	23.895
2	20.776	16.232	14.104

Table 4.1: *Required SNR (in dB) for all possible numbers of eigenvectors, $M = 2$ and a target BER $= 10^{-3}$, in the three 1-tap cell environments.*

Figure 4.4 shows that $K = 2$ eigenvectors were used in all three cell types, as this is the K that yields the lowest required SNR in all of them. This is confirmed by the results of Table 4.1, which show that the $K = 2$ choice yields the lowest required SNR in all three cell types. It is worth noting that in the macro cell, although the angular spread is relatively small ($\delta = 10^{\text{o}}$) and the correlation coefficient high ($\rho_{\text{adj}} = 0.988$) so that one would expect that one eigenvector (i.e. maximum SNR) would be able to yield the lowest required SNR, minimum BER has actually used two eigenvectors instead. This is also confirmed by the results of Table 4.1. However, Table 4.1 shows that in the case of $M = 2$ in the macro cell, two eigenvectors are marginally better than one eigenvector (by about 0.2 dB). Also, since we have $K = M = 2$ in all the cells, the performance of minimum BER is essentially the same as that of space-time spreading with the same number of antennas ($M = 2$). Thus, the results are the same as those

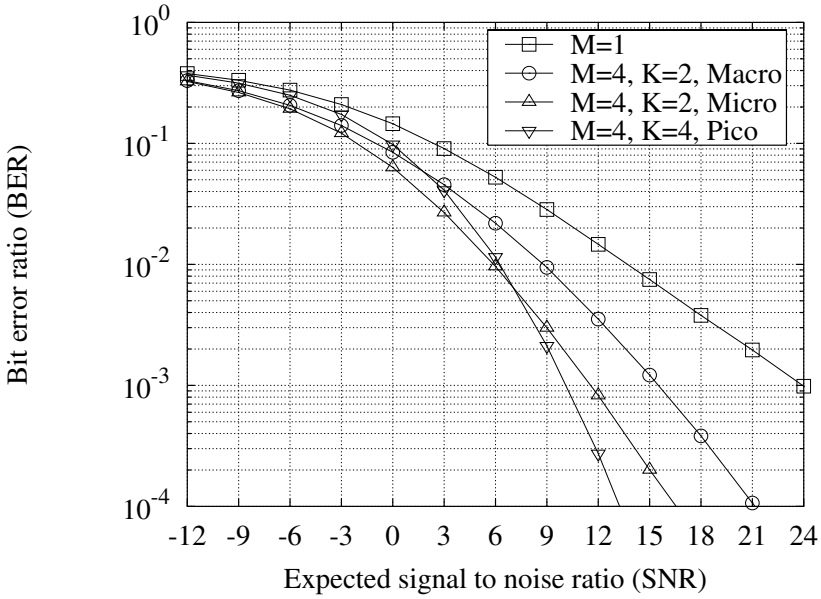

Figure 4.5: *Simulation results of minimum BER for $M = 4$ in the macro, micro and pico cell.*

K ($M = 4$)	**Macro cell** ($\rho_{\text{adj}} = 0.988$ when $D = \frac{\lambda}{2}$)	**Micro cell** ($\rho_{\text{adj}} = 0.825$ when $D = \frac{\lambda}{2}$)	**Pico cell** ($\rho_{\text{adj}} = 0.035$ when $D = \frac{\lambda}{2}$)
1	18.083	19.761	23.337
2	15.213	11.519	13.701
3	16.944	11.879	11.152
4	18.193	13.101	10.075

Table 4.2: *Required SNR (in dB) for all possible numbers of eigenvectors, $M = 4$ and a target BER $= 10^{-3}$, in the three 1-tap cell environments.*

of Figure 3.10(a) (page 45), and the same comments that were made in the discussion of that figure are also valid here.

Next, Figure 4.5 shows simulation results for $M = 4$ in the three 1-tap cells. It shows that in both macro and micro cells two eigenvectors were used, while in the pico cell four eigenvectors were used. These results are also confirmed by Table 4.2. Again, despite the small angular spread and the high correlation coefficient, the lowest required SNR in the macro cell is not yielded by one eigenvector (i.e. maximum SNR) but two eigenvectors. Furthermore, now the one eigenvector case is worse than the two eigenvector case not by a small amount as in the case of $M = 2$, but by about 2.9 dB. The performance in the macro and micro cell (which use the same number

of eigenvectors) is very similar for very low SNR values. Also, as the SNR increases the performance in the micro cell becomes better, which may be unexpected as the same number of antennas and eigenvectors are used by the base station in both cells. Nevertheless, the larger angular spread of the micro cell is reflected on the correlation matrix and becomes the major factor that affects the values of its eigenvalues and the subspace(s) spanned by its eigenvectors or sets of eigenvectors. Thus, although the subspace spanned by the two 'largest' eigenvectors is used for data signal transmission in both cells, the larger angular spread of the micro cell results in a subspace that is more efficient in terms of power transfer and yields a higher gain. This is the same effect as when a diversity technique performs better in a cell with larger angular spread than in a cell with smaller angular spread due to higher diversity gain, even though it uses the same number of antennas in both cells (e.g. Figures 3.10(a)–3.10(c) and Figures 3.16(a)–3.16(c)). Additionally, the performance in the pico cell (where a larger number of eigenvectors is used by the base station) is worse than that in the macro and micro cell for small SNR values, but becomes better than the performance in these both cells for large SNR values. In the previous section we described that when the base station uses K eigenvectors, the power of the transmitted data signal is proportional to $1/K$. Subsequently, when the SNR is small (i.e. the benefit from the diversity gain is small) and K increases (decreasing the beamforming gain due to the $1/K$ factor) the performance becomes worse. However, when the SNR increases, even though the beamforming gain may be small due to increased K, the benefit from the diversity gain also increases and eventually prevails, improving the overall performance. This is the reason why the performance in the pico cell is worse than that in the macro and micro cell for small SNR, but becomes better than both as SNR increases.

Next, Figure 4.6 shows simulation results for $M = 8$ in the three 1-tap cells. The number of eigenvectors that the base station uses is $K = 2$ in the macro cell, $K = 4$ in the micro cell and $K = 8$ in the pico cell. This means that K increases with angular spread (i.e. transition from macro to micro to pico cell), which is expected as the beamwidth of a uniform linear antenna array with $M = 8$ elements is relatively narrow (Figure A.2 on page 165), and more beams are needed as the angular spread increases. Moreover, the K values that were used by the base station are also confirmed by the results of Table 4.3. Since K always increases as the channel conditions change from macro to micro to pico cell, the phenomenon of the performance becoming worse with increasing K for small SNR values and then improving considerably for larger SNR values which was observed in Figure 4.5, is also apparent here. It is worth noting that the performance in the micro cell becomes better than that in the macro cell

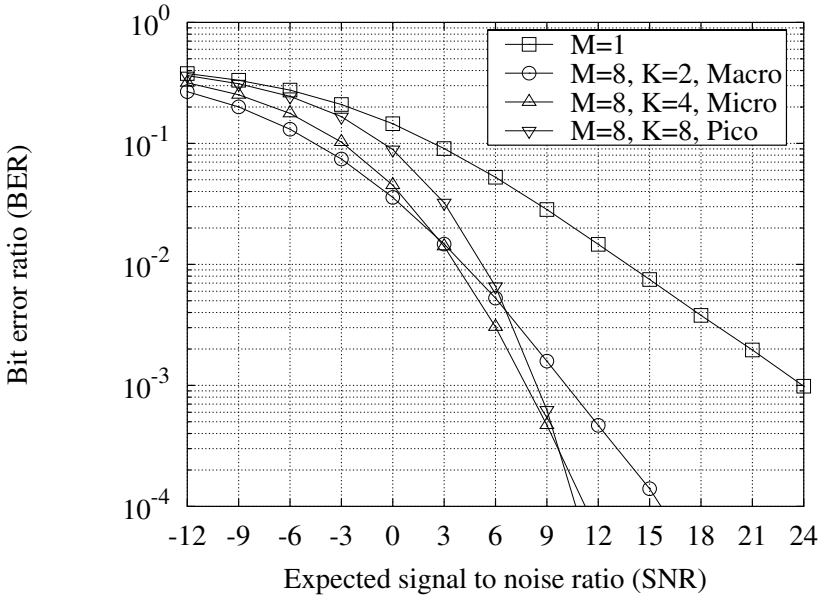

Figure 4.6: *Simulation results of minimum BER for $M = 8$ in the macro, micro and pico cell.*

at a relatively small SNR value (about 2.85 dB), while the performance in the pico cell becomes better than that in the micro cell at a relatively large SNR value (about 9.8 dB). The reason for this may be that the transition from $K = 2$ to $K = 4$ (transition from macro to micro cell) is not too large in terms of beamforming gain loss and the diversity gain is able to compensate for this loss at relatively small SNR values. The transition from $K = 4$ to $K = 8$ (transition from micro to pico cell), on the other hand, is (much) larger in terms of beamforming gain loss and the diversity gain is able to compensate for this loss only at relatively large SNR values.

K ($M = 8$)	**Macro cell** ($\rho_{\text{adj}} = 0.988$ when $D = \frac{\lambda}{2}$)	**Micro cell** ($\rho_{\text{adj}} = 0.825$ when $D = \frac{\lambda}{2}$)	**Pico cell** ($\rho_{\text{adj}} = 0.035$ when $D = \frac{\lambda}{2}$)
1	15.487	19.184	22.827
2	9.871	9.635	13.058
3	11.341	7.602	10.507
4	12.588	7.435	9.413
5	13.558	8.471	8.848
6	14.349	9.259	8.511
7	15.019	9.929	8.378
8	15.599	10.508	8.291

Table 4.3: *Required SNR (in dB) for all possible numbers of eigenvectors, $M = 8$ and a target BER $= 10^{-3}$, in the three 1-tap cell environments.*

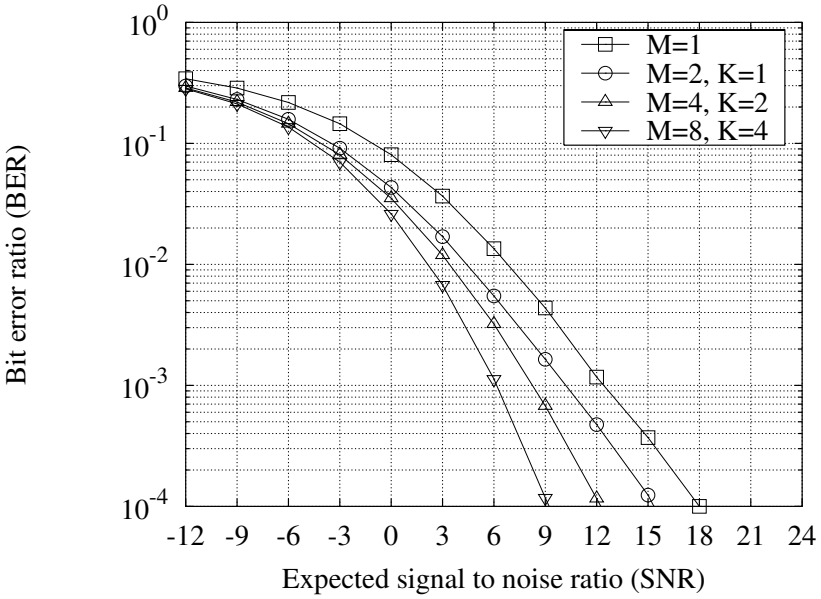

Figure 4.7: *Simulation results of minimum BER for* $M = 1, 2, 4, 8$ *in the 2-tap scenario.*

Figure 4.7 shows simulation results of minimum BER in the 2-tap scenario with the two taps of Table 3.2 (page 43). When $M = 2$, the base station uses $K = 1$ eigenvector and the performance is essentially the same as that of the technique maximum SNR with $M = 2$ in the same scenario (Figure 3.12(d) on page 48). In this case there is only additional beamforming gain with respect to the single-antenna transmitter, but no additional diversity gain. This becomes apparent by the fact that the $M = 2$ curve is shifted to the left by about 2.5 dB with respect to the $M = 1$ curve (i.e. there is additional beamforming gain of approximately 2.5 dB), and it is almost parallel to the $M = 1$ curve (i.e. there is no additional diversity gain to change the slope of the $M = 2$ curve). When $M = 4$, the number of eigenvectors that the base station uses is increased from 1 to 2, providing additional diversity gain but no additional beamforming gain. This becomes apparent by the fact that the $M = 4$ curve is not shifted for small SNR values with respect to the $M = 2$ curve (i.e. there is no additional beamforming gain to cause the shift), and its slope becomes gradually steeper than that of the $M = 2$ curve (i.e. there is additional diversity gain which increases the slope of the $M = 4$ curve). When $M = 8$, K is increased from 2 to 4, providing again additional diversity gain but no beamforming gain with respect to the $M = 4$ curve. This becomes apparent by the fact that the $M = 8$ curve is not shifted for small SNR values with respect to the $M = 4$ curve, and its slope becomes gradually steeper than that of the $M = 4$ curve.

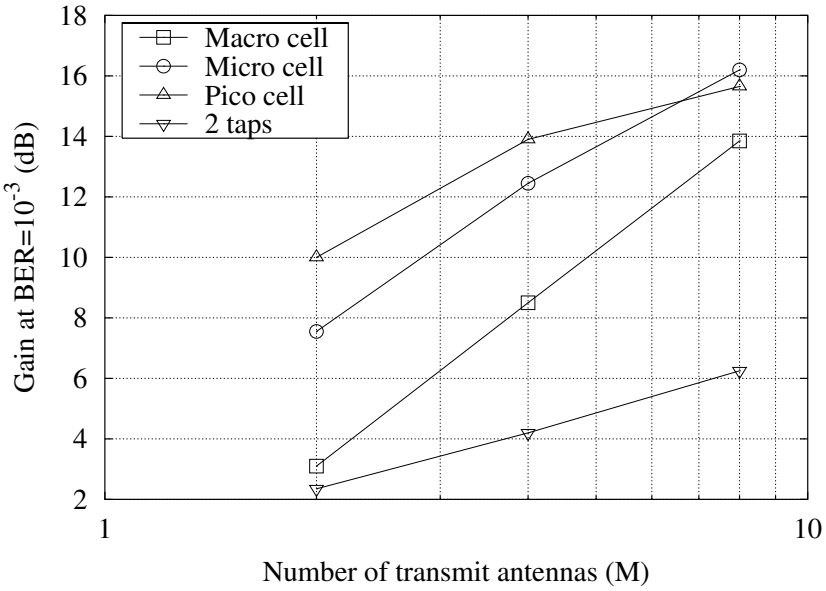

Figure 4.8: *Gain of minimum BER over the single antenna transmitter at BER* = 10^{-3}.

Finally, Figure 4.8 contains a summary of the results in Figures 4.4–4.7, and depicts the minimum BER gain over the single-antenna transmitter at BER = 10^{-3} as a function of M in both the 1-tap and 2-tap channel propagation environments. It shows that the gain over the single-antenna transmitter in dB increases almost linearly with $\log(M)$ in both the macro and micro cells. In the pico cell, nevertheless, increasing M above 4 starts to give diminishing returns. Also, since in the pico cell K is equal to M for all M values, the minimum BER performance is essentially the same as that of space-time spreading, and the pico cell curve of Figure 4.8 is the same as the pico cell curve of Figure 3.11 (page 46). Therefore, as has been noted in the discussion of the results of Figure 3.11, it is expected that when the number of antennas M becomes larger than 4, the technique will give diminishing returns in terms of additional diversity gain, as this gain is already high due to the very small correlation coefficient of the pico cell ($\rho_{\text{adj}} = 0.035$ for $D = \frac{\lambda}{2}$). Finally, in the 2-tap scenario, the gain over the single-antenna transmitter in dB increases linearly with $\log(M)$. Nevertheless, the 2-tap curve is less steep than both the macro and micro curves (that is, the gain in dB increases with $\log(M)$ at a lower rate in the 2-tap scenario than in the macro and micro cells), probably because in this case there is already multipath diversity resulting from the two taps.

4.5 Comparison of simulation results

The simulation results of minimum BER will be compared to the simulation results of the techniques of Chapter 3 in this section. The same method as in section 3.4 of Chapter 3 will be used here for the comparison of the results. That is, the performance loss that results from using minimum BER instead of transmit antenna array will be calculated at BER = 10^{-3} for each cell environment and M value, and the results will be added to those of Figures 3.22–3.25. This will enable us to compare the performance of minimum BER with the performance of the other techniques (especially the open loop ones). As in section 3.4, the smaller the performance loss, the better the technique performs.

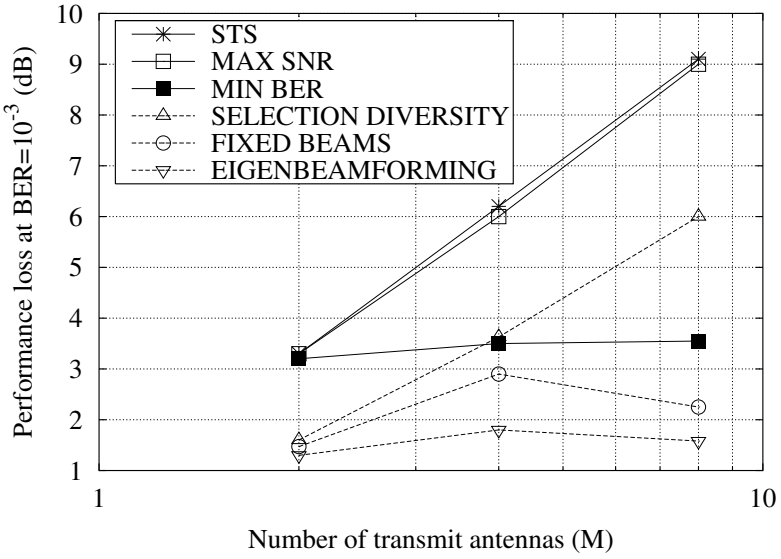

Figure 4.9: *Performance loss of the techniques at BER = 10^{-3}, including minimum BER, compared to TXAA in the macro cell.*

Figure 4.9 shows the performance loss of each technique with respect to transmit antenna array at BER = 10^{-3}, as a function of the number of transmit antennas in the macro cell (it is essentially the same as Figure 3.22 of page 59, but with additional results for minimum BER). Solid curves correspond to open loop techniques while dashed curves correspond to closed loop techniques. The results show that when $M = 2$, minimum BER provides performance very similar to that of the other two open loop techniques. However, the minimum BER performance loss increases very little with $\log(M)$ (less than 0.35 dB when M increases from 2 to 8), in contrast with the other two open loop techniques whose performance loss increases by a much

larger amount with log(M). This means that minimum BER is able to exploit the underlying structure of the macro cell much better than the other open loop techniques, providing the best performance among them when $M = 4$ and $M = 8$ in this scenario. Also, the minimum BER performance is better than that of the closed loop technique selection diversity for $M = 4$ and $M = 8$ (it is marginally better when $M = 4$ and better by a larger amount when $M = 8$). This can be attributed to the fact that selection diversity lacks beamforming gain and yields only diversity gain, which is small in the highly correlated environment of the macro cell (as has also been noted in Chapter 3). In addition, when $M = 4$ minimum BER performs almost as well as the closed loop technique fixed beams.

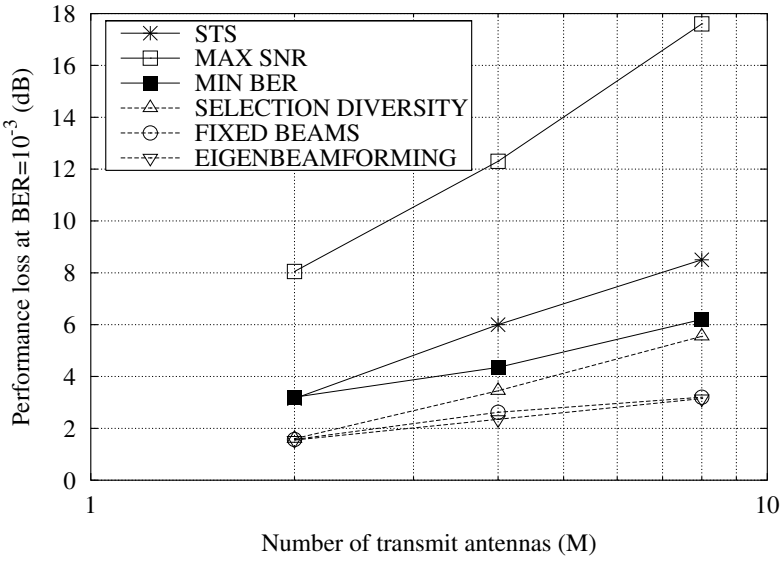

Figure 4.10: *Performance loss of the techniques at BER* $= 10^{-3}$*, including minimum BER, compared to TXAA in the micro cell.*

Next, Figure 4.10 shows the performance loss of each technique with respect to transmit antenna array at BER $= 10^{-3}$, as a function of the number of transmit antennas in the micro cell (it is essentially the same as Figure 3.23 of page 60, but with additional results for minimum BER). The results show that when $M = 2$ minimum BER yields the same performance as space-time spreading, while both of them are much better than maximum SNR. However, as M increases minimum BER is again able to exploit the channel environment better than space-time spreading, becoming better than it for $M = 4$ and $M = 8$ (by about 1.65 dB and 2.3 dB respectively). Also, as M increases the difference between the minimum BER and selection diversity performance becomes smaller, and the former approaches the latter closely for $M = 4$

and $M = 8$ (within 0.9 dB and 0.65 dB respectively).

Next, Figure 4.11 shows the performance loss of each technique with respect to transmit antenna array at BER = 10^{-3}, as a function of the number of transmit antennas in the pico cell (it is essentially the same as Figure 3.24 of page 62, but with additional results for minimum BER). The results of this figure show that the minimum BER performance is almost identical to the performance of the space-time technique. This is also confirmed by the results of Figures 4.4–4.6, which show that the number of eigenvectors that the base station uses in the pico cell is equal to the number of antennas ($K = M$), making the minimum BER performance essentially the same as that of space-time spreading.

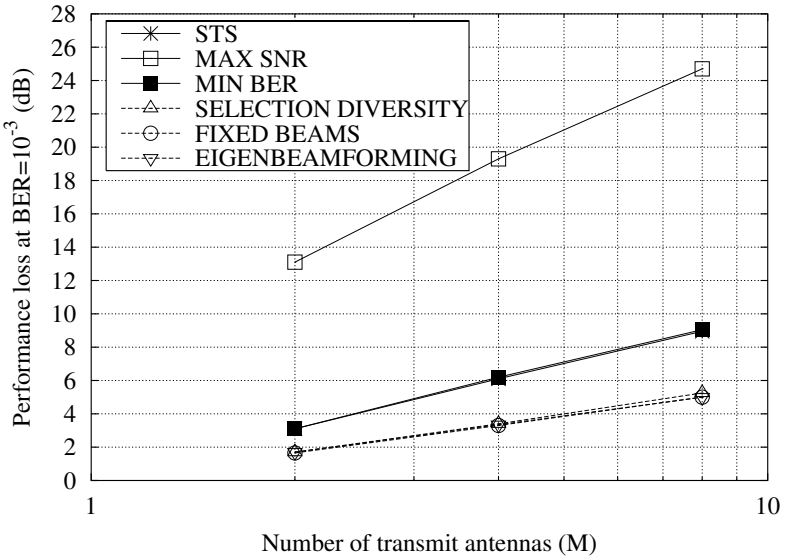

Figure 4.11: *Performance loss of the techniques at BER = 10^{-3}, including minimum BER, compared to TXAA in the pico cell.*

Finally, Figure 4.12 shows the performance loss of each technique with respect to transmit antenna array at BER = 10^{-3}, as a function of the number of transmit antennas in the 2-tap scenario (it is essentially the same as Figure 3.25 of page 63, but with additional results for minimum BER). The results show that when $M = 2$, minimum BER is the same as maximum SNR, while both of them are better than space-time spreading. Also, even though the minimum BER performance loss increases when M becomes larger than 2, the technique is still better than space-time spreading, while it also becomes better than maximum SNR (whose performance loss increases by a much larger amount than minimum BER). In addition, minimum BER is

better than the closed loop technique selection diversity for all M values. This is probably because selection diversity uses only one antenna element for downlink transmission so it lacks beamforming gain (even though it benefits from the information feedback about the antenna element with the highest SNR).

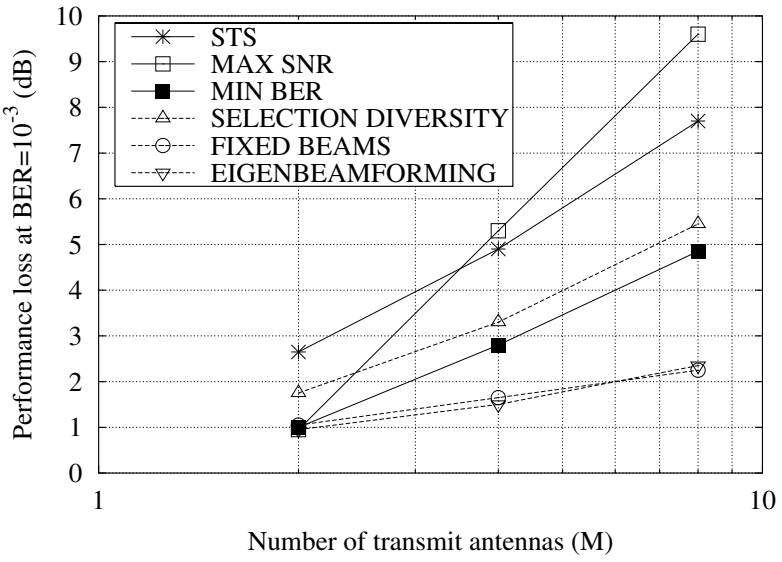

Figure 4.12: *Performance loss of the techniques at BER* $= 10^{-3}$*, including minimum BER, compared to TXAA in the 2-tap channel propagation environment.*

Figures 4.9–4.12 show that in general minimum BER provides the largest performance improvement over the other open loop techniques when the number of antennas is relatively large (i.e. $M = 4$ and $M = 8$). When M is relatively large, the possible number of eigenvectors that can be used by the base station is also large. Therefore, the technique can choose from a larger number of possible solutions to the optimisation problem of minimising the required SNR for the target BER. That is, it has more 'freedom' to yield a better solution and a larger performance improvement. On the other hand, when M is small (i.e. $M = 2$) the technique can only choose either $K = 1$ or $K = 2$, providing performance identical to that of another open loop technique (maximum SNR or space-time spreading, respectively). Figures 4.9–4.11 show also that minimum BER provides the largest performance improvement in the macro and micro cell, while in the pico cell its performance is the same as that of space-time spreading. This confirms the argument that minimum BER is most beneficial in channel environments with small to moderate angular spread.

Finally, in minimum BER the base station attempts to minimise the SNR (i.e. transmit power)

that is needed to achieve a specific target BER at the mobile station by using a specific number of eigenvectors as beamformers. However, this does not guarantee that the target BER will be achieved eventually at the mobile station, as the final BER is also affected by other factors not taken into account here, such as multiple access interference (MAI). Thus, the transmit power may have to be increased in order to achieve the target BER. However, the final transmit power (including any potential increase because of other factors) is still minimised by the minimum BER technique.

4.6 Summary

In this chapter we examined the decomposition of the channel into independent components by means of eigenvalue decomposition of its correlation matrix. The observations of this examination motivated the investigation of the combination of the channel components and space-time processing as an efficient open loop approach to the downlink data signal transmission. The approach was applied to optimise a performance criterion which attempts to minimise the transmit power required to achieve a target BER at the mobile station. This is done by employing for downlink transmission the number of channel components that provides the lowest required SNR to achieve the target BER at the mobile receiver. We named this scheme minimum BER. As the channel conditions (in the form of angle of arrival/departure and angular spread) change, the technique can use a different number of components for data signal transmission, optimising performance in all channel conditions. Also, the technique can be operated in an open loop mode by using the eigenvectors of the uplink channel correlation matrix for downlink transmission (similarly to maximum SNR, described in section 3.1.2, page 31).

The theoretical performance of minimum BER in a 1-tap scenario was calculated in terms of the eigenvalues of the mean channel correlation matrix, and it was shown that its behaviour varies from pure beamforming all the way to pure diversity. Beamforming gain only is provided when the technique uses only the principal channel component for downlink transmission. The SNR in this case is proportional to the principal eigenvalue of the channel correlation matrix. When the number of the used channel components is larger than one and smaller than the number of transmit antennas in the base station, the technique provides hybrid beamforming and diversity gain in the domain of eigenvalues. The order of the diversity part of the gain is the same as the number of components used, which in turn is determined by the channel conditions as represented by the angle of arrival/departure and angular spread. The SNR in this

case is proportional to the sum of the eigenvalues corresponding to the channel components used for downlink transmission. Finally, when the number of the used components is equal to the number of transmit antennas in the base station, the technique yields the same performance as space-time spreading, which is a pure diversity technique. This means that it effectively provides only diversity gain, the order of which is equal to the number of transmit antennas.

Furthermore, minimum BER was simulated by means of Monte Carlo simulation in an open loop mode. The simulations were performed in three representative 1-tap cells and one 2-tap scenario, and the results were compared to those of the techniques of Chapter 3. The comparisons showed that minimum BER provides the best performance among all the examined open loop techniques at the BER for which its performance was optimised. In addition, the results showed that in general minimum BER is mostly beneficial in scenarios with small to moderate angular spread values. This may be explained by the fact that none of the existing open loop techniques yields the maximum expected performance in these conditions. Moreover, the performance improvement provided by the technique generally increases as the number of base station transmit antennas increases. This may be explained by the fact that, as the number of transmit antennas increases, the optimisation procedure gains more 'freedom' to yield a better solution.

Chapter 5
Effect of imperfect parameter estimation on the performance of downlink antenna array techniques

In the simulation results presented in Chapters 3 and 4 we assumed that both the base station and the mobile station had access to perfect (i.e. noiseless) estimates of all the unknown parameters which they needed. This assumption simplified the simulations and reduced the simulation time, facilitating the comparison of different techniques under the same conditions. Nevertheless, this is generally not true in practice, since the needed parameters are practically estimated by means of **pilot** and **feedback** signals transmitted by the base and/or mobile station [8, 72, 81, 123, 149, 185]. **Pilot** signals are signals whose value is known at both the transmitter and the receiver, and are transmitted at known and pre-defined time intervals to facilitate procedures such as synchronisation between transmitter and receiver, and estimation of various parameters needed by the receiver and/or the transmitter. **Feedback** signals are signals which are used for transmission of various parameters from one end of the transmission link (e.g. mobile station) to the other end (e.g. base station), and are generally transmitted when these parameters are needed or their value changes and must be updated. Examples of parameters that usually need to be estimated in practice include the coefficients of the uplink and downlink channel, and the channel correlation matrix. Since the pilot signals used for parameter estimation are noisy, the procedure of estimating the needed parameters from them results in noisy parameter estimates. Consequently, the performance of the techniques in practice will be poorer than is depicted in the figures containing simulation results in Chapters 3 and 4. The impact of the noisy parameter estimates is important, since it is a major factor affecting the overall performance.

In this chapter, we examine various types of pilot signals and their effect on the performance of the downlink antenna array algorithms in which they are used. A number of different types of pilot signals are described, along with the procedure of estimating the relevant parameters from them, and then their impact on the performance of various algorithms is examined by means

of computer simulations. This examination shows that in general different algorithms need to estimate different parameters by means of different types of pilot signals, and even the same kind of pilot signals may have different impact on different algorithms. Also, depending on the type of pilot signals and the parameters that are estimated from them, the impact often depends on the number of transmit antennas in the base station and/or the SNR value, and sometimes even on the channel scenario.

5.1 Two basic approaches to the transmission of pilot signals

Before moving on to the description of various types of pilot signals, we shall briefly describe two basic approaches to the transmission of pilot signals, and the multiplexing of these signals with the data signals over time. These approaches were not chosen because they are the only ones or the most efficient ones, but because they are useful in presenting the basic concepts which will be used in the simulations of this chapter.

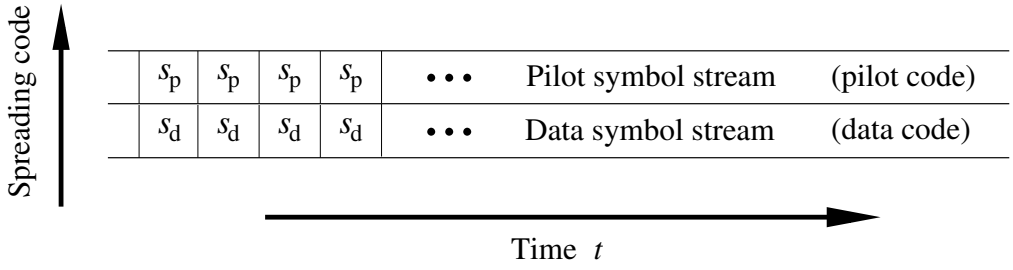

Figure 5.1: *Simple schematic representation of a sequence of pilot symbols s_p which is transmitted at the same time as the sequence of the data symbols s_d (e.g. using different spreading codes).*

According to the first approach, the pilot signals s_p are transmitted at the same time as the data signals s_d, each having the form of a stream of continuous symbols, as shown in Figure 5.1. To avoid excessive mutual interference between the pilot and data symbol streams, the transmitter may use different orthogonal spreading codes for the two streams. This may not eliminate the mutual interference completely as the orthogonality between the two codes may be lost due to multipath propagation (see Figure 2.12 on page 21), but usually such interference is not too significant. The pilot and data streams may also be I/Q code multiplexed, as is noted in the specifications of [9] and shown schematically in Figure 2.7 (page 13). Furthermore, in the case where the signals of Figure 5.1 are transmitted from base station to mobile station(s),

it is not necessary that each mobile station of a given cell sector be allocated its own distinct pilot spreading code, but the same pilot spreading code may be shared among all users of the cell sector in question to avoid wasting resources in the form of spreading codes. Moreover, while in Figure 5.1 the data and pilot signals have the same duration, in practice their duration may be different, as noted in the specifications of [9].

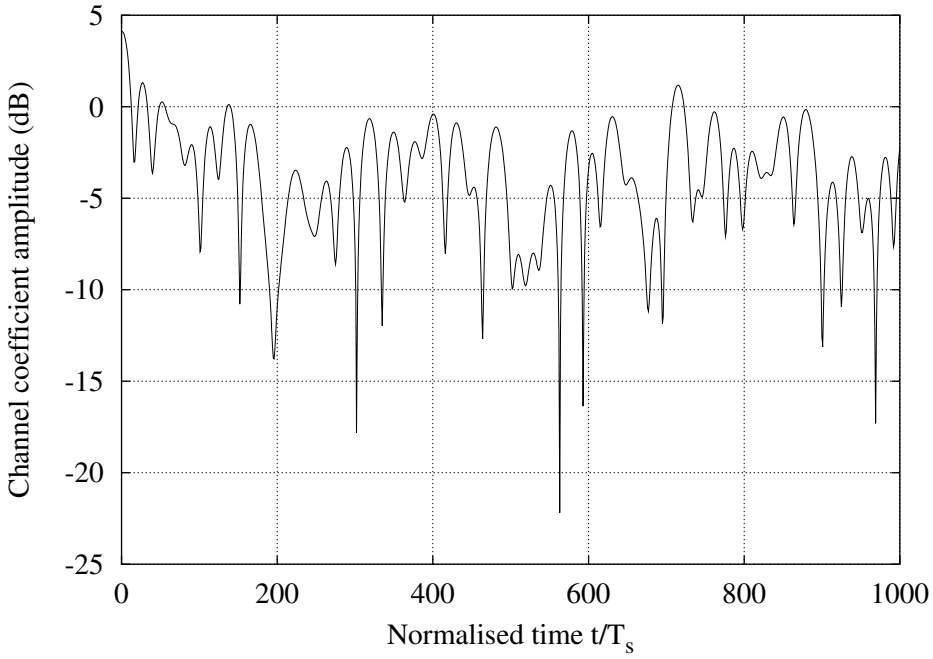

Figure 5.2: *Rapid variation of the channel amplitude (in dB) over time due to large Doppler frequency shift (maximum Doppler frequency shift $f_{D,max}$ = 220 Hz and symbol period T_s = 104.2 μsec). The plot was generated by implementing equation (2.5) (page 21) on a computer.*

Since pilot signals are transmitted continuously, this approach may be useful in cases where the parameters that need to be estimated from pilot signals change rapidly and their continuous estimation is necessary to obtain estimates that are close to their real values. An example of such a parameter is the amplitude of a channel which is rapidly changing over time, due to large Doppler frequency shift of a fast moving mobile user. The rapid variation of the amplitude of such a channel is shown in Figure 5.2 for a maximum Doppler frequency shift of $f_{D,\max}$ = 220 Hz and a symbol period of T_s = 104.2 μsec (comparison of Figure 5.2 with Figure 2.14 on page 23, where $f_{D,\max}$ = 110 Hz, shows that the channel fading is more rapid in the former, i.e. a given negative threshold such as −5 dB or −10 dB is crossed many more times per time unit in Figure 5.2 than in Figure 2.14).

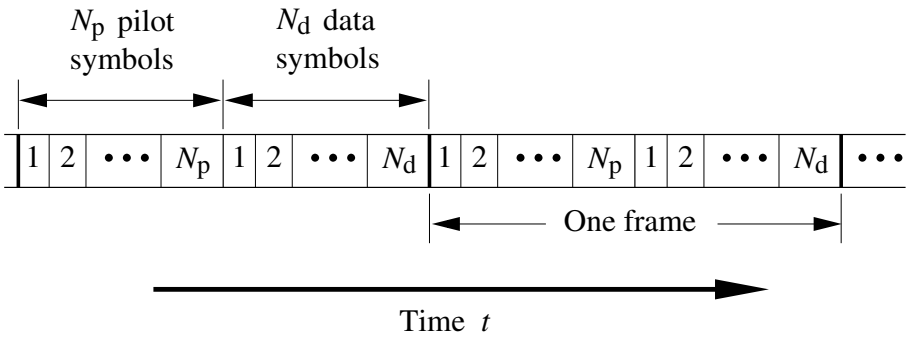

Figure 5.3: *Simple schematic representation of two frames over time, each of which includes a sequence of N_p pilot symbols followed by a sequence of N_d data symbols.*

Another basic approach to the pilot signal transmission is shown in Figure 5.3. It does not involve continuous pilot signal transmission, but uses the concept of 'frames'. Each frame is basically a group of symbols, containing N_p pilot symbols time multiplexed with N_d data symbols. This scheme is described in the specifications of the downlink of third generation mobile communication systems [9] (Figure 2.8 on page 14 also shows a schematic diagram of it[1]), and is also used in current GSM systems. In principle, the needed parameters are estimated during the transmission of the pilot symbols and their estimated values are then used during the transmission of the data symbols. Since the pilot signals are not transmitted continually but periodically, this approach may be suitable for estimation of parameters that do not change rapidly over time. Examples of such parameters include channels where the maximum Doppler frequency shift is much smaller than the number of frames per second, and the mean correlation matrix of the channel (and, consequently, its eigenvalues and eigenvectors) which changes relatively slowly as it is averaged over fading. Also, an advantage of this scheme is that the pilot and data symbols do not produce interference to each other. Finally, even though the pilot symbols of each frame in Figure 5.3 are grouped together over time and transmitted as a group, in practice they may also be mixed with the data symbols and transmitted in smaller groups or even individually within each frame, depending on the particular communication system implementation. In the next section we will describe how various parameters are estimated from pilot signals, making use of the two basic approaches that were described in this section.

[1] In Figure 2.8 each frame contains additional signals, such as transmit power control (TPC) and transport format combination indicator (TFCI) signals, but for simplicity these signals are not shown in Figure 5.3 since they are not relevant to the context of this chapter.

5.2 Parameter estimation from pilot signals

In this section we will describe various pilot and feedback signals, as well as the procedure employed to estimate the required parameters from them.

5.2.1 Estimation of downlink channel at mobile station

When the base station transmits the data signal to the intended mobile station, the latter must estimate either the channel or its impact on the transmitted signal, in order to be able to coherently demodulate the received signal and obtain an estimate of the transmitted data signal[2]. The estimates of the channel or its impact are practically obtained by means of pilot signals, which have known values and are transmitted from base station to mobile station at known time intervals to facilitate their acquisition by the latter.

For instance, if $s_d(t)$ is the data signal to be transmitted from base to mobile station, a simple beamforming base station (e.g. the base station of the maximum SNR or fixed beams techniques) typically transmits the vector signal $\mathbf{x}_d^{\mathrm{H}}(t)$ which is written as follows

$$\mathbf{x}_d^{\mathrm{H}}(t) = \sqrt{E_d} c_d(t) s_d(t) \mathbf{w}^{\mathrm{H}}, \tag{5.1}$$

where E_d is the transmit power of the data signal, $c_d(t)$ the spreading code corresponding to the data signal of the intended mobile user (which may be real or complex) and $\mathbf{w}^{\mathrm{H}} \in \mathbb{C}^{1\times M}$ the beamforming vector[3]. The single-antenna mobile receiver receives the signal $y_d(t)$ which, after de-spreading with the code $c_d(t)$ (or $c_d^{\mathrm{H}}(t)$, in case of complex spreading codes [160]), is written as

$$y_d(t) = \sqrt{E_d} s_d(t) \underbrace{\mathbf{w}^{\mathrm{H}} \mathbf{h}_d}_{\zeta_d} + n(t) = \sqrt{E_d} \zeta_d s_d(t) + n(t), \tag{5.2}$$

where $\mathbf{h}_d \in \mathbb{C}^{M\times 1}$ is a sample of the channel vector taken by the mobile station at the time of reception of $y_d(t)$, $n(t)$ is a sample of a white Gaussian stochastic process [162] representing the thermal noise due to the electronics of the receiver which appears as an additive noise term [176], and the complex number ζ_d represents the combined effect of the weight vector and

[2]The same happens when a mobile station transmits a data signal to the base station, as the latter generally has to estimate either the channel or its impact on the transmitted signal, but here we will only concern ourselves with the transmission from base station to mobile station (i.e. downlink).

[3]The transmitted signal in practical mobile communication systems typically includes additional factors such as error correction codes, scrambling codes and cell-specific codes [8], but these are not included in equation (5.1) for the sake of simplicity

the channel on the transmitted data signal (which was referred to as the 'impact' of the channel on the transmitted signal in the beginning of this section). The mobile receiver now obtains an estimate $\hat{s}_d(t)$ of the transmitted signal $s_d(t)$ as follows

$$\hat{s}_d(t) = \zeta_d^* y_d(t) = \underbrace{\sqrt{E_d}|\zeta_d|^2}_{\tilde{E}_d} s_d(t) + \underbrace{\zeta_d^* n(t)}_{\tilde{n}(t)} = \tilde{E}_d s_d(t) + \tilde{n}(t). \tag{5.3}$$

However, in order to obtain the estimate $\hat{s}_d(t)$ as shown in the above equation, the mobile receiver needs to know the impact of the channel on the transmitted signal, which is represented by the complex number ζ_d as noted above. To this end, the base station transmits pilot signals which are used by the mobile station to obtain ζ_d. More specifically, if the base station transmits a pilot signal $s_p(t)$, similarly to the data signal $s_d(t)$, with a value that is known to the mobile station (e.g. $s_p(t) = 1$, in the case of real BPSK signals[4]), the latter receives the corresponding signal $y_p(t)$ which, after de-spreading with the spreading code used by the base station during transmission of $s_p(t)$, is written as

$$y_p(t) = \sqrt{E_p} s_p(t) \underbrace{\mathbf{w}^{\mathrm{H}} \mathbf{h}_p}_{\zeta_p} + n(t) = \sqrt{E_p} \zeta_p s_p(t) + n(t), \tag{5.4}$$

where E_p is the transmit power corresponding to the pilot signal, $\mathbf{h}_p \in \mathbb{C}^{M\times 1}$ is a sample of the channel vector taken by the mobile station at the time of reception of $y_p(t)$, $n(t)$ is a sample of a white Gaussian stochastic process representing the thermal noise due to the electronics of the receiver, and the complex number ζ_p represents the combined effect of the weight vector and the channel on the transmitted pilot signal. Assuming for simplicity of analysis that $s_p(t) = 1$ and that the mobile station knows the power of the transmitted pilot signal[5], it uses $y_p(t)$ to obtain an estimate $\hat{\zeta}_p$ of ζ_p as follows

$$\hat{\zeta}_p = \frac{1}{\sqrt{E_p}} y_p(t) = \zeta_p + \frac{n(t)}{\sqrt{E_p}}. \tag{5.5}$$

We note that, as it is intuitively expected, the higher the power of the pilot signal E_p, the more closely the $\hat{\zeta}_p$ estimate is to the real value of ζ_p.

In the above simple analysis, if the pilot signals are transmitted as shown in Figure 5.1, the

[4] We note that the actual values of the pilot signals are not very important. Nevertheless, they may need careful design when the pilot signals are also used for synchronisation purposes.

[5] This may not be true in a practical system with fast power control.

channel affecting the pilot signals is the same as that affecting the data signals $\mathbf{h}_p = \mathbf{h}_d$ and, thus, $\zeta_p = \zeta_d$. On the other hand, if the pilot signals are transmitted as shown in Figure 5.3, the mobile station obtains N_p estimates of the ζ_p parameter from the N_p pilot signals, written as $\hat{\zeta}_{p,i}$, $i = 1..N_p$. These estimates can now be used to calculate the $\hat{\zeta}_p$ that will be used in equation (5.3). For instance, they can be averaged (after possibly being weighted) as follows

$$\hat{\zeta}_p = \frac{1}{N_p} \sum_{i=1}^{N_p} \hat{\zeta}_{p,i}. \tag{5.6}$$

Also, if the pilot signals are grouped in smaller groups which are mixed with the data signals within each frame of Figure 5.3, the averaging process can be applied to different groups individually. Once $\hat{\zeta}_p$ is obtained using either equation (5.5) or (5.6), it can be used in the place of ζ_d in equation (5.3) for the acquisition of the data signal estimate $\hat{s}_d(t)$.

The procedure of channel estimation that was described above applies in general to all the beamforming techniques that were analysed in Chapters 3 and 4. More specifically, it applies to maximum SNR, transmit antenna array, fixed beams and eigenbeamforming, which use one beam for data signal transmission. Also, in the case of the minimum BER technique, if it uses more than one eigenbeam for data signal transmission, the above procedure applies to each of the eigenbeams. That is, the base station transmits pilot signals through each eigenbeam and the mobile station estimates the impact of the channel on each of them according to the above procedure. Furthermore, the same basic principle applies also to the diversity techniques space-time spreading and selection diversity. More specifically, in space-time spreading with M transmit antennas the mobile station needs to estimate all M channel coefficients. Therefore, the base station transmits pilot signals from all M antennas in a way that the mobile station is able to differentiate among them (e.g. by using M different pilot spreading codes on the M antennas, as done by means of the downlink common pilot channel (CPICH) [9]). Then, the mobile station repeats the process of obtaining $\hat{\zeta}_p$ (which was described in the last paragraph) for each of the M channel coefficients. We note that in this case the ζ_p parameter of equations (5.2)–(5.5) does not contain the effects of any weight vector (since there is not one), but just represents one coefficient of the channel vector. Finally, the procedure of downlink channel estimation in selection diversity is the same as in space-time spreading, but now only one of the M channel coefficients is estimated, since the base station uses only one antenna element for data signal transmission.

5.2.2 Estimation of channel correlation matrix

Pilot signals are also used for the estimation of the mean channel correlation matrix in techniques where this is needed (e.g. maximum SNR). Since the mean channel correlation matrix is calculated from the channel vector itself, its estimation is basically equivalent to the problem of estimating the channel vector. This procedure was described in the previous section and everything that was said there applies also here. However, given that the channel correlation matrix is typically needed at the base station, its estimation involves two different approaches: 1) estimation of the downlink correlation matrix at the mobile station and then feedback of the matrix or (some of) its eigenvectors to the base station, and 2) estimation of the uplink correlation matrix at the base station.

Let us examine the former case first. The mobile station estimates the downlink channel from pilot signals transmitted by the base station. If the pilot signals are transmitted continually as shown in Figure 5.1, the mobile station can estimate the downlink channel vector $\mathbf{h}$ over each pilot symbol and then use this channel vector to update the correlation matrix $\mathbf{R}$ as follows [48]

$$\mathbf{R}_{\text{new}} = \alpha\mathbf{R}_{\text{old}} + (1-\alpha)\mathbf{h}_{\text{cur}}\mathbf{h}_{\text{cur}}^{\text{H}} = \alpha\mathbf{R}_{\text{old}} + (1-\alpha)\mathbf{R}_{\text{cur,INST}}, \tag{5.7}$$

where $\mathbf{R}_{\text{new}}$ is the updated correlation matrix, $\mathbf{R}_{\text{old}}$ denotes the value of the correlation matrix before the update, α is called the 'forgetting factor' with $0 < \alpha < 1$, $\mathbf{h}_{\text{cur}}$ represents the channel vector estimated during the current pilot symbol and $\mathbf{R}_{\text{cur,INST}}$ is the current instantaneous correlation matrix calculated from the current channel vector $\mathbf{h}_{\text{cur}}$. Consequently, the correlation matrix includes information about past, but recent, channel conditions, as well as information about the new channel conditions, both of which are necessary for the averaging process. Once the correlation matrix is updated, then it is either fed back to the base station, or it is subject to eigenvalue decomposition and (some of) its eigenvectors are fed back to the base station[6]. If the channel conditions change relatively slowly, the update of the correlation matrix may not be performed over every pilot symbol but less often (e.g. every 5 or 10 symbols). This is done to decrease the computational load needed for its update and its further processing (such as eigenvalue decomposition), and the feedback rate required for sending it or (some of) its eigenvectors back to the base station. On the other hand, if the pilot signals are transmitted in groups

[6]As noted in Chapter 3, in the 3GPP specifications for closed loop transmit diversity with $M = 2$ transmit antennas, the mobile station feeds back to base station the phase (and possibly amplitude) adjustment of the second antenna with respect to the first antenna [11].

as shown in Figure 5.3, the mobile station can obtain the N_p correlation matrices over the N_p pilot symbols and then update the old value of the correlation matrix as shown in equation (5.7). The updated correlation matrix is then processed further as above.

Now let us move on to the case where the base station estimates and uses the uplink channel correlation matrix. On this occasion, the base station needs to estimate the uplink channel from pilot signals transmitted by the mobile station. However, the mobile station may not be able to transmit pilot signals continuously as shown in Figure 5.1 due to power shortage (since it is practically powered by batteries). Therefore, it is more likely that the mobile station transmits pilot signals in groups as shown in Figure 5.3, which will be discussed here. The transmission of pilot signals in groups by the mobile station is the same as the corresponding pilot signal transmission by the base station, which was described in the previous section. More specifically, the base station can obtain the N_p correlation matrices over the N_p pilot symbols, and use them to update the old correlation matrix as shown in equation (5.7). Finally, once the updated correlation matrix becomes available, it can decompose it into eigenvalues and eigenvectors which will be used for downlink transmission.

In equation (5.7), each sample of the channel vector $\mathbf{h}_{\text{cur}} \in \mathbb{C}^{M\times 1}$ contains the noiseless channel vector, perturbed by noise, and can be written as follows

$$\mathbf{h}_{\text{cur}} = \mathbf{h} + \mathbf{n}, \tag{5.8}$$

where $\mathbf{h} \in \mathbb{C}^{M\times 1}$ is the noiseless channel vector while $\mathbf{n} \in \mathbb{C}^{M\times 1}$ represents the noise vector due to noisy estimates of the M channel coefficients. Therefore, each sample of the instantaneous channel correlation matrix $\mathbf{R}_{\text{cur,INST}} \in \mathbb{C}^{M\times M}$ contains the noiseless instantaneous correlation matrix plus a number of noise terms:

$$\mathbf{R}_{\text{cur,INST}} = \mathbf{h}_{\text{cur}}\mathbf{h}_{\text{cur}}^{\text{H}} = \mathbf{h}\mathbf{h}^{\text{H}} + \mathbf{h}\mathbf{n}^{\text{H}} + \mathbf{n}\mathbf{h}^{\text{H}} + \mathbf{n}\mathbf{n}^{\text{H}}. \tag{5.9}$$

From the last equation, the mean value of the instantaneous sample correlation matrix can be calculated as follows

$$\begin{aligned}\overline{\mathbf{R}}_{\text{cur,INST}} = \text{E}[\mathbf{R}_{\text{cur,INST}}] &= \underbrace{\text{E}[\mathbf{h}\mathbf{h}^{\text{H}}]}_{\overline{\mathbf{R}}} + \underbrace{\text{E}[\mathbf{h}\mathbf{n}^{\text{H}}]}_{0} + \underbrace{\text{E}[\mathbf{n}\mathbf{h}^{\text{H}}]}_{0} + \underbrace{\text{E}[\mathbf{n}\mathbf{n}^{\text{H}}]}_{\sigma_n^2\mathbf{I}} \\ &= \overline{\mathbf{R}} + \sigma_n^2\mathbf{I},\end{aligned} \tag{5.10}$$

where $\overline{\mathbf{R}} \in \mathbb{C}^{M\times M}$ is the mean value of the noiseless correlation matrix, σ_n^2 denotes the noise power spectral density and $\mathbf{I} \in \mathbb{C}^{M\times M}$ is the identity matrix (the two middle terms are equal to zero because the noiseless channel vector $\mathbf{h}$ is statistically independent of the noise vector $\mathbf{n}$). This suggests that the effect of the noise in the channel coefficient estimates is on average equivalent to adding the matrix $\sigma_n^2\mathbf{I}$ (scaled by $(1-\alpha)$) to the noiseless correlation matrix each time a new channel vector sample is taken into account in equation (5.7).

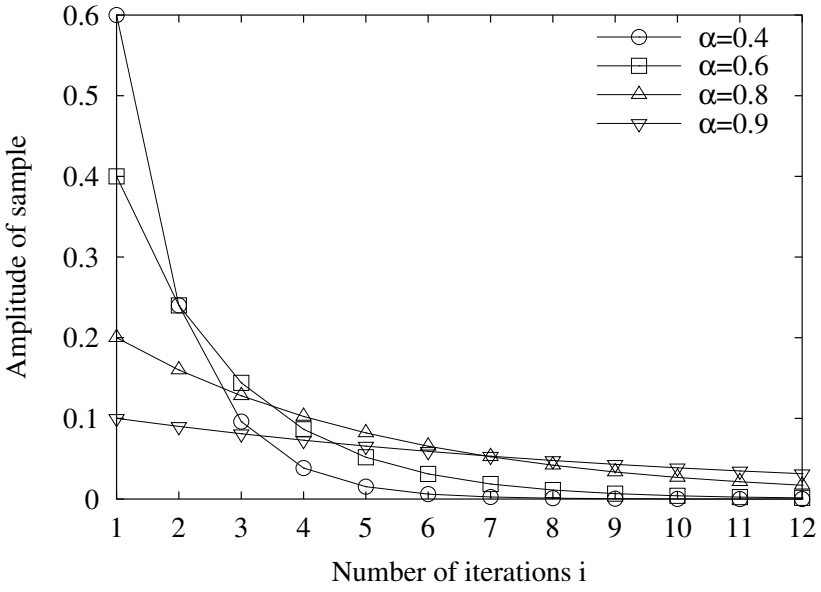

Figure 5.4: *Channel vector sample amplitude decay as the number of iterations increases for* $\alpha = 0.4, 0.6, 0.8$ *and* 0.9.

It is interesting to analyse further the behaviour of the process of obtaining the correlation matrix according to equation (5.7). In particular, our interest will focus on how long a particular channel vector sample (in the form of $\mathbf{R}_{\text{cur,INST}}$) contributes to the correlation matrix, and how many samples are effectively included in the correlation matrix. From equation (5.7), we note that the first time that a new channel vector sample is taken into account in the correlation matrix calculation (first iteration), this sample has an amplitude of $1-\alpha$. Also, after the i-th iteration ($i \geq 2$) the sample's amplitude is equal to $\alpha^{i-1}(1-\alpha)$. Figure 5.4 shows the amplitude of the sample as a function of the number of iterations for various values of the forgetting factor α. The figure suggests that the sample amplitude decay is strongly dependent on the value of α. When α is small (closer to zero), the amplitude is initially large but decays rapidly with the number of iterations. This means that new samples initially provide a large contribution to the correlation matrix, but their contribution does not last over many iterations.

The correlation matrix in this case includes mostly recent channel information. This may be useful in environments where the channel conditions (in the form of angle of arrival/departure and angular spread) change relatively fast and the correlation between recent and past temporal channel samples is relatively low, and past samples contain little information about the current conditions. In addition, the effective number of samples in the updated correlation matrix is small, since their amplitude (and consequently their contribution) becomes small quickly as the number of iterations increases (that is, the 'memory' of the process is small). On the other hand, when α is large (closer to one), the sample amplitude is initially smaller but decays more smoothly with the number of iterations. This means that new samples do not provide a large contribution to the correlation matrix, but their contribution lasts over more iterations. The correlation matrix in this case includes recent channel information as well as a good portion of past channel information. This may be useful in environments where the channel conditions (in the form of angle of arrival/departure and angular spread) change relatively slowly and the correlation between recent and past temporal channel samples is higher, and past samples contain more information about the current conditions. Moreover, the effective number of samples in the updated correlation matrix is now larger, since their amplitude (and consequently their contribution) takes more iterations to decay (that is, the 'memory' of the process is now larger).

While the above analysis may be characterised 'qualitative', the number of iterations after which each channel sample does not contribute to the correlation matrix can be quantified. It is generally known (and can be proven experimentally) that if two quantities are summed up and the second quantity is about 10 dB or more smaller than the first one, then it contributes very little to the final sum, which is almost equal to the first quantity. Therefore, we can calculate the ratio ϵ (in dB) of the amplitude of a particular sample after the i-th iteration ($\alpha^{i-1}(1-\alpha)$) over the amplitude of a new sample $(1-\alpha)$ as follows

$$\epsilon = 10\log_{10}\left(\frac{\alpha^{i-1}(1-\alpha)}{1-\alpha}\right) = 10\log_{10}\left(\alpha^{i-1}\right), \tag{5.11}$$

and assume that if the number of iterations i is such that ϵ is smaller than -10 dB, the sample in question has ceased to contribute significantly to the correlation matrix. Figure 5.5 shows the number of iterations that are necessary to make ϵ smaller than -10, -20 and -30 dB, as a function of α. If we choose the curve of -10 dB, we see that as α increases, the sample ceases to contribute significantly to the correlation matrix after a higher number of iterations. Also, given that during each iteration exactly one sample more is added to the correlation

matrix estimate, the number of iterations represents also the effective number of samples in the correlation matrix. Consequently, the memory of the process increases with α, which confirms the 'qualitative' observations of the last paragraph. The other two curves (-20 and -30 dB) exhibit the same trend, so the conclusion holds regardless of the threshold that we choose for ϵ. Finally, we note that in the extreme case of $\alpha \to 0$ the effective number of samples approaches unity (memory approaches zero), while in the other extreme case of $\alpha \to 1$ the effective number of samples approaches infinity (memory length approaches infinity).

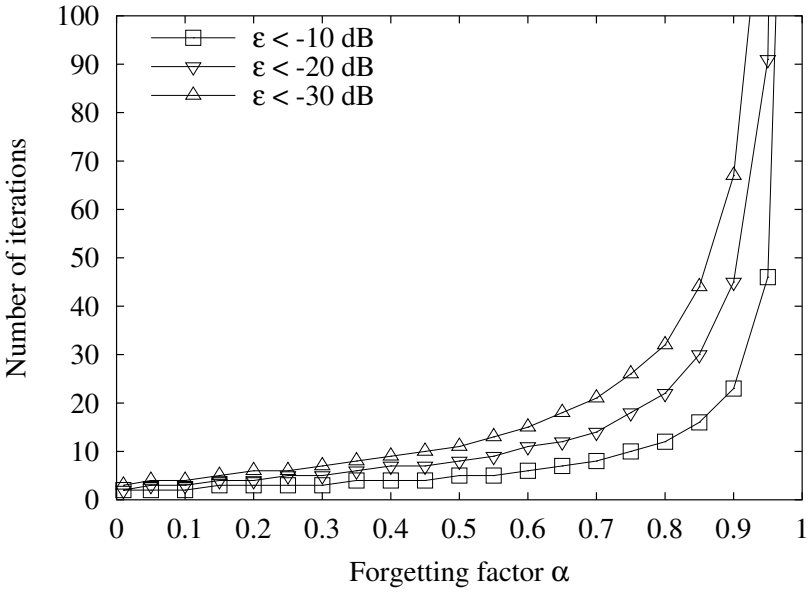

Figure 5.5: *Effective number of channel vector samples in the estimated correlation matrix as a function of the forgetting factor α.*

5.2.3 Selection of highest SNR diversity branch (antenna or beam)

Another type of pilot signal is the one that is used for selection of the antenna or beam that yields the highest SNR at the mobile receiver in the techniques selection diversity (description on page 36) and fixed beams (description on page 38), respectively. These pilot signals are transmitted by the base station through each antenna or beam, and used at the mobile station to measure the SNR of the M antennas or beams. From equation (5.4), if $s_{p,i}(t)$ is the pilot signal transmitted by the base station through the i-th diversity branch (antenna or beam), the signal that the mobile station receives is written as (after de-spreading with the corresponding

spreading code)

$$y_{p,i}(t) = \sqrt{E_{p,i}}\zeta_{p,i}s_{p,i}(t) + n(t), \tag{5.12}$$

where $\zeta_{p,i}$ was called the 'impact' of the channel on the transmitted pilot signal. If $s_{p,i}(t)$ is transmitted through the i-th transmit antenna of the base station (that is, in selection diversity), then $\zeta_{p,i}$ represents only a sample of the channel coefficient h_i between this i-th antenna and the single receiving antenna, taken by the mobile station at the moment of reception of $y_{p,i}(t)$, $\zeta_{p,i} = h_i$ with $i = 1..M$. On the other hand, if $s_{p,i}(t)$ is transmitted through the i-th beam formed by the base station (that is, in fixed beams), then $\zeta_{p,i}$ includes both the weight vector corresponding to the i-th beam $\mathbf{w}_i^{\mathrm{H}}$ and a sample of the channel vector $\mathbf{h}_i$ which affects the signal of this beam, taken at the moment of reception of $y_{p,i}(t)$, $\zeta_{p,i} = \mathbf{w}_i^{\mathrm{H}}\mathbf{h}_i$ with $i = 1..M$. In both cases, $\zeta_{p,i}$ is a complex number. Selecting the diversity branch with the highest SNR is equivalent to selecting the branch with the largest instantaneous received power when the average noise power is the same on all branches [27, 53]. Consequently, the mobile station selects the diversity branch with the largest instantaneous received power, which for the i-th branch is given by

$$A_i = |y_{p,i}(t)|^2. \tag{5.13}$$

This procedure may result in the selection of the wrong diversity branch, since the instantaneous received power of each branch is influenced by the noise term $n(t)$, as shown in equation (5.12).

In the above description, if the pilot signals are transmitted in a continuous fashion as in Figure 5.1, the mobile station has the chance to measure the SNR of the M antennas or beams over each pilot symbol, and send an index to the highest SNR antenna or beam to the base station. However, this would require a high rate feedback path, since information would need to be sent back to base station over each symbol, which may affect the uplink data rate of the system negatively. Thus, the mobile station in practice measures the SNR of the antennas or beams not over every pilot symbol but less often. For small to moderate angular spread values the frequency of these SNR measurements is expected to be higher for antennas than for beams, because a particular beam is anticipated to be used for transmission longer than a particular antenna. This is because the instantaneous SNR of an antenna changes faster and needs more frequent estimation than that of a beam, since the former is affected mainly by fast fading (Rayleigh distributed fading [24,45,63,104,176,210]) while the latter is affected mostly by slow fading (log-normal distributed fading). However, for large angular spread values the SNR of beams varies more rapidly than for small angular spread and needs to be measured as frequently

as that of antennas.

If the pilot signals are transmitted in groups within a frame as in Figure 5.3, the mobile station can average the instantaneous received power of each diversity branch over the N_p pilot symbols[7]. The branch which yields the largest average received power over these symbols is then chosen for transmission of the N_d data symbols that follow. If the channel changes rapidly, the received power measurements (especially those of an antenna) may become quickly out of date and may no longer represent reality, especially during the transmission of the data symbols that are closer to the end of the sequence of the N_d data symbols. In this case it may be useful to make smaller groups of pilot symbols and interleave them with the data symbols, so that the received power measurements are updated more often.

5.2.4 Feedback of highest SNR diversity branch (antenna or beam)

Once the diversity branch (antenna or beam) that yields the highest SNR at the mobile receiver has been identified as described above, an index to it is sent from mobile station back to base station, which then uses only this diversity branch for data signal transmission. If the number of diversity branches is M, the index that is fed back to the base station must be able to represent M different states, so the number of binary bits b that it must contain is given by

$$b = \text{ceil}\left(\log_2(M)\right), \tag{5.14}$$

where ceil(x) denotes the smallest integer number that is equal to or greater than the real number x. Also, since these feedback bits are transmitted from mobile station to base station through the channel, they are subject to distortions due to the random nature of the channel and the thermal noise of the base station receiver electronics. Therefore, the value of the index to the highest SNR diversity branch that the base station receives may change because of these distortions, and the base station may eventually use the wrong branch for data signal transmission. This results in additional performance loss, the amount of which is strongly related to the bit error ratio (BER) of the feedback path.

[7]We note that the SNR of each branch is expected to increase if it is integrated (or averaged) over multiple symbols. However, this will affect the SNR values of all the branches in the same way and will not alter the relationship among them.

5.3 Performance loss due to noisy parameter estimation

In this section we will examine the effect of the pilot and feedback signals that were described in the above few sections on the performance of various techniques by means of Monte Carlo simulations. Simulation results of the techniques will be obtained by estimating the necessary parameters through pilot signals. Then, these results will be compared to the simulation results obtained by assuming noiseless estimates of the necessary parameters, and the effect of noisy parameter estimates will be discussed. The carrier frequency used in the simulations is $f_c = 2$ GHz, the transmit antenna spacing is $D = \frac{\lambda}{2}$ and the pilot symbols have the same duration as the data symbols, unless otherwise indicated. The bit error ratio is calculated by counting and averaging the errors at the mobile receiver over a total of 10^6 data symbols transmitted by the base station.

Some of the parameters that can be estimated from pilot signals and were described in the above sections, apply to more than one downlink antenna array technique. For example, the downlink channel (or its impact on the transmitted data signal) must be estimated by the mobile station for coherent demodulation of the received signal in all the techniques. However, in order to avoid repetition of multiple sets of simulation results that effectively convey the same information, the effects of each parameter will be simulated using only selected technique(s). For instance, it is not worth presenting simulation results for all the techniques when the downlink channel is estimated at the mobile station using pilot signals, since this procedure has the same effect on the performance of all the techniques. The technique(s) that will be used for simulation of the effects of each parameter will be selected in such a way that all the relevant phenomena are exposed, while trying to minimise repetition of multiple sets of simulation results which lead to the same conclusions. Table 5.1 shows the technique(s) that will be used to simulate the effects of estimating each described parameter from pilot signals. For example, the technique space-time spreading will be used to simulate the effects of channel coefficient estimation for coherent demodulation at the mobile receiver. The technique transmit antenna array will also be used for the same purpose, as it involves the additional step of channel coefficient quantisation and feedback to base station for weight vector calculation. The table also includes brief descriptions of the procedures that will be used in each simulation, while more detailed descriptions will be given in the relevant sections. Furthermore, wherever the effect of a parameter estimation procedure on the performance of a particular technique is the same in all channel scenarios (macro, micro and pico cell), the technique will only be simulated in one scenario, which is

Parameter to be estimated	Antenna array technique to be simulated
Channel coefficient(s)	Space-time spreading (*estimation of downlink channel coefficients at mobile receiver from pilot signals transmitted by base station*) Transmit antenna array (*estimation of downlink channel coefficients at mobile receiver from pilot signals transmitted by base station, quantisation of coefficients at mobile station and feedback of them to base station, use of received channel coefficients for downlink weight vector calculation at base station*)
Correlation matrix	Maximum SNR (*estimation of uplink channel vector at base station from pilot signals transmitted by mobile station, calculation of uplink correlation matrix from uplink channel vector at base station*) Minimum BER (*same procedure as in maximum SNR*)
Selection of highest SNR branch	Selection diversity (*highest SNR antenna is chosen by mobile station from pilot signals transmitted by base station*) Fixed beams (*highest SNR beam is chosen by mobile station from pilot signals transmitted by base station*)
Feedback of highest SNR branch	Selection diversity (*index to highest SNR antenna is sent from mobile to base station*) Fixed beams (*index to highest SNR beam is sent from mobile to base station*)

Table 5.1: *Downlink antenna array technique(s) that will be used to simulate the effects of estimation of each described parameter from pilot signals.*

usually the one that enables it to provide its best performance (for instance, diversity techniques will be simulated in the pico cell where the diversity gain is maximum). On the other hand, if the parameter scenario plays an important role, the technique will be simulated in all the interesting scenarios. Table 5.2 shows the channel scenario in which each technique will be simulated, along with the characteristics of each scenario for easy reference.

5.3.1 Effect of noisy channel estimates

First we discuss the effect of noisy channel estimates at the mobile station and/or the base station. The techniques that will be used for this purpose are space-time spreading and transmit antenna array. The channel conditions for the simulations of both techniques are those of a pico cell, where the signals of different antenna elements are highly uncorrelated ($\rho_{\text{adj}} = 0.035$)

Antenna array technique	**Channel scenario**
Space-time spreading	Pico cell (AOD = 0^o, AS = 120^o, $\rho_{\text{adj}} = 0.035$)
Transmit antenna array	Pico cell (AOD = 0^o, AS = 120^o, $\rho_{\text{adj}} = 0.035$)
Maximum SNR	Macro cell (AOD = 15^o, AS = 10^o, $\rho_{\text{adj}} = 0.988$)
Minimum BER	Macro cell (AOD = 15^o, AS = 10^o, $\rho_{\text{adj}} = 0.988$) Micro cell (AOD = 30^o, AS = 45^o, $\rho_{\text{adj}} = 0.825$)
Selection diversity	Pico cell (AOD = 0^o, AS = 120^o, $\rho_{\text{adj}} = 0.035$)
Fixed beams	Macro cell (AOD = 15^o, AS = 10^o, $\rho_{\text{adj}} = 0.988$) Micro cell (AOD = 30^o, AS = 45^o, $\rho_{\text{adj}} = 0.825$) Pico cell (AOD = 0^o, AS = 120^o, $\rho_{\text{adj}} = 0.035$)

Table 5.2: *Channel scenario(s) in which the simulations of each technique are performed, along with the angle of departure (AOD) and angular spread (AS) of each scenario.*

and the diversity gain is maximised [104, 180, 250]. We assume that the base station transmits pilot signals through each transmit antenna in a continuous mode (as in Figure 5.1). Also, the mobile receiver estimates the downlink channel coefficients over each pilot symbol and uses these estimates for coherent demodulation of the corresponding data symbol (in transmit antenna array the estimated coefficients are also fed back to the base station which uses them for calculation of the weight vector). The *total* power $E_{p,\text{dB}}$ allocated to pilot signals across all M antennas is $E_{add,\text{dB}}$ dB higher than the total power $E_{s,\text{dB}}$ allocated to data signals

$$E_{p,\text{dB}} = E_{s,\text{dB}} + E_{add,\text{dB}}. \tag{5.15}$$

The total pilot power is equally shared among the M transmit antennas. Therefore, the power dedicated to the pilot signal of each transmit antenna (and consequently to the estimation of each channel coefficient) *decreases* as M increases. To minimise simulation time, the channel coefficients of consecutive data symbols are made uncorrelated with each other[8]. This is achieved by generating a different set of the Q scattered signals of equation (2.5) and recalculating the M channel coefficients anew over each data symbol (as in the simulations of Chapter 3).

Let us examine space-time spreading first. Figure 5.6 shows simulation results of space-time

[8]We note that this does not alter the simulation results, since the basic concept of estimating each channel coefficient from the corresponding pilot signal over each data symbol is again used. Also, generating temporally uncorrelated channel coefficients is equivalent to assuming very large Doppler frequency shift $f_{D,\max} \to \infty$. The latter does not affect the results in any way if the mobile station estimates the channel coefficients from pilot signals over each data symbol.

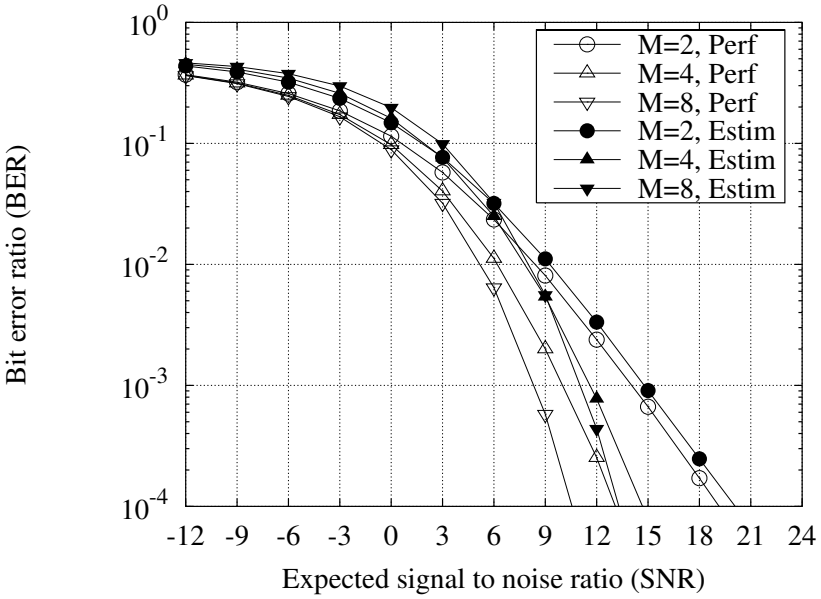

Figure 5.6: *Effect of noisy channel estimates (used by mobile station for coherent demodulation) on the performance of space-time spreading (pico cell). Total pilot power fixed and 10 dB higher than data power ($E_{add,dB} = 10$ dB).*

spreading with the above assumptions and $E_{add,\mathrm{dB}} = 10$ dB. Also, in order to facilitate comparison, it contains simulation results for the case in which the mobile station uses noiseless (perfect) downlink channel estimates and all other assumptions are as above (these results are essentially the same as the pico cell results of Figure 3.10 on page 45). The figure shows that estimation of the channel coefficients from noisy pilot signals at the mobile receiver results in a performance loss L_p. The loss does not increase as SNR increases, since the (total) pilot power is always 10 dB higher than the (total) data power. However, the loss increases with M ($L_p \simeq 0.8$ dB when $M = 2$, $L_p \simeq 1.6$ dB when $M = 4$ and $L_p \simeq 2.75$ dB when $M = 8$, all loss values measured at BER $= 10^{-3}$). This is because the pilot power dedicated to the estimation of each channel coefficient decreases with M and, therefore, the estimates of the channel coefficients become less accurate as M increases, leading to larger performance loss. Furthermore, when SNR is low (e.g. SNR $\lessapprox 3$ dB) the performance worsens with increasing M [160] (i.e. the performance with $M = 8$ is worse than that with $M = 4$ which in turn is worse than that with $M = 2$). This is because the pilot power dedicated to the estimation of each channel coefficient is already low (due to low SNR) and it becomes even lower each time M increases, resulting in less accurate channel coefficient estimates and ultimately larger performance loss. In addition, the benefit from the diversity gain is small (due to small SNR) and not able to compensate for

the increasingly larger loss. Nevertheless, this diversity gain benefit increases with SNR and starts to compensate for the loss for larger SNR values (e.g. SNR $\gtrapprox$ 3 dB).

In order to investigate the effect of the additional pilot power $E_{add,\mathrm{dB}}$, Figure 5.7 shows the loss L_p due to noisy channel estimates at the mobile receiver with respect to the noiseless channel estimates case at BER = 10^{-3}, as a function of $E_{add,\mathrm{dB}}$ and for $M = 2, 4, 8$ transmit antennas in the pico cell. As it is expected, the results suggest that the loss decreases as $E_{add,\mathrm{dB}}$ increases, since more power is dedicated to the estimation of the channel coefficients and, thus, the estimates are improved.

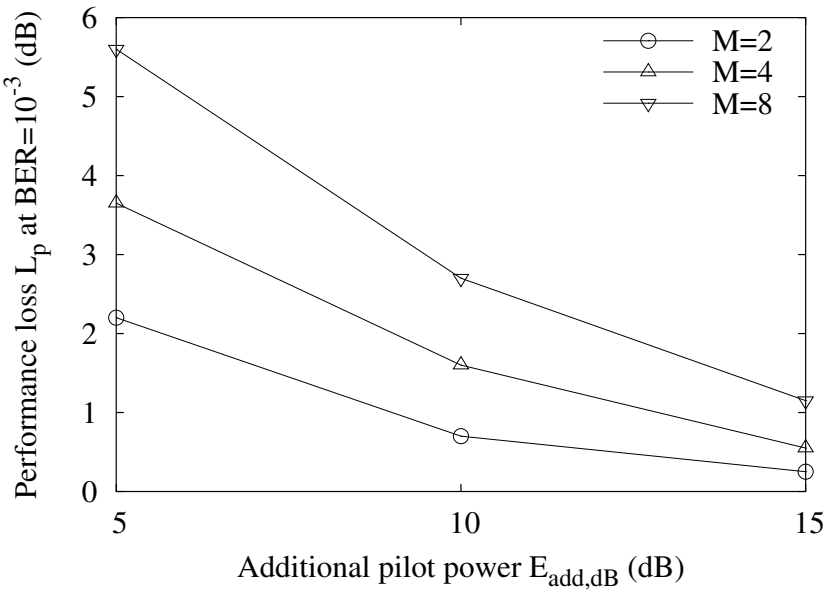

Figure 5.7: *Performance loss L_p in space-time spreading at BER = 10^{-3} due to noisy channel estimates (used by mobile station for coherent demodulation) with respect to the noiseless channel estimates case, as a function of the additional pilot power $E_{add,dB}$, and for $M = 2, 4, 8$ transmit antennas (pico cell).*

In the case where the pilot power of *each* transmit antenna is 10 dB higher than the total power of the data signal across all M antennas (i.e. the *total* pilot power across all M antennas effectively increases with M), the loss does not increase with M but is the same for all M values [120]. This is depicted in Figure 5.8, where the pilot power allocated to *each* transmit antenna is 10 dB higher than the total data signal power across all M transmit antennas (all other assumptions are the same as above). The loss now is the same for all M values and equal to about 0.5 dB. This means that if we plot the loss L_p at BER = 10^{-3} as a function of $E_{add,\mathrm{dB}}$

for $M = 2, 4, 8$ (as in Figure 5.7), the curves for $M = 2, 4, 8$ will overlap with one another. However, this approach has the significant disadvantage of increasing the total power allocated to pilot signals to high levels as M increases, which is not desired in practical implementations of mobile communication systems.

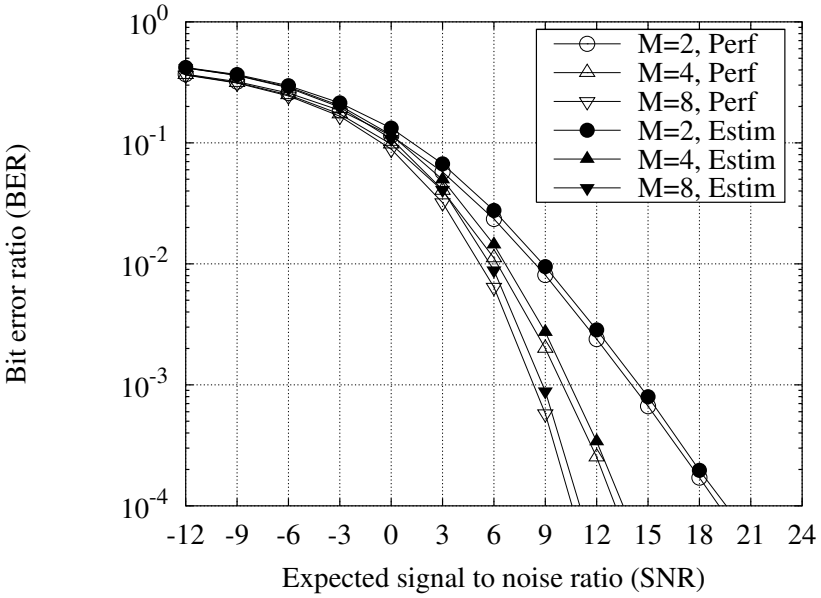

Figure 5.8: *Effect of noisy channel estimates (used by mobile station for coherent demodulation) on the performance of space-time spreading (pico cell). Total pilot power increases with M: pilot power of each antenna is 10 dB higher than total data power.*

Now we turn our attention to transmit antenna array. In this technique, not only does the mobile station use the estimated channel coefficients for coherent demodulation of the received data signals, but it also sends them back to the base station, which uses them for calculation of the weight vector. However, in order to send the coefficients back to the base station, the mobile station has to quantise them [176, 179]. The quantisation process introduces additional noise to the coefficients which will be accounted for in the simulations, according to the quantisation noise analysis of [179]. In order to quantise the i-th complex channel coefficient $h_i = h_i^{\mathrm{R}} + \jmath h_i^{\mathrm{I}} = |h_i| e^{\jmath \phi_{h_i}}$, $i = 1..M$, the mobile station can quantise either its real and imaginary part (h_i^{R} and h_i^{I}, respectively) or its amplitude and phase ($|h_i|$ and ϕ_{h_i}, respectively). We choose to quantise the real and imaginary part, as this allows for easier analysis of the quantisation noise effects. Also, we will discuss only the quantisation of the real part h_i^{R}, but everything that will be said applies also to the imaginary part h_i^{I}. To elaborate, we assume that the quantiser uses

words of $b+1$ bits and its range R_Q is equal to the range of the real part $R_{h_i^{\mathrm{R}}}$, $R_Q = R_{h_i^{\mathrm{R}}}$ (that is, the quantiser introduces no 'signal clipping' errors). The parameter h_i^{R} is a random variable following a Gaussian distribution with statistical mean $\overline{h_i^{\mathrm{R}}} = 0$ and variance $\sigma^2_{h_i^{\mathrm{R}}} = \frac{1}{2}$. Therefore, about 99% of the time its value is limited as follows $-3\sigma^2_{h_i^{\mathrm{R}}} \lessapprox h_i^{\mathrm{R}} \lessapprox 3\sigma^2_{h_i^{\mathrm{R}}}$, so its range is $R_{h_i^{\mathrm{R}}} \simeq 3\sigma^2_{h_i^{\mathrm{R}}} - (-3\sigma^2_{h_i^{\mathrm{R}}}) = 6\sigma^2_{h_i^{\mathrm{R}}} = 6\frac{1}{2} = 3$ [162, 176]. We assume that the quantisation noise n_q is uniform over $\left[-\frac{\Delta}{2}, \frac{\Delta}{2}\right]$ [179], where Δ is the step (or resolution) of the quantiser given by the following expression

$$\Delta = \frac{R_Q}{2^{b+1}}. \tag{5.16}$$

Also, the power of the quantisation noise is determined by the following relation which gives the signal to quantisation noise (power) ratio (SQNR)

$$\mathrm{SQNR} = 10\log_{10}\left(\frac{P_{h_i^{\mathrm{R}}}}{P_{n_q}}\right) = 10\log_{10}\left(\frac{\sigma^2_{h_i^{\mathrm{R}}}}{\sigma^2_{n_q}}\right) = \cdots = 6.02b + 1.25 \quad (\mathrm{dB}). \tag{5.17}$$

In summary, we simulate the effects of the quantisation process on the real part by adding to it an additional quantisation noise term n_q, which is uniform over $\left[-\frac{\Delta}{2}, \frac{\Delta}{2}\right]$ and has a power determined by equation (5.17) (when a word of $b+1$ bits is used for the quantisation). As noted above, we follow the same process also for the imaginary part h_i^{I}. In addition, the channel coefficients used by the base station for the calculation of the weight vector contain noise, because they are estimated at the mobile station from noisy pilot signals (which are transmitted by the base station). The *total* power of these pilot signals is $E_{add,\mathrm{dB}} = 10$ dB higher than the power of the data signals.

Figure 5.9 shows simulation results of transmit antenna array in the pico cell with the above assumptions. Again the *total* power $E_{p,\mathrm{dB}}$ allocated to pilot signals across all M antennas is 10 dB higher than the total power $E_{s,\mathrm{dB}}$ allocated to data signals, and this pilot power is equally shared among the M transmit antennas. The length of the word used for quantisation of the real and imaginary parts of each channel coefficient is 1 bit (that is, each channel coefficient uses a total of 2 bits for its quantisation). Also, in order to facilitate comparison, the figure contains simulation results for the case where both the mobile and base station use noiseless (perfect) downlink channel estimates and all other assumptions are as above (these results are essentially the same as the pico cell results of Figure 3.14 on page 50). The results show that the combined effects of the channel coefficient estimation noise and the quantisation noise generally result in fairly large performance loss. When SNR is small the performance is dominated by

the thermal noise in the received signal (whose power is much higher than the data signal power), and the effects of the quantisation noise do not become apparent. However, as SNR increases, the thermal noise becomes less significant and the effects of the quantisation noise start to dominate the performance. Also, the results suggest that the quantisation noise results in large performance loss, which is attributed to the fact that the number of bits used for the quantisation of the channel coefficients is small, and their quantised values are not very accurate representations of their real values.

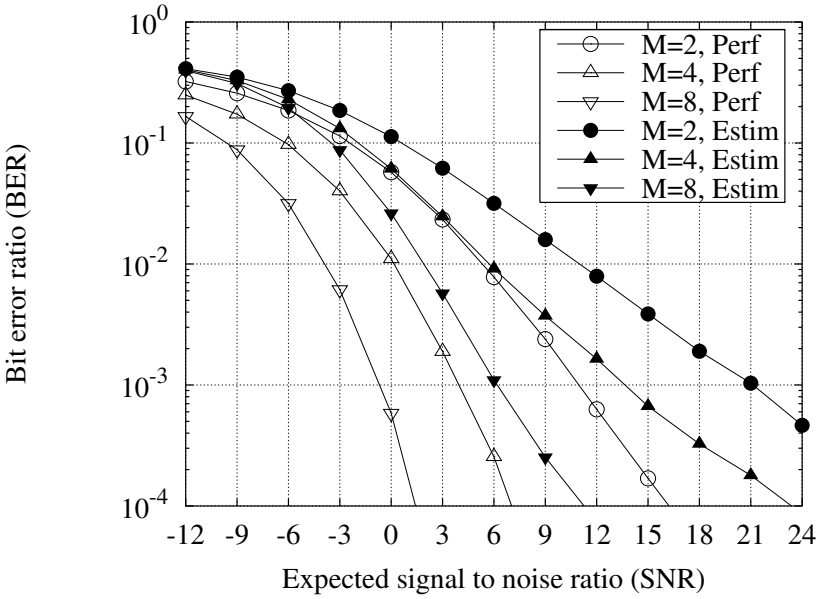

Figure 5.9: *Combined effect of noisy channel estimates (used by mobile station for coherent demodulation) and quantised channel coefficients (used by base station for weight vector calculation) on the performance of transmit antenna array (pico cell). Total pilot power is 10 dB higher than data power ($E_{add,dB}$ = 10 dB), and 1 bit is used for quantisation of real and imaginary part of each channel coefficient (2 bits per channel coefficient).*

Additionally, in order to examine the effect of using different numbers of quantisation bits, Figure 5.10 shows the performance loss L_p at BER $= 10^{-3}$ due to channel estimation and quantisation noise with respect to the noiseless channel estimates case, as a function of the number of bits used for quantisation of each channel coefficient $2(b+1)$ for $M = 2, 4, 8$ transmit antennas and $E_{add,\mathrm{dB}} = 10$ dB in the pico cell. The results suggest that as the number of quantisation bits increases, the loss becomes generally smaller. This is expected, since when the number of quantisation bits becomes larger the quantised channel coefficients become more

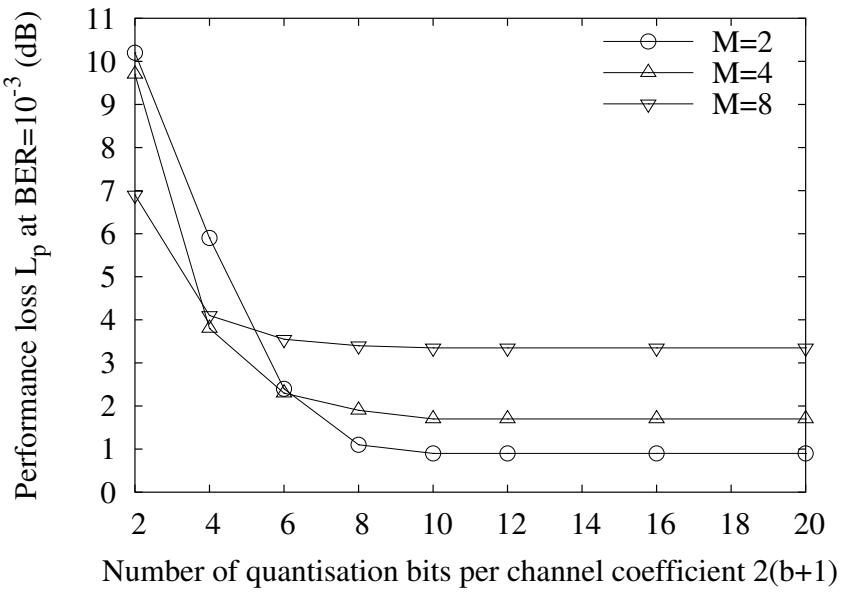

Figure 5.10: *Performance loss L_p in transmit antenna array at BER = 10^{-3} due to channel estimation and quantisation noise with respect to the noiseless and non-quantised channel estimates case, as a function of the number of bits for quantisation of each channel coefficient ($2(b+1)$), and for $M = 2, 4, 8$ transmit antennas (pico cell). Total pilot power is 10 dB higher than data power ($E_{add,dB} = 10$ dB).*

accurate representations of the actual coefficients, and the performance loss due to quantisation noise decreases. However, when $2(b + 1)$ increases above 10 the loss does not decrease further and there is no additional performance improvement. This means that when $2(b + 1) = 10$ the quantised channel coefficient values are already highly accurate representations of their real values, and increasing the number of bits further does not help improve the performance (at least at BER = 10^{-3}). Also, the loss decreases with $2(b + 1)$ more rapidly when M is small ($M = 2$) than when M is large ($M = 8$), and eventually, when $2(b + 1) \geq 10$ and the loss is purely due to estimation noise, it becomes smaller for small M than for large M. This means that when M is small most of the performance loss at BER = 10^{-3} is due to quantisation noise, while when M is large most of the performance loss at BER = 10^{-3} is due to estimation noise. Furthermore, the phenomenon that when $2(b + 1) \geq 10$ the loss increases with M, is the same as that of Figure 5.6 and happens for the same reason (namely, the pilot power allocated to the estimation of each channel coefficient decreases as M increases, leading to less accurate channel coefficient estimates and larger performance loss). Finally, Figure 5.10 shows that increasing the value of $2(b+1)$ yields a larger performance improvement when $2(b+1)$ is close

to 2 than when it is close to 10 (that is, increasing $2(b+1)$ from 2 to 4 yields larger improvement than increasing it from 8 to 10). This means that it is not necessary to use 10 quantisation bits per channel coefficient to obtain all the performance improvement, since (depending on M) a number of 4–8 bits yields most of this improvement.

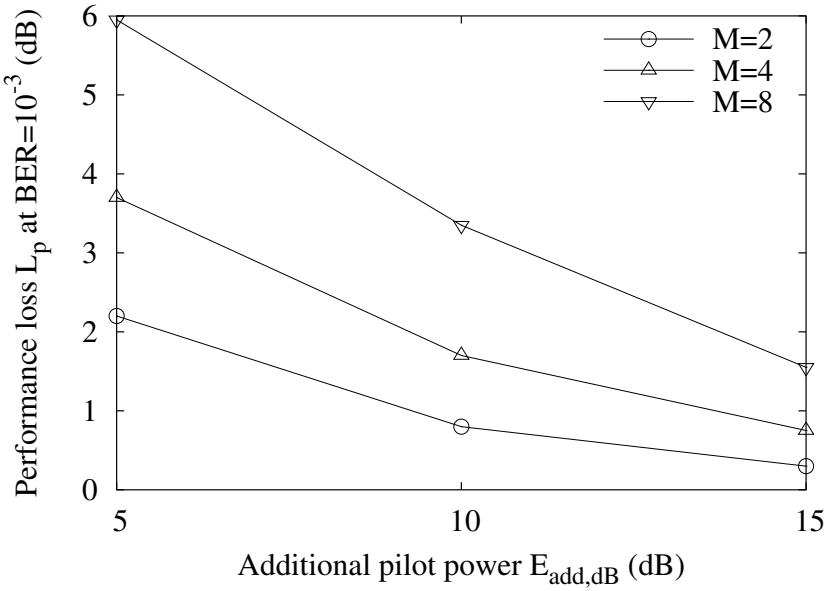

Figure 5.11: *Performance loss L_p in transmit antenna array at BER = 10^{-3} due to channel estimation noise with respect to the noiseless channel estimates case, as a function of the additional pilot power $E_{add,dB}$, and for $M = 2, 4, 8$ transmit antennas (pico cell). 10 bits are used for quantisation of each channel coefficient.*

Finally, it is interesting to investigate the effect of using different values of $E_{add,\mathrm{dB}}$. This is accomplished better when the effects of the quantisation noise have been eliminated, so we will use $2(b + 1) = 10$. Figure 5.11 shows the performance loss L_p at BER = 10^{-3} due to channel estimation noise with respect to the noiseless channel estimates case, as a function of the additional pilot power $E_{add,\mathrm{dB}}$ for $M = 2, 4, 8$ transmit antennas in the pico cell. The results show the same trend as those of Figure 5.7 and, as expected, suggest that when $E_{add,\mathrm{dB}}$ increases the loss L_p decreases.

5.3.2 Effect of noisy correlation matrix estimates

Next we move on to study the effects of imperfect correlation matrix estimates. In particular, we examine how the performance of the techniques maximum SNR and minimum BER de-

teriorates when the base station does not have access to perfect correlation matrix estimates, but obtains these estimates from pilot signals transmitted by the mobile station. We will examine the former technique first. We assume that the mobile station transmits pilot signals with power $E_{add,\mathrm{dB}}$ dB higher than that of data signals. The duration of each symbol (data or pilot) is $T_s = 14.205$ μsec while the maximum Doppler frequency shift is $f_{D,\max} = 110$ Hz (this corresponds to a mobile station speed of about 60 Km/h or 37.5 m/h at a carrier frequency of $f_c = 2$ GHz). The base station uses the pilot signals to estimate the uplink channel vector $\mathbf{h}_{\mathrm{UL}}$ and calculate the uplink mean correlation matrix $\mathbf{R}_{\mathrm{UL}}$ as shown in equation (5.7). To avoid excessive computational load at the base station, the uplink correlation matrix estimate is not updated over every data symbol but with a rate equal to the maximum Doppler frequency shift (that is, it is updated 110 times per second). Each time the correlation matrix is updated by the base station, its eigenvalue decomposition is performed and its principal eigenvector is used as weight vector until the next update. As in Chapter 3, the uplink and downlink carrier frequencies are $f_{\mathrm{UL},c} = 2.14$ GHz and $f_{\mathrm{DL},c} = 1.95$ GHz respectively, while the transmit antenna spacing is $D = \frac{\lambda_{\mathrm{MID}}}{2}$, where λ_{MID} is the wavelength of the carrier frequency $f_{\mathrm{MID},c} = \frac{f_{\mathrm{UL},c}+f_{\mathrm{DL},c}}{2}$. The simulations are performed in the macro cell where the technique provides the highest gain over the single-antenna transmitter.

Figure 5.12 shows simulation results for $E_{add,\mathrm{dB}} = 5, 10, 15$ dB, forgetting factor $\alpha = 0.2$ (i.e. α closer to zero) and $M = 2, 4, 8$ transmit antennas. Also, in order to facilitate comparison, it contains simulation results for the case in which the base station uses noiseless uplink channel correlation matrix and all other assumptions are as above (these results are essentially the same as the macro cell results of Figure 3.12 on page 48). The results of all the sub-figures of Figure 5.12 suggest that the noisy correlation matrix estimates result in some performance loss, and that the largest loss occurs when SNR is small. This happens because the pilot signal power is low when SNR is small, resulting in highly noisy channel coefficient estimates. Also, we observe that the performance loss at BER values of interest (i.e. $10^{-3} \lessapprox \mathrm{BER} \lessapprox 10^{-2}$) is generally not large, even for large M values. This may be because the noise that is present in the uplink channel coefficient estimates is not sufficiently large to alter the main directional information conveyed by the channel vector. Thus, the noise in the correlation matrix is not sufficiently large to affect the principal eigenvector (usually called the 'signal subspace') too much, but affects mainly the 'smaller' components which represent the eigenvectors corresponding to the smaller eigenvalues (usually called the 'noise subspace'). Consequently, although the calculated principal eigenvector is noisy, the noise contained in it is not capable of altering its directional

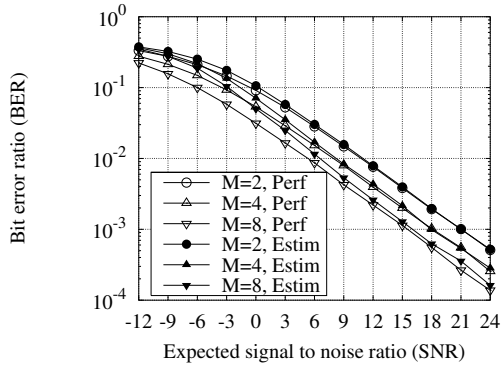

(a) Total pilot power is 5 dB higher than data power ($E_{add,\mathrm{dB}}$ = 5 dB)

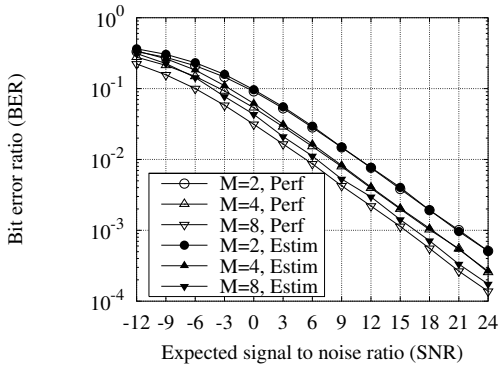

(b) Total pilot power is 10 dB higher than data power ($E_{add,\mathrm{dB}}$ = 10 dB)

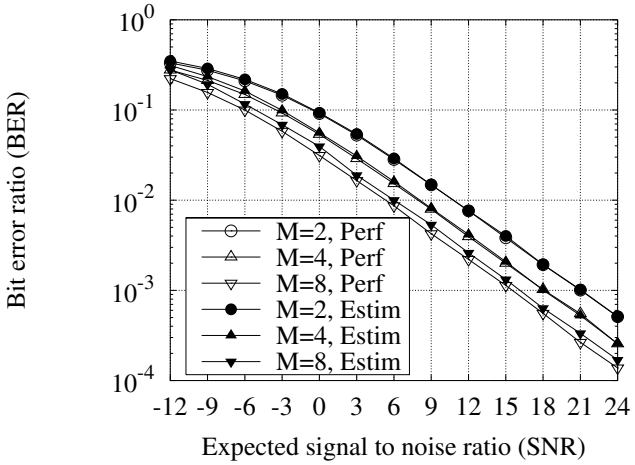

(c) Total pilot power is 15 dB higher than data power ($E_{add,\mathrm{dB}}$ = 15 dB)

Figure 5.12: *Effect of noisy uplink correlation matrix estimates (used by base station for calculation of weight vector in the form of the principal eigenvector) on the performance of maximum SNR (macro cell) for various $E_{add,dB}$ values. Forgetting factor is α = 0.2.*

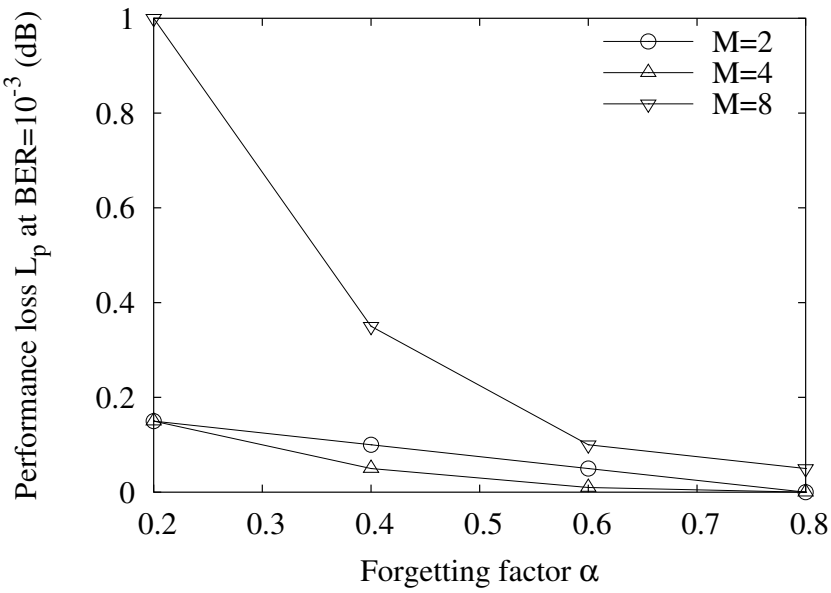

Figure 5.13: *Performance loss in maximum SNR at BER* $= 10^{-3}$ *due to noisy correlation matrix estimates (used by base station for weight vector calculation) with respect to the noiseless correlation matrix estimates case, as a function of the forgetting factor* α*, for* $M = 2, 4, 8$ *transmit antennas and* $E_{add,dB} = 10$ *(macro cell).*

information to such a degree that could change its radiation pattern dramatically and result in large performance loss.

In addition, in order to examine the effect of the parameter α, Figure 5.13 shows the performance loss at BER = 10^{-3} due to noisy correlation matrix estimates with respect to the noiseless correlation matrix estimates case, as a function of α, for $M = 2, 4, 8$ transmit antennas and $E_{add,\mathrm{dB}} = 10$ dB in the macro cell. As has also been noted above, the figure suggests that the performance loss is generally small, and that it decreases as the forgetting factor α increases (i.e. as the effective number of channel vector samples included in the correlation matrix estimate increases). This means that the presence of past channel information in the correlation matrix is important and can improve the performance (even though the improvement can be characterised small). This is especially true in a scenario where the channel parameters (in the form of angle of arrival/departure and angular spread) do not change over time, as in the assumed macro cell.

Next we examine the effect of noisy correlation matrix estimate on the performance of minimum BER. The procedure of estimating the correlation matrix at base station from uplink

channel samples and all the other assumptions are the same as in maximum SNR. Also, since the optimisation process that selects the number of eigenvectors to be used as beamformers in minimum BER is based on the values of the M eigenvalues, the performance of the technique depends strongly on accurate eigenvalue estimates. In order to obtain accurate eigenvalue estimates, the base station must use a large α value (e.g. $\alpha > 0.95$), given that a large α results in a large number of channel vector samples contributing to the correlation matrix, improving the estimates of the eigenvalues [61] (especially of the smaller ones). If a smaller α is used, the estimates of the eigenvalues (especially of the smaller ones) may not be very accurate, so the optimisation process may not succeed in selecting the actual optimum number of eigenvectors to be used as beamformers. Therefore, the value of the forgetting factor used in the simulations is $\alpha = 0.99$. We note that using a large forgetting factor improves the eigenvalue estimates without having any negative side-effects (such as, for example, additional computational load/complexity).

Figure 5.14 shows simulation results of minimum BER for $E_{add,\mathrm{dB}} = 10$ dB and $M = 2, 4, 8$ transmit antennas in the macro and micro cell[9]. A target BER of 10^{-3} was used in the optimisation process that selects the number of eigenvectors to be used as beamformers (that is, the number of eigenvectors K used as beamformers is selected so that it provides the lowest required SNR at BER = 10^{-3}). Also, in order to facilitate comparison, the figure contains simulation results for the case in which the base station uses noiseless uplink channel correlation matrix and all other assumptions are as above. The results show that the performance with noisy correlation matrix estimate for $M = 4, 8$ does not match the performance with noiseless correlation matrix when SNR is small in both scenarios. However, the noisy and noiseless correlation matrix performance curves match each other when SNR becomes larger. When SNR is small, the power of the pilot signals is (relatively) small and the noise that is present in the channel coefficient estimates obtained from these pilot signals, and, consequently, in the correlation matrix estimate, is (relatively) large. This noise affects mainly the smaller eigenvalues of the correlation matrix (the 'noise subspace') and effectively alters their values (to a certain degree). Therefore, the optimisation process uses the altered eigenvalues and selects a K that is not equal to the actual optimal K, resulting in discrepancy between the performance with noiseless correlation matrix and the performance with noisy correlation matrix estimate.

[9]Results are not shown for the pico cell, because in this scenario minimum BER yields performance identical to that of space-time spreading (Figure 4.11 on page 86) which is much more likely to be used in such a case given that it is simpler than minimum BER.

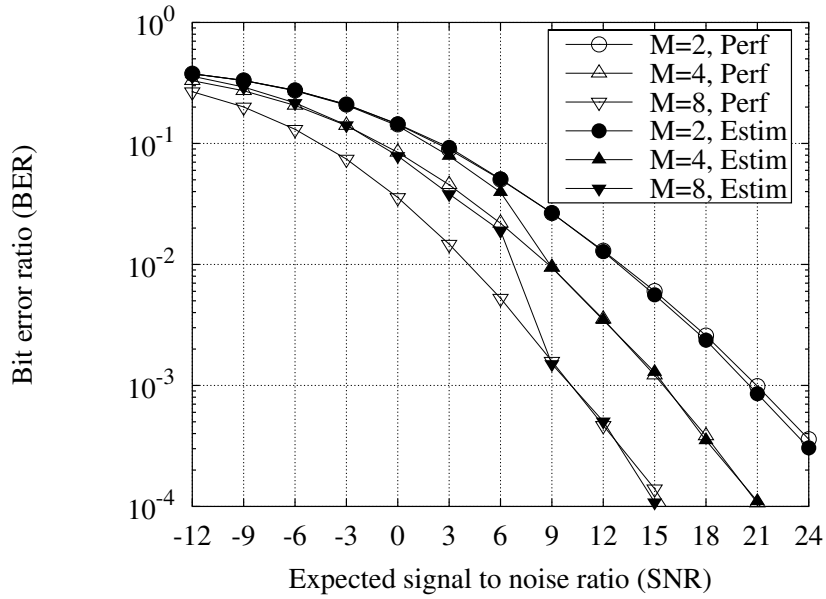

(a) Macro cell

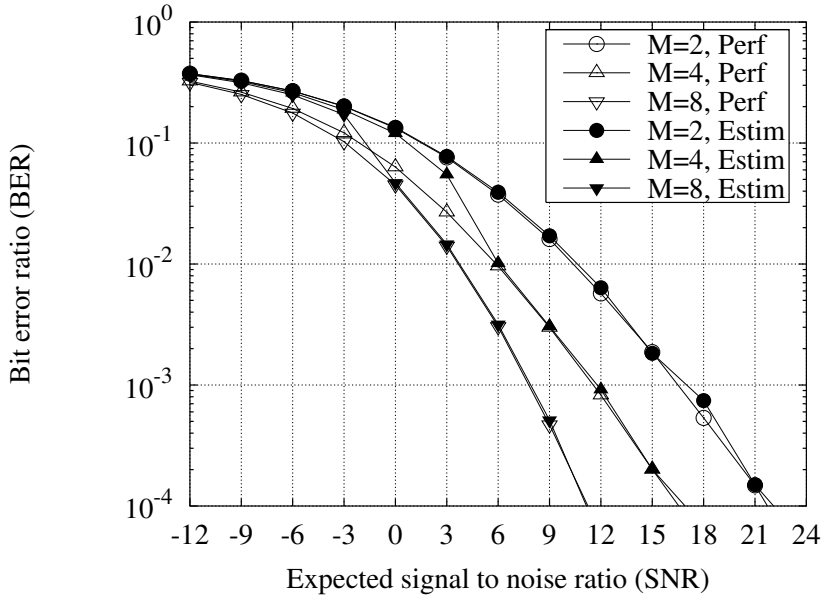

(b) Micro cell

Figure 5.14: *Effect of noisy uplink correlation matrix estimate (used by base station for calculation of its eigenvectors) on the performance of minimum BER. Total pilot power is 10 dB higher than data power ($E_{add,dB} = 10$ dB), while forgetting factor is* $\alpha = 0.99$.

Nevertheless, when SNR becomes larger the noise in the channel coefficient estimates becomes smaller and it does not affect the smaller eigenvalues of the estimated correlation matrix to the same degree as before. Therefore, the values of these eigenvalues are more accurate and the optimisation process which is based on them is able to select the actual optimum K. Hence, in this case the performance with noisy correlation matrix estimate matches that with noiseless correlation matrix. This is indicative of the significance of accurate eigenvalue estimates in the minimum BER technique.

The results also suggest that when SNR is large and the estimates of all the eigenvalues are accurate, the performance with noisy correlation matrix estimate is very similar to that with noiseless correlation matrix; that is, the performance loss due to noisy channel coefficient estimates is negligible. A possible explanation for this phenomenon is as follows. When a noiseless correlation matrix is used, the number of eigenvectors K to be used as beamformers is selected once in the beginning and is then kept constant throughout the simulation (this is because the correlation matrix does not change over time and there is no reason for the base station to go through the optimisation process more than once, since the same K will be selected again). On the other hand, when the correlation matrix is estimated from pilot signals, the value of its elements changes (even slightly) each time the matrix is updated. This means that its eigenvalues, as well as the radiation pattern of its eigenvectors (eigenbeams), also change each time the matrix is updated. Thus, the base station must go through the process that selects the optimum K each time the correlation matrix is updated, as a different K may provide the lowest required SNR for the target BER after the correlation matrix update. This frequent optimisation enhances the performance adaptively, and effectively compensates for the loss due to noisy channel coefficient estimates.

Finally, in order to examine the effect of the additional pilot power $E_{add,\mathrm{dB}}$, Figure 5.15 shows simulation results for $E_{add,\mathrm{dB}} = 5$ and 15 dB, for $M = 2, 4, 8$ in the micro cell (simulation results in the macro cell exhibit the same trend, so they are not shown to avoid repetition of multiple result sets which are similar to each other). Comparison of Figures 5.15(a), 5.15(b) and 5.14(b) suggests that when $M = 2$ the parameter $E_{add,\mathrm{dB}}$ does not affect the performance significantly. However, when $M = 4, 8$ the parameter $E_{add,\mathrm{dB}}$ appears to play an important role: as $E_{add,\mathrm{dB}}$ increases, the SNR value after which the noiseless and noisy correlation matrix performance curves match each other decreases. For instance, if $M = 4$ the two performance curves match each other for SNR $\gtrapprox$ 9 dB when $E_{add,\mathrm{dB}} = 5$ dB, for SNR $\gtrapprox$ 6 dB when $E_{add,\mathrm{dB}} = 10$ dB and

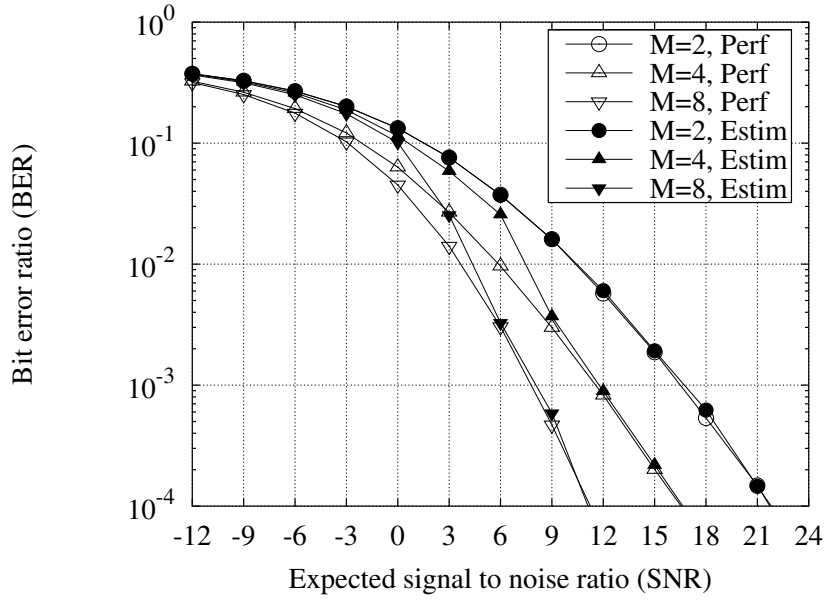

(a) Pilot power is 5 dB higher than data power ($E_{add,\mathrm{dB}} = 5$ dB)

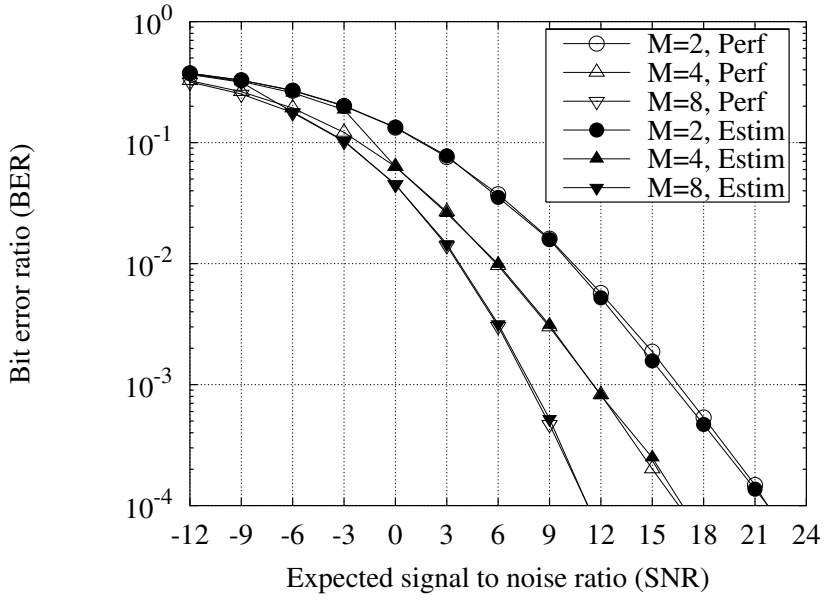

(b) Pilot power is 15 dB higher than data power ($E_{add,\mathrm{dB}} = 15$ dB)

Figure 5.15: *Effect of the additional pilot power $E_{add,dB}$ on the performance of minimum BER for $M = 2, 4, 8$ transmit antennas in the micro cell. Forgetting factor is $\alpha = 0.99$*

for SNR $\gtrapprox$ 0 dB when $E_{add,\mathrm{dB}} = 15$ dB. This is because, as $E_{add,\mathrm{dB}}$ increases, the pilot signal power also increases and the eigenvalue estimates become 'accurate' at lower SNR values. Also, this relationship between $E_{add,\mathrm{dB}}$ and the SNR value after which the two performance curves match each other may have implications for the system performance. For instance, if $E_{add,\mathrm{dB}}$ is so low that the eigenvalue estimates become accurate for an SNR larger than the SNR which yields the target BER, the optimisation process is very likely to fail to select the optimum K for the target BER, affecting the performance negatively. This could happen, for example, in Figure 5.15(a) for $M = 4$ or 8 and a target BER = 10^{-1}. Therefore, the $E_{add,\mathrm{dB}}$ value should be such that it provides accurate eigenvalue estimates at an SNR smaller than the SNR which yields the target BER.

5.3.3 Effect of noisy selection of highest SNR diversity branch (antenna or beam)

In this section we discuss the use of pilot signals for the selection of the highest SNR antenna or beam in the techniques selection diversity or fixed beams respectively. We assume that the base station transmits pilot signals through each diversity branch (antenna or beam) in frames as in Figure 5.3, with $N_p = 4$ and $N_d = 20$ (ratio of number of pilot symbols over number of data symbols $\eta = \frac{N_p}{N_d} = \frac{4}{20} = 0.2$). The duration of both data and pilot symbols is $T_s = 14.205$ μsec while the maximum Doppler frequency shift is $f_{D,\max} = 110$ Hz. The number of diversity branches in both techniques is M (in selection diversity the number of branches is equal to the number of transmit antennas M, while in fixed beams the number of branches is equal to the number of beams N_B, which is also $N_\mathrm{B} = M$ as we have noted on page 39). The total power allocated to pilot signals across all M branches is $E_{add,\mathrm{dB}}$ dB higher than the total power of the data signals. The mobile station measures and averages the instantaneous received power of each branch over the N_p pilot symbols[10], and determines which branch yields the highest instantaneous power, when this is averaged over these pilot symbols. Then, it feeds an index to this branch back to base station which uses this branch for transmission of the N_d data symbols that follow. In this section we simulate only the effects of selecting the highest SNR branch from noisy pilot signals, while we assume that the feedback of the index to this branch from mobile to base station is performed noiselessly. Also, we assume that the mobile station has perfect knowledge of the downlink channel coefficients during the transmission of the N_d data

[10] As we noted earlier in this chapter, the averaging process has the effect of improving the SNR of the M diversity branches, but since it affects all of them in the same fashion, it does not alter the relationship among their SNR values which is the parameter of interest in this section.

symbols, so their demodulation is also carried out noiselessly. These assumptions eliminate all other sources of performance degradation due to pilot signals except for the noisy selection of the best branch, so we can discuss its impact on the performance separately.

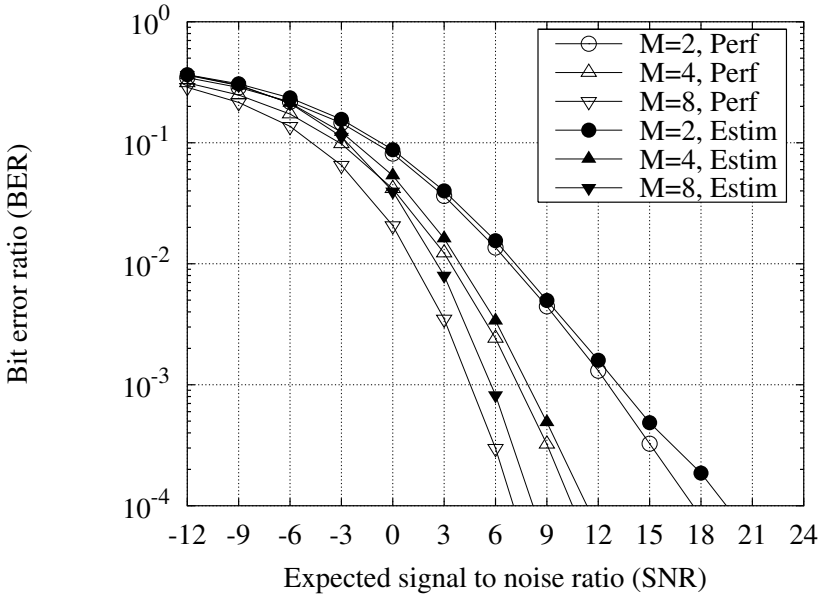

Figure 5.16: *Effect of noisy highest SNR antenna selection by the mobile station on the performance of selection diversity (pico cell). Total pilot power is 10 dB higher than data power ($E_{add,dB} = 10$ dB).*

Figure 5.16 shows simulation results of selection diversity in the pico cell with the above assumptions, for $M = 2, 4, 8$ transmit antennas and $E_{add,\mathrm{dB}} = 10$ dB. To facilitate comparison, it also shows simulation results in a case where the base station knows which antenna yields the highest SNR over each data symbol and uses it for transmission of the data symbols. The results show that the performance loss L_p due to noisy highest SNR antenna selection at the mobile station increases with the number of antennas M ($L_p \simeq 0.55$ dB when $M = 2$, $L_p \simeq 0.65$ dB when $M = 4$ and $L_p \simeq 1.2$ dB when $M = 8$, all loss values measured at BER $= 10^{-3}$). This is because the pilot power dedicated to the estimation of each antenna's SNR becomes smaller as M increases, leading to less accurate SNR estimates and increased performance loss. Also, for very small SNR values (e.g. SNR $\lessapprox -6$ dB), larger M values yield (slightly) worse performance. However, the amount by which the performance worsens is very small and much smaller than the corresponding amount observed in the space-time spreading simulation in section 5.3.1. This may be because selection diversity provides higher diversity gain than space-time spreading, as it takes advantage of the feedback information about the highest SNR

antenna from the mobile station.

In addition, in order to investigate the effect of the additional pilot power $E_{add,\mathrm{dB}}$, Figure 5.17 shows the performance loss L_p due to noisy highest SNR antenna selection with respect to the noiseless highest SNR antenna selection case at BER = 10^{-3}, as a function of $E_{add,\mathrm{dB}}$ for $M = 2, 4, 8$ transmit antennas in the pico cell. As it is expected, the results suggest that the loss decreases as $E_{add,\mathrm{dB}}$ increases, since more power is dedicated to the selection of the antenna with the highest SNR and, thus, this selection is improved resulting in smaller loss values.

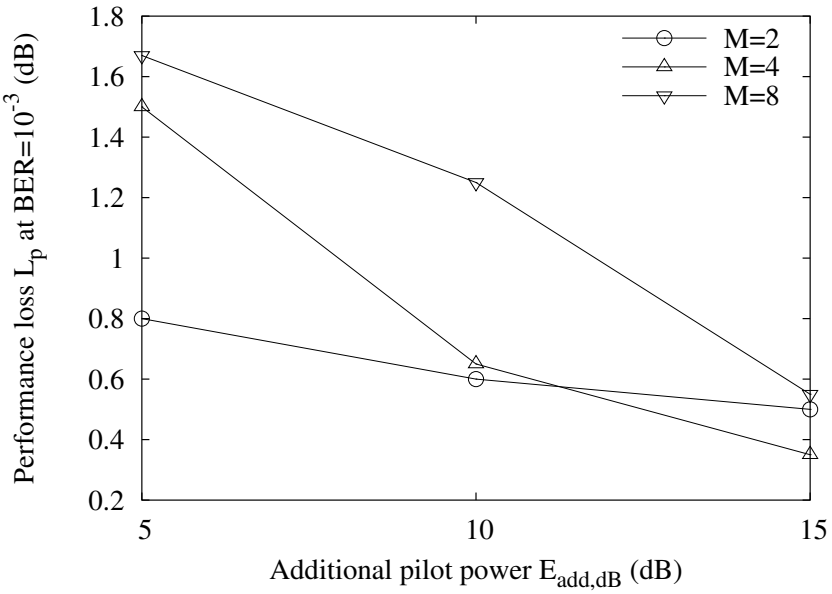

Figure 5.17: *Performance loss L_p in selection diversity at BER = 10^{-3} due to noisy highest SNR antenna selection with respect to the noiseless highest SNR antenna selection case, as a function of the additional pilot power $E_{add,dB}$, and for $M = 2, 4, 8$ transmit antennas (pico cell).*

Next, Figure 5.18 shows simulation results of fixed beams in the pico cell with the assumptions noted above, for $M = 2, 4, 8$ transmit antennas and $E_{add,\mathrm{dB}} = 10$ dB. It also shows simulation results in a case where the base station knows which beam yields the highest SNR over each data symbol and uses it for transmission of the data symbols. The results suggest again that the performance loss L_p due to noisy highest SNR beam selection increases with the number of antennas M ($L_p \simeq 0.55$ dB when $M = 2$, $L_p \simeq 0.65$ dB when $M = 4$ and $L_p \simeq 1.2$ dB when $M = 8$, all loss values measured at BER = 10^{-3}). As in selection diversity, this is because the pilot power dedicated to the estimation of each beam's SNR becomes smaller as M increases,

resulting in less accurate SNR estimates and increased performance loss. Also, the loss values due to noisy highest SNR branch selection in fixed beams and selection diversity, and the results of Figures 5.18 and 5.16 for the same M are very similar to each other. This suggests that when the signals of the M antennas are uncorrelated (i.e. pico cell), fixed beams performs similarly to selection diversity (the similarity between the performance of the two techniques in the pico cell is also apparent in Figure 3.24 on page 62). Furthermore, contrary to selection diversity, larger M values do not result in worse performance when SNR is small. This may be because fixed beams provides beamforming gain in addition to its diversity gain, which compensates for the loss due to increasingly worse SNR estimates when SNR is small and M increases.

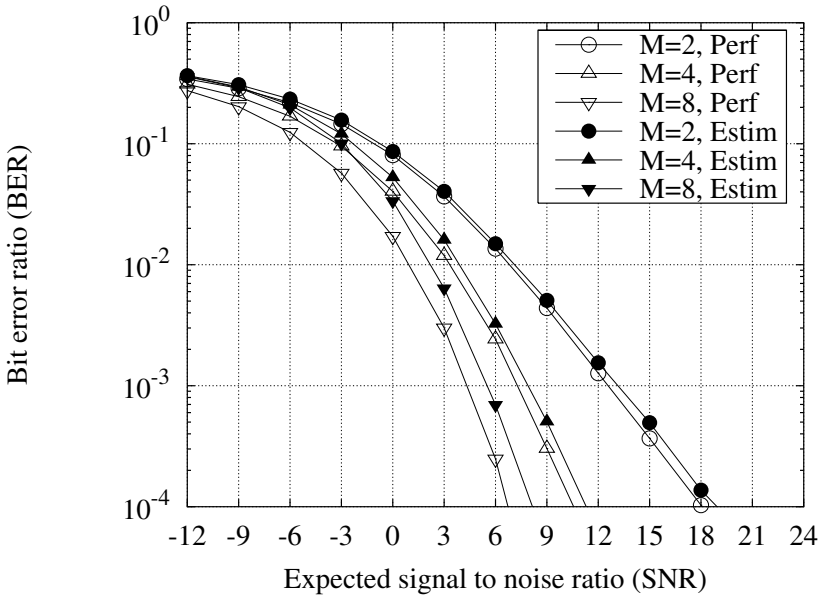

Figure 5.18: *Effect of noisy highest SNR beam selection by the mobile station on the performance of fixed beams (pico cell). Total pilot power is 10 dB higher than data power ($E_{add,dB} = 10$ dB).*

The effect of the additional pilot power $E_{add,\mathrm{dB}}$ in fixed beams is very similar to that in selection diversity, which for the pico cell is shown in Figure 5.17. However, because of the directional transmission by means of beams, the channel scenario appears to play an important role in fixed beams. To examine the effect of different channel scenarios, Figure 5.19 shows the loss due to noisy highest SNR beam selection with respect to the noiseless highest SNR beam selection case at BER = 10^{-3} in the three scenarios (macro, micro and pico cell) for $M = 2, 4, 8$ transmit antennas ($E_{add,\mathrm{dB}} = 10$ dB). The results suggest that as the angular spread becomes smaller (that is, transition from pico to micro to macro cell), the loss for a particular M becomes larger.

When the angular spread is large, even if the wrong beam is selected by the mobile station, it illuminates a significant portion of the angular spread so the loss is not large. On the other hand, when the angular spread is smaller, a beam other than the one with the highest SNR may illuminate a (very) small part of it, causing the loss to increase. Also, the figure suggests that larger M values are affected more than smaller ones. When M is small the beamwidth is relatively large (Figure A.2 on page 165) and even if the wrong beam is selected by the mobile station, it illuminates a significant portion of the angular spread so the loss is not large. When M is larger the beamwidth is smaller and a beam other than the one with the highest SNR may illuminate a (very) small part of the angular spread, resulting in increased loss values.

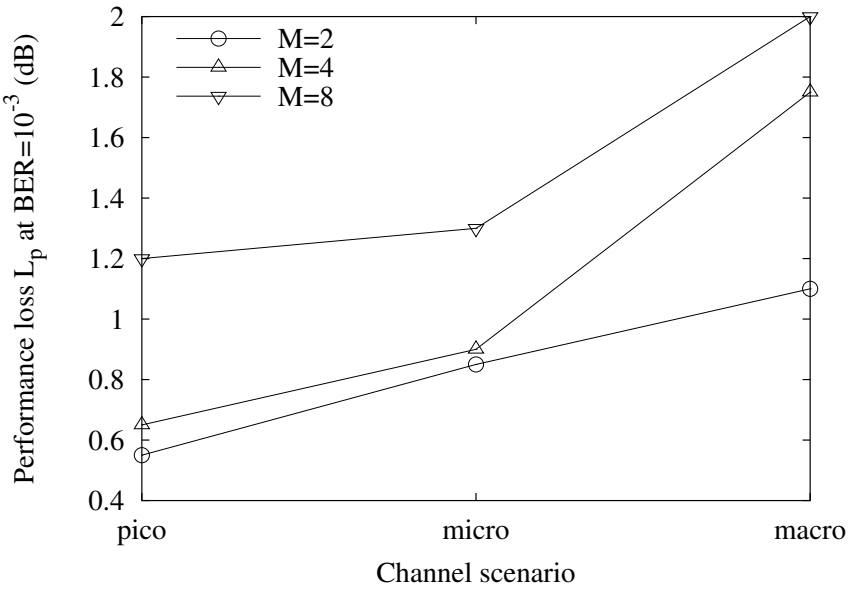

Figure 5.19: *Performance loss L_p in fixed beams at BER = 10^{-3} due to noisy highest SNR beam selection with respect to the noiseless highest SNR beam selection case, in the three channel scenarios for $M = 2, 4, 8$ transmit antennas. Total pilot power is 10 dB higher than data power ($E_{add,dB} = 10$ dB).*

5.3.4 Effect of noisy feedback of highest SNR diversity branch (antenna or beam)

Finally, in this section we discuss the effects of errors due to noise on the feedback path used to feed an index to the highest SNR diversity branch (antenna or beam) from mobile to base station in selection diversity and fixed beams. We assume that the highest SNR branch is selected at the mobile station from noiseless pilot signals (i.e. the mobile station has perfect knowledge of

which branch yields the highest average SNR over the $N_p = 4$ pilot symbols). Then, in order to simulate a fixed BER (e.g. BER = 10^{-2}) on the feedback path between mobile and base station, we first transform the index to the highest SNR branch from decimal into binary form. Next, we alter the value of each binary digit of the index with probability BER = 10^{-2} and transform the resulting binary number back into decimal form. Finally, we assume that the base station uses the diversity branch that the resulting decimal number points to for transmission of the $N_d = 20$ data symbols that follow to mobile station. All other assumptions and parameters are the same as in the previous section. The above simulation of the two techniques is also performed using an error-free (or noiseless) feedback path, and the results are compared with those of the simulations that use the noisy feedback path with BER = 10^{-2}.

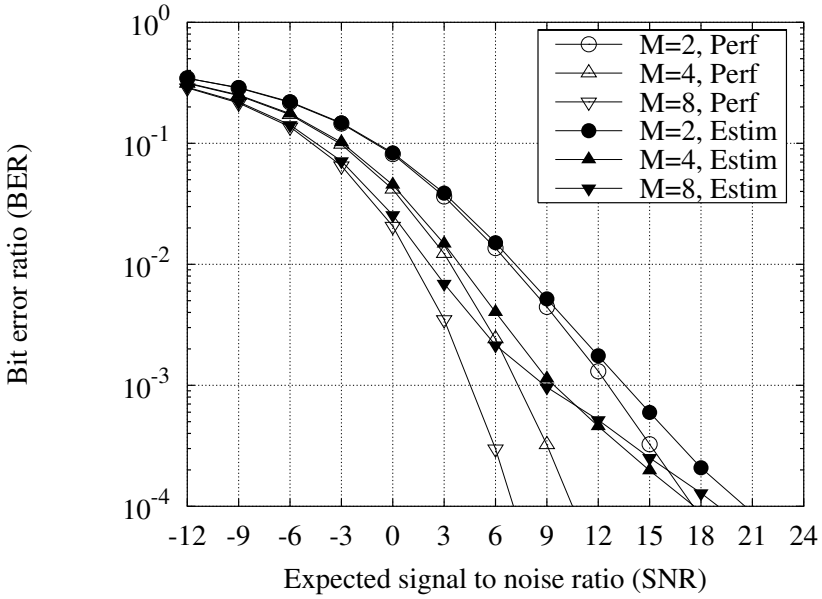

Figure 5.20: *Effect of noisy highest SNR antenna feedback from mobile station to base station on the performance of selection diversity (pico cell). BER of feedback path is* 10^{-2}.

Figure 5.20 shows simulation results of selection diversity using both a feedback path with BER = 10^{-2} and an error-free (i.e. noiseless) feedback path in the pico cell. The results show that for very small SNR values the noisy feedback path does not affect the performance, which is similar to that of the noiseless feedback path case. When the SNR value is very small the data signal power is much smaller than the thermal noise power. Thus, the dominant source of errors is the thermal noise in the received signal and the impact of the errors due to noisy feedback path is somewhat 'concealed'. However, as SNR increases the data signal power

becomes gradually larger than that of the thermal noise, and the errors due to this noise become gradually less important than the errors due to noisy feedback path. Consequently, as SNR becomes larger the errors due to noisy feedback path become gradually more important and they start to dominate the system performance. In addition, the performance loss due to noisy feedback path becomes larger as the number of transmit antennas M increases. This may be because when an error occurs and the wrong antenna is used for data signal transmission by the base station, the distance that can potentially occur between the highest SNR antenna and the antenna that is erroneously used for transmission increases with M, resulting in smaller correlation between the channel coefficients of the two antennas (the correlation as a function of the distance between two antennas is shown in Figure 2.16 on page 26).

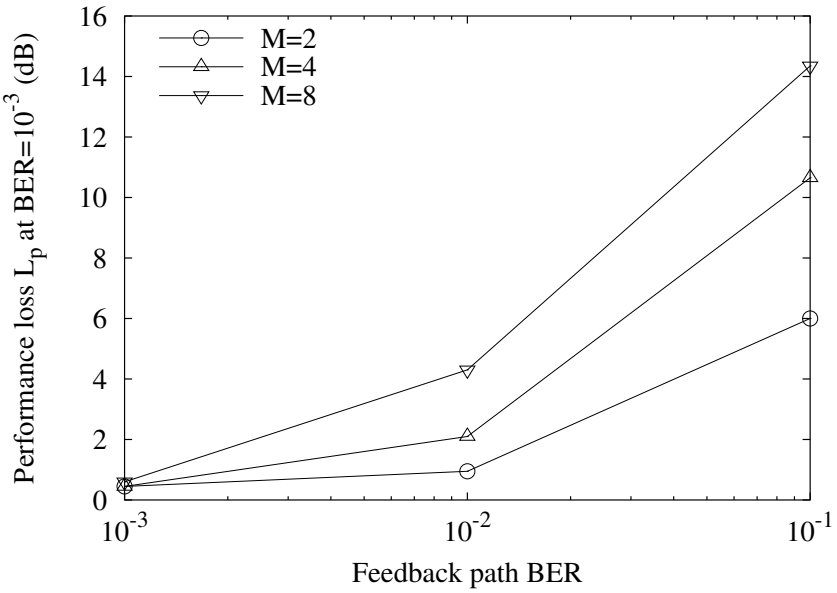

Figure 5.21: *Performance loss L_p in selection diversity at BER = 10^{-3} due to noisy highest SNR antenna feedback with respect to the noiseless highest SNR antenna feedback case, as a function of the BER of the feedback path (pico cell).*

In order to examine the effect of different feedback BER values, Figure 5.21 shows the performance loss L_p at BER = 10^{-3} due to noisy feedback path as a function of the feedback BER for $M = 2, 4, 8$ transmit antennas in the pico cell. The figure suggests that the loss decreases as the feedback BER decreases, since in this case less errors occur on the feedback path and the true highest SNR antenna is used more times on average.

Next, Figure 5.22 shows simulation results of fixed beams using both a feedback path with

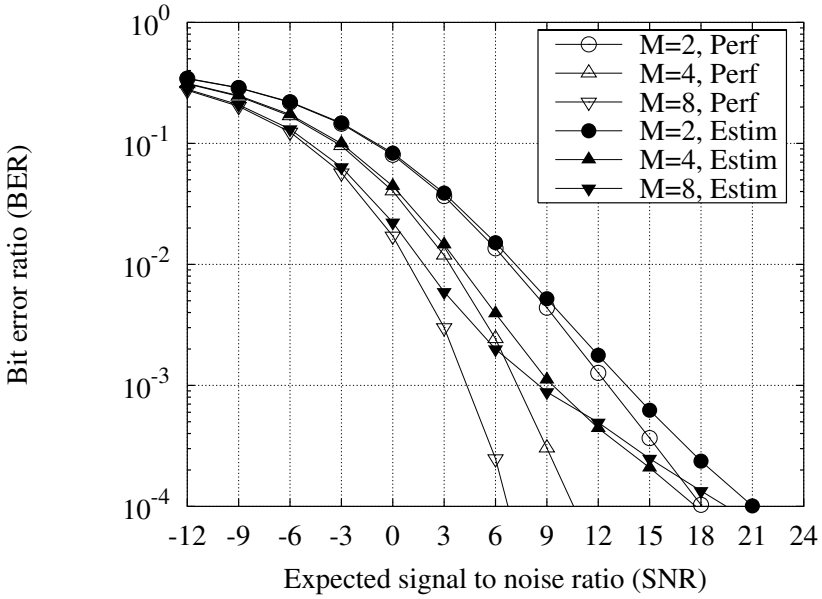

Figure 5.22: *Effect of noisy highest SNR beam feedback from mobile station to base station on the performance of fixed beams (pico cell). BER of feedback path is* 10^{-2}.

BER = 10^{-2} and a noiseless feedback path, also in the pico cell. The results show similar trends to those of Figure 5.20 for the same reasons. Also, the performance loss due to noisy feedback path is very similar to that of selection diversity. This is because the angular spread of the pico cell is (very) large, and even if the non-highest SNR beam is used for data signal transmission, this is able to illuminate a significant portion of the channel components so that the power that reaches the mobile receiver is not reduced by a large amount. This situation is similar to that of selection diversity, where even if the non-highest SNR antenna is used for data signal transmission, the power that reaches the mobile receiver is not reduced by a large amount, because of the (almost) omnidirectional transmission of all M linear antennas on the horizontal plane[11]. However, if the angular spread becomes smaller, using a non-highest SNR beam for data signal transmission may illuminate a very small portion of the signal components, resulting in larger performance loss. This is depicted in Figure 5.23 which shows the performance loss L_p due to noisy highest SNR beam feedback for a feedback BER = 10^{-2} in the three channel scenarios (macro, micro and pico cell). The figure shows that the loss becomes indeed larger as the angular spread becomes smaller (that is, transition from pico to micro to macro cell).

[11]In this case the received power at the mobile receiver in selection diversity is affected mainly by the multipath fading of the channel over time and not by the antenna pattern, since the latter is the same for all M linear transmit antennas of the base station and has an almost constant amplitude in all horizontal directions over $[-60^o, 60^o]$.

Finally, both Figure 5.22 and Figure 5.23 show that the loss due to noisy feedback path becomes larger as the number of transmit antennas M increases. This may be because when an error occurs and the wrong beam is used for data signal transmission by the base station, the distance that can potentially occur between the direction of the highest SNR beam and the direction of the beam that is erroneously used for transmission increases with M (this can be seen in Figures 3.7 and A.4 on pages 39 and 167 respectively), resulting in a smaller portion of the channel components being potentially illuminated. Additionally, the beamwidth of the main lobe decreases with M (Figure A.2 on page 165) and even if the distance between the two beams is small, the impact on the performance may be (relatively) large.

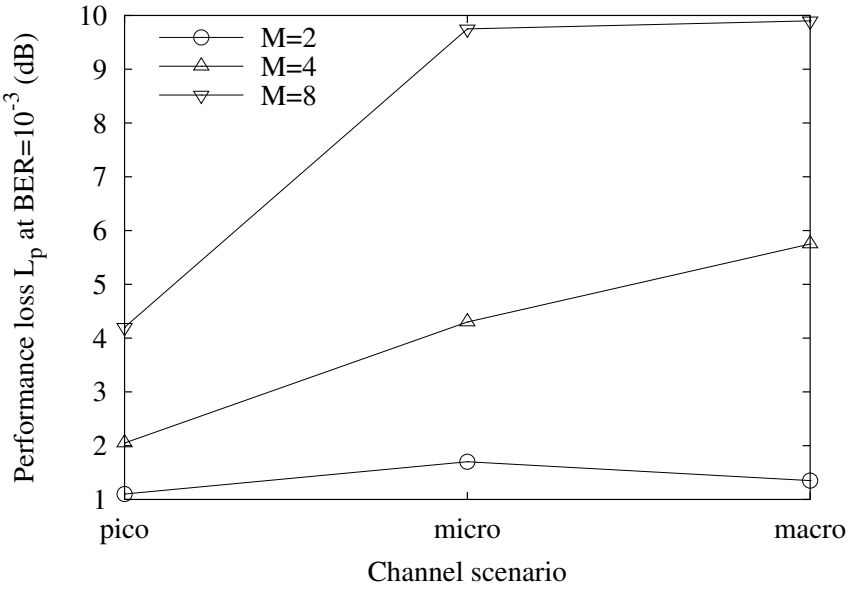

Figure 5.23: *Performance loss L_p in fixed beams at BER = 10^{-3} due to noisy feedback of the highest SNR beam with respect to the noiseless feedback of the highest SNR beam, in the three channel scenarios for $M = 2, 4, 8$ transmit antennas. BER of feedback path is 10^{-2}.*

5.4 Summary

In this chapter we discussed the impact of estimating various parameters that are needed at the base and/or mobile station from pilot signals on the performance of various downlink antenna array algorithms. Two basic approaches to the transmission of pilot signals were briefly introduced to facilitate presentation of various parameter estimation techniques. One of them

involves continuous pilot signal transmission, while the other involves pilot signal transmission in frames. Next, approaches to the estimation of various parameters from pilot signals were discussed. The estimated parameters included the channel vector, the channel correlation matrix and the identification of the highest SNR transmit antenna or beam by the mobile station. The details of the channel correlation matrix estimation from pilot signals were also examined, and the memory of this process was expressed as a function of the forgetting factor α. Also, we discussed feedback of the downlink channel coefficients and the index to the highest SNR transmit antenna or beam from mobile to base station. Next, these approaches were applied to various downlink antenna array techniques by means of computer simulations and the impact on their performance was discussed.

The results showed that estimation of the needed parameters from (noisy) pilot signals in most cases results in performance loss. The amount and form of the loss is related to the parameter estimated from pilot signals. Also, the loss might depend on the number of transmit antennas M in the base station, the SNR value and/or the channel scenario. More specifically, estimation of the M downlink channel coefficients from pilot signals at the mobile receiver results in performance loss which in general increases with M, when the total pilot power allocated to the estimation of the M coefficients is fixed. The same holds for the case where the downlink channel coefficients are fed back to the base station, where they are used for calculation of the weight vector. In this case, there is additional noise which results from the quantisation of the channel coefficients that are to be fed back to base station. The amount of this noise is related to the number of bits used by the quantiser of the mobile station: the larger the number of quantisation bits, the smaller the performance loss becomes. Also, estimation of the principal eigenvector of the mean channel correlation matrix from (noisy) pilot signals in the technique maximum SNR does not degrade performance by a large amount, since the noise in the matrix affects mainly the components corresponding to the smaller eigenvalues, and not the principal one. The parameter α plays an important role in this case, with larger α values increasing the memory of the correlation matrix estimation process and yielding smaller performance loss in general. Furthermore, a large α results in more accurate estimates of the smaller eigenvalues in the technique minimum BER, enhancing its performance. In addition, the frequent selection of the number of eigenvectors that provides the lowest SNR for the target BER in this technique, compensates for most of the effect of the noisy correlation matrix estimate and helps it to yield performance very close to the noiseless correlation matrix case. Moreover, when the highest SNR transmit antenna or beam is selected from (noisy) pilot signals by the mobile station,

the performance loss increases with the number of antennas, if the total pilot power allocated to the M antennas or beams is fixed. Finally, when the feedback of the index to the highest SNR antenna or beam from mobile to base station is noisy, the performance degrades. The performance loss in this case is related to the bit error ratio (BER) of the feedback path, with smaller BER values providing smaller loss. Also, the technique fixed beams appears to be more sensitive to this type of noise than the technique selection diversity, since selection of the wrong beam may have a greater impact on the performance than selection of the wrong antenna (especially if the number of transmit antennas M is large and/or the angular spread is small).

Chapter 6

Impact of frequency division duplex on open loop downlink beamforming using eigenbeams

In this chapter we examine the effects of the separation between the carrier frequencies of the uplink and downlink channels due to frequency division duplex (which, in the remainder of this thesis will be called frequency division duplex gap (FDD gap), f_{FDD}) on the performance of open loop downlink beamforming techniques that make use of eigenbeams. First, the correlation between the uplink and downlink eigenvectors (or equivalently, eigenbeams) will be expressed in terms of f_{FDD}, and it will be shown to decrease as f_{FDD} increases (that is, the eigenbeams become less related with each other as f_{FDD} increases). The increasingly smaller correlation between the eigenbeams due to FDD gap results in performance loss, L_{FDD}, which is also expressed in terms of f_{FDD} and is shown to be an increasing function of f_{FDD} (that is, the loss increases as f_{FDD} increases). Next, a simple approach to compensating for the above frequency division duplex effects is applied, and it is shown that it increases the correlation between the uplink and downlink eigenbeams and compensates for most of the performance loss. Finally, comparison of this approach with an existing compensation technique shows that, even though the latter is more complex and sophisticated than the former, it yields very similar compensation performance.

6.1 Effects of frequency division duplex

In previous chapters we have seen that the base station generally needs some information about the downlink channel (in the form of its correlation matrix's eigenvectors, or eigenbeams) in order to optimise performance. For instance, the base station of maximum SNR and minimum BER needs knowledge of the eigenvalues/eigenbeams of the mean downlink channel correlation matrix in order to yield the maximum possible gain. The technique eigenbeamforming

(described in section 3.2.4 on page 41) uses explicitly the eigenvectors of the downlink channel correlation matrix, so it is not affected by frequency division duplex and thus will not be considered in this chapter. As we have also seen, the downlink eigenbeam information can be estimated at the mobile station (by means of pilot signals) and then sent to the base station (by means of feedback signals), but this may affect the system capacity negatively. However, when the FDD gap is relatively small, there is a strong relationship between the average statistical properties of the uplink and downlink channels [182] (in the form of their second order statistics as represented by the mean correlation matrices). In this case, the base station may minimise the need for the above pilot and feedback signals by operating the antenna array in an open loop fashion, through estimation of the required eigenvalues and/or eigenbeams from the uplink channel and use of them for downlink transmission. However, this approach introduces a performance loss, L_{FDD}, which increases with FDD gap. This section will examine the effects of the FDD gap, f_{FDD}, on the correlation between the uplink and downlink eigenbeams and on the received signal power (or equivalently its SNR).

6.1.1 Decorrelation between uplink and downlink eigenbeams

Given that the base station uses the uplink eigenbeams in the place of the downlink ones, a parameter of interest is the correlation between corresponding uplink and downlink eigenbeams. With this in mind, let us assume that the base station uses a uniform linear antenna array with M transmit antenna elements, the FDD gap is f_{FDD} and the transmit antenna spacing is $D = \frac{\lambda_{ref}}{2}$, where λ_{ref} is the wavelength of the 'reference' carrier frequency $f_{ref} = 2$ GHz ($\lambda_{ref} = \frac{v_l}{f_{ref}}$, where $v_l = 3 \times 10^8$ m/sec is the speed of light). Then, we define the uplink and downlink carrier frequencies as $f_{\mathrm{UL},c} = f_{ref} - \frac{f_{FDD}}{2}$ and $f_{\mathrm{DL},c} = f_{ref} + \frac{f_{FDD}}{2}$, respectively. Next, we can calculate the uplink $\mathbf{R}_{\mathrm{UL}}(f_{FDD})$ and downlink $\mathbf{R}_{\mathrm{DL}}(f_{FDD})$ mean channel correlation matrices in a certain channel scenario and for the above f_{FDD} value (using equations (A.2) and (A.3) of page 157), and obtain their eigenvectors. Finally, it is easy to define the correlation $\rho_i(f_{FDD})$, $i = 1..M$, between the i-th uplink eigenvector, $\mathbf{u}_{\mathrm{UL},i}(f_{FDD}) \in \mathbb{C}^{M\times 1}$, and the i-th downlink eigenvector, $\mathbf{u}_{\mathrm{DL},i}(f_{FDD}) \in \mathbb{C}^{M\times 1}$, in this channel scenario and for the specified f_{FDD} value as

$$\rho_i(f_{FDD}) = |\mathbf{u}^{\mathrm{H}}_{\mathrm{DL},i}(f_{FDD})\mathbf{u}_{\mathrm{UL},i}(f_{FDD})|, \tag{6.1}$$

where the H superscript denotes complex conjugate transpose and $|z|$ is the amplitude of the complex number z. The parameter $\rho_i(f_{FDD})$ provides a measure of the relation between the two

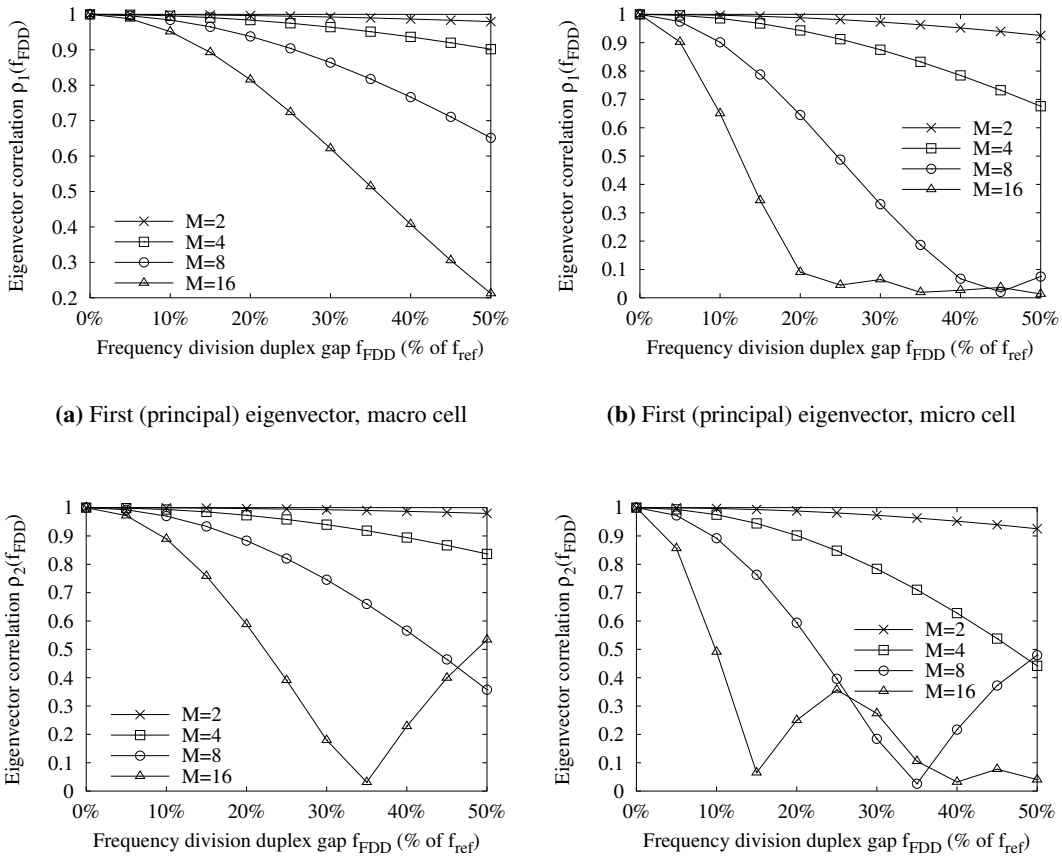

(a) First (principal) eigenvector, macro cell

(b) First (principal) eigenvector, micro cell

(c) Second eigenvector, macro cell

(d) Second eigenvector, micro cell

Figure 6.1: *Correlation between uplink and downlink eigenvectors as a function of frequency division duplex gap and for* $M = 2, 4, 8, 16$ *in the macro and micro cells.*

eigenvectors in the given channel scenario and when the FDD gap is f_{FDD}. We vary the value of f_{FDD} from 0 up to 50% of the reference carrier frequency (i.e. up to 1 GHz) with a step of 0.1 GHz, and plot the corresponding $\rho_i(f_{FDD})$ values for $i = 1, 2$ (i.e. for the first (principal) and second eigenvectors) in Figure 6.1. The figure includes correlation values for $M = 2, 4, 8, 16$ transmit antennas in the macro and micro cells. There are no results for the pico cell, since the two considered beamforming techniques are rather unlikely to be used in this scenario as has been noted in earlier chapters. As is expected, the results suggest that the uplink and downlink eigenvectors become less correlated as the FDD gap increases. Also, the eigenvector correlation decreases as the number of transmit antennas M increases. A possible explanation for this may be that as M increases the eigenvectors consist of more elements, so more elements differ from

each other between the two eigenvectors of equation (6.1) as M increases, resulting in smaller overall correlation. In addition, the figure suggests that the correlation of a particular pair of uplink and downlink eigenvectors (e.g. the pair of the principal eigenvectors) decreases with the angular spread (that is, transition from macro to micro cell). Finally, correlation results for pairs of uplink and downlink eigenvectors of higher order (that is, pairs of the 3-rd, 4-th, $\cdots$, M-th eigenvectors) exhibit similar trends, so they are not shown here.

6.1.2 Performance loss

The fact that the correlation between uplink and downlink eigenvectors decreases with FDD gap, suggests that the performance of open loop beamforming techniques that use the 'raw' uplink eigenbeams deteriorates with FDD gap. In this section the performance loss due to FDD gap is quantified for the open loop techniques maximum SNR and minimum BER. Let us deal with the former first. From equation (3.3) (page 31), assuming that the FDD gap is f_{FDD}, the transmit power and noise power is unit ($E_s = 1$ and $\sigma_n^2 = 1$ respectively) and the base station uses the uplink principal eigenvector $\mathbf{u}_{\mathrm{UL},1}(f_{FDD})$ for downlink transmission, the expected SNR of the received signal at the mobile receiver for this f_{FDD} value is given by

$$\mathrm{SNR}_{\mathrm{MAXSNR}}(f_{FDD}) = \mathbf{u}_{\mathrm{UL},1}^{\mathrm{H}}(f_{FDD})\mathbf{R}_{\mathrm{DL}}(f_{FDD})\mathbf{u}_{\mathrm{UL},1}(f_{FDD}), \tag{6.2}$$

where $\mathbf{R}_{\mathrm{DL}}(f_{FDD})$ is the mean downlink channel correlation matrix for the above f_{FDD} value. Also, in the case of $f_{FDD} = 0$, the uplink and downlink mean correlation matrices are the same and the base station can obtain the latter by estimating the former (e.g. through pilot signals). Then, it can obtain the downlink principal eigenvector $\mathbf{u}_{\mathrm{DL},1}(f_{FDD} = 0)$ by eigenvalue decomposition and use it for downlink transmission, so the expected SNR becomes

$$\mathrm{SNR}_{\mathrm{MAXSNR}}(f_{FDD} = 0) = \mathbf{u}_{\mathrm{DL},1}^{\mathrm{H}}(f_{FDD} = 0)\mathbf{R}_{\mathrm{DL}}(f_{FDD} = 0)\mathbf{u}_{\mathrm{DL},1}(f_{FDD} = 0) = e_{\mathrm{DL},1}, \tag{6.3}$$

where $e_{\mathrm{DL},1}$ is the maximum eigenvalue of $\mathbf{R}_{\mathrm{DL}}(f_{FDD} = 0)$. Finally, we can define the SNR performance loss due to FDD gap $L_{FDD}(f_{FDD})$ as a function of f_{FDD}, as follows

$$\begin{aligned} L_{FDD}(f_{FDD}) &= 10\log_{10}\left(\frac{\mathrm{SNR}_{\mathrm{MAXSNR}}(f_{FDD})}{\mathrm{SNR}_{\mathrm{MAXSNR}}(f_{FDD} = 0)}\right) \\ &= 10\log_{10}\left(\frac{\mathbf{u}_{\mathrm{UL},1}^{\mathrm{H}}(f_{FDD})\mathbf{R}_{\mathrm{DL}}(f_{FDD})\mathbf{u}_{\mathrm{UL},1}(f_{FDD})}{e_{\mathrm{DL},1}}\right). \end{aligned} \tag{6.4}$$

The parameter $L_{FDD}(f_{FDD})$ provides a measure of the SNR performance loss when the FDD gap is f_{FDD}. As we did for calculation of the eigenvector correlation in the last section, we vary f_{FDD} from 0 up to 50% of the reference carrier frequency and plot the corresponding values of the parameter $L_{FDD}(f_{FDD})$ in the macro cell, in Figure 6.2. We note that the negative sign of $L_{FDD}(f_{FDD})$ is expected, as it effectively means that $\mathrm{SNR}_{\mathrm{MAXSNR}}(f_{FDD})$ is smaller than $e_{\mathrm{DL},1}$ (i.e. there *is* performance loss). The results show that the loss increases with the FDD gap f_{FDD} and the number of transmit antennas M, which is consistent with the eigenvector correlation results of Figure 6.1. Also, when $f_{FDD} = 0.1 \times f_{ref}$ (i.e. $f_{FDD} = 0.2$ GHz, which is close to 0.19 GHz specified in [8]) the loss is small ($L_{FDD}(f_{FDD}) < 0.4$ dB) for all shown M values.

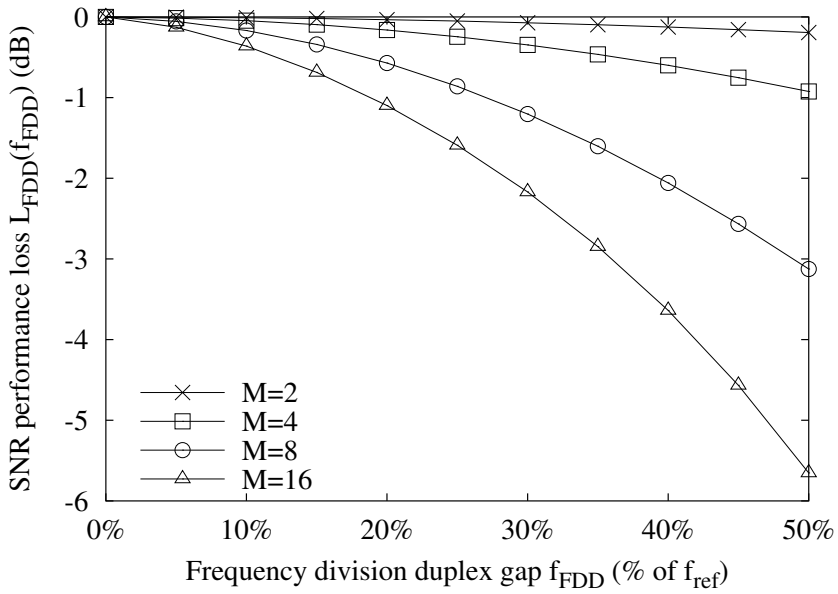

Figure 6.2: *SNR performance loss in the maximum SNR technique as a function of frequency division duplex gap and for $M = 2, 4, 8, 16$ in the macro cell.*

Now we turn our attention to the performance loss due to FDD in the minimum BER technique. Again we assume that the FDD gap is f_{FDD} and the base station uses the K 'largest' eigenvectors of the uplink channel correlation matrix $\mathbf{u}_{\mathrm{UL},i}(f_{FDD})$, $i = 1..K$, for downlink transmission. For notation convenience, we arrange the K eigenvectors in the matrix $\mathbf{U}_{\mathrm{UL}}(f_{FDD}) \in \mathbb{C}^{M\times K}$ as

$$\mathbf{U}_{\mathrm{UL}}(f_{FDD}) = \left[\mathbf{u}_{\mathrm{UL},1}(f_{FDD}) \;\; \mathbf{u}_{\mathrm{UL},2}(f_{FDD}) \;\; \cdots \;\; \mathbf{u}_{\mathrm{UL},K}(f_{FDD})\right]. \tag{6.5}$$

Then, assuming again that the transmit power and noise power is unit ($E_s = 1$ and $\sigma_n^2 = 1$ respectively), the expected SNR of the received signal at the mobile receiver for this f_{FDD}

value is given by

$$\mathrm{SNR}_{\mathrm{MINBER}}(f_{FDD}) = \frac{1}{K}\mathrm{trace}\left[\mathbf{U}_{\mathrm{UL}}^{\mathrm{H}}(f_{FDD})\mathbf{R}_{\mathrm{DL}}(f_{FDD})\mathbf{U}_{\mathrm{UL}}(f_{FDD})\right]. \tag{6.6}$$

Also, in the case of $f_{FDD} = 0$, the uplink and downlink mean correlation matrices are the same and the base station can obtain the latter by estimating the former. Then, it can obtain the K largest downlink eigenvectors $\mathbf{u}_{\mathrm{DL},i}(f_{FDD} = 0)$, $i = 1..K$, by eigenvalue decomposition and use them for downlink transmission. Arranging these eigenvectors in the matrix $\mathbf{U}_{\mathrm{DL}}(f_{FDD} = 0) \in \mathbb{C}^{M\times K}$ we have

$$\mathbf{U}_{\mathrm{DL}}(f_{FDD} = 0) = \left[\mathbf{u}_{\mathrm{DL},1}(f_{FDD} = 0)\ \ \mathbf{u}_{\mathrm{DL},2}(f_{FDD} = 0)\ \ \cdots\ \ \mathbf{u}_{\mathrm{DL},K}(f_{FDD} = 0)\right]. \tag{6.7}$$

Then, the expected SNR of the received signal at the mobile receiver for this f_{FDD} value becomes

$$\begin{aligned}\mathrm{SNR}_{\mathrm{MINBER}}(f_{FDD} = 0) &= \frac{1}{K}\mathrm{trace}\left[\mathbf{U}_{\mathrm{DL}}^{\mathrm{H}}(f_{FDD} = 0)\mathbf{R}_{\mathrm{DL}}(f_{FDD} = 0)\mathbf{U}_{\mathrm{DL}}(f_{FDD} = 0)\right] \\ &= \frac{1}{K}\left(e_{\mathrm{DL},1} + e_{\mathrm{DL},2} + \cdots + e_{\mathrm{DL},K}\right) = \frac{1}{K}\sum_{i=1}^{K} e_{\mathrm{DL},i},\end{aligned} \tag{6.8}$$

where $e_{\mathrm{DL},i}$, $i = 1..K$, are the K largest eigenvalues of $\mathbf{R}_{\mathrm{DL}}(f_{FDD} = 0)$. Therefore, the SNR performance loss $L_{FDD}(f_{FDD})$ can now be obtained as

$$\begin{aligned}L_{FDD}(f_{FDD}) &= 10\log_{10}\left(\frac{\mathrm{SNR}_{\mathrm{MINBER}}(f_{FDD})}{\mathrm{SNR}_{\mathrm{MINBER}}(f_{FDD} = 0)}\right) \\ &= 10\log_{10}\left(\frac{\mathrm{trace}\left[\mathbf{U}_{\mathrm{UL}}^{\mathrm{H}}(f_{FDD})\mathbf{R}_{\mathrm{DL}}(f_{FDD})\mathbf{U}_{\mathrm{UL}}(f_{FDD})\right]}{\sum_{i=1}^{K} e_{\mathrm{DL},i}}\right).\end{aligned} \tag{6.9}$$

Now, we vary f_{FDD} from 0 up to 50% of the reference carrier frequency and plot the corresponding values of the parameter $L_{FDD}(f_{FDD})$ in the macro and micro cells, in Figure 6.3. The figure shows that the performance loss increases as both the FDD gap f_{FDD} and number of transmit antennas M increase, which is also consistent with the eigenvector correlation results of Figure 6.1. Comparison of Figures 6.3(a) and 6.2 shows that the macro cell loss due to FDD in the minimum BER technique is smaller than the corresponding loss in the maximum SNR for the same M. This is probably because the former operates in general more efficiently than the latter, as it uses the optimum number of eigenvectors for downlink transmission instead of only the principal one. Also, Figure 6.3 illustrates that the loss for a given M depends on the

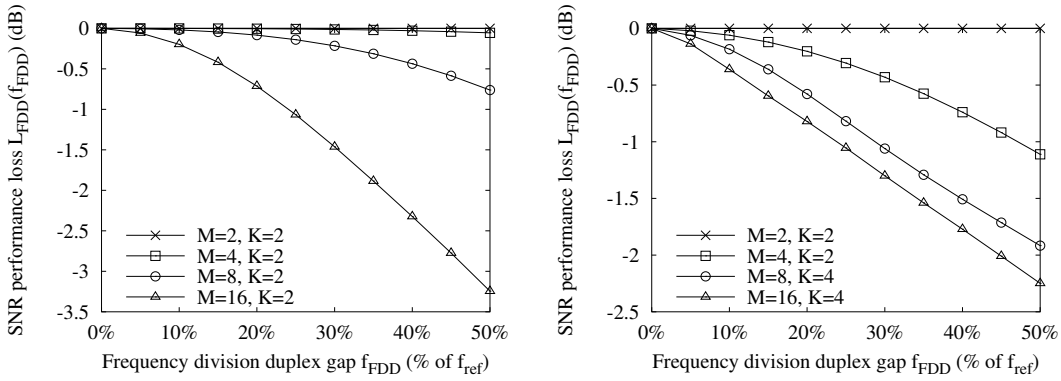

(a) Macro cell

(b) Micro cell

Figure 6.3: *SNR performance loss in the minimum BER technique as a function of frequency division duplex gap and for* $M = 2, 4, 8, 16$ *in the macro and micro cells.*

channel scenario, as it is generally different in the two cells. Finally, again we observe that when $f_{FDD} = 0.1 \times f_{ref}$ (i.e. $f_{FDD} = 0.2$ GHz) the loss is small for all shown M values in both cells ($L_{FDD}(f_{FDD}) < 0.2$ dB in the macro cell and $L_{FDD}(f_{FDD}) < 0.4$ dB in the micro cell).

6.2 Compensating for the frequency division duplex effects

In this section we will examine a simple but efficient approach to compensating for the FDD effects. Even though the results of the previous section suggest that the performance loss due to FDD for f_{FDD} and M values specified in [8] for third generation systems is not large, an efficient FDD compensation technique would give future mobile communication systems the freedom to use larger f_{FDD} and M values. In addition, if the FDD compensation technique is simple and does not impose a prohibitive computational (or other) load, it may be exploited in third generation systems to improve their performance (although the improvement may be small), wherever the highest possible performance is of great importance.

The basic principle behind the compensation technique is that, instead of using the 'raw' eigenvectors of the uplink correlation matrix for downlink transmission, the base station can translate the uplink correlation matrix to the downlink carrier frequency and use its eigenvectors. This approach effectively relies on the fact that the uplink directional information be also valid for the downlink, which is usually true [166] (unless f_{FDD} is unusually large). To this end, the

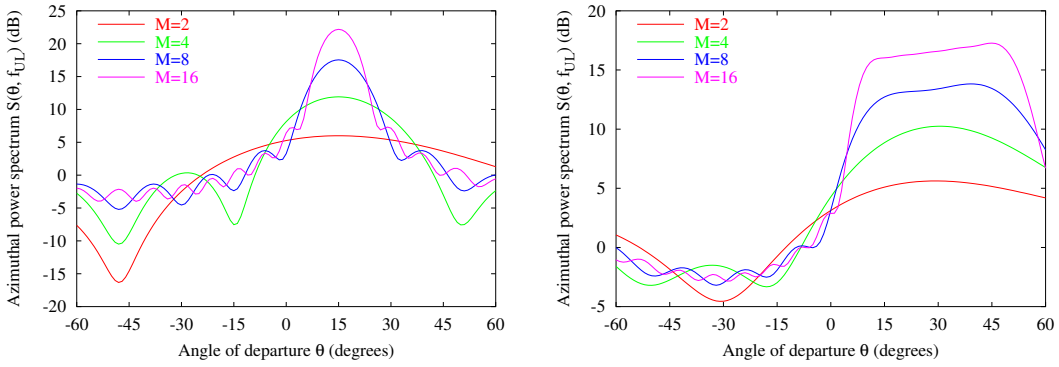

(a) Macro cell

(b) Micro cell

Figure 6.4: *Uplink azimuthal power spectrum estimate delivered by the conventional beamformer technique for $M = 2, 4, 8, 16$ in the macro and micro cells. The power spectrum estimate was calculated using equation (6.10) with $\theta_{step} = 1^o$.*

base station calculates the uplink azimuthal power spectrum $S(\theta, f_{\mathrm{UL}})$ of the intended user, and translates the information conveyed by this spectrum to the downlink carrier frequency to obtain an estimate of the downlink correlation matrix. The calculation of the uplink azimuthal power spectrum can be carried out relatively easily by the base station, since the latter can use the uplink channel estimates that it has to obtain anyway for coherent demodulation of the signal received from the intended mobile user. A simple way of obtaining $S(\theta, f_{\mathrm{UL}})$ is as follows

$$S(\theta, f_{\mathrm{UL}}) = \mathbf{v}^{\mathrm{H}}(\theta, f_{\mathrm{UL}})\mathbf{R}_{\mathrm{UL}}(f_{\mathrm{UL}})\mathbf{v}(\theta, f_{\mathrm{UL}}), \tag{6.10}$$

where $\mathbf{v}(\theta, f_{\mathrm{UL}}) = \left[1 \; e^{\jmath\frac{2\pi D}{\lambda_{\mathrm{UL}}}\sin(\theta)} \; \cdots \; e^{\jmath\frac{2\pi D}{\lambda_{\mathrm{UL}}}(M-1)\sin(\theta)}\right]^{\mathrm{T}}$ is a steering vector at the uplink carrier frequency with the main beam in the azimuthal direction $\theta \in [-60^{\mathrm{o}}, 60^{\mathrm{o}}]$ (D is the transmit antenna spacing, λ_{UL} is the wavelength of the uplink carrier frequency and the T superscript denotes transpose) and $\mathbf{R}_{\mathrm{UL}}(f_{\mathrm{UL}})$ is the estimate of the uplink correlation matrix at the base station. Since a common steering vector (conventional beamformer) is used, this method is called the 'conventional beamformer' technique. The spectrum $S(\theta, f_{\mathrm{UL}})$ is sampled at angular intervals of θ_{step} degrees (that is, the direction of the main beam θ is varied from -60^{o} to 60^{o} with a step of θ_{step} degrees). Figure 6.4 shows the azimuthal power spectrum $S(\theta, f_{\mathrm{UL}})$ of the macro and micro cells for $M = 2, 4, 8, 16$, calculated according to equation (6.10) with $\theta_{step} = 1^{\mathrm{o}}$ (the uplink correlation matrix as given by equations (A.2) and (A.3) of page 157 was used). In both channel scenarios the peaks of the spectrum appear over the azimuthal areas

where the angular spread occurs, while their width covers most of the angular spread area.

Once the base station calculates the uplink spectrum $S(\theta, f_{\mathrm{UL}})$, it uses it to obtain an estimate of the channel correlation matrix $\hat{\mathbf{R}}_{\mathrm{DL}}(f_{\mathrm{DL}})$ at the downlink carrier frequency f_{DL} as

$$\begin{aligned}
\hat{\mathbf{R}}_{\mathrm{DL}}(f_{\mathrm{DL}}) = \sum_{i=1}^{N} \Bigg\{ & P_i \left[\mathbf{v}(\theta_i, f_{\mathrm{DL}}) \mathbf{v}^{\mathrm{H}}(\theta_i, f_{\mathrm{DL}}) \right] \\
& + \underbrace{\sum_{l=1}^{N_l} P_l \left[\mathbf{v}(\theta_i - l\theta_{step}, f_{\mathrm{DL}}) \mathbf{v}^{\mathrm{H}}(\theta_i - l\theta_{step}, f_{\mathrm{DL}}) \right] \Big|_{N_l \,:\, P_l^{\mathrm{dB}} \geq P_i^{\mathrm{dB}} - P_{threshold}^{\mathrm{dB}} \text{ for all } l \in [1, N_l]}}_{\mathbf{R}_{left}(i)} \\
& + \underbrace{\sum_{r=1}^{N_r} P_r \left[\mathbf{v}(\theta_i + r\theta_{step}, f_{\mathrm{DL}}) \mathbf{v}^{\mathrm{H}}(\theta_i + r\theta_{step}, f_{\mathrm{DL}}) \right] \Big|_{N_r \,:\, P_r^{\mathrm{dB}} \geq P_i^{\mathrm{dB}} - P_{threshold}^{\mathrm{dB}} \text{ for all } r \in [1, N_r]}}_{\mathbf{R}_{right}(i)} \Bigg\} \\
\Rightarrow \hat{\mathbf{R}}_{\mathrm{DL}}(f_{\mathrm{DL}}) = \sum_{i=1}^{N} \Big\{ & P_i \left[\mathbf{v}(\theta_i, f_{\mathrm{DL}}) \mathbf{v}^{\mathrm{H}}(\theta_i, f_{\mathrm{DL}}) \right] + \mathbf{R}_{left}(i) + \mathbf{R}_{right}(i) \Big\}, \qquad (6.11)
\end{aligned}$$

where θ_i, $i = 1..N$, are the azimuthal directions where the main peaks of $S(\theta, f_{\mathrm{UL}})$ occur, while P_i, $i = 1..N$, are the corresponding (linear) amplitudes of these peaks. In order for a peak to be taken into account in the $\hat{\mathbf{R}}_{\mathrm{DL}}(f_{\mathrm{DL}})$ estimate, its amplitude P_i^{dB} (in dB) must be at most 10 dB smaller than the amplitude of the maximum peak $P_{\max}^{\mathrm{dB}}$ of the spectrum (i.e. $P_i^{\mathrm{dB}} \geq P_{\max}^{\mathrm{dB}} - 10$). Furthermore, whenever a spectrum peak is taken into account in the $\hat{\mathbf{R}}_{\mathrm{DL}}(f_{\mathrm{DL}})$ estimate, two more terms are added to this estimate, $\mathbf{R}_{left}(i)$ and $\mathbf{R}_{right}(i)$, which basically account for the angular spread on either side of the peak (this is an improvement since the technique was first presented in [121]). The term $\mathbf{R}_{left}(i)$ accounts for the part of the angular spread that is on the left of the i-th peak, and includes the correlation matrices of N_l steering vectors; the main beam direction of the l-th steering vector is $l \times \theta_{step}$ degrees leftward from the main beam direction of the i-th peak (i.e. $\theta_l = \theta_i - l \times \theta_{step}$). The number of correlation matrices N_l included in $\mathbf{R}_{left}(i)$ is such that the amplitude of the spectrum (in dB) in the respective directions is at most $P_{threshold}^{\mathrm{dB}}$ dB smaller than the spectrum amplitude (in dB) in the direction of the i-th peak (i.e. $N_l : P_l^{\mathrm{dB}} \geq P_i^{\mathrm{dB}} - P_{threshold}^{\mathrm{dB}}$ for all $l \in [1, N_l]$). Similarly, the term $\mathbf{R}_{right}(i)$ accounts for the part of the angular spread that is on the right of the i-th peak, and includes the correlation matrices of N_r steering vectors; the main beam direction of the r-th steering vector is $r \times \theta_{step}$ degrees rightward from the main beam direction of the i-th peak (i.e. $\theta_r = \theta_i + r \times \theta_{step}$). The number of correlation matrices N_r included in $\mathbf{R}_{right}(i)$ is such that the amplitude of the spectrum (in dB) in the respective directions is at most $P_{threshold}^{\mathrm{dB}}$ dB smaller than the spectrum

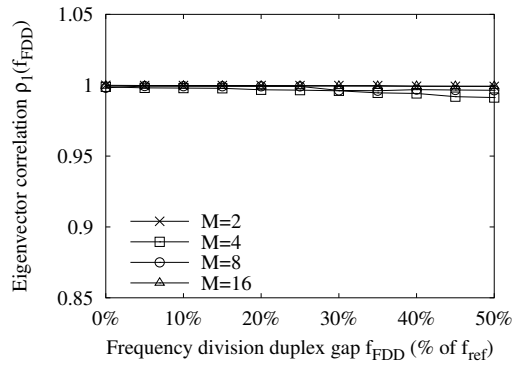

(a) First (principal) eigenvector, macro cell

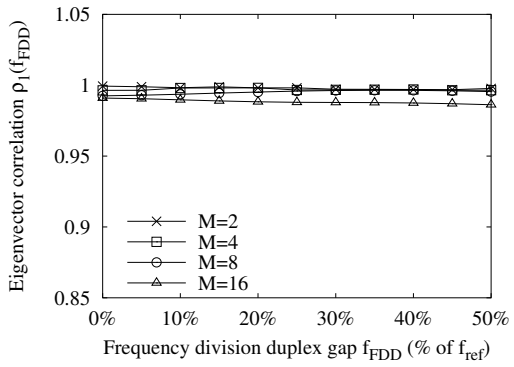

(b) First (principal) eigenvector, micro cell

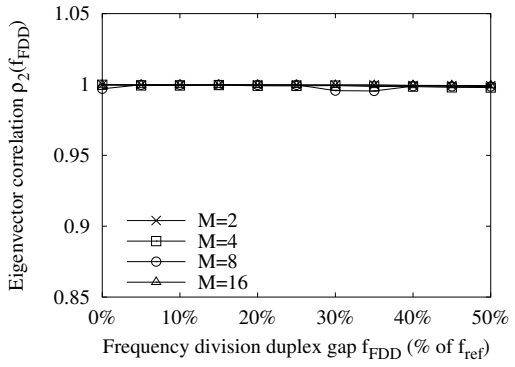

(c) Second eigenvector, macro cell

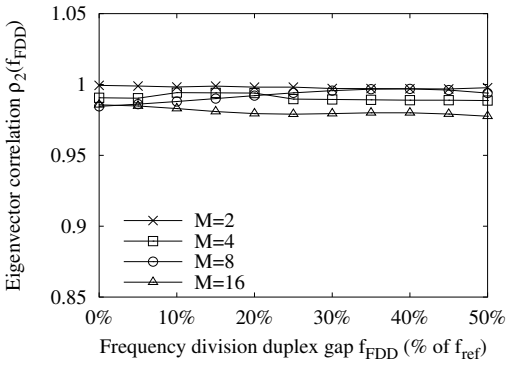

(d) Second eigenvector, micro cell

Figure 6.5: *Correlation between actual downlink eigenvectors and downlink eigenvectors estimated using the conventional beamformer technique, as a function of frequency division duplex gap and for* $M = 2, 4, 8, 16$ *in the macro and micro cells.*

amplitude (in dB) in the direction of the i-th peak (i.e. $N_r : P_r^{\text{dB}} \geq P_i^{\text{dB}} - P_{threshold}^{\text{dB}}$ for all $r \in [1, N_r]$). We have found experimentally that the optimum value for $P_{threshold}^{\text{dB}}$ is 1 dB when $M = 2$ and 2 dB when $M = 4, 8, 16$. Finally, all the linear amplitudes of equation (6.11) are normalised as follows

$$\sum_{i=1}^{N} \left\{ P_i + \sum_{l=1}^{N_l} P_l + \sum_{r=1}^{N_r} P_r \right\} = 1. \tag{6.12}$$

After obtaining $\hat{\mathbf{R}}_{\text{DL}}(f_{\text{DL}})$, the base station performs its eigenvalue decomposition and uses its eigenvalues and/or eigenvectors (depending on the technique) for downlink transmission.

A measure of the performance of the above compensation technique is its impact on the correl-

ation between the actual downlink eigenvectors and the eigenvectors of the estimated downlink correlation matrix, and on the SNR performance loss. First, in order to calculate the eigenvector correlation, we use the same assumptions and parameters as those of section 6.1.1 and calculate the mean uplink $\mathbf{R}_{\mathrm{UL}}(f_{FDD})$ and downlink $\mathbf{R}_{\mathrm{DL}}(f_{FDD})$ correlation matrices for a given f_{FDD} (using again equations (A.2) and (A.3) of page 157). The downlink correlation matrix is subject to an eigenvalue decomposition and its eigenvectors $\mathbf{u}_{\mathrm{DL},i}(f_{FDD}) \in \mathbb{C}^{M\times 1}$, $i = 1..M$, are obtained. The uplink correlation matrix is subject to the above compensation technique to yield an estimate of the downlink correlation matrix $\hat{\mathbf{R}}_{\mathrm{DL}}(f_{FDD})$, which is then also subject to an eigenvalue decomposition and its eigenvectors $\hat{\mathbf{u}}_{\mathrm{DL},i}(f_{FDD}) \in \mathbb{C}^{M\times 1}$, $i = 1..M$, are obtained. Finally, the correlation $\rho_i(f_{FDD})$ between the i-th eigenvector $\mathbf{u}_{\mathrm{DL},i}(f_{FDD})$ of the actual downlink correlation matrix and the i-th eigenvector $\hat{\mathbf{u}}_{\mathrm{DL},i}(f_{FDD})$ of the estimated downlink correlation matrix is obtained as

$$\rho_i(f_{FDD}) = |\mathbf{u}^{\mathrm{H}}_{\mathrm{DL},i}(f_{FDD})\hat{\mathbf{u}}_{\mathrm{DL},i}(f_{FDD})|. \tag{6.13}$$

The value of f_{FDD} is varied from 0 to 50% of f_{ref} with a step of 0.1 GHz, and the corresponding $\rho_i(f_{FDD})$ for $i = 1, 2$ (i.e. for the first and second eigenvectors) is plotted in Figure 6.5. The figure includes correlation values for $M = 2, 4, 8, 16$ transmit antennas in the macro and micro cells. Comparison of Figure 6.5 with Figure 6.1 shows that the correlation is increased dramatically, and is now very close to one for all shown f_{FDD} values. This means that the two 'largest' eigenvectors of the estimated downlink correlation matrix are highly accurate estimates of the corresponding actual downlink eigenvectors.

Now we move on to the calculation of the SNR performance loss in maximum SNR and minimum BER, after applying FDD compensation using the conventional beamformer method. We start with maximum SNR. Given that the base station uses the principal eigenvector $\hat{\mathbf{u}}_{\mathrm{DL},1}(f_{FDD})$ of the estimated downlink correlation matrix for downlink transmission, and using the same assumptions and parameters as in section 6.1.2, the expected SNR of the received signal at the mobile receiver for a given f_{FDD} value is

$$\mathrm{SNR}_{\mathrm{MAXSNR}}(f_{FDD}) = \hat{\mathbf{u}}^{\mathrm{H}}_{\mathrm{DL},1}(f_{FDD})\mathbf{R}_{\mathrm{DL}}(f_{FDD})\hat{\mathbf{u}}_{\mathrm{DL},1}(f_{FDD}), \tag{6.14}$$

where $\mathbf{R}_{\mathrm{DL}}(f_{FDD})$ is the actual mean downlink correlation matrix for the above f_{FDD} value. In the case of $f_{FDD} = 0$, the $\mathrm{SNR}_{\mathrm{MAXSNR}}(f_{FDD} = 0)$ value is given by equation (6.3). Therefore,

the SNR loss $L_{FDD}(f_{FDD})$ as a function of f_{FDD} is given by

$$L_{FDD}(f_{FDD}) = 10\log_{10}\left(\frac{\mathrm{SNR}_{\mathrm{MAXSNR}}(f_{FDD})}{\mathrm{SNR}_{\mathrm{MAXSNR}}(f_{FDD}=0)}\right)$$
$$= 10\log_{10}\left(\frac{\hat{\mathbf{u}}^{\mathrm{H}}_{\mathrm{DL},1}(f_{FDD})\mathbf{R}_{\mathrm{DL}}(f_{FDD})\hat{\mathbf{u}}_{\mathrm{DL},1}(f_{FDD})}{e_{\mathrm{DL},1}}\right). \quad (6.15)$$

The value of $L_{FDD}(f_{FDD})$ is plotted in Figure 6.6 for f_{FDD} from 0 to 50% of f_{ref} with a step of 0.1 GHz and $M = 2, 4, 8, 16$, in the macro cell. The loss is close to zero for $M = 2$, it is very small for $M = 4, 8$ ($L_{FDD}(f_{FDD}) < 0.15$ dB and $L_{FDD}(f_{FDD}) < 0.3$ dB respectively), and it is small even for $M = 16$ ($L_{FDD}(f_{FDD}) \leq 0.7$ dB), over all shown f_{FDD} values. Also, comparison with Figure 6.2 shows that the loss is greatly decreased, which is most likely due to the translation of the uplink correlation matrix into the downlink carrier frequency.

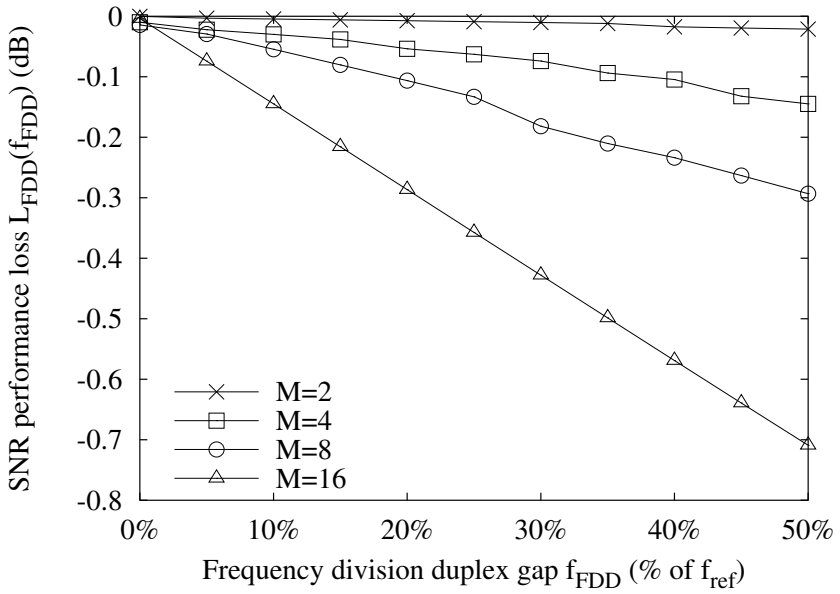

Figure 6.6: *SNR performance loss as a function of frequency division duplex gap in the maximum SNR technique after FDD effect compensation by the conventional beamformer technique for $M = 2, 4, 8, 16$ in the macro cell.*

Now consider the calculation of the SNR loss in the minimum BER technique after FDD compensation by means of the conventional beamformer technique. Let us assume that when the FDD gap is f_{FDD} the base station uses the K 'largest' eigenvectors $\hat{\mathbf{u}}_{\mathrm{DL},i}(f_{FDD})$, $i = 1..K$, of the estimated downlink correlation matrix for downlink transmission. Again, we arrange the K

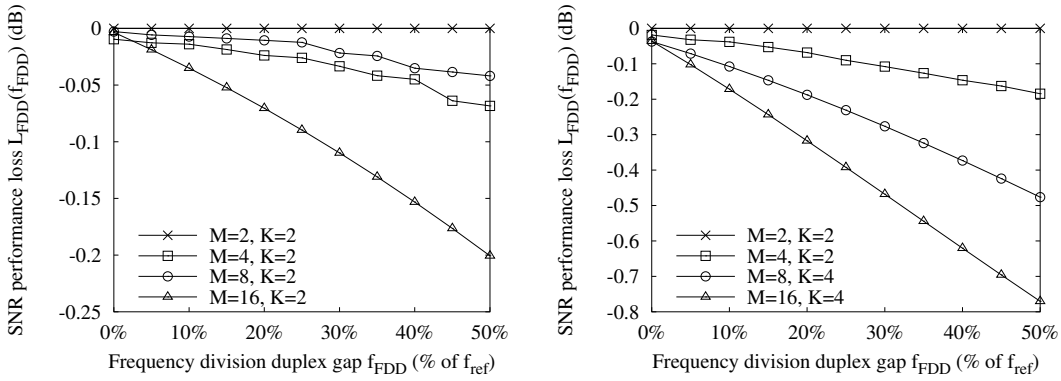

(a) Macro cell **(b)** Micro cell

Figure 6.7: *SNR performance loss as a function of frequency division duplex gap in the minimum BER technique after FDD effect compensation by the conventional beamformer technique for* $M = 2, 4, 8, 16$ *in the macro and micro cells.*

eigenvectors in a matrix $\hat{\mathbf{U}}_{\mathrm{DL}}(f_{FDD}) \in \mathbb{C}^{M\times K}$ for notation convenience

$$\hat{\mathbf{U}}_{\mathrm{DL}}(f_{FDD}) = \left[\hat{\mathbf{u}}_{\mathrm{DL},1}(f_{FDD})\ \ \hat{\mathbf{u}}_{\mathrm{DL},2}(f_{FDD})\ \ \cdots\ \ \hat{\mathbf{u}}_{\mathrm{DL},K}(f_{FDD})\right]. \tag{6.16}$$

Then, the expected SNR of the received signal at the mobile receiver for this f_{FDD} value is given by

$$\mathrm{SNR}_{\mathrm{MINBER}}(f_{FDD}) = \frac{1}{K}\mathrm{trace}\left[\hat{\mathbf{U}}^{\mathrm{H}}_{\mathrm{DL}}(f_{FDD})\mathbf{R}_{\mathrm{DL}}(f_{FDD})\hat{\mathbf{U}}_{\mathrm{DL}}(f_{FDD})\right], \tag{6.17}$$

where $\mathbf{R}_{\mathrm{DL}}(f_{FDD})$ is the actual mean downlink correlation matrix for the above f_{FDD} value. Also, in the case of $f_{FDD} = 0$, the expected SNR is given by equation (6.8). Hence, the SNR performance loss $L_{FDD}(f_{FDD})$ can be obtained as

$$\begin{aligned} L_{FDD}(f_{FDD}) &= 10\log_{10}\left(\frac{\mathrm{SNR}_{\mathrm{MINBER}}(f_{FDD})}{\mathrm{SNR}_{\mathrm{MINBER}}(f_{FDD}=0)}\right) \\ &= 10\log_{10}\left(\frac{\mathrm{trace}\left[\hat{\mathbf{U}}^{\mathrm{H}}_{\mathrm{DL}}(f_{FDD})\mathbf{R}_{\mathrm{DL}}(f_{FDD})\hat{\mathbf{U}}_{\mathrm{DL}}(f_{FDD})\right]}{\sum_{i=1}^{K} e_{\mathrm{DL},i}}\right). \end{aligned} \tag{6.18}$$

The value of $L_{FDD}(f_{FDD})$ is plotted in Figure 6.7 for f_{FDD} from 0 to 50% of f_{ref} with a step of 0.1 GHz and $M = 2, 4, 8, 16$, in the macro and micro cells. Figure 6.7(a) illustrates that the loss in the macro cell is very small ($L_{FDD}(f_{FDD}) \leq 0.2$ dB) for all M and over all shown f_{FDD} values, while comparison with Figure 6.3(a) suggests that the FDD effect compensation benefits mostly the larger M values (i.e. $M = 8, 16$)—but the loss for $M = 2, 4$ is small without

FDD effect compensation anyway. Also, Figure 6.7(b) illustrates that the loss in the micro cell is in general small, although it is a bit larger than that of the macro cell for the same M. In addition, comparison with Figure 6.3(b) shows that the loss reduction because of conventional beamformer FDD compensation is generally smaller in the micro cell than in the macro cell (apart from the case of $M = 4$ where the loss reduction is larger in the micro cell, probably because in this case the loss without FDD compensation is very small in the macro cell, making the margin for improvement very small).

6.3 Comparison with an existing compensation technique

In this section the conventional beamformer compensation technique will be compared with an existing compensation technique. The latter was first presented in [100] and was later improved in [101]. The fundamental principle is similar in both techniques. That is, in both techniques the uplink correlation matrix is estimated and then used to calculate the uplink azimuthal power spectrum, which is in turn used to obtain an estimate of the downlink channel correlation matrix. However, there are differences in key points between the two techniques. In particular, the way of calculating the uplink azimuthal power spectrum from the uplink correlation matrix, as well as that of obtaining the downlink channel correlation matrix from this spectrum, differ between the two techniques. More specifically, in the existing technique the uplink azimuthal power spectrum $S(\theta, f_{\mathrm{UL}})$ is calculated from the uplink correlation matrix $\mathbf{R}_{\mathrm{UL}}(f_{\mathrm{UL}})$ as

$$S(\theta, f_{\mathrm{UL}}) = \frac{1}{\mathbf{v}^{\mathrm{H}}(\theta, f_{\mathrm{UL}})\mathbf{R}_{\mathrm{UL}}^{-1}(f_{\mathrm{UL}})\mathbf{v}(\theta, f_{\mathrm{UL}})}, \tag{6.19}$$

where $\mathbf{R}_{\mathrm{UL}}^{-1}(f_{\mathrm{UL}})$ denotes the inverse of $\mathbf{R}_{\mathrm{UL}}(f_{\mathrm{UL}})$. Since the above expression resembles the minimum variance distortionless response filter, we call this compensation technique the 'minimum variance' technique. We note that this is more computationally expensive than equation (6.10) (especially for larger M), since it requires the additional step of inverting $\mathbf{R}_{\mathrm{UL}}(f_{\mathrm{UL}})$. The uplink azimuthal power spectrum of the macro and micro cells is obtained as in section 6.2, but using equation (6.19) instead of equation (6.10), and it is plotted in Figure 6.8 for $M = 2, 4, 8, 16$. The maxima of the azimuthal power spectrum occur over the angular spread areas, while their width extends over most of it. Also, the spectrum is (greatly) suppressed over azimuthal directions that do not correspond to angular spread areas (especially for larger M).

After calculation of the uplink azimuthal power spectrum $S(\theta, f_{\mathrm{UL}})$, this spectrum is modified

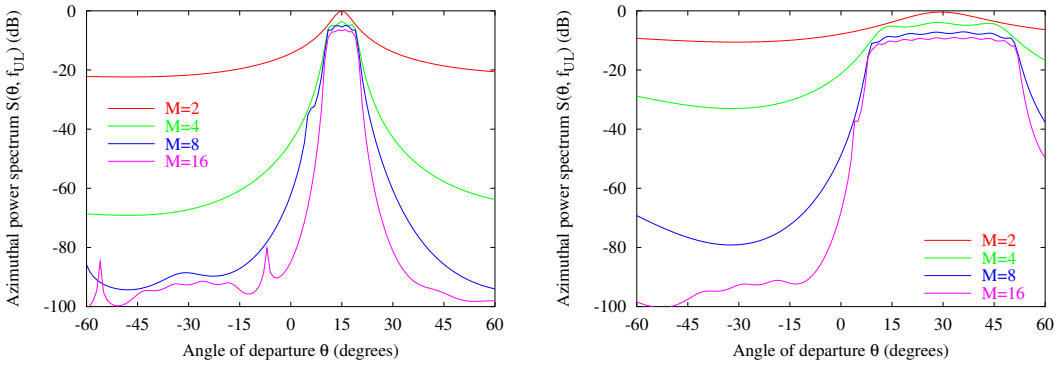

(a) Macro cell

(b) Micro cell

Figure 6.8: *Uplink azimuthal power spectrum estimate delivered by the minimum variance technique for $M = 2, 4, 8, 16$ in the macro and micro cells. The power spectrum estimate was calculated using equation (6.19) with $\theta_{step} = 1^o$.*

to avoid 'beam-pointing errors' as described in [101], so the modified uplink power spectrum $S_{mod}(\theta, f_{\mathrm{UL}})$ is produced. This process basically 'removes' from $S(\theta, f_{\mathrm{UL}})$ the azimuthal directions over which the uplink spectrum has very small amplitude by multiplication with an appropriate rectangular window. The modified spectrum is then integrated over the azimuth to yield an estimate of the downlink correlation matrix $\hat{\mathbf{R}}_{\mathrm{DL}}(f_{\mathrm{DL}})$

$$\hat{\mathbf{R}}_{\mathrm{DL}}(f_{\mathrm{DL}}) = \int_{\theta} S_{mod}(\theta, f_{\mathrm{UL}})\mathbf{v}(\theta, f_{\mathrm{DL}})\mathbf{v}^{\mathrm{H}}(\theta, f_{\mathrm{DL}}). \tag{6.20}$$

Finally, the base station can obtain the eigenvalues and/or eigenvectors of $\hat{\mathbf{R}}_{\mathrm{DL}}(f_{\mathrm{DL}})$ and use them for downlink transmission.

As in the last section, in order to examine the impact of the above FDD compensation technique on the uplink and downlink eigenvector correlation, we use the same assumptions and parameters as those of section 6.1.1 and calculate the mean uplink $\mathbf{R}_{\mathrm{UL}}(f_{FDD})$ and downlink $\mathbf{R}_{\mathrm{DL}}(f_{FDD})$ correlation matrices for a given f_{FDD} (using equations (A.2) and (A.3) of page 157). The downlink correlation matrix is subject to eigenvalue decomposition so that its eigenvectors $\mathbf{u}_{\mathrm{DL},i}(f_{FDD}) \in \mathbb{C}^{M\times 1}$, $i = 1..M$, are obtained. The uplink correlation matrix is subject to the above FDD compensation technique to yield an estimate of the downlink correlation matrix $\hat{\mathbf{R}}_{\mathrm{DL}}(f_{FDD})$, which is then also subject to eigenvalue decomposition and its eigenvectors $\hat{\mathbf{u}}_{\mathrm{DL},i}(f_{FDD}) \in \mathbb{C}^{M\times 1}$, $i = 1..M$, are obtained. Finally, the correlation $\rho_i(f_{FDD})$ between the

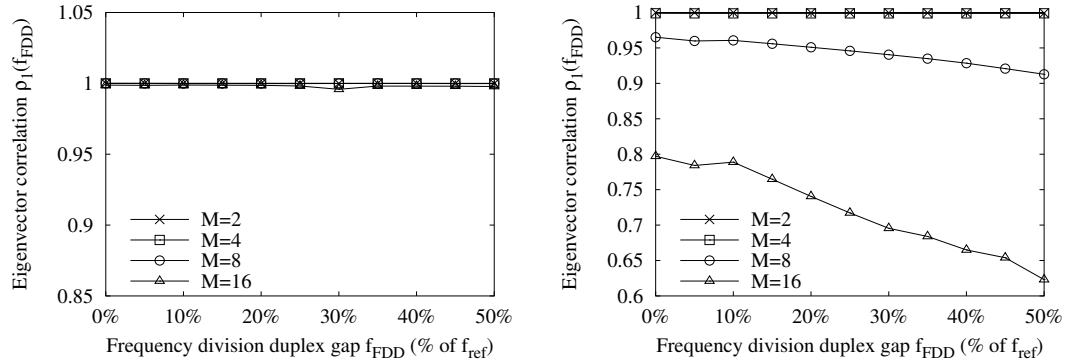

(a) First (principal) eigenvector, macro cell

(b) First (principal) eigenvector, micro cell

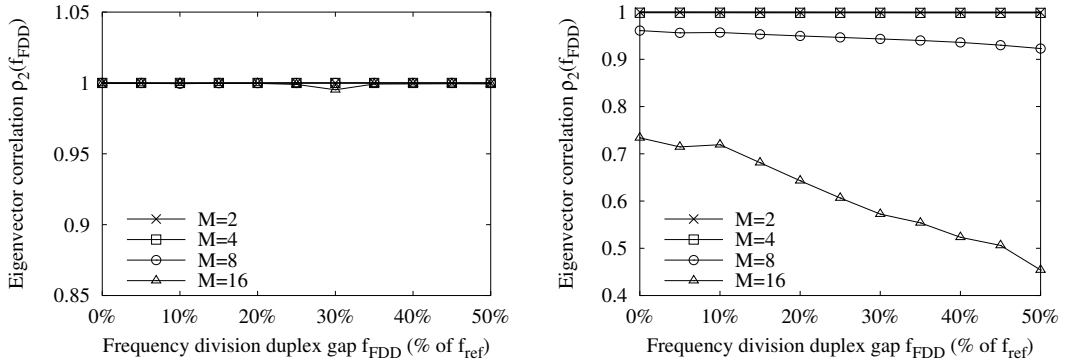

(c) Second eigenvector, macro cell

(d) Second eigenvector, micro cell

Figure 6.9: *Correlation between actual downlink eigenvectors and downlink eigenvectors estimated using the minimum variance technique, as a function of frequency division duplex gap and for* $M = 2, 4, 8, 16$ *in the macro and micro cells.*

i-th eigenvector $\mathbf{u}_{\mathrm{DL},i}(f_{FDD})$ of the actual downlink correlation matrix and the i-th eigenvector $\hat{\mathbf{u}}_{\mathrm{DL},i}(f_{FDD})$ of the estimated downlink correlation matrix is calculated as in equation (6.13). The value of f_{FDD} is varied from 0 to 50% of f_{ref} with a step of 0.1 GHz, and the corresponding $\rho_i(f_{FDD})$ for $i = 1, 2$ (i.e. for the first and second eigenvectors) is plotted in Figure 6.9. The figure includes correlation values for $M = 2, 4, 8, 16$ transmit antennas in the macro and micro cells. The eigenvector correlation in the macro cell is very close to one for all M values. In the micro cell, however, the eigenvector correlation is close to one for $M = 2, 4, 8$ but becomes lower with f_{FDD} for $M = 16$.

Next, we examine the impact of FDD effect compensation through the minimum variance technique on the SNR performance loss of the maximum SNR technique. As in the last section,

the loss $L_{FDD}(f_{FDD})$ for a given f_{FDD} value is given by equation (6.15), but the eigenvector $\hat{\mathbf{u}}^{\mathrm{H}}_{\mathrm{DL},1}(f_{FDD})$ is now the principal eigenvector of the estimated downlink correlation matrix obtained from equation (6.20). The value of $L_{FDD}(f_{FDD})$ is plotted in Figure 6.10 for f_{FDD} from 0 to 50% of f_{ref} with a step of 0.1 GHz and $M = 2, 4, 8, 16$, in the macro cell. The results of this figure are very similar to those of Figure 6.6 (actually the minimum variance technique yields slightly better SNR performance than the conventional beamformer technique for $M = 4, 8$). This means that although the conventional beamformer technique is less complex than the minimum variance technique (since it does not require matrix inversion), it yields almost the same loss reduction as it.

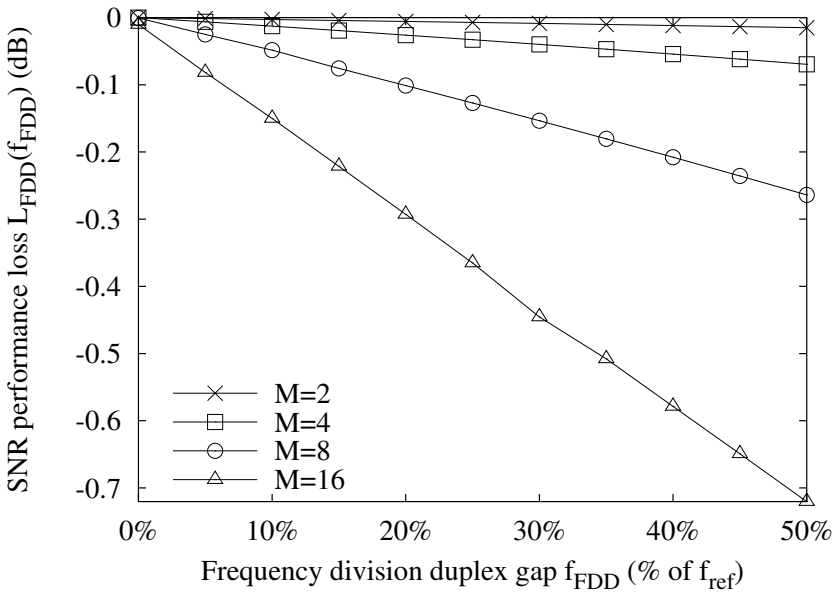

Figure 6.10: *SNR performance loss as a function of frequency division duplex gap in the maximum SNR technique after FDD effect compensation by the minimum variance technique for* $M = 2, 4, 8, 16$ *in the macro cell.*

Finally, we examine the SNR performance loss reduction in the minimum BER technique. The loss $L_{FDD}(f_{FDD})$ for a given f_{FDD} value is again given by equation (6.18), but the eigenvectors $\hat{\mathbf{u}}^{\mathrm{H}}_{\mathrm{DL},i}(f_{FDD})$, $i = 1..K$, are now those of the estimated downlink correlation matrix obtained from equation (6.20). The value of $L_{FDD}(f_{FDD})$ is plotted in Figure 6.11 for f_{FDD} from 0 to 50% of f_{ref} with a step of 0.1 GHz and $M = 2, 4, 8, 16$, in the macro and micro cells. Again the results of this figure are very similar to those of Figure 6.7. In addition, regarding the case with $M = 16$ transmit antennas, the loss reduction of Figure 6.11(b) is very similar to that of Figure 6.7(b), even though the correlation of Figures 6.9(b) and 6.9(d) is not as high as that of Figures

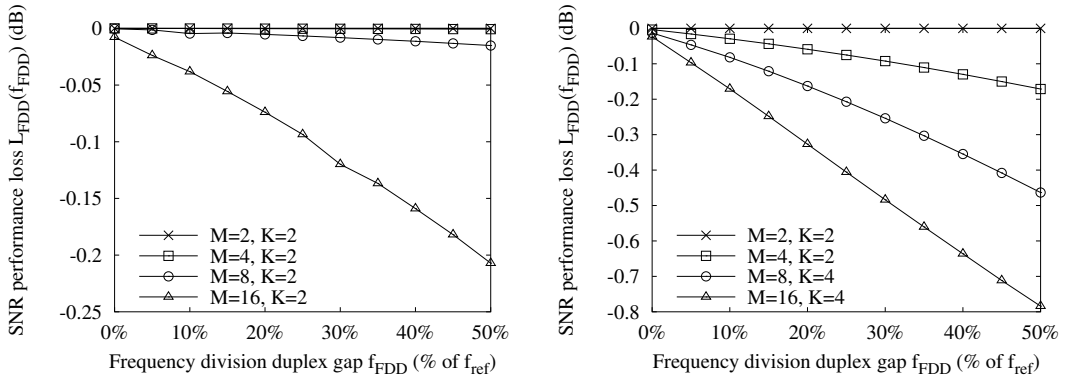

(a) Macro cell

(b) Micro cell

Figure 6.11: *SNR performance loss as a function of frequency division duplex gap in the minimum BER technique after FDD effect compensation by the minimum variance technique for* $M = 2, 4, 8, 16$ *in the macro and micro cells.*

6.5(b) and 6.5(d). This may suggest that the correlation between the actual and estimated downlink eigenvectors might not be the most important factor. Rather, the translation of the uplink directional information into the downlink carrier frequency seems to be more important. The conclusion that this translation appears to play an important role was also drawn in [121], where the angular spread was not accounted for in the calculation of the downlink correlation matrix estimate (i.e. equation (6.11) did not include the terms $\mathbf{R}_{left}(i)$ and $\mathbf{R}_{right}(i)$).

6.4 Summary

In this chapter we examined the impact of frequency division duplex gap on the performance of open loop downlink beamforming techniques that make use of eigenbeams (the techniques maximum SNR and minimum BER were examined). The correlation between uplink and downlink eigenbeams was shown to decrease with increasing FDD gap and M. Thus, when the above two techniques make use of the 'raw' uplink eigenbeams for downlink transmission, their performance deteriorates with increasing FDD gap and M. Next, a simple technique for compensating for these FDD effects was investigated. First, the technique uses the uplink channel correlation matrix to calculate the uplink azimuthal power spectrum. Next, it obtains an estimate of the downlink channel correlation matrix through translation of the directional information of the uplink azimuthal power spectrum into the downlink carrier frequency, in a

simple manner. This technique was shown to improve the correlation between the uplink and downlink eigenbeams and to reduce the performance loss considerably. Comparison of this technique with an existing compensation technique illustrated that although the latter is more complex, it does not provide a significant additional performance improvement.

Chapter 7
Concluding remarks

In this thesis, antenna array techniques that can be employed on the downlink of WCDMA mobile communication systems were examined. The presented work can be split into three logical parts: the first part includes comparison of a number of downlink antenna array techniques in various channel scenarios and using the same assumptions (Chapter 3), the second part includes examination of the performance of minimum BER and comparison of it with the other array techniques (Chapter 4), and the third part includes results related to performance loss in the above techniques due to various phenomena (i.e. effects of noisy estimates of various parameters and the frequency division duplex effect—Chapters 5 and 6 respectively). Following is a summary of the main conclusions of each part, along with a number of possible directions for future work.

Regarding the comparison of the downlink array techniques in Chapter 3, it was shown that in general pure diversity techniques (e.g. space-time spreading) do not perform well in environments with high correlation among the signals of the M array elements, because the benefit from the diversity gain is small. Beamforming techniques (e.g. maximum SNR) perform generally better in such environments. However, the performance of pure diversity techniques may be practically improved in these environments by simply increasing the transmit array spacing. Hybrid algorithms that combine diversity and beamforming gain (e.g. fixed beams and eigenbeamforming) appear to perform well in a variety of different channel environments, but usually require some kind of information feedback from mobile to base station. When such information feedback can be used, these algorithms can be employed to improve performance. As a rule, the higher the feedback rate and the more complex the base station, the larger the performance improvement. Nonetheless, in environments like the pico cell, even simple algorithms (e.g. selection diversity) yield performance equal to that of the more complex algorithms (e.g. eigenbeamforming). Also, a noteworthy result is that the technique fixed beams yields performance very similar to that of eigenbeamforming in a number of scenarios, even though it uses a (much) lower feedback rate. A possible explanation is that, in these scenarios, the differences of the two techniques are ‘suppressed’ while their similarities are emphasised.

In addition, it was shown that, depending on the technique and the channel scenario, increasing the number of base station transmit antennas does not always improve performance as it may be intuitively expected. An example of this behaviour is the technique maximum SNR in the pico cell.

In the next part of the thesis (Chapter 4), the decomposition of the channel into independent components by means of eigenvalue decomposition of its correlation matrix was examined. This led to the investigation of the combination of the channel components and space-time coding as an efficient open loop approach to the downlink data signal transmission. The approach was applied to optimise a performance criterion which attempts to minimise the transmit power required to achieve a target BER at the mobile receiver, by using a specific number of channel components. This scheme was named minimum BER. Theoretical performance calculation of minimum BER in a channel propagation environment with one tap in terms of the eigenvalues of the mean channel correlation matrix, showed that its behaviour varies from pure beamforming to pure diversity. The exact nature and amount of the performance improvement yielded by this technique, depends on the channel conditions and the number of base station transmit antennas.

The open loop mode of minimum BER was also simulated in three representative 1-tap cells and one 2-tap scenario, and the results were compared to those of the techniques of Chapter 3. The comparisons showed that minimum BER provides the best performance among all the examined open loop techniques at the BER for which its performance was optimised. Additionally, minimum BER is in general mostly beneficial in scenarios with small to moderate angular spread values. This may be explained by the fact that none of the existing open loop techniques yields the maximum expected performance in these conditions. Moreover, the performance improvement provided by the technique generally increases as the number of base station transmit antennas increases. This may be explained by the fact that, as the number of transmit antennas increases, the optimisation procedure of minimum BER gains more 'freedom' to yield a better solution.

In the first half of the third part of the thesis (Chapter 5), the impact of estimating various parameters that are needed at the base and mobile station from pilot signals on the performance of various downlink antenna array algorithms was discussed. The estimated parameters included the channel vector, the channel correlation matrix and the identification of the highest SNR transmit antenna or beam by the mobile station. The details of the channel correlation

matrix estimation from pilot signals were also examined, and the memory of this process was expressed as a function of the forgetting factor α. In addition, feedback of the downlink channel coefficients and the index to the highest SNR transmit antenna or beam from mobile to base station was discussed. Next, the effect of noisy estimates of the above parameters on the performance of various downlink antenna array techniques was examined through computer simulations.

The results suggested that the noisy parameter estimates result in performance loss in most cases, while the exact amount and form of the loss is usually related to the estimated parameter. Also, the loss might depend on the number of transmit antennas M in the base station, the SNR value and/or the channel scenario. As a rule, the more power is allocated to the pilot signals from which the parameters are estimated, the smaller the performance loss. The loss from estimation of the M downlink channel coefficients from pilot signals at the mobile receiver generally increases with M, when the total allocated pilot power is fixed. The same holds for the case where the downlink channel coefficients are sent to base station, where they are used for calculation of the weight vector, but now there is additional noise resulting from the quantisation of the channel coefficients. The amount of this noise is related to the number of bits used by the mobile station quantiser: the more quantisation bits, the smaller the loss. Also, noisy estimates of the correlation matrix principal eigenvector in the technique maximum SNR do not degrade performance by a large amount, since this eigenvector is not affected too much by the noise in the matrix. The forgetting factor α is important in this case, as larger α values increase the memory of the correlation matrix estimation process and generally yield smaller performance loss. Furthermore, a large α results in more accurate estimates of the smaller eigenvalues in the technique minimum BER, enhancing its performance. In addition, the frequent selection of the number of eigenvectors that provides the lowest SNR for the target BER in this technique, compensates for most of the effect of the noisy correlation matrix estimate and enables it to yield performance very close to the noiseless correlation matrix case. Moreover, when the highest SNR transmit antenna or beam is selected from (noisy) pilot signals by the mobile station, the performance loss increases with the number of antennas, if the total pilot power allocated to the M antennas or beams is fixed. Finally, noisy feedback of the index to the highest SNR antenna or beam from mobile to base station degrades performance. The performance loss in this case is related to the feedback path BER, with smaller BER values providing smaller loss.

In the second half of the third part of the thesis (Chapter 6), the impact of the frequency division duplex gap on the performance of open loop downlink beamforming techniques that make use of eigenbeams was discussed. In particular, the techniques maximum SNR and minimum BER were examined. First, the correlation between corresponding uplink and downlink eigenbeams was shown to decrease with increasing FDD gap and number of transmit antennas (M). The increasingly smaller correlation of the eigenbeams means that, when the above two techniques make use of the 'raw' uplink eigenbeams for downlink transmission, their performance deteriorates with increasing FDD gap and M. Next, a simple technique for compensating for these FDD effects was investigated. First, the technique uses the uplink channel correlation matrix to calculate the uplink azimuthal power spectrum. Then, it obtains an estimate of the downlink channel correlation matrix through translation of the directional information of the uplink azimuthal power spectrum into the downlink carrier frequency, in a simple manner. This procedure was shown to improve the correlation between corresponding eigenbeams of the estimated downlink correlation matrix and the real downlink correlation matrix, and to reduce the performance loss due to FDD gap considerably. Comparison of this technique with an existing compensation technique illustrated that although the latter is more complex, it does not provide a significant additional performance improvement.

Also, the theoretical BER versus SNR performance of a number of downlink antenna array techniques was also calculated in terms of the mean channel correlation matrix and equation (2.9), in Chapters 3 and 4. Comparison of the theoretical performance results with simulation ones in appendix B showed that they match very well, suggesting that the above method of calculating the performance is correct.

Concerning possible extensions to this work, it would be interesting to compare the downlink antenna array techniques of Chapter 3 in a multi-user scenario. However, the relationship among the performance of the techniques is not anticipated to change drastically in such a scenario. Also, regarding the technique minimum BER, an interesting direction for future work is the use of complex data symbols and the combination of the K transmit eigenbeams with orthogonal transmit diversity instead of space-time spreading. In addition, the modification of the minimum BER performance optimisation criterion so that non-white noise is taken into account (e.g. inter-symbol interference (ISI) and multiple access interference (MAI)), is another interesting extension.

Appendix A
Various auxiliary equations and figures

This appendix contains various auxiliary equations and figures that help the presentation of the work of the thesis.

A.1 Analytical expressions for the mean channel correlation matrix

If the mean correlation matrix of the n-th tap of the channel is written as follows

$$\mathbf{R}_n = \begin{bmatrix} r_{n,11} & r_{n,12} & \cdots & r_{n,1M} \\ r_{n,21} & r_{n,22} & \cdots & r_{n,2M} \\ \vdots & \vdots & \ddots & \vdots \\ r_{n,M1} & r_{n,M2} & \cdots & r_{n,MM} \end{bmatrix} \tag{A.1}$$

the real and imaginary parts of its complex entries are given by the following expressions [190]:

real part of $r_{n,ij}$

$$\Re\left\{r_{n,ij}\right\} = J_0[z(i-j)] + 2\sum_{m=1}^{\infty} J_{2m}[z(i-j)]\cos(2m\theta)\frac{\sin(m\delta)}{m\delta}, \tag{A.2}$$

imaginary part of $r_{n,ij}$

$$\Im\left\{r_{n,ij}\right\} = 2\sum_{m=0}^{\infty} J_{2m+1}[z(i-j)]\sin[(2m+1)\theta]\frac{\sin\left[(2m+1)\frac{\delta}{2}\right]}{(2m+1)\frac{\delta}{2}}, \tag{A.3}$$

where J_m denotes the Bessel function of integer order m, θ is the central angle of departure/arrival as defined in Figure 2.11 (page 20), δ is the angular spread as defined in the same figure and the scalar z is given by

$$z = 2\pi\frac{D}{\lambda} = 2\pi\tilde{D}. \tag{A.4}$$

A.2 Analysis of minimum BER for $K = 4$

This section presents analysis of the technique minimum BER for $K = 4$ eigenbeams. To elaborate, if the base station calculates that $K = 4$ eigenbeams provide the lowest required SNR, the intended mobile user's data symbol stream $s(t)$ is divided into four symbol substreams $s_i(t)$, $i = 1..4$, as in space-time spreading [160]. The base station then uses four consecutive symbol periods, T_i, $i = 1..4$, to transmit the vector signals $\mathbf{x}_i^{\mathrm{H}}(t) \in \mathbb{C}^{1\times M}$, $i = 1..4$, respectively, where

$$\mathbf{x}_1^{\mathrm{H}}(t) = \sqrt{\frac{E_s}{4}}\left[s_1(t)c(t)\mathbf{u}_1^{\mathrm{H}} + s_2(t)c(t)\mathbf{u}_2^{\mathrm{H}} + s_3(t)c(t)\mathbf{u}_3^{\mathrm{H}} + s_4(t)c(t)\mathbf{u}_4^{\mathrm{H}}\right] \quad (\text{over } \mathrm{T}_1) \tag{A.5}$$

$$\mathbf{x}_2^{\mathrm{H}}(t) = \sqrt{\frac{E_s}{4}}\left[s_2(t)c(t)\mathbf{u}_1^{\mathrm{H}} - s_1(t)c(t)\mathbf{u}_2^{\mathrm{H}} - s_4(t)c(t)\mathbf{u}_3^{\mathrm{H}} + s_3(t)c(t)\mathbf{u}_4^{\mathrm{H}}\right] \quad (\text{over } \mathrm{T}_2) \tag{A.6}$$

$$\mathbf{x}_3^{\mathrm{H}}(t) = \sqrt{\frac{E_s}{4}}\left[s_3(t)c(t)\mathbf{u}_1^{\mathrm{H}} + s_4(t)c(t)\mathbf{u}_2^{\mathrm{H}} - s_1(t)c(t)\mathbf{u}_3^{\mathrm{H}} - s_2(t)c(t)\mathbf{u}_4^{\mathrm{H}}\right] \quad (\text{over } \mathrm{T}_3) \tag{A.7}$$

$$\mathbf{x}_4^{\mathrm{H}}(t) = \sqrt{\frac{E_s}{4}}\left[s_4(t)c(t)\mathbf{u}_1^{\mathrm{H}} - s_3(t)c(t)\mathbf{u}_2^{\mathrm{H}} + s_2(t)c(t)\mathbf{u}_3^{\mathrm{H}} - s_1(t)c(t)\mathbf{u}_4^{\mathrm{H}}\right] \quad (\text{over } \mathrm{T}_4) \tag{A.8}$$

and E_s is the power of each data substream across the $K = 4$ eigenbeams, $c(t)$ is the intended mobile user's spreading code (which may be real or complex) and $\mathbf{u}_i \in \mathbb{C}^{M\times 1}$, $i = 1..4$, denote the four eigenvectors of $\mathbf{R}_{\mathrm{DL}}$ (mean downlink correlation matrix) that correspond to its four largest eigenvalues e_i, $i = 1..4$, respectively. Assuming that there is flat fading, the intended mobile station receives the signals $y_i(t)$, $i = 1..4$, due to transmission of the vector signals $\mathbf{x}_i^{\mathrm{H}}(t)$, $i = 1..4$, respectively, which after despreading with the spreading code $c(t)$ (or $c^*(t)$ in case of complex codes, where the asterisk denotes complex conjugate) are written as

$$y_1(t) = \sqrt{\frac{E_s}{4}}\left[s_1(t)\mathbf{u}_1^{\mathrm{H}} + s_2(t)\mathbf{u}_2^{\mathrm{H}} + s_3(t)\mathbf{u}_3^{\mathrm{H}} + s_4(t)\mathbf{u}_4^{\mathrm{H}}\right]\mathbf{h} + n_1 \tag{A.9}$$

$$y_2(t) = \sqrt{\frac{E_s}{4}}\left[s_2(t)\mathbf{u}_1^{\mathrm{H}} - s_1(t)\mathbf{u}_2^{\mathrm{H}} - s_4(t)\mathbf{u}_3^{\mathrm{H}} + s_3(t)\mathbf{u}_4^{\mathrm{H}}\right]\mathbf{h} + n_2 \tag{A.10}$$

$$y_3(t) = \sqrt{\frac{E_s}{4}}\left[s_3(t)\mathbf{u}_1^{\mathrm{H}} + s_4(t)\mathbf{u}_2^{\mathrm{H}} - s_1(t)\mathbf{u}_3^{\mathrm{H}} - s_2(t)\mathbf{u}_4^{\mathrm{H}}\right]\mathbf{h} + n_3 \tag{A.11}$$

$$y_4(t) = \sqrt{\frac{E_s}{4}}\left[s_4(t)\mathbf{u}_1^{\mathrm{H}} - s_3(t)\mathbf{u}_2^{\mathrm{H}} + s_2(t)\mathbf{u}_3^{\mathrm{H}} - s_1(t)\mathbf{u}_4^{\mathrm{H}}\right]\mathbf{h} + n_4 \tag{A.12}$$

where $\mathbf{h} \in \mathbb{C}^{M\times 1}$ denotes a sample of the instantaneous vector of the single channel tap, while n_i, $i = 1..4$, denote samples of a white Gaussian stochastic process and appear as additive noise

terms. In the calculation of $y_i(t)$, $i = 1..4$, we have assumed that the channel vector $\mathbf{h}$ does not change significantly over the four consecutive symbol periods T_i, $i = 1..4$, (this is the default assumption in space-time spreading, too). The mobile station receiver uses the received signals $y_i(t)$, $i = 1..4$, to obtain an estimate $\hat{s}_i(t)$, $i = 1..4$, of the data signals $s_i(t)$, $i = 1..4$, respectively, as follows

$$\begin{aligned}\hat{s}_1 &= \Re\left\{(\mathbf{u}_1^{\mathrm{H}}\mathbf{h})^* y_1 - (\mathbf{u}_2^{\mathrm{H}}\mathbf{h})^* y_2 - (\mathbf{u}_3^{\mathrm{H}}\mathbf{h})^* y_3 - (\mathbf{u}_4^{\mathrm{H}}\mathbf{h})^* y_4\right\} \\ &= \left(\sqrt{\frac{E_s}{4}}\sum_{i=1}^{4}\mathbf{u}_i^{\mathrm{H}}\mathbf{h}\mathbf{h}^{\mathrm{H}}\mathbf{u}_i\right) s_1(t) + \Re\{\tilde{n}_1\}\end{aligned} \tag{A.13}$$

$$\begin{aligned}\hat{s}_2 &= \Re\left\{(\mathbf{u}_2^{\mathrm{H}}\mathbf{h})^* y_1 + (\mathbf{u}_1^{\mathrm{H}}\mathbf{h})^* y_2 - (\mathbf{u}_4^{\mathrm{H}}\mathbf{h})^* y_3 + (\mathbf{u}_3^{\mathrm{H}}\mathbf{h})^* y_4\right\} \\ &= \left(\sqrt{\frac{E_s}{4}}\sum_{i=1}^{4}\mathbf{u}_i^{\mathrm{H}}\mathbf{h}\mathbf{h}^{\mathrm{H}}\mathbf{u}_i\right) s_2(t) + \Re\{\tilde{n}_2\}\end{aligned} \tag{A.14}$$

$$\begin{aligned}\hat{s}_3 &= \Re\left\{(\mathbf{u}_3^{\mathrm{H}}\mathbf{h})^* y_1 + (\mathbf{u}_4^{\mathrm{H}}\mathbf{h})^* y_2 + (\mathbf{u}_1^{\mathrm{H}}\mathbf{h})^* y_3 - (\mathbf{u}_2^{\mathrm{H}}\mathbf{h})^* y_4\right\} \\ &= \left(\sqrt{\frac{E_s}{4}}\sum_{i=1}^{4}\mathbf{u}_i^{\mathrm{H}}\mathbf{h}\mathbf{h}^{\mathrm{H}}\mathbf{u}_i\right) s_3(t) + \Re\{\tilde{n}_3\}\end{aligned} \tag{A.15}$$

$$\begin{aligned}\hat{s}_4 &= \Re\left\{(\mathbf{u}_4^{\mathrm{H}}\mathbf{h})^* y_1 - (\mathbf{u}_3^{\mathrm{H}}\mathbf{h})^* y_2 + (\mathbf{u}_2^{\mathrm{H}}\mathbf{h})^* y_3 + (\mathbf{u}_1^{\mathrm{H}}\mathbf{h})^* y_4\right\} \\ &= \left(\sqrt{\frac{E_s}{4}}\sum_{i=1}^{4}\mathbf{u}_i^{\mathrm{H}}\mathbf{h}\mathbf{h}^{\mathrm{H}}\mathbf{u}_i\right) s_4(t) + \Re\{\tilde{n}_4\}\end{aligned} \tag{A.16}$$

where $\Re$ denotes the real part of a complex number and each of the terms $\tilde{n}_i$, $i = 1..4$, represents a linear combination of the noise terms n_i, $i = 1..4$, perturbed by the eigenvectors $\mathbf{u}_i$, $i = 1..4$, and the channel vector Hermitian $\mathbf{h}^{\mathrm{H}}$, similarly to equations (4.6) and (4.7) on page 74. Calculation of the mean SNR from any of the estimated signals $\hat{s}_i$, $i = 1..4$, similarly to equation (4.8) on page 74 yields

$$\mathrm{SNR}_{\mathrm{MINBER}} = \frac{E_s}{4}\frac{\sum_{i=1}^{4} e_i}{\sigma_n^2}, \tag{A.17}$$

where e_i, $i = 1..4$, are the four largest eigenvalues of $\mathbf{R}_{\mathrm{DL}}$, and σ_n^2 denotes the noise power spectral density.

A.3 Analysis of minimum BER for $K = 8$

This section presents analysis of the technique minimum BER for $K = 8$ eigenbeams. If the base station calculates that $K = 8$ eigenbeams provide the lowest required SNR, the intended mobile user's data symbol stream $s(t)$ is divided into eight symbol substreams $s_i(t)$, $i = 1..8$, as in space-time spreading [160]. The base station then uses eight consecutive symbol periods, T_i, $i = 1..8$, to transmit the vector signals $\mathbf{x}_i^{\mathrm{H}}(t) \in \mathbb{C}^{1\times M}$, $i = 1..8$, respectively, where

$$\mathbf{x}_1^{\mathrm{H}}(t) = \sqrt{\frac{E_s}{8}}[s_1(t)c(t)\mathbf{u}_1^{\mathrm{H}} + s_2(t)c(t)\mathbf{u}_2^{\mathrm{H}} + s_3(t)c(t)\mathbf{u}_3^{\mathrm{H}} + s_4(t)c(t)\mathbf{u}_4^{\mathrm{H}} + s_5(t)c(t)\mathbf{u}_5^{\mathrm{H}} + s_6(t)c(t)\mathbf{u}_6^{\mathrm{H}} + s_7(t)c(t)\mathbf{u}_7^{\mathrm{H}} + s_8(t)c(t)\mathbf{u}_8^{\mathrm{H}}] \quad (\text{over } \mathrm{T}_1) \tag{A.18}$$

$$\mathbf{x}_2^{\mathrm{H}}(t) = \sqrt{\frac{E_s}{8}}[s_2(t)c(t)\mathbf{u}_1^{\mathrm{H}} - s_1(t)c(t)\mathbf{u}_2^{\mathrm{H}} - s_4(t)c(t)\mathbf{u}_3^{\mathrm{H}} + s_3(t)c(t)\mathbf{u}_4^{\mathrm{H}} - s_6(t)c(t)\mathbf{u}_5^{\mathrm{H}} + s_5(t)c(t)\mathbf{u}_6^{\mathrm{H}} + s_8(t)c(t)\mathbf{u}_7^{\mathrm{H}} - s_8(t)c(t)\mathbf{u}_8^{\mathrm{H}}] \quad (\text{over } \mathrm{T}_2) \tag{A.19}$$

$$\mathbf{x}_3^{\mathrm{H}}(t) = \sqrt{\frac{E_s}{8}}[s_3(t)c(t)\mathbf{u}_1^{\mathrm{H}} + s_4(t)c(t)\mathbf{u}_2^{\mathrm{H}} - s_1(t)c(t)\mathbf{u}_3^{\mathrm{H}} - s_2(t)c(t)\mathbf{u}_4^{\mathrm{H}} - s_7(t)c(t)\mathbf{u}_5^{\mathrm{H}} - s_8(t)c(t)\mathbf{u}_6^{\mathrm{H}} + s_5(t)c(t)\mathbf{u}_7^{\mathrm{H}} + s_6(t)c(t)\mathbf{u}_8^{\mathrm{H}}] \quad (\text{over } \mathrm{T}_3) \tag{A.20}$$

$$\mathbf{x}_4^{\mathrm{H}}(t) = \sqrt{\frac{E_s}{8}}[s_4(t)c(t)\mathbf{u}_1^{\mathrm{H}} - s_3(t)c(t)\mathbf{u}_2^{\mathrm{H}} + s_2(t)c(t)\mathbf{u}_3^{\mathrm{H}} - s_1(t)c(t)\mathbf{u}_4^{\mathrm{H}} - s_8(t)c(t)\mathbf{u}_5^{\mathrm{H}} + s_7(t)c(t)\mathbf{u}_6^{\mathrm{H}} - s_6(t)c(t)\mathbf{u}_7^{\mathrm{H}} + s_5(t)c(t)\mathbf{u}_8^{\mathrm{H}}] \quad (\text{over } \mathrm{T}_4) \tag{A.21}$$

$$\mathbf{x}_5^{\mathrm{H}}(t) = \sqrt{\frac{E_s}{8}}[s_5(t)c(t)\mathbf{u}_1^{\mathrm{H}} + s_6(t)c(t)\mathbf{u}_2^{\mathrm{H}} + s_7(t)c(t)\mathbf{u}_3^{\mathrm{H}} + s_8(t)c(t)\mathbf{u}_4^{\mathrm{H}} - s_1(t)c(t)\mathbf{u}_5^{\mathrm{H}} - s_2(t)c(t)\mathbf{u}_6^{\mathrm{H}} - s_3(t)c(t)\mathbf{u}_7^{\mathrm{H}} - s_4(t)c(t)\mathbf{u}_8^{\mathrm{H}}] \quad (\text{over } \mathrm{T}_5) \tag{A.22}$$

$$\mathbf{x}_6^{\mathrm{H}}(t) = \sqrt{\frac{E_s}{8}}[s_6(t)c(t)\mathbf{u}_1^{\mathrm{H}} - s_5(t)c(t)\mathbf{u}_2^{\mathrm{H}} + s_8(t)c(t)\mathbf{u}_3^{\mathrm{H}} - s_7(t)c(t)\mathbf{u}_4^{\mathrm{H}} + s_2(t)c(t)\mathbf{u}_5^{\mathrm{H}} - s_1(t)c(t)\mathbf{u}_6^{\mathrm{H}} + s_4(t)c(t)\mathbf{u}_7^{\mathrm{H}} - s_3(t)c(t)\mathbf{u}_8^{\mathrm{H}}] \quad (\text{over } \mathrm{T}_6) \tag{A.23}$$

$$\mathbf{x}_7^{\mathrm{H}}(t) = \sqrt{\frac{E_s}{8}}[s_7(t)c(t)\mathbf{u}_1^{\mathrm{H}} - s_8(t)c(t)\mathbf{u}_2^{\mathrm{H}} - s_5(t)c(t)\mathbf{u}_3^{\mathrm{H}} + s_6(t)c(t)\mathbf{u}_4^{\mathrm{H}} + s_3(t)c(t)\mathbf{u}_5^{\mathrm{H}} - s_4(t)c(t)\mathbf{u}_6^{\mathrm{H}} - s_1(t)c(t)\mathbf{u}_7^{\mathrm{H}} + s_2(t)c(t)\mathbf{u}_8^{\mathrm{H}}] \quad \text{(over } \mathrm{T}_7\text{)} \tag{A.24}$$

$$\mathbf{x}_8^{\mathrm{H}}(t) = \sqrt{\frac{E_s}{8}}[s_8(t)c(t)\mathbf{u}_1^{\mathrm{H}} + s_7(t)c(t)\mathbf{u}_2^{\mathrm{H}} - s_6(t)c(t)\mathbf{u}_3^{\mathrm{H}} - s_5(t)c(t)\mathbf{u}_4^{\mathrm{H}} + s_4(t)c(t)\mathbf{u}_5^{\mathrm{H}} + s_3(t)c(t)\mathbf{u}_6^{\mathrm{H}} - s_2(t)c(t)\mathbf{u}_7^{\mathrm{H}} - s_1(t)c(t)\mathbf{u}_8^{\mathrm{H}}] \quad \text{(over } \mathrm{T}_8\text{)} \tag{A.25}$$

and E_s is the power of each data substream across the $K = 8$ eigenbeams, $c(t)$ is the intended mobile user's spreading code (which may be real or complex) and $\mathbf{u}_i \in \mathbb{C}^{M\times 1}$, $i = 1..8$, denote the eight eigenvectors of $\mathbf{R}_{\mathrm{DL}}$ (mean downlink correlation matrix) that correspond to its eight largest eigenvalues e_i, $i = 1..8$, respectively. Assuming that there is flat fading, the intended mobile station receives the signals $y_i(t)$, $i = 1..8$, due to transmission of the vector signals $\mathbf{x}_i^{\mathrm{H}}(t)$, $i = 1..8$, respectively, which after despreading with the spreading code $c(t)$ (or $c^*(t)$ in case of complex codes, where the asterisk denotes complex conjugate) are written as

$$y_1(t) = \sqrt{\frac{E_s}{8}}[s_1(t)\mathbf{u}_1^{\mathrm{H}} + s_2(t)\mathbf{u}_2^{\mathrm{H}} + s_3(t)\mathbf{u}_3^{\mathrm{H}} + s_4(t)\mathbf{u}_4^{\mathrm{H}} + s_5(t)\mathbf{u}_5^{\mathrm{H}} + s_6(t)\mathbf{u}_6^{\mathrm{H}} + s_7(t)\mathbf{u}_7^{\mathrm{H}} + s_8(t)\mathbf{u}_8^{\mathrm{H}}]\mathbf{h} + n_1 \tag{A.26}$$

$$y_2(t) = \sqrt{\frac{E_s}{8}}[s_2(t)\mathbf{u}_1^{\mathrm{H}} - s_1(t)\mathbf{u}_2^{\mathrm{H}} - s_4(t)\mathbf{u}_3^{\mathrm{H}} + s_3(t)\mathbf{u}_4^{\mathrm{H}} - s_6(t)\mathbf{u}_5^{\mathrm{H}} + s_5(t)\mathbf{u}_6^{\mathrm{H}} + s_8(t)\mathbf{u}_7^{\mathrm{H}} - s_7(t)\mathbf{u}_8^{\mathrm{H}}]\mathbf{h} + n_2 \tag{A.27}$$

$$y_3(t) = \sqrt{\frac{E_s}{8}}[s_3(t)\mathbf{u}_1^{\mathrm{H}} + s_4(t)\mathbf{u}_2^{\mathrm{H}} - s_1(t)\mathbf{u}_3^{\mathrm{H}} - s_2(t)\mathbf{u}_4^{\mathrm{H}} - s_7(t)\mathbf{u}_5^{\mathrm{H}} - s_8(t)\mathbf{u}_6^{\mathrm{H}} + s_5(t)\mathbf{u}_7^{\mathrm{H}} + s_6(t)\mathbf{u}_8^{\mathrm{H}}]\mathbf{h} + n_3 \tag{A.28}$$

$$y_4(t) = \sqrt{\frac{E_s}{8}}[s_4(t)\mathbf{u}_1^{\mathrm{H}} - s_3(t)\mathbf{u}_2^{\mathrm{H}} + s_2(t)\mathbf{u}_3^{\mathrm{H}} - s_1(t)\mathbf{u}_4^{\mathrm{H}} - s_8(t)\mathbf{u}_5^{\mathrm{H}} + s_7(t)\mathbf{u}_6^{\mathrm{H}} - s_6(t)\mathbf{u}_7^{\mathrm{H}} + s_5(t)\mathbf{u}_8^{\mathrm{H}}]\mathbf{h} + n_4 \tag{A.29}$$

$$y_5(t) = \sqrt{\frac{E_s}{8}}[s_5(t)\mathbf{u}_1^{\mathrm{H}} + s_6(t)\mathbf{u}_2^{\mathrm{H}} + s_7(t)\mathbf{u}_3^{\mathrm{H}} + s_8(t)\mathbf{u}_4^{\mathrm{H}} - s_1(t)\mathbf{u}_5^{\mathrm{H}} - s_2(t)\mathbf{u}_6^{\mathrm{H}} - s_3(t)\mathbf{u}_7^{\mathrm{H}} - s_4(t)\mathbf{u}_8^{\mathrm{H}}]\mathbf{h} + n_5 \tag{A.30}$$

$$y_6(t) = \sqrt{\frac{E_s}{8}}[s_6(t)\mathbf{u}_1^{\mathrm{H}} - s_5(t)\mathbf{u}_2^{\mathrm{H}} + s_8(t)\mathbf{u}_3^{\mathrm{H}} - s_7(t)\mathbf{u}_4^{\mathrm{H}} + s_2(t)\mathbf{u}_5^{\mathrm{H}} - s_1(t)\mathbf{u}_6^{\mathrm{H}} + s_4(t)\mathbf{u}_7^{\mathrm{H}} - s_3(t)\mathbf{u}_8^{\mathrm{H}}]\mathbf{h} + n_6 \tag{A.31}$$

$$y_7(t) = \sqrt{\frac{E_s}{8}}[s_7(t)\mathbf{u}_1^{\mathrm{H}} - s_8(t)\mathbf{u}_2^{\mathrm{H}} - s_5(t)\mathbf{u}_3^{\mathrm{H}} + s_6(t)\mathbf{u}_4^{\mathrm{H}} + s_3(t)\mathbf{u}_5^{\mathrm{H}} - s_4(t)\mathbf{u}_6^{\mathrm{H}} - s_1(t)\mathbf{u}_7^{\mathrm{H}} + s_2(t)\mathbf{u}_8^{\mathrm{H}}]\mathbf{h} + n_7 \tag{A.32}$$

$$y_8(t) = \sqrt{\frac{E_s}{8}}[s_8(t)\mathbf{u}_1^{\mathrm{H}} + s_7(t)\mathbf{u}_2^{\mathrm{H}} - s_6(t)\mathbf{u}_3^{\mathrm{H}} - s_5(t)\mathbf{u}_4^{\mathrm{H}} + s_4(t)\mathbf{u}_5^{\mathrm{H}} + s_3(t)\mathbf{u}_6^{\mathrm{H}} - s_2(t)\mathbf{u}_7^{\mathrm{H}} - s_1(t)\mathbf{u}_8^{\mathrm{H}}]\mathbf{h} + n_8 \tag{A.33}$$

where $\mathbf{h} \in \mathbb{C}^{M\times 1}$ denotes a sample of the instantaneous vector of the single channel tap, while n_i, $i = 1..8$, denote samples of a white Gaussian stochastic process and appear as additive noise terms. In the calculation of $y_i(t)$, $i = 1..8$, we have assumed that the channel vector $\mathbf{h}$ does not change significantly over the eight consecutive symbol periods T_i, $i = 1..8$, (this is the default assumption in space-time spreading, too). The mobile station receiver uses the received signals $y_i(t)$, $i = 1..8$, to obtain an estimate $\hat{s}_i(t)$, $i = 1..8$, of the data signals $s_i(t)$, $i = 1..8$, respectively, as follows

$$\hat{s}_1 = \Re\Big\{(\mathbf{u}_1^{\mathrm{H}}\mathbf{h})^* y_1 - (\mathbf{u}_2^{\mathrm{H}}\mathbf{h})^* y_2 - (\mathbf{u}_3^{\mathrm{H}}\mathbf{h})^* y_3 - (\mathbf{u}_4^{\mathrm{H}}\mathbf{h})^* y_4 - (\mathbf{u}_5^{\mathrm{H}}\mathbf{h})^* y_5 - (\mathbf{u}_6^{\mathrm{H}}\mathbf{h})^* y_6 - (\mathbf{u}_7^{\mathrm{H}}\mathbf{h})^* y_7 - (\mathbf{u}_8^{\mathrm{H}}\mathbf{h})^* y_8\Big\} = \left(\sqrt{\frac{E_s}{8}}\sum_{i=1}^{8}\mathbf{u}_i^{\mathrm{H}}\mathbf{h}\mathbf{h}^{\mathrm{H}}\mathbf{u}_i\right) s_1(t) + \Re\{\tilde{n}_1\} \tag{A.34}$$

$$\hat{s}_2 = \Re\Big\{(\mathbf{u}_2^{\mathrm{H}}\mathbf{h})^* y_1 + (\mathbf{u}_1^{\mathrm{H}}\mathbf{h})^* y_2 - (\mathbf{u}_4^{\mathrm{H}}\mathbf{h})^* y_3 + (\mathbf{u}_3^{\mathrm{H}}\mathbf{h})^* y_4 - (\mathbf{u}_6^{\mathrm{H}}\mathbf{h})^* y_5 + (\mathbf{u}_5^{\mathrm{H}}\mathbf{h})^* y_6 + (\mathbf{u}_8^{\mathrm{H}}\mathbf{h})^* y_7 - (\mathbf{u}_7^{\mathrm{H}}\mathbf{h})^* y_8\Big\} = \left(\sqrt{\frac{E_s}{8}}\sum_{i=1}^{8}\mathbf{u}_i^{\mathrm{H}}\mathbf{h}\mathbf{h}^{\mathrm{H}}\mathbf{u}_i\right) s_2(t) + \Re\{\tilde{n}_2\} \tag{A.35}$$

$$\hat{s}_3 = \Re\Big\{(\mathbf{u}_3^{\mathrm{H}}\mathbf{h})^* y_1 + (\mathbf{u}_4^{\mathrm{H}}\mathbf{h})^* y_2 + (\mathbf{u}_1^{\mathrm{H}}\mathbf{h})^* y_3 - (\mathbf{u}_2^{\mathrm{H}}\mathbf{h})^* y_4 - (\mathbf{u}_7^{\mathrm{H}}\mathbf{h})^* y_5 - (\mathbf{u}_8^{\mathrm{H}}\mathbf{h})^* y_6 + (\mathbf{u}_5^{\mathrm{H}}\mathbf{h})^* y_7 + (\mathbf{u}_6^{\mathrm{H}}\mathbf{h})^* y_8\Big\} = \left(\sqrt{\frac{E_s}{8}}\sum_{i=1}^{8}\mathbf{u}_i^{\mathrm{H}}\mathbf{h}\mathbf{h}^{\mathrm{H}}\mathbf{u}_i\right) s_3(t) + \Re\{\tilde{n}_3\} \tag{A.36}$$

$$\hat{s}_4 = \Re\Big\{(\mathbf{u}_4^{\mathrm{H}}\mathbf{h})^* y_1 - (\mathbf{u}_3^{\mathrm{H}}\mathbf{h})^* y_2 + (\mathbf{u}_2^{\mathrm{H}}\mathbf{h})^* y_3 + (\mathbf{u}_1^{\mathrm{H}}\mathbf{h})^* y_4 - (\mathbf{u}_8^{\mathrm{H}}\mathbf{h})^* y_5 + (\mathbf{u}_7^{\mathrm{H}}\mathbf{h})^* y_6 - (\mathbf{u}_6^{\mathrm{H}}\mathbf{h})^* y_7 + (\mathbf{u}_5^{\mathrm{H}}\mathbf{h})^* y_8\Big\} = \left(\sqrt{\frac{E_s}{8}}\sum_{i=1}^{8}\mathbf{u}_i^{\mathrm{H}}\mathbf{h}\mathbf{h}^{\mathrm{H}}\mathbf{u}_i\right) s_4(t) + \Re\{\tilde{n}_4\} \tag{A.37}$$

$$\hat{s}_5 = \Re\Big\{(\mathbf{u}_5^{\mathrm{H}}\mathbf{h})^* y_1 + (\mathbf{u}_6^{\mathrm{H}}\mathbf{h})^* y_2 + (\mathbf{u}_7^{\mathrm{H}}\mathbf{h})^* y_3 + (\mathbf{u}_8^{\mathrm{H}}\mathbf{h})^* y_4 + (\mathbf{u}_1^{\mathrm{H}}\mathbf{h})^* y_5 - (\mathbf{u}_2^{\mathrm{H}}\mathbf{h})^* y_6 - (\mathbf{u}_3^{\mathrm{H}}\mathbf{h})^* y_7 - (\mathbf{u}_4^{\mathrm{H}}\mathbf{h})^* y_8\Big\} = \left(\sqrt{\frac{E_s}{8}}\sum_{i=1}^{8}\mathbf{u}_i^{\mathrm{H}}\mathbf{h}\mathbf{h}^{\mathrm{H}}\mathbf{u}_i\right) s_5(t) + \Re\{\tilde{n}_5\} \tag{A.38}$$

$$\hat{s}_6 = \Re\Big\{(\mathbf{u}_6^{\mathrm{H}}\mathbf{h})^* y_1 - (\mathbf{u}_5^{\mathrm{H}}\mathbf{h})^* y_2 + (\mathbf{u}_8^{\mathrm{H}}\mathbf{h})^* y_3 - (\mathbf{u}_7^{\mathrm{H}}\mathbf{h})^* y_4 + (\mathbf{u}_2^{\mathrm{H}}\mathbf{h})^* y_5 + (\mathbf{u}_1^{\mathrm{H}}\mathbf{h})^* y_6 + (\mathbf{u}_4^{\mathrm{H}}\mathbf{h})^* y_7 - (\mathbf{u}_3^{\mathrm{H}}\mathbf{h})^* y_8\Big\} = \left(\sqrt{\frac{E_s}{8}}\sum_{i=1}^{8}\mathbf{u}_i^{\mathrm{H}}\mathbf{h}\mathbf{h}^{\mathrm{H}}\mathbf{u}_i\right) s_6(t) + \Re\{\tilde{n}_6\} \tag{A.39}$$

$$\hat{s}_7 = \Re\Big\{(\mathbf{u}_7^{\mathrm{H}}\mathbf{h})^* y_1 - (\mathbf{u}_8^{\mathrm{H}}\mathbf{h})^* y_2 - (\mathbf{u}_5^{\mathrm{H}}\mathbf{h})^* y_3 + (\mathbf{u}_6^{\mathrm{H}}\mathbf{h})^* y_4 + (\mathbf{u}_3^{\mathrm{H}}\mathbf{h})^* y_5 - (\mathbf{u}_4^{\mathrm{H}}\mathbf{h})^* y_6 + (\mathbf{u}_1^{\mathrm{H}}\mathbf{h})^* y_7 + (\mathbf{u}_2^{\mathrm{H}}\mathbf{h})^* y_8\Big\} = \left(\sqrt{\frac{E_s}{8}}\sum_{i=1}^{8}\mathbf{u}_i^{\mathrm{H}}\mathbf{h}\mathbf{h}^{\mathrm{H}}\mathbf{u}_i\right) s_7(t) + \Re\{\tilde{n}_7\} \tag{A.40}$$

$$\hat{s}_8 = \Re\Big\{(\mathbf{u}_8^{\mathrm{H}}\mathbf{h})^* y_1 + (\mathbf{u}_7^{\mathrm{H}}\mathbf{h})^* y_2 - (\mathbf{u}_6^{\mathrm{H}}\mathbf{h})^* y_3 - (\mathbf{u}_5^{\mathrm{H}}\mathbf{h})^* y_4 + (\mathbf{u}_4^{\mathrm{H}}\mathbf{h})^* y_5 + (\mathbf{u}_3^{\mathrm{H}}\mathbf{h})^* y_6 - (\mathbf{u}_2^{\mathrm{H}}\mathbf{h})^* y_7 + (\mathbf{u}_1^{\mathrm{H}}\mathbf{h})^* y_8\Big\} = \left(\sqrt{\frac{E_s}{8}}\sum_{i=1}^{8}\mathbf{u}_i^{\mathrm{H}}\mathbf{h}\mathbf{h}^{\mathrm{H}}\mathbf{u}_i\right) s_8(t) + \Re\{\tilde{n}_8\} \tag{A.41}$$

where $\Re$ denotes the real part of a complex number and each of the terms $\tilde{n}_i$, $i = 1..8$, represents a linear combination of the noise terms n_i, $i = 1..8$, perturbed by the eigenvectors $\mathbf{u}_i$, $i = 1..8$, and the channel vector Hermitian $\mathbf{h}^{\mathrm{H}}$, similarly to equations (4.6) and (4.7) on page 74. Calculation of the mean SNR from any of the estimated signals $\hat{s}_i$, $i = 1..8$, similarly to equation (4.8) on page 74 yields

$$\mathrm{SNR}_{\mathrm{MINBER}} = \frac{E_s}{8}\frac{\sum_{i=1}^{8} e_i}{\sigma_n^2}, \tag{A.42}$$

where e_i, $i = 1..8$, are the eight largest eigenvalues of $\mathbf{R}_{\mathrm{DL}}$, and σ_n^2 denotes the noise power spectral density.

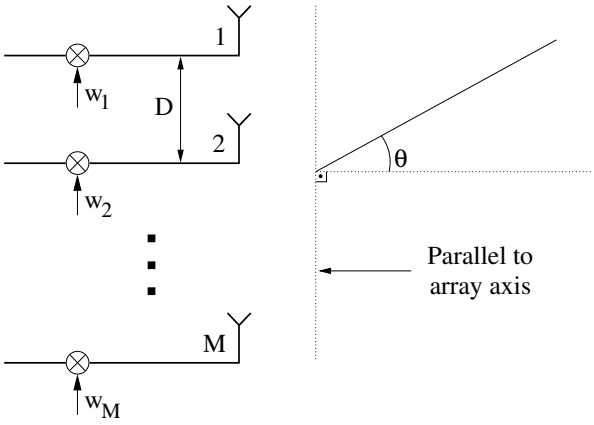

Figure A.1: *Uniform linear array (ULA) with M elements.*

A.4 Beamwidth of a uniform linear antenna array

In this section we plot the beamwidth of the main beam of the radiation pattern of a uniform linear array (ULA) as a function of the direction of this beam. The ULA that will be used for this purpose is shown in Figure A.1, with an element spacing of $D = \frac{\lambda}{2}$ (the antenna elements are omnidirectional over the azimuth), where λ is the carrier wavelength. Let us assume that the complex weights w_i, $i = 1..M$, are such that the difference between the phase of the i-th and $i+1$-th array element is $\Delta\phi = \phi_{i+1} - \phi_i = -\frac{2\pi D}{\lambda}\cos(\psi) = -2\pi\tilde{D}\cos(\psi)$, where ψ is a constant. With these assumptions, the absolute value of the amplitude of the electrical field $\Lambda(\theta)$ of the ULA is given as a function of θ by the following equation [118]

$$\Lambda(\theta) = \left| \frac{\sin\left\{M\frac{\pi D}{\lambda}(\sin(\psi) - \sin(\theta))\right\}}{\sin\left\{\frac{\pi D}{\lambda}(\sin(\psi) - \sin(\theta))\right\}} \right|, \tag{A.43}$$

where $|r|$ is the absolute value of the real number r. The maximum of the electrical field is $\Lambda(\theta) = M$ and occurs in the direction $\theta = \psi$. This means that the main beam can be steered in the desired direction through proper adjustment of the phases of the signals of the M array elements by means of the complex weights w_i, $i = 1..M$, and without mechanical movement of the array. This is a well known principle with many applications (e.g. airport surveillance systems). Therefore, for the numerical calculation of the beamwidth of the main beam of the

power radiation pattern when this beam is in the direction $\theta_{\text{main beam}}$ ($\theta_{\text{main beam}} \in [0^{\text{o}}, 90^{\text{o}}]$), first we set $\psi = \theta_{\text{main beam}}$ and $\theta = \theta_{\text{main beam}}$. Then, we decrease the value of θ by a small step θ_{step} (e.g. $\theta_{\text{step}} = 0.05^{\text{o}}$) and calculate $\Lambda(\theta)$ for each resulting θ. While $20\log_{10}\left(\frac{\Lambda(\theta)}{M}\right) > -3$ dB, the decrease of θ continues. Assuming that this ratio becomes equal to (or just smaller than) -3 dB for $\theta = \theta_{\text{crit}}$, then the 3 dB beamwidth of the main beam is $2 \times (\theta_{\text{main beam}} - \theta_{\text{crit}})$ (of course, the accuracy of the 3 dB beamwidth calculation is subject to θ_{step}). This process is repeated for $M = 2, 4, 8, 16$ and the results are plotted in Figure A.2.

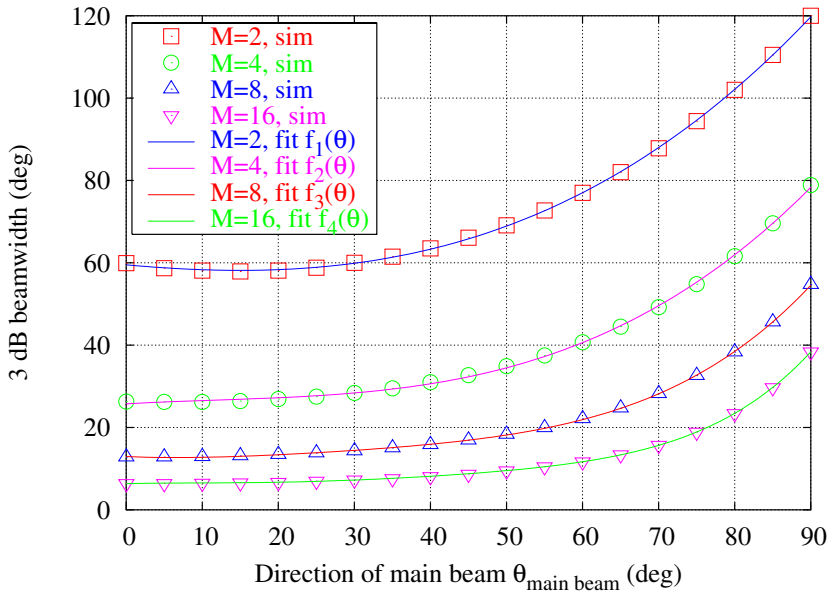

Figure A.2: *3 dB beamwidth of a uniform linear array as a function of the direction of the main beam for $M = 2, 4, 8, 16$.*

Also, in order to obtain analytical expressions for easy calculation of the 3 dB beamwidth of the main beam as a function of its direction, the curves of Figure A.2 have been subject to a polynomial fit. The resulting polynomials are written below and are also plotted in Figure A.2, where it can be seen that there is very good agreement between the actual and the fitted values.

$$f_1(\theta) = 5.43484 \times 10^{-5}\theta^3 + 4.42043 \times 10^{-3}\theta^2 - 0.169094\theta + 59.5173 \tag{A.44}$$

$$f_2(\theta) = 9.79329 \times 10^{-5}\theta^3 - 3.48158 \times 10^{-3}\theta^2 + 0.104064\theta + 25.7536 \tag{A.45}$$

$$f_3(\theta) = 1.51878 \times 10^{-6}\theta^4 - 1.54869 \times 10^{-4}\theta^3 + 7.68774 \times 10^{-3}\theta^2 \\ -8.26359 \times 10^{-2}\theta + 12.9521 \quad \text{(A.46)}$$

$$f_4(\theta) = 2.74958 \times 10^{-8}\theta^5 - 4.14827 \times 10^{-6}\theta^4 + 2.43027 \times 10^{-4}\theta^3 - 4.89048 \times 10^{-3}\theta^2 \\ +4.72174 \times 10^{-2}\theta + 6.34313 \quad \text{(A.47)}$$

A.5 Spatial beam configuration in fixed beams for $M = 2, 8$

In this section we plot the spatial configuration of the beams of the transmit uniform linear array of the technique fixed beams (described in section 3.2.3 on page 38) for $M = 2$ and $M = 8$. The number of beams N_B used in fixed beams in this thesis is equal to the number of transmit antenna elements, $N_B = M$. The N_B beams are uniformly distributed over the 120° of a cell sector. Figure A.3 shows the spatial beam configuration when $N_B = M = 2$, while Figure A.4 shows the spatial beam configuration when $N_B = M = 8$, both for a carrier frequency of 2 GHz and an antenna element spacing of $D = \frac{\lambda}{2}$.

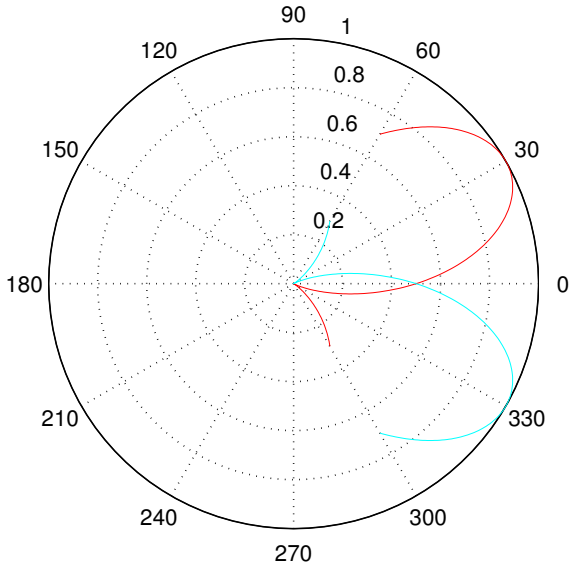

Figure A.3: *Uniform spatial beam configuration in fixed beams for $N_B = M = 2$.*

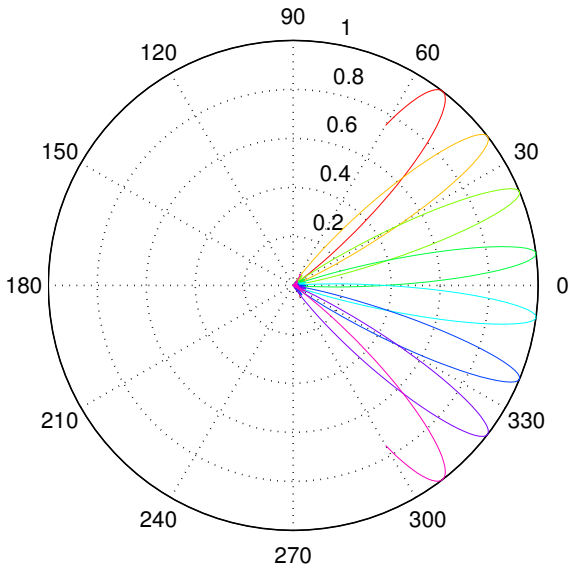

Figure A.4: *Uniform spatial beam configuration in fixed beams for* $N_B = M = 8$.

Appendix B
Comparison of theoretical and simulation results

In chapter 3 the theoretical BER versus SNR performance of the techniques *space-time spreading*, *maximum SNR* and *transmit antenna array*, was calculated in a frequency flat fading scenario by using the eigenvalues of the mean channel correlation matrix in equation (2.9). The theoretical BER versus SNR performance of *minimum BER* was also calculated in the same way in chapter 4. In order to show that this approach leads to correct results for the performance of the above mentioned algorithms, in this appendix we will compare the theoretical results obtained by using the eigenvalues of the mean channel correlation matrix in equation (2.9) with simulation results for each of the above techniques. The comparison will show that the theoretical and simulation results match very well, confirming that the above approach of calculating the theoretical performance of the algorithms is correct.

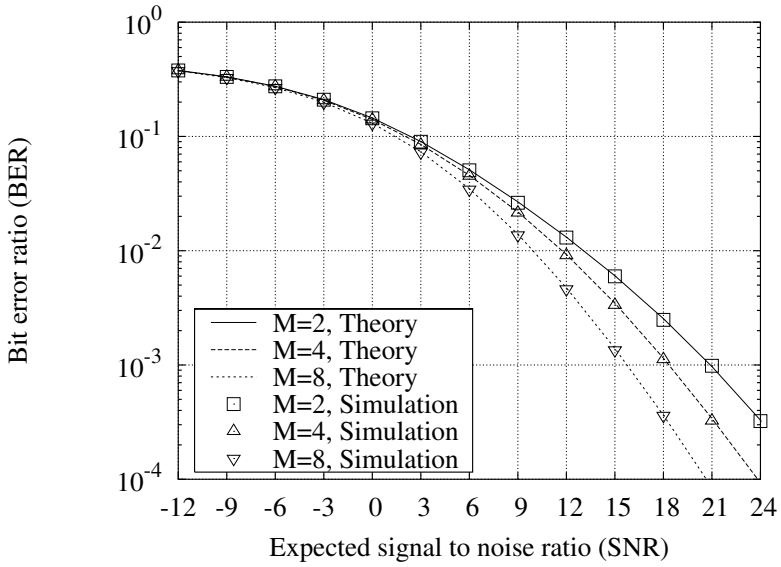

Figure B.1: *Comparison of theoretical and simulation results of space-time spreading in the macro cell.*

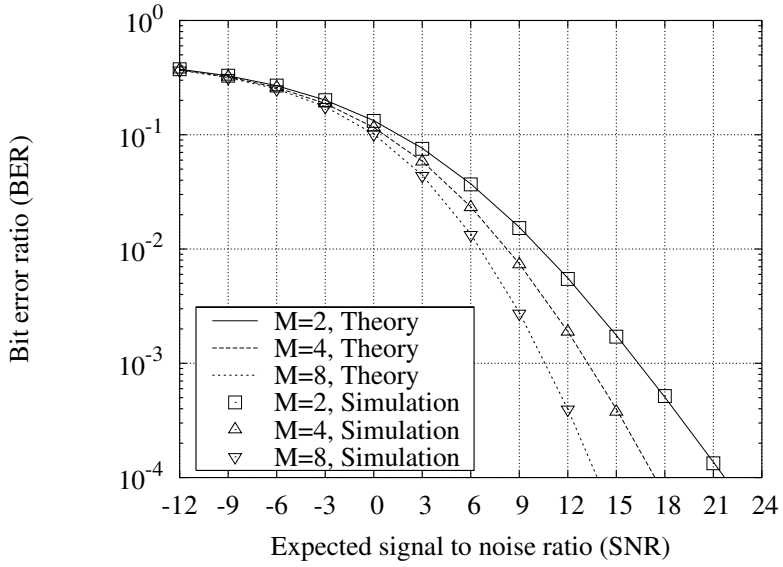

Figure B.2: *Comparison of theoretical and simulation results of space-time spreading in the micro cell.*

B.1 Space-time spreading

In this section theoretical performance results will be compared to simulation results for the technique *space-time spreading*. The simulation results are the same as those presented in section 3.3.1.1 of chapter 3 (page 44). For the calculation of the theoretical performance results, in order to be consistent with the simulations, we assume the same parameters as in the simulations. That is, the downlink carrier frequency is $f_{\mathrm{DL},c} = 2$ GHz and the spacing of the transmit antenna array is $D = \frac{\lambda_{\mathrm{DL}}}{2}$, where λ_{DL} is the wavelength of the downlink carrier frequency $f_{\mathrm{DL},c}$. Let us assume that the base station uses M transmit antennas, the downlink carrier frequency $f_{\mathrm{DL},c}$ and transmit antenna spacing D are as above, and the channel environment where the base station operates has a central angle of departure θ and an angular spread δ (see Figure 2.11 on page 20). Then, in order to obtain the theoretical performance results in this scenario, we first calculate the mean channel correlation matrix $\mathbf{R} \in \mathbb{C}^{M \times M}$ using the above values of M, D, λ_{DL}, θ and δ in equations A.2 and A.3 of appendix A. Next, the correlation matrix is decomposed into eigenvalues e_i, $i = 1..M$, and eigenvectors $\mathbf{u}_i \in \mathbb{C}^{M \times 1}$, $i = 1..M$. If the (linear) value of SNR is γ, the M eigenvalues are then multiplied by $\gamma \frac{1}{M}$ (as indicated by equation (3.2) of page 31) and used in equation (2.9) (page 28) to calculate the BER that corresponds to this SNR value. The SNR value is equal to the ratio of the power of each transmitted data bit across all M transmit antennas E_s, over the power spectral density of the additive white Gaussian noise

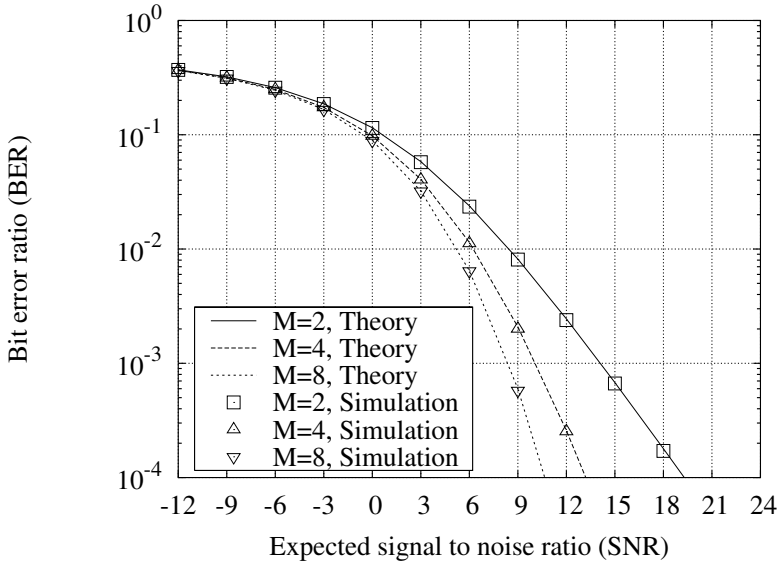

Figure B.3: *Comparison of theoretical and simulation results of space-time spreading in the pico cell.*

σ_n^2

$$\gamma = \frac{E_s}{\sigma_n^2} \tag{B.1}$$

(in the actual calculations we assume that $\sigma_n^2 = 1$). In the figures containing the results we plot the SNR value in dB, rather than the linear one, which is obtained as $\mathrm{SNR}_{\mathrm{dB}} = 10\log_{10}(\gamma)$. The SNR is varied from -12 dB to 24 dB with a step of 3 dB, and the BER corresponding to each SNR value is calculated according to the above procedure. This procedure is repeated for $M = 2, 4, 8$ in the macro, micro and pico cell, and the results are plotted in figures B.1, B.2 and B.3 respectively.

Furthermore, the eigenvalues of the mean channel correlation matrix that are used in the above procedure, have been calculated for $M = 2, 4, 8$ in the macro, micro and pico cell and are shown in Table B.1 which is located toward the end of this appendix on page 179. These eigenvalues can be obtained by calculating the mean channel correlation matrix using the parameters of the three cell types in equations A.2 and A.3 of appendix A. Also, by using these eigenvalues in equation (2.9) according to the procedure described above, one can obtain the theoretical results of figures B.1, B.2 and B.3.

Figure B.1 shows that the theoretical results match the simulation results very well for all shown SNR and M values in the macro cell. In addition, figures B.2 and B.3 show that the theoretical

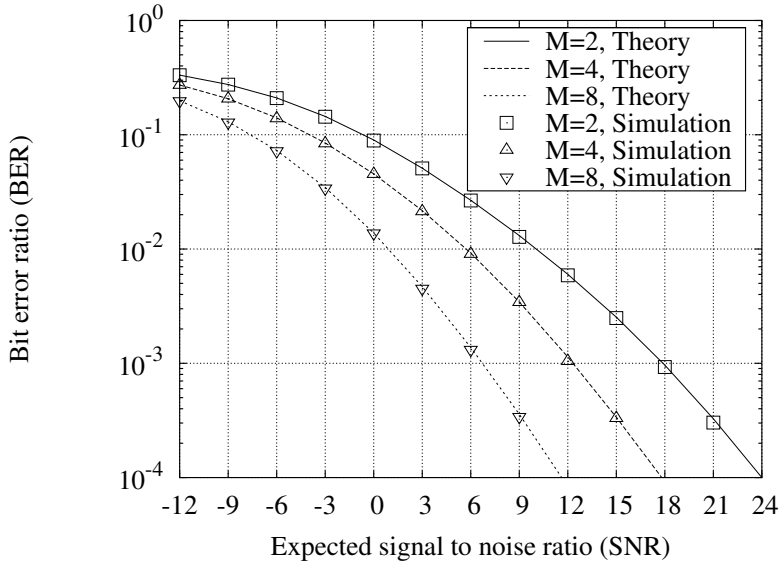

Figure B.4: *Comparison of theoretical and simulation results of transmit antenna array in the macro cell.*

results also match the simulation results very well for all shown SNR and M values in the micro and pico cell respectively. Therefore, the theoretical performance results match the simulation ones very well in all cell types for the case of space-time spreading.

B.2 Transmit antenna array

In this section theoretical performance results will be compared to simulation results for the technique *transmit antenna array*. The simulation results of this section are the same as those presented in section 3.3.2.1 of chapter 3 (page 50). Again, for the calculation of the theoretical performance results we assume the same parameters as in the simulations, in order to be consistent with the simulations. This means that the downlink carrier frequency is $f_{\mathrm{DL},c} = 2$ GHz and the spacing of the transmit antenna array is $D = \frac{\lambda_{\mathrm{DL}}}{2}$, where λ_{DL} is the wavelength of the downlink carrier frequency $f_{\mathrm{DL},c}$. The procedure of calculating the theoretical performance of transmit antenna array is the same as that of space-time spreading. The only difference is that now the eigenvalues are not multiplied by $\gamma\frac{1}{M}$ as in space-time spreading, but by γ, as indicated by equation (3.9) on page 35 (this effectively means that there is beamforming gain in transmit antenna array, which is not present in space-time spreading). The theoretical results are compared to the simulation ones for $M = 2, 4, 8$ in the macro, micro and pico cell, and the

results are plotted in figures B.4, B.5 and B.6 respectively.

Figure B.4 shows that the theoretical results match the simulation results very well for all shown SNR and M values in the macro cell. In addition, figures B.5 and B.6 show that the theoretical results also match the simulation results very well for all shown SNR and M values in the micro and pico cell respectively. Therefore, the theoretical performance results match the simulation ones very well in all cell types for the case of transmit antenna array.

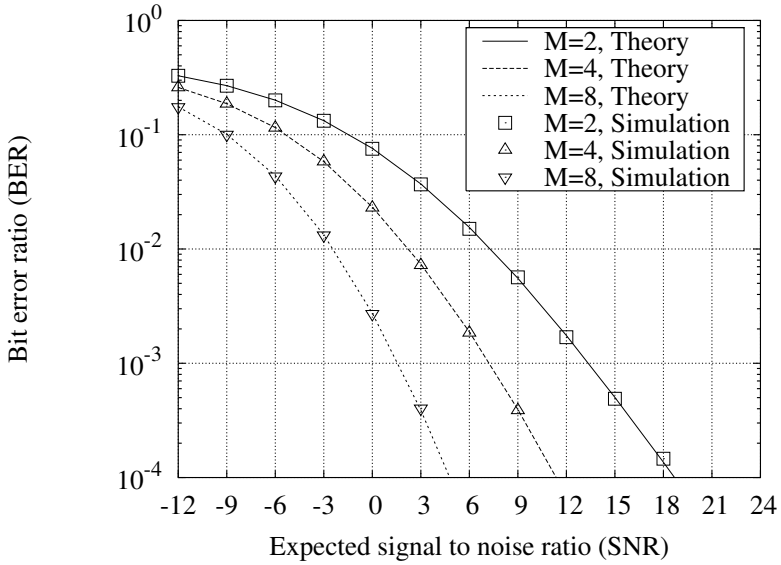

Figure B.5: *Comparison of theoretical and simulation results of transmit antenna array in the micro cell.*

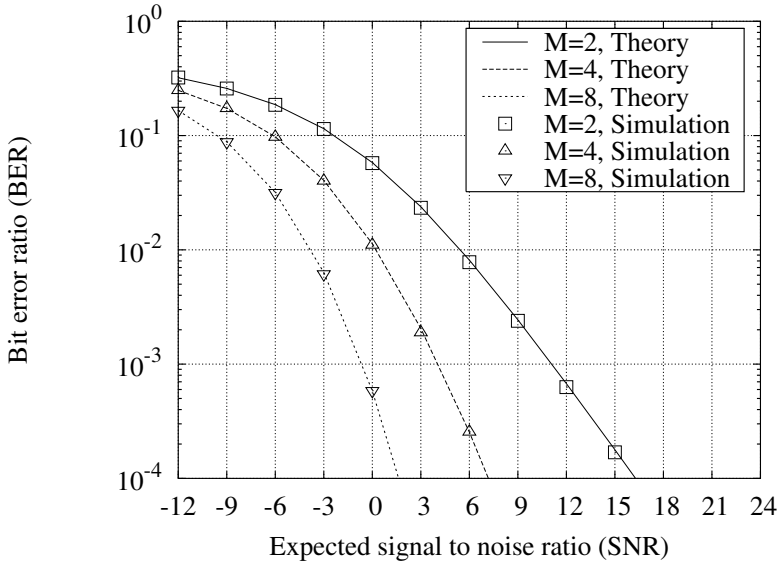

Figure B.6: *Comparison of theoretical and simulation results of transmit antenna array in the pico cell.*

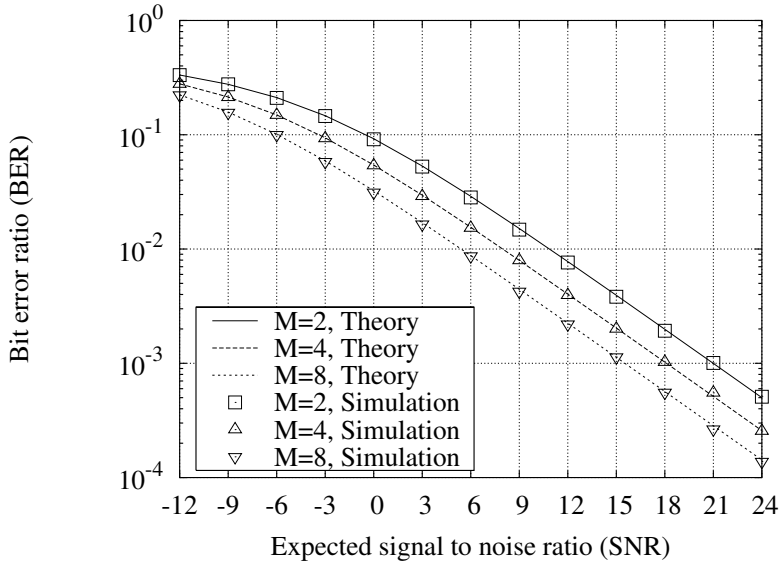

Figure B.7: *Comparison of theoretical and simulation results of maximum SNR in the macro cell.*

B.3 Maximum SNR

In this section theoretical performance results will be compared to simulation results for the technique *maximum SNR*. The simulation results of this section are the same as those presented in section 3.3.1.2 of chapter 3 (page 47). Again, in order to be consistent with the assumptions in the simulations,in the calculation of the theoretical performance results we assume that the uplink and downlink carrier frequencies are $f_{\mathrm{UL},c} = 2.14$ GHz and $f_{\mathrm{DL},c} = 1.95$ GHz respectively, while the transmit antenna spacing is $D = \frac{\lambda_{\mathrm{MID}}}{2}$, where λ_{MID} is the wavelength of the carrier frequency $f_{\mathrm{MID},c} = \frac{f_{\mathrm{UL},c}+f_{\mathrm{DL},c}}{2}$. Moreover, as in the simulations, the base station uses the principal eigenvector $\mathbf{u}_{\mathrm{UL,max}}$ of the uplink mean channel correlation matrix $\mathbf{R}_{\mathrm{UL}}$ as beamformer on the downlink. This means that only the maximum eigenvalue will be used in the calculations. Because the uplink and downlink channels use different carrier frequencies, the eigenvalues of $\mathbf{R}_{\mathrm{UL}}$ do not represent the contribution of the corresponding eigenvectors any more and cannot be used directly in equation (2.9). Thus, the procedure of obtaining the theoretical performance results must be changed as described below. First of all, we assume that the central angle of departure θ and angular spread δ of the downlink channel is the same as the angle of arrival and angular spread of the uplink channel, respectively (this assumption was also made in the simulations of maximum SNR). Then, we use the values of M, D, λ_{UL}, λ_{DL}, θ

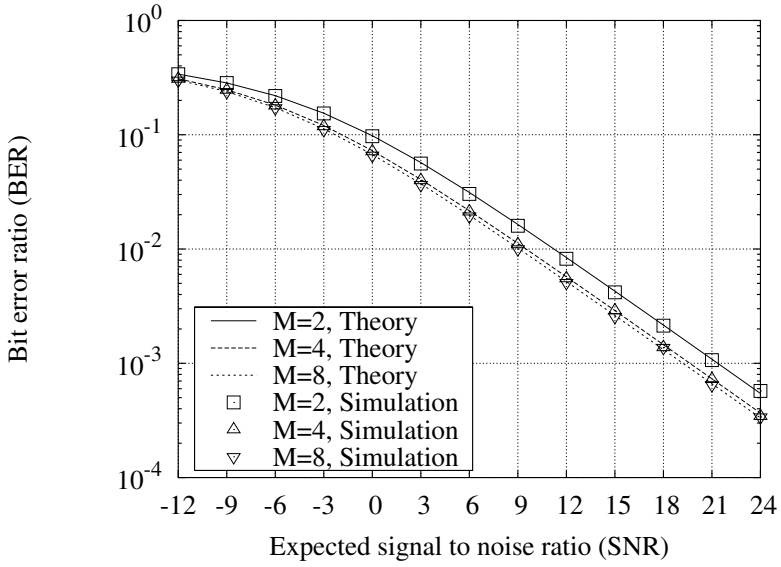

Figure B.8: *Comparison of theoretical and simulation results of maximum SNR in the micro cell.*

and δ that correspond to the channel environment under investigation in equations A.2 and A.3 of appendix A, to calculate both the uplink $\mathbf{R}_{\mathrm{UL}}$ and downlink $\mathbf{R}_{\mathrm{DL}}$ mean correlation matrices (the two matrices differ because $f_{\mathrm{UL},c} \neq f_{\mathrm{DL},c}$ and $\lambda_{\mathrm{UL}} \neq \lambda_{\mathrm{DL}}$). Next, we perform the eigenvalue decomposition of the uplink correlation matrix $\mathbf{R}_{\mathrm{UL}}$ and obtain the matrix $\mathbf{E}_{\mathrm{eff}} \in \mathbb{R}^{M \times M}$ as follows

$$\mathbf{E}_{\mathrm{eff}} = \mathbf{U}_{\mathrm{UL}}^{\mathrm{H}} \mathbf{R}_{\mathrm{DL}} \mathbf{U}_{\mathrm{UL}}, \tag{B.2}$$

where $\mathbf{U}_{\mathrm{UL}} \in \mathbb{C}^{M \times M}$ is a matrix whose columns are equal to the eigenvectors of $\mathbf{R}_{\mathrm{UL}}$ and the H superscript denotes complex conjugate transpose. The $\mathbf{E}_{\mathrm{eff}}$ matrix is diagonal and its i-th diagonal element $e_{\mathrm{eff},i}$ represents the contribution of the i-th eigenvector $\mathbf{u}_{\mathrm{UL},i}$, $i = 1..M$, of $\mathbf{R}_{\mathrm{UL}}$. The diagonal elements of $\mathbf{E}_{\mathrm{eff}}$ are called 'effective eigenvalues', and their values for $M = 2, 4, 8$ in the macro, micro and pico cell are shown in Table B.2 at the end of this appendix on page 180. For each M value and in each channel scenario, the largest effective eigenvalue is multiplied by the linear SNR value γ and then used in equation (2.9) to give the BER corresponding to this SNR value in the considered conditions (the largest effective eigenvalue in each case is typed in a **bold** type face in Table B.2). Again the SNR value is varied from -12 dB to 24 dB, and the results for $M = 2, 4, 8$ in the macro, micro and pico cell are shown in figures B.7, B.8 and B.9, respectively. The three figures show that there is very good agreement between the theoretical and simulation results in all the examined cell types.

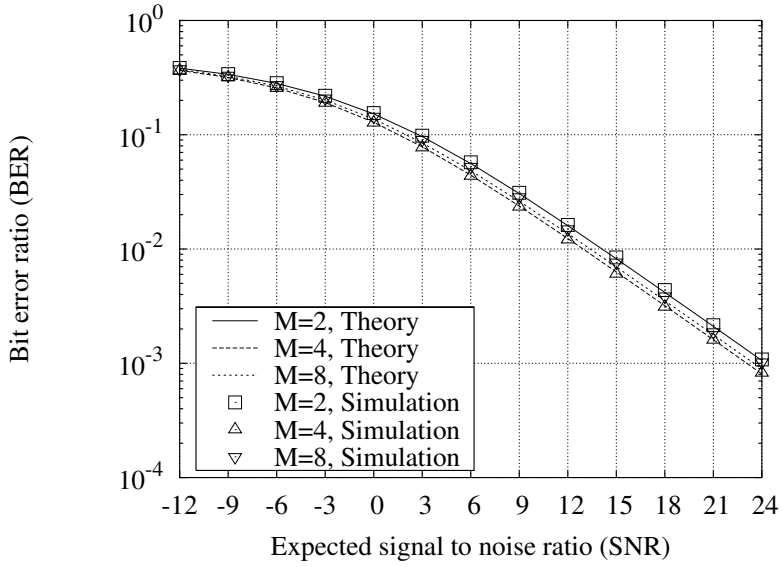

Figure B.9: *Comparison of theoretical and simulation results of maximum SNR in the pico cell.*

B.4 Minimum BER

In this section theoretical performance results will be compared with simulation results for the technique *minimum BER*. The simulation results of this section are the same as those presented in section 4.4 of chapter 4 (page 76). Again, in order to be consistent with the assumptions in the simulations, we assume that the uplink and downlink carrier frequencies are $f_{\mathrm{UL},c} = 2.14$ GHz and $f_{\mathrm{DL},c} = 1.95$ GHz respectively, while the transmit antenna spacing is $D = \frac{\lambda_{\mathrm{MID}}}{2}$, where λ_{MID} is the wavelength of the carrier frequency $f_{\mathrm{MID},c} = \frac{f_{\mathrm{UL},c}+f_{\mathrm{DL},c}}{2}$. Furthermore, as in the simulations, the technique is operated in an open loop fashion and the base station uses the eigenvectors of the uplink mean channel correlation matrix $\mathbf{R}_{\mathrm{UL}}$ for the transmission of data signals on the downlink. Because the uplink and downlink channels use different carrier frequencies, the effective eigenvalues of Table B.2 are used. If the number of eigenvectors used by the base station is K and the linear SNR value is γ, the K largest effective eigenvalues are multiplied by $\gamma\frac{1}{K}$ and then used in equation (2.9) to give the BER corresponding to this SNR value in the considered channel conditions. The SNR value is varied from -12 dB to 24 dB, and the results for $M = 2, 4, 8$ in the macro, micro and pico cell are shown in figures B.10, B.11 and B.12, respectively. Again, the three figures show that there is very good agreement between the theoretical and simulation results in all the examined cell types and for all M values.

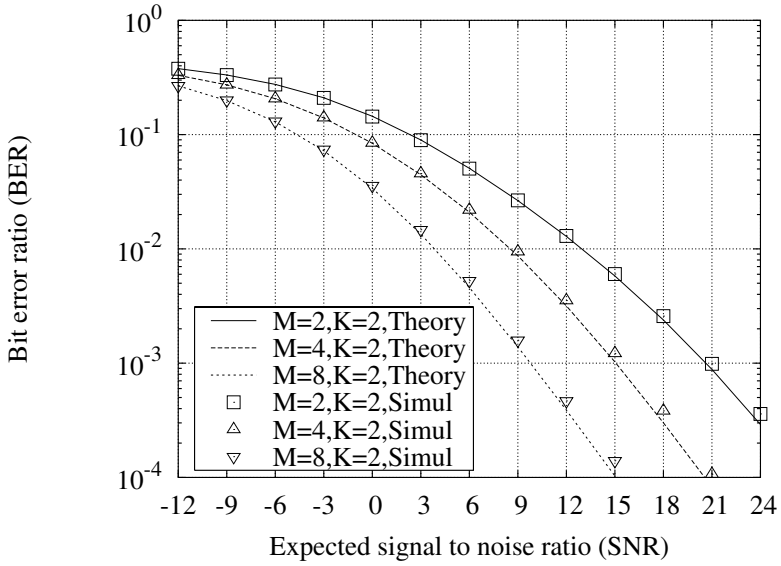

Figure B.10: *Comparison of theoretical and simulation results of minimum BER in the macro cell.*

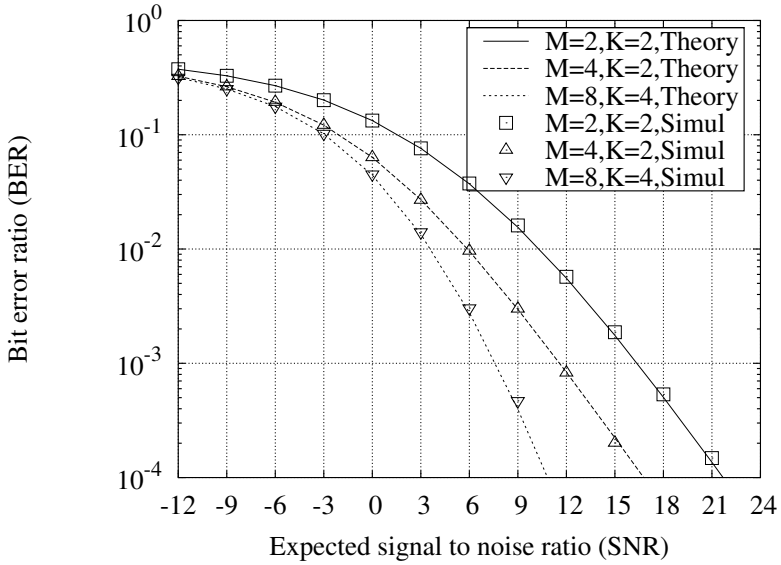

Figure B.11: *Comparison of theoretical and simulation results of minimum BER in the micro cell.*

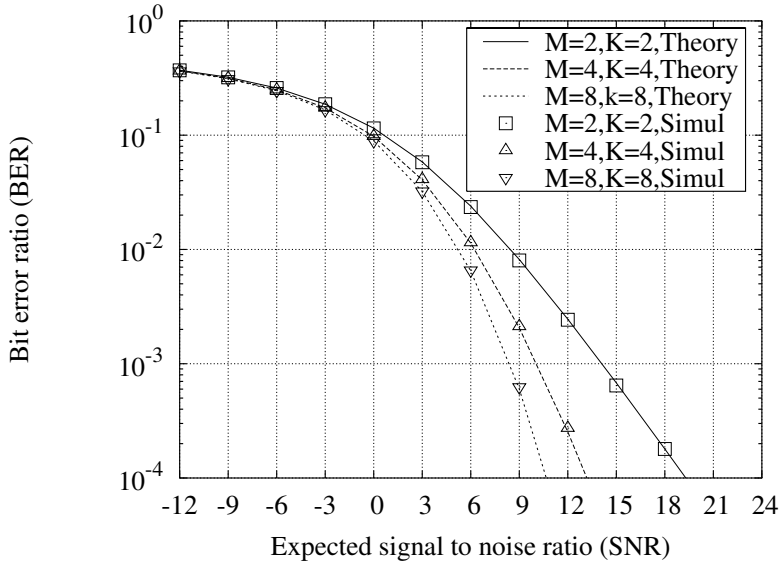

Figure B.12: *Comparison of theoretical and simulation results of minimum BER in the pico cell.*

Cell type	$M = 2$ **TX antennas** (2 eigenvalues)	$M = 4$ **TX antennas** (4 eigenvalues)	$M = 8$ **TX antennas** (8 eigenvalues)
	1.98837	3.88616	7.11981
Macro cell	0.01163	0.11340	0.86198
(AOD = 15°,	–	0.00044	0.01808
AS = 10°,	–	0	0.00013
$\rho_{\text{adj}} = 0.988$	–	–	0
when $D = \frac{\lambda}{2}$)	–	–	0
	–	–	0
	–	–	0
	1.82491	2.71283	3.12290
Micro cell	0.17509	1.17944	2.69241
(AOD = 30°,	–	0.10602	1.75698
AS = 45°,	–	0.00170	0.39859
$\rho_{\text{adj}} = 0.825$	–	–	0.02826
when $D = \frac{\lambda}{2}$)	–	–	0.00085
	–	–	0.00001
	–	–	0
	1.03531	1.21122	1.33456
Pico cell	0.96469	1.08519	1.26659
(AOD = 1°,	–	0.97769	1.09123
AS = 120°,	–	0.72590	1.07696
$\rho_{\text{adj}} = 0.035$	–	–	1.00242
when $D = \frac{\lambda}{2}$)	–	–	0.98239
	–	–	0.96024
	–	–	0.28561

Table B.1: *Eigenvalues of the mean channel correlation matrix that were used for the calculation of the theoretical performance of space-time spreading and transmit antenna array for* $M = 2, 4, 8$ *in the macro, micro and pico cells.*

Cell type	$M = 2$ **TX antennas** (2 eigenvalues)	$M = 4$ **TX antennas** (4 eigenvalues)	$M = 8$ **TX antennas** (8 eigenvalues)
	1.98600	**3.86409**	**6.98003**
Macro cell	0.01400	0.13499	0.98303
(AOD = 15°,	–	0.00092	0.03640
AS = 10°,	–	0	0.00053
$\rho_{\text{adj}} = 0.988$	–	–	0
when $D = \frac{\lambda}{2}$)	–	–	0
	–	–	0
	–	–	0
	1.82405	**2.71176**	**2.99054**
Micro cell	0.17595	1.16576	2.72775
(AOD = 30°,	–	0.11985	1.74803
AS = 45°,	–	0.00263	0.48107
$\rho_{\text{adj}} = 0.825$	–	–	0.05050
when $D = \frac{\lambda}{2}$)	–	–	0.00206
	–	–	0.00004
	–	–	0
	0.93744	**1.22927**	1.11020
Pico cell	**1.06256**	0.96069	**1.30824**
(AOD = 1°,	–	0.81418	1.17966
AS = 120°,	–	0.99586	1.10594
$\rho_{\text{adj}} = 0.035$	–	–	1.04380
when $D = \frac{\lambda}{2}$)	–	–	1.00680
	–	–	0.98609
	–	–	0.25927

Table B.2: *Effective eigenvalues that were used for the calculation of the theoretical performance of maximum SNR and minimum BER for $M = 2, 4, 8$ in the macro, micro and pico cells. Bold type face represents the maximum effective eigenvalues in each case.*

Appendix C
Publications

The author of this thesis has the following publications:

- ◇ Antonis C. Koutalos, John S. Thompson and Peter M. Grant, "Antenna array techniques for mobile communications systems", PGNet 2000 Symposium, JM University of Liverpool, Liverpool, UK, 19–20 June 2000.

- ◇ † Antonis C. Koutalos, John S. Thompson and Peter M. Grant, "Downlink adaptive antenna techniques for WCDMA", IEEE Vehicular Technology Conference (VTC), Birmingham, Alabama, USA, volume 3, pages 1135–1139, 6–9 May, 2002.

- ◇ † Antonis C. Koutalos and John S. Thompson, "Pilot signal effects on adaptive antenna arrays in FDD wideband CDMA", IEEE International Symposium on Spread Spectrum Techniques and Applications (ISSSTA), Prague, Czech Republic, volume 2, pages 531–535, 2–5 September, 2002.

- ◇ † Antonis C. Koutalos and John S. Thompson, "Effect of frequency division duplex on open loop downlink beamforming in WCDMA systems", IEEE Vehicular Technology Conference (VTC), Vancouver, BC, Canada, volume 2, pages 686–690, 24–28 September, 2002.

- ◇ Antonis C. Koutalos and John S. Thompson, "Adaptive antenna array techniques for the downlink of WCDMA communication systems", Submitted to IEE Proceedings Communications.

- ◇ Antonis C. Koutalos and John S. Thompson, "Performance loss due to imperfect parameter estimation in FDD downlink antenna array techniques", Submitted to European Transactions on Telecommunications.

† Included in this appendix.

Downlink Adaptive Antenna Techniques for WCDMA

Antonis C Koutalos†, John S Thompson & Peter M Grant
Signals and Systems Group, Department of Electronics and Electrical Engineering,
The University of Edinburgh, Edinburgh, EH9 3JL, UK.
Email: Antonis.Koutalos@ee.ed.ac.uk, John.Thompson@ee.ed.ac.uk

Abstract— **This paper analyses candidate adaptive algorithms for operating antenna arrays on the downlink of wideband code division multiple access (WCDMA) systems, including diversity, beamforming and hybrid schemes. The algorithms are simulated and compared with each other under different channel environments and for various numbers of transmit antennas. Furthermore, a new blind downlink technique is proposed, which optimises performance in all channel environments according to a flexible criterion and yields the best performance among the presented blind techniques.**

Keywords— **Adaptive antennas, smart antennas, downlink diversity, downlink beamforming.**

I. Introduction

Communication in mobile communication systems using WCDMA suffers mainly from the effects of two phenomena, fading and co-channel interference (CCI), which affect bit error ratio (BER) performance. Antenna arrays can effectively combat both of them by offering diversity, beamforming and hybrid gain [1], [2], [3], [4], [5], thus improving BER performance. This paper analyses a number of downlink antenna array techniques for WCDMA systems operating in frequency division duplex (FDD) mode. The techniques are simulated by means of Monte Carlo simulations in various channel conditions and for various numbers of antennas. Also, a new blind hybrid technique is introduced, which optimises performance by periodically measuring and adapting to channel conditions, to satisfy a flexible criterion.

The outline of the paper is as follows. The next section introduces the system model that we assume. Section III presents diversity techniques, section IV analyses beamforming techniques and section V investigates hybrid techniques. Also, in section V we propose the new blind hybrid algorithm. Finally, in section VI we compare all the presented techniques and in section VII we draw our conclusions.

II. System Model

This work assumes that the base station (BS) is equipped with a uniform linear array (ULA) containing M elements, while mobile stations (MS) use a single antenna. The schematic diagram of a BS operating in a 120^{o} sector of a cell is shown in Fig. 1. The distance between adjacent elements is denoted by D. Although signals are transmitted in all directions over $[-60^{\text{o}}, 60^{\text{o}}]$, only signals whose angle of departure (AOD) lies in $[\theta - \delta/2, \theta + \delta/2]$ contribute to the signal received at the MS, due to MS and scatterer locations. The parameter θ is the central AOD, while δ is the angular spread (AS) which arises from the fact that the signal is scattered by objects in the channel before being received. The BS controls adaptively each

†Antonis C Koutalos gratefully acknowledges the departmental sponsorship which supports his studies.

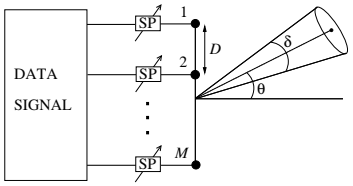

Fig. 1. Schematic diagram of a base station using a uniform linear array.

element by means of a signal processor (SP).

The channel vector of the l-th temporal tap of the downlink channel is modeled as follows:

$$\mathbf{h}_l(t) = \sqrt{\frac{P_l}{Q_l}} \sum_{q=1}^{Q_l} e^{j(\phi_q + 2\pi f_q t)} \underbrace{\begin{bmatrix} 1 \\ e^{j\{\frac{2\pi D}{\lambda}\sin(\theta_q)\}} \\ \vdots \\ e^{j\{\frac{2\pi D}{\lambda}(M-1)\sin(\theta_q)\}} \end{bmatrix}}_{\mathbf{a}(\theta_q)} \quad (1)$$

where P_l is the tap power, Q_l the number of scattered signals (components) contributing to the tap, ϕ_q the random phase of the q-th component uniformly distributed over $[0, 2\pi]$, f_q the Doppler frequency shift of the q-th component and θ_q the AOD of the q-th component uniformly distributed over $[\theta - \delta/2, \theta + \delta/2]$. Also, λ is the wavelength of the carrier frequency f_c, and $\mathbf{a}(\theta_q)$ the array steering vector.

The mean channel correlation matrix (CCM) $\mathbf{R}_l^{\text{DL}}$ of the l-th downlink tap is obtained as $\mathbf{R}_l^{\text{DL}} = \text{E}\left[\mathbf{h}_l(t)\mathbf{h}_l(t)^{\text{H}}\right]$, where E[•] denotes expectation and the H superscript complex conjugate transpose. Its eigenvalue decomposition (EVD) will play an important role in analysing the performance of some of the algorithms. By performing the EVD of $\mathbf{R}_l^{\text{DL}}$ we express it as a function of its eigenvalues and eigenvectors

$$\mathbf{R}_l^{\text{DL}} = \mathbf{U}\mathbf{E}\mathbf{U}^{\text{H}} = \sum_{i=1}^{M} e_i(\mathbf{u}_i\mathbf{u}_i^{\text{H}}), \quad (2)$$

where $\mathbf{E}$ is a diagonal matrix whose diagonal entries are equal to the eigenvalues $e_1, e_2, \cdots, e_M$ of $\mathbf{R}_l^{\text{DL}}$ (in descending order) and $\mathbf{U}$ is a matrix whose columns are equal to the corresponding eigenvectors $\mathbf{u}_1, \mathbf{u}_2, \cdots, \mathbf{u}_M$ [6].

We assume that the BS transmits the vector signal $\mathbf{x}(t)^{\text{H}} \in C^{1\times M}$ at time t. For flat fading, the MS receives the signal

$$y(t) = \mathbf{x}(t)^{\text{H}}\mathbf{h}(t) + n(t) \quad (3)$$

where $\mathbf{h}(t)$ is the channel vector and $n(t)$ is white Gaussian noise. For frequency selective fading the received signal is given by the convolution of the transmitted signal and the channel.

The techniques to be presented can be split into two categories with respect to mobile feedback they need to estimate the downlink channel: 1) those that need some kind of feedback (non-blind techniques) and 2) those that do not need feedback (blind techniques). In non-blind techniques the MS feeds information back to BS once per time slot. The next three sections will present diversity, beamforming and hybrid techniques, respectively, while information about the amount of feedback that each technique needs will be given after its description.

III. Diversity Techniques

Downlink diversity techniques will be presented in this section. In principle, diversity techniques deliver to the receiver a number of different versions of the same data signal, which are combined to obtain an estimate of this signal [3].

A. Space-Time Spreading

Space-time spreading (STS) is a recently proposed diversity technique for real signal constellations [7]. If M antennas are used at the BS, the data stream s of a user is split into M substreams s_i, $i = 1..M$, and his spreading code $\mathbf{c}$ is used to construct M new spreading codes $\mathbf{c}_i$, $i = 1..M$. Then, each antenna transmits a function of all M data substreams and spreading codes. The received signal $\mathbf{y}$ at the single-antenna MS receiver is a linear superposition of the M transmitted signals perturbed by noise. The receiver cross-correlates the received signal with each $\mathbf{c}_i^{\mathrm{H}}$, thus decoupling the M transmitted signals and obtaining an estimate $\hat{s}_i$ of the i-th data substream. STS is a blind technique, as it does not need feedback from MS to BS.

The signal-to-noise ratio (SNR) of the decision signal at the MS receiver is $\mathrm{SNR}_{\mathrm{STS}} = \left(\sum_{i=1}^{M} |h_i|^2\right)/(M\sigma_n^2)$, where h_i is the channel coefficient between the i-th antenna at the BS and the single antenna at the MS, while σ_n^2 denotes the noise power spectral density. Therefore, STS with M antennas provides M-order diversity gain. This gain increases as the correlation between two adjacent antenna elements, ρ_{adj}, decreases ($0 \leq \rho_{\mathrm{adj}} \leq 1$). In the STS simulation we use a downlink carrier frequency of $f_c^{\mathrm{DL}} = 2$ GHz and a spacing of $D = \lambda/2$.

B. Selection Diversity

According to selection diversity, pilot signals are transmitted from each element of the array. The MS receiver measures the mean SNR of the M received pilot signals and decides which element yields the highest mean SNR. This information is fed back to BS, which then uses *only* this element to transmit data signals to this MS receiver. Selection diversity is a non-blind technique which needs $\mathrm{ceil}(\log_2(M))$ feedback bits ($\mathrm{ceil}(x)$ denotes the smallest integer that is greater than or equal to x).

Selection diversity yields diversity gain, but lacks beamforming gain as it uses only one antenna for transmission. In the simulations we use $f_c^{\mathrm{DL}} = 2$ GHz, $D = \lambda/2$ and assume that the BS knows which antenna yields the highest SNR at the MS receiver.

IV. Beamforming Techniques

In this section we will present beamforming techniques, which radiate power only in the intended receiver direction thus improving the SNR of the decision signal and minimising CCI.

A. Fixed Beams

In this technique, a fixed number of beams are formed by the BS to cover the 120^{o} sector [8]. Pilot signals are transmitted through each beam and the MS receiver measures which one yields the highest mean SNR. This information is fed back to BS, which then uses *only* this beam to transmit data signals to this MS receiver. Fixed beams is non-blind, and if it uses N_{B} beams, it needs $\mathrm{ceil}(\log_2(N_{\mathrm{B}}))$ feedback bits.

The main gain type of this scheme is beamforming gain. Also, some diversity gain will be present in environments with large δ. In the simulations we use $N_{\mathrm{B}} = M$ beams uniformly distributed over $[-60^{\mathrm{o}}, 60^{\mathrm{o}}]$ to cover the 120^{o} sector, the downlink carrier frequency is $f_c^{\mathrm{DL}} = 2$ GHz, the spacing is $D = \lambda/2$, while we assume that the BS knows which beam yields the highest SNR at the MS receiver.

B. Maximum SNR

This technique's objective is to maximise the mean SNR of the received signal by multiplying the transmitted signal by the appropriate weight vector (beamformer) $\mathbf{w}^{\mathrm{H}} \in C^{1\times M}$ [9]. The mean SNR of the decision signal at the MS receiver for flat fading is $\mathrm{SNR}_{\mathrm{MAXSNR}} = (\mathbf{w}^{\mathrm{H}}\mathrm{E}\left[\mathbf{h}\mathbf{h}^{\mathrm{H}}\right]\mathbf{w})/\sigma_n^2 = (\mathbf{w}^{\mathrm{H}}\mathbf{R}^{\mathrm{DL}}\mathbf{w})/\sigma_n^2$, where $\mathbf{h} \in C^{M\times 1}$ is the downlink channel vector, $\mathbf{R}^{\mathrm{DL}}$ its mean CCM and σ_n^2 the noise power spectral density. The beamformer $\mathbf{w}$ is chosen so that the mean SNR is maximised, while keeping the transmitted power equal to that of a single-antenna BS. The solution to this problem is the unit-norm principal eigenvector $\mathbf{u}_{\mathrm{max}}$ of $\mathbf{R}^{\mathrm{DL}}$ (the eigenvector corresponding to the maximum eigenvalue e_{max}), $\mathbf{w}^{\mathrm{H}} = \mathbf{u}_{\mathrm{max}}^{\mathrm{H}}$. Replacing $\mathbf{R}^{\mathrm{DL}}$ from equation (2) and $\mathbf{w}$, to the SNR expression we have $\mathrm{SNR}_{\mathrm{MAXSNR}} = \left(\mathbf{u}_{\mathrm{max}}^{\mathrm{H}}\left[\sum_{i=1}^{M} e_i\left(\mathbf{u}_i\mathbf{u}_i^{\mathrm{H}}\right)\right]\mathbf{u}_{\mathrm{max}}\right)/\sigma_n^2 = e_{\mathrm{max}}/\sigma_n^2$, i.e. the mean SNR is proportional to the maximum eigenvalue of the mean downlink CCM. In case of frequency selective fading with N taps, the mean CCMs of all downlink taps are summed $\mathbf{R}_{\mathrm{SUM}}^{\mathrm{DL}} = \sum_{i=1}^{N}\mathrm{E}\left[\mathbf{h}_i\mathbf{h}_i^{\mathrm{H}}\right]$, and the weight vector is set equal to the principal eigenvector of $\mathbf{R}_{\mathrm{SUM}}^{\mathrm{DL}}$.

In our simulations we use the principal eigenvector of the uplink CCM $\mathbf{R}^{\mathrm{UL}}$ as beamformer, the uplink and downlink carrier frequencies are $f_c^{\mathrm{UL}} = 2.14$ GHz and $f_c^{\mathrm{DL}} = 1.95$ GHz respectively, while the spacing is $D = \lambda^{\mathrm{MID}}/2$, where λ^{MID} is the wavelength of the carrier frequency $f_c^{\mathrm{MID}} = (f_c^{\mathrm{UL}} + f_c^{\mathrm{DL}})/2$.

V. Hybrid Techniques

Downlink techniques that combine both diversity and beamforming gain will be presented in this section. Also, further investigation of the EVD of the mean CCM will lead to a new hybrid technique without mobile feedback which optimises performance in all channel environments according to a flexible criterion.

A. Transmit Antenna Array

Transmit antenna array (TXAA) is the transmit equivalent of maximal ratio combining reception [10]. Again the data signal is multiplied by a weight vector $\mathbf{w}^{\mathrm{H}} \in C^{1\times M}$ and then transmitted, but the objective now is to maximise the instantaneous SNR of the decision signal at the MS receiver. For flat fading and an M-element array, the weight vector is given by $\mathbf{w}^{\mathrm{H}} = \left(1/\sqrt{\mathbf{h}\mathbf{h}^{\mathrm{H}}}\right)\mathbf{h}^{\mathrm{H}} = \left(1/\sqrt{\sum_{i=1}^{M}|h_i|^2}\right)\mathbf{h}^{\mathrm{H}}$, where $\mathbf{h}$ de-

notes the downlink channel vector and h_i the channel coefficient between the i-th antenna at the BS and the single antenna at the MS. The mean SNR of the decision signal at the MS receiver is $\text{SNR}_{\text{TXAA}} = \left(\sum_{i=1}^{M} |h_i|^2\right)/\sigma_n^2$, where σ_n^2 denotes the noise power spectral density. TXAA yields M-order diversity gain as well as beamforming gain. In case of frequency selective fading with N taps, the instantaneous CCMs of all downlink taps are summed $\mathbf{R}_{\text{SUM}}^{\text{INST}} = \sum_{i=1}^{N} \mathbf{h}_i \mathbf{h}_i^{\text{H}}$, and the weight vector is set equal to the principal eigenvector of $\mathbf{R}_{\text{SUM}}^{\text{INST}}$.

The number of feedback bits needed by TXAA depends on M and the quantisation scheme that is used to quantise the channel coefficients h_i that will be fed back to BS. This number is larger than that of selection diversity and fixed beams (i.e. higher rate feedback is needed by TXAA). In the simulations we use $f_c^{\text{DL}} = 2$ GHz and $D = \lambda/2$, while the BS is assumed to know the downlink channel vector prior to transmission.

B. Minimum BER

The MAX SNR algorithm and the EVD of the mean CCM will be investigated further in this section. This investigation will result in the proposal of a new hybrid algorithm.

B.1 Motivation

When the principal eigenvector of $\mathbf{R}^{\text{DL}}$ is used as beamformer, the SNR of the MAX SNR algorithm is proportional to the maximum eigenvalue of $\mathbf{R}^{\text{DL}}$. Replacing $\mathbf{R}^{\text{DL}}$ from equation (2) to the SNR expression of MAX SNR and using the i-th eigenvector as beamformer, it is shown that the SNR is proportional to the i-th eigenvalue, $\text{SNR} = e_i/\sigma_n^2$. This means that the amplitude of the i-th eigenvalue is an indication of how efficiently the power is transferred across the downlink channel to MS, if the i-th eigenvector is used as beamformer.

Fig. 2 shows the amplitude of the eigenvalues of $\mathbf{R}^{\text{DL}}$ for a 4-element array as a function of δ (spacing is $D = \lambda/2$ and AOD $= 0^{\text{o}}$). For small values of δ there is a dominant eigenvalue and only the direction indicated by the dominant eigenvector transfers the power efficiently. However, as δ increases, the amplitude of the smaller eigenvalues increases, too, and becomes comparable to that of the dominant one. This means that the directions indicated by the eigenvectors corresponding to these eigenvalues become also efficient in power transfer, and using only the dominant eigenvector does not exploit fully the underlying structure of the channel.

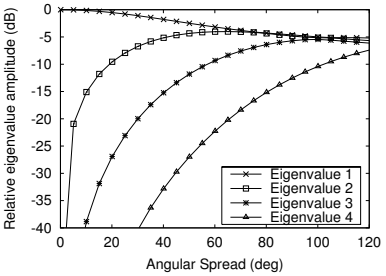

Fig. 2. Eigenvalue amplitude as a function of δ ($M = 4$, $D = \lambda/2$, AOA $= 0^{\text{o}}$).

To investigate and quantify the potential diversity gain of using more than one eigenvector, we will plot the required SNR for a target BER $= 10^{-3}$, when various numbers of eigenvectors are used as beamformers. Using the principal eigenvector provides a mean SNR proportional to the largest eigenvalue, so using the K eigenvectors that correspond to the K largest eigenvalues is expected to yield K diversity paths with mean SNR values proportional to the K largest eigenvalues. Since the eigenvectors are mutually orthogonal [6], the K diversity paths are mutually uncorrelated and equation (14-5-28) of [3] can be used.

Fig. 3 shows the required SNR as a function of AS, for the target BER and various numbers of eigenvectors. The number of elements is $M = 4$, spacing $D = \lambda/2$ and AOD $= 0^{\text{o}}$. The $K = 1$ curve corresponds to MAX SNR performance and the $K = M$ curve corresponds to STS performance. The figure shows that $K = 1$ needs the lowest SNR only if δ is smaller than about 4^{o}. For AS larger than 4^{o} a $K > 1$ needs the lowest SNR for the specified target BER. For example, if $4^{\text{o}} \leq \delta \leq 45^{\text{o}}$, $K = 2$ needs the lowest SNR, while if $\delta > 97^{\text{o}}$ $K = M$ (STS) needs the lowest SNR. For other M and/or target BER values the curves are shifted upward or downward, but the trend is always the same: the optimum solution is $K = 1$ for small δ, $K = M$ for large δ and $1 < K < M$ for moderate δ. Next we propose an algorithm which uses the optimum K in all channel scenarios.

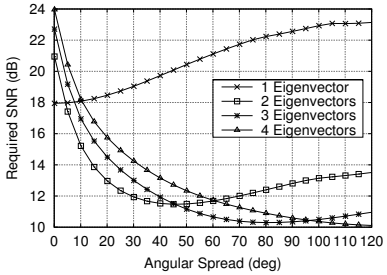

Fig. 3. Required SNR for a target BER $= 10^{-3}$ and various numbers of eigenvectors as a function of δ ($M = 4$, $D = \lambda/2$, AOA $= 0^{\text{o}}$).

B.2 Algorithm description

We propose combining the K eigenvectors (eigenbeams) according to a space-time technique [11], such as STS. In reference [12] space-time coding was applied to 'normal' beams for complex data symbols and $M = 2$. Here, we apply space-time coding to eigenbeams and real data symbols for an arbitrary M. Also, the authors in reference [13] discuss generally the application of space-time codes to eigenbeams, but do not analyse it. Here, we propose a specific combination of space-time coding and eigenbeams and analyse its performance.

The BS determines the target BER according to other system requirements, such as voice or service quality at the MS. It then uses equation (14-5-28) of [3] to calculate the K requiring the lowest SNR for this BER. Finally, it combines the K dominant eigenbeams according to STS and transmits to the intended MS. We call this scheme Minimum BER (MIN BER). For instance, if $K = 2$ eigenbeams need the lowest SNR for the specified target BER, the user's real data sequence s is divided into two subsequences s_1 and s_2, as in STS. The BS then uses the symbol periods T_1 and T_2 to transmit the signals $\mathbf{x}_1^{\text{H}}$ and

$\mathbf{x}_2^{\mathrm{H}}$, respectively, where

$$\mathbf{x}_1^{\mathrm{H}} = \sqrt{\frac{E_s}{2}}(s_1 c(t)\mathbf{u}_1^{\mathrm{H}} + s_2 c(t)\mathbf{u}_2^{\mathrm{H}}) \qquad \text{(over T}_1\text{)} \quad (4)$$

$$\mathbf{x}_2^{\mathrm{H}} = \sqrt{\frac{E_s}{2}}(s_2 c(t)\mathbf{u}_1^{\mathrm{H}} - s_1 c(t)\mathbf{u}_2^{\mathrm{H}}) \qquad \text{(over T}_2\text{)}, \quad (5)$$

where E_s is the signal power, $c(t)$ the user's spreading code and $\mathbf{u}_1$ and $\mathbf{u}_2$ the two dominant eigenvectors of $\mathbf{R}^{\mathrm{DL}}$. Under flat fading conditions, the MS receives the signal y_1 due to $\mathbf{x}_1^{\mathrm{H}}$ and the signal y_2 due to $\mathbf{x}_2^{\mathrm{H}}$, which after despreading are written as

$$y_1 = \mathbf{x}_1^{\mathrm{H}}\mathbf{h} + n_1 = \sqrt{\frac{E_s}{2}}(s_1\mathbf{u}_1^{\mathrm{H}} + s_2\mathbf{u}_2^{\mathrm{H}})\mathbf{h} + n_1 \quad (6)$$

$$y_2 = \mathbf{x}_2^{\mathrm{H}}\mathbf{h} + n_2 = \sqrt{\frac{E_s}{2}}(s_2\mathbf{u}_1^{\mathrm{H}} - s_1\mathbf{u}_2^{\mathrm{H}})\mathbf{h} + n_2 \quad (7)$$

where $\mathbf{h}$ is the channel vector while n_1 and n_2 denote white Gaussian noise. It is assumed that the channel does not change significantly over the two symbol periods (default assumption in STS). Then, the aquisition of the estimates $\hat{s}_1$ and $\hat{s}_2$ of s_1 and s_2, respectively, is performed as in STS. The mean SNR of the decision signal is SNR $= E_s(e_1 + e_2)/(2\sigma_n^2)$, where e_1 and e_2 are the two largest eigenvalues of $\mathbf{R}^{\mathrm{DL}}$, and σ_n^2 denotes the noise power spectral density. Hence, MIN BER achieves the expected 2-fold diversity gain by using two eigenvectors. Since there is an STS scheme for any number of antennas and real signal constellations [11], the same approach can be applied to any K. In the general case of K eigenvectors, the SNR is proportional to $\left(\sum_{i=1}^{K} e_i\right)/K$, which shows that K-fold diversity gain in the domain of eigenbeams is achieved. In case of frequency selective fading with N taps, the mean CCMs of all downlink taps are summed $\mathbf{R}_{\mathrm{SUM}}^{\mathrm{DL}} = \sum_{i=1}^{N} \mathrm{E}\left[\mathbf{h}_i\mathbf{h}_i^{\mathrm{H}}\right]$, and the eigenvectors of $\mathbf{R}_{\mathrm{SUM}}^{\mathrm{DL}}$ are used.

Performance is optimised according to the target BER, which is a *flexible* criterion as it can be changed to meet other system requirements such as voice or service quality at the MS. MIN BER is especially beneficial in environments with moderate AS, where neither diversity nor beamforming techniques yield the maximum expected gain. Also, its ability to move from a pure beamforming technique ($K = 1$) to a pure diversity technique ($K = M$), allows it to adaptively provide the optimum solution in all channel environments.

In the simulations the BS uses the eigenvectors of the mean uplink CCM $\mathbf{R}^{\mathrm{UL}}$ as beamformers, so MIN BER is operated in a blind mode. Also, the uplink and downlink carrier frequencies are $f_c^{\mathrm{UL}} = 2.14$ GHz and $f_c^{\mathrm{DL}} = 1.95$ GHz, respectively, while the spacing is $D = \lambda^{\mathrm{MID}}/2$, where λ^{MID} is the wavelength of the carrier frequency $f_c^{\mathrm{MID}} = (f_c^{\mathrm{UL}} + f_c^{\mathrm{DL}})/2$.

C. Eigenbeamforming

In this technique, if the downlink channel consists of N resolvable taps, the MS performs the EVD of the mean CCM $\mathbf{R}_l^{\mathrm{DL}}$, $l = 1..N$ of all of them [13]. With M antennas at the BS, a set of MN eigenvalues is obtained. The eigenbeams corresponding to the L largest eigenvalues are sent to the BS. Then, the MS calculates which of the L eigenbeams yields the highest SNR over every time slot. This information is fed back to the BS which uses only this eigenbeam as beamformer to transmit data signals to this MS. The number of feedback bits needed for the L eigenbeams to be sent to BS and to be updated when the long term properties of the channel change, depends on L and the quantisation scheme used. Also, $\mathrm{ceil}(\log_2(L))$ feedback bits are needed to pick the eigenbeam yielding the highest SNR over every time slot.

Here we will simulate a slight modification of the technique. The MS sums the mean CCMs of all downlink taps $\mathbf{R}_{\mathrm{SUM}}^{\mathrm{DL}} = \sum_{l=1}^{N} \mathbf{R}_l^{\mathrm{DL}}$, performs the EVD of $\mathbf{R}_{\mathrm{SUM}}^{\mathrm{DL}}$ and sends all its eigenvectors to the BS. Finally, the MS calculates which eigenbeam yields the highest SNR over every time slot and sends this information back to the BS,which uses this eigenbeam for data transmission to the MS. The downlink carrier frequency is $f_c^{\mathrm{DL}} = 2$ GHz, the spacing is $D = \lambda/2$ and the BS is assumed to know which eigenbeam must be used over every time slot.

VI. Simulation Result Comparisons

In this section we compare simulation results of all techniques in terms of BER vs SNR performance for BPSK modulation, in both flat and frequency selective fading. All techniques transmit unit power for fair comparison, while the MS receiver is assumed capable of obtaining noiseless estimates of the downlink channel coefficients h_i, $i = 1..M$.

Type of cell	**AOD** (deg)	**AS** (deg)	ρ_{adj}
Macro	15	10	0.988
Micro	30	45	0.825

TABLE I
CELL TYPES USED IN FLAT FADING SIMULATIONS

Table I shows the cell types and their parameters, which have been used in the simulations of flat fading conditions [14]. Also, table II shows the parameters of the two taps used in the simulation of the frequency selective conditions.

Tap	**Power** (dB)	**AOD** (deg)	**AS** (deg)	ρ_{adj}
# 1	0	2	10	0.987
# 2	-3	30	25	0.943

TABLE II
TAPS USED IN FREQUENCY SELECTIVE FADING SIMULATIONS

Simulation results for 4 antennas in the macro cell environment are shown in Fig. 4. Dashed curves correspond to blind techniques, while solid curves correspond to non-blind techniques. The results show that TXAA yields the best performance of all techniques providing the lower bound, though at the expense of high rate feedback. Eigenbeamforming approaches the lower bound to within 1.8dB at BER $= 10^{-3}$, but requires high rate feedback. MIN BER approaches the lower bound to within 3dB and is better than all blind techniques at BER $= 10^{-3}$, but at higher BERs it is worse than MAX SNR.

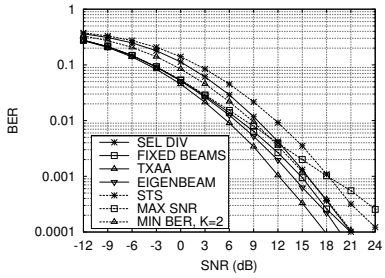

Fig. 4. Comparison of all techniques in the macro cell for $M = 4$.

This is because the diversity gain of using two eigenvectors ($K = 2$) prevails only at higher SNRs (lower BERs). Also, MIN BER has been optimised for target BER $= 10^{-3}$. Fixed beams has the same performance as MAX SNR for low SNRs, which is attributed to the particular channel environment, as the central AOD coincides with the maximum radiation of a beam of fixed beams. However, it becomes better than MAX SNR at higher SNRs due to diversity gain. STS is worse than all blind techniques for low SNR (<18dB), but improves significantly for higher SNR (>18dB) because of the diversity nature of its gain. Finally, selection diversity yields the worst performance of all non-blind techniques at all shown SNR values. This is due to its lack of beamforming gain and the low diversity gain of the macro cell.

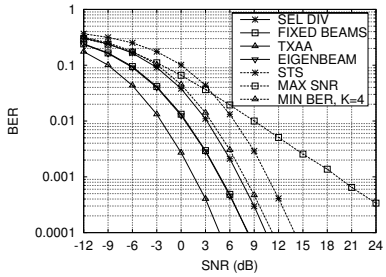

Fig. 5. Comparison of all techniques in the micro cell for $M = 8$.

Next, Fig. 5 shows simulation results for 8 antennas in the micro cell. Although MAX SNR uses more antennas, it performs worse than previously as there is no preferred direction of transmission because of large AS. MIN BER is again better than all other blind techniques, especially at higher SNR (>-6dB). Selection diversity improves significantly due to the higher diversity gain of the richer scattering environment of the micro cell, and is marginally better than MIN BER (within 0.7dB). Fixed beams provides equal-strength (partially) correlated beams while eigenbeamforming provides unequal-strength uncorrelated eigenbeams, both of which can be seen as a transformation in space. In the micro cell, both transformations when combined with selection diversity yield similar results.

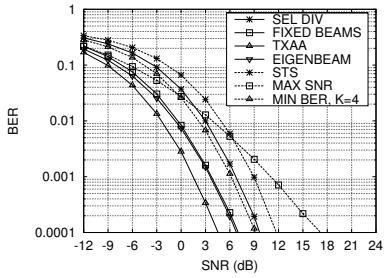

Fig. 6. Comparison of all techniques for frequency selective fading and $M = 8$.

Simulation results under a frequency selective fading scenario with the two taps of table II and $M = 8$ are shown in Fig. 6. We assume that the two taps are resolved by the mobile RAKE receiver and there is no interference between them. Again, TXAA yields the lower bound while fixed beams and eigenbeamforming perform within about 1.8dB away from it at BER $= 10^{-3}$. Also, fixed beams starts off together with MAX SNR at very low SNR but performs much better than it at higher SNR (about 7dB better at BER $= 10^{-3}$), as it benefits from diversity gain. MIN BER is worse than MAX SNR at low SNR (<0dB), but becomes better than all blind techniques at higher SNR (>0dB). Finally, selection diversity is now marginally worse than MIN BER.

All results show that non-blind techniques perform in general better than blind ones, which is expected as they use mobile feedback information about the downlink channel. The gain over the blind techniques is an indication of how much the performance can be improved by introducing mobile feedback.

VII. Conclusions

Candidate downlink adaptive antenna techniques for WCDMA systems have been analysed and simulated in this paper. Comparison results show that TXAA provides the lower bound on the performance and eigenbeamforming performs closely to it, but they require high rate feedback. Blind beamforming techniques such as MAX SNR do not perform efficiently in environments with large AS. Non-blind techniques perform better than blind ones, providing an indication of how much the performance can be improved by using mobile feedback. Also, a new blind hybrid technique has been introduced, which periodically measures the channel (in the form of its mean CCM) and adapts to it to satisfy a flexible criterion. Its behaviour ranges from pure beamforming to pure diversity, optimising the performance under all channel conditions.

References

[1] IEEE Personal Communications Magazine, Special Issue on Smart Antennas, February 1998. Vol. 5, No. 1.

[2] A. J. Paulraj and C. B. Papadias. Space-time processing for wireless communications. *IEEE Signal Processing Magazine*, 14(6):49–83, November 1997.

[3] J. G. Proakis. *Digital communications*. McGraw-Hill, 3rd edition, 1995.

[4] J. S. Thompson, P. M. Grant, and B. Mulgrew. Smart antenna arrays for CDMA systems. *IEEE Personal Communications Magazine*, 3(5):16–25, October 1996.

[5] J. S. Thompson, J. E Hudson, P. M. Grant, and B. Mulgrew. CDMA downlink beamforming for frequency selective channels. In *PIMRC'99*, pages 233–237, 1999.

[6] S. Haykin. *Adaptive filter theory*. Prentice-Hall International Editions, 3rd edition, 1996.

[7] B. Hochwald, T. L. Marzetta, and C. B. Papadias. A transmitter diversity scheme for wideband CDMA systems based on space-time spreading. *IEEE Journal on Selected Areas in Communications*, 19(1):48–60, January 2001.

[8] E. Tiirola and J. Ylitalo. Performance evaluation of fixed-beam beamforming in WCDMA downlink. In *IEEE Vehicular Technology Conference*, volume 2, May 15-18 2000. Tokyo, Japan.

[9] G. G. Raleigh, S. N. Diggavi, V. K. Jones, and A. Paulraj. A blind adaptive transmit antenna algorithm for wireless communication. In *IEEE International Conference on Communications*, volume 3, pages 1494–1499, June 1995. Seattle.

[10] K. Rohani, M. Harrison, and K. Kuchi. A comparison of base station transmit diversity methods for third generation cellular standards. In *IEEE Vehicular Technology Conference*, pages 351–355, 16-20 May 1999. Houston, USA.

[11] V. Tarokh, H. Jafarkhani, and A. R. Calderbank. Space-ime block codes from orthogonal designs. *IEEE Transactions on Information Theory*, 45(5):1456–1467, July 1999.

[12] M. Katz and J. Ylitalo. Extension of space-time coding to beamforming WCDMA base stations. In *IEEE Vehicular Technology Conference*, volume 2, pages 1230–1234, May 15-18 2000. Tokyo, Japan.

[13] C. Bruner, J. S. Hammerschmidt, and J. A. Nossek. Downlink eigenbeamforming in WCDMA. In *European Wireless*, pages 195–200, September 12-14 2000. Dresden, Germany.

[14] Siemens TSGR1#16 R1-00-1180. Simulation parameters for TX diversity simulations using correlated antennas. In *3GPP TSG RAN WG1*, 10-13 October 2000. Pusan, Korea.

Pilot Signal Effects on Adaptive Antenna Arrays in FDD wideband CDMA

Antonis C Koutalos† & John S Thompson
Signals and Systems Group, Department of Electronics and Electrical Engineering,
The University of Edinburgh, Edinburgh, EH9 3JL, UK.
Email: Antonis.Koutalos@ee.ed.ac.uk, John.Thompson@ee.ed.ac.uk

Abstract— **This paper discusses the effect of pilot signals on the performance of adaptive antenna array algorithms. The adaptive antennas are employed on the downlink of wideband code division multiple access (WCDMA) mobile communication systems which operate in frequency division duplex (FDD) mode. The algorithms are first simulated under a scenario where all required parameters are known to both base station (BS) and mobile station (MS). Also, different types of pilot signals are described and the algorithms are simulated under a scenario where these pilot signals are used to estimate the required parameters. The impact of the different types of pilot signals on the performance of the algorithms is then discussed.**

Keywords— **Adaptive antennas, antenna arrays, pilot signals.**

I. Introduction

Adaptive antenna arrays are employed in BSs of mobile communication systems, as they can improve the mean signal-to-noise ratio (SNR) and suppress co-channel interference (CCI). Among the first applications of antenna arrays was that of signal reception on the uplink (MS to BS link) [1], [2], [3]. Recently, there has been increasing interest in employing them also on the downlink (BS to MS link) [4], [5]. However, in FDD systems the downlink is more challenging than the uplink because the BS has no direct access to the channel vector and other parameters it may need (e.g. which antenna or beam to use for data signal transmission to the intended MS). These parameters are practically obtained by means of pilot signals.

Pilot signals are transmitted by the BS and are used by the MS to estimate the downlink channel vector and any other required parameters. Some of these parameters are used by the MS itself, while others are fed back to BS which uses them for data signal transmission to the MS. The MS may also transmit pilot signals so that the BS estimates the necessary parameters. Nevertheless, the estimated parameters contain noise, since the pilot signals used to estimate them are noisy, which affects the system performance.

This paper presents simulation results for a number of downlink antenna array techniques without pilot signals (i.e. the MS and BS are assumed to know all the required parameters perfectly) and with pilot signals (i.e. pilot signals are used to estimate the required parameters). The results are then compared to each other and the effects of different types of pilot signals on the performance of each technique are discussed.

†Antonis C Koutalos gratefully acknowledges the financial support of his studies by the Electronics & Electrical Engineering Department of the University of Edinburgh, Edinburgh, Scotland.

The organisation of the paper is as follows. Section II addresses the system model that is assumed while section III introduces the techniques that will be simulated in the paper. Finally, section IV presents the simulation results and discusses the pilot signal effects on the performance of the techniques, and section V draws our conclusions.

II. System Model

Each cell of the system is divided into three sectors of 120^{o} each. The BS is assumed to employ a uniform linear array (ULA) with M elements to transmit signals to MSs, which use a single-element antenna to receive signals. If s_{d} is the data signal to be transmitted to a MS and $c(t)$ the spreading code of this MS (which is complex in general and has unit norm), the BS transmits the vector signal $\mathbf{x}(t)^{\text{H}} = \sqrt{E_{\text{s}}} s_{\text{d}} c(t) \mathbf{w}^{\text{H}}$, where E_{s} is the power of the data signal, $\mathbf{w}^{\text{H}} \in C^{1\times M}$ is the weight vector (or beamformer) that the BS uses and the H superscript denotes complex conjugate transpose of a vector. The MS receives a signal which, after cross-correlation with $c(t)^{\text{H}}$, is written as $y = \sqrt{E_{\text{s}}} s_{\text{d}} \mathbf{w}^{\text{H}} \mathbf{h} + n = \sqrt{E_{\text{s}}} s_{\text{d}} \zeta + n$, where $\mathbf{h} \in C^{M\times 1}$ is the downlink channel vector, n denotes additive white Gaussian noise and ζ contains the combined effects of the weight vector and the channel vector. The downlink channel is modeled as follows:

$$\mathbf{h}(t) = \sqrt{\frac{P}{Q}} \sum_{\text{q}=1}^{Q} e^{j(\phi_{\text{q}} + 2\pi f_{\text{q}} t)} \begin{bmatrix} 1 \\ e^{j\{\frac{2\pi D}{\lambda}\sin(\theta_{\text{q}})\}} \\ \vdots \\ e^{j\{\frac{2\pi D}{\lambda}(M-1)\sin(\theta_{\text{q}})\}} \end{bmatrix}$$

where P is the channel power, Q the number of scattered signals (components) contributing to the channel, ϕ_{q} the random phase of the q-th component uniformly distributed over $[0, 2\pi]$, f_{q} the Doppler frequency shift of the q-th component and θ_{q} the angle-of-departure (AOD) of the q-th component with respect to the perpendicular to the array axis. The AOD θ_{q} is uniformly distributed over $[\Theta - \delta/2, \Theta + \delta/2]$, where Θ is the central AOD and δ is the angular spread (AS) of the channel. Also, λ is the wavelength of the carrier frequency f_{c} and D the array element spacing.

The BS transmits pilot signals so that the MS can estimate either $\mathbf{h}$ or ζ (depending on the technique) and obtain an estimate $\hat{s}_{\text{d}}$ of the data signal from the received signal y. Also, in techniques where the BS needs information about the uplink channel, the MS transmits pilot signals from which this information is obtained. Finally, if the BS needs information about the downlink channel in order to calculate the weight vector $\mathbf{w}^{\text{H}}$, it transmits pilot signals from which the MS obtains downlink channel information. This information is then

fed back to the BS by means of feedback signals.

III. Description of Techniques

In this section we briefly describe the antenna array techniques that will be simulated in section IV. In the description of each technique we will focus on the parameters that need to be estimated via pilot signals.

A. Space-Time Spreading

Space-time spreading (STS) is a diversity technique in which the data signal is coded according to a space-time coding scheme, and then transmitted through each antenna element [6], [7]. The MS cross-correlates the received signal with the appropriate spreading codes, thus decoupling the signals transmitted from each element and obtaining an estimate of the initial transmitted data signal. Due to the coding scheme, the BS does not need downlink channel information, but the MS needs to estimate this channel in order to demodulate the received signal. Therefore, in the simulations the BS transmits pilot signals which are used by the MS to estimate the downlink channel.

B. Maximum SNR

Maximum SNR (MAX SNR) is a beamforming technique that maximises the expected SNR of the decision signal at the MS receiver [8]. For this purpose, it uses the principal eigenvector $\mathbf{u}_{\max}^{\mathrm{DL}}$ of the downlink channel correlation matrix (CCM) $\mathbf{R}^{\mathrm{DL}}$ as beamformer ($\mathbf{u}_{\max}^{\mathrm{DL}}$ is the eigenvector corresponding to the maximum eigenvalue $e_{\max}^{\mathrm{DL}}$ of $\mathbf{R}^{\mathrm{DL}}$). The downlink CCM is defined as $\mathbf{R}^{\mathrm{DL}} = \mathrm{E}\left[\mathbf{h}^{\mathrm{DL}}(t)\mathbf{h}^{\mathrm{DL}}(t)^{\mathrm{H}}\right]$, where $\mathbf{h}^{\mathrm{DL}}(t)$ is the downlink channel vector and $\mathrm{E}[\bullet]$ denotes the expectation operation.

The MS can calculate the downlink CCM $\mathbf{R}^{\mathrm{DL}}$ and its principal eigenvector $\mathbf{u}_{\max}^{\mathrm{DL}}$, and feed either the CCM or the eigenvector back to the BS. This requires a reliable feedback path from MS to BS. Alternatively, the BS can calculate the uplink CCM $\mathbf{R}^{\mathrm{UL}}$ and use its principal eigenvector $\mathbf{u}_{\max}^{\mathrm{UL}}$ as beamformer. Then, the feedback path is avoided, but in FDD systems there will be some performance degradation because the uplink and the downlink channels do not use the same carrier frequency and their CCMs are not exactly the same. In our simulations the BS will calculate $\mathbf{R}^{\mathrm{UL}}$ from pilot signals transmitted by the MS, and will use its principal eigenvector $\mathbf{u}_{\max}^{\mathrm{UL}}$ as beamformer.

C. Selection Diversity

Selection diversity is a diversity scheme, in which the BS transmits pilot signals from each antenna element which are used by the MS to measure which antenna yields the highest SNR ('best' antenna) [9]. This information is fed back to the BS, which then uses *only* this best antenna to transmit data signals to this MS. The number of pilot bits needed to feed back an index to the best antenna is $\mathrm{ceil}(\log_2(M))$ ($\mathrm{ceil}(x)$ denotes the smallest integer that is greater than or equal to x).

Selecting the antenna with the highest SNR, is analogous to selecting the antenna with the largest instantaneous power when the average noise power is the same for all antennas [9]. However, the instantaneous power of the pilot signals of each antenna is influenced by noise and, thus, the best antenna selection by the MS may be incorrect, resulting in performance loss. Also, even if the best antenna is selected correctly at the MS, this information has to be fed back to BS. The noise that is present in the feedback signals from MS to BS can cause the BS to use the wrong antenna for data signal transmission to MS. In the simulations we simulate the effects of these both phenomena.

D. Fixed Beams

Fixed beams is a beamforming technique [10]. The BS sets up a fixed number of beams, N_{B}, to cover the cell sector that it serves and transmits pilot signals through each beam. The MS measures the beam that yields the highest SNR ('best' beam) and feeds this information back to the BS, which uses *only* this best beam to transmit signals to this MS. The number of pilot bits needed to feed back an index to the best beam is $\mathrm{ceil}(\log_2(N_{\mathrm{B}}))$.

The selection of the best beam is performed similarly to the selection of the best antenna in selection diversity. Therefore, the basic sources of errors and performance loss in fixed beams are similar to those in selection diversity. Namely, the best beam may not be selected correctly by the MS due to noise in the pilot signals, or the index to the best beam that the MS feeds back to BS may be corrupted due to noise in the feedback signals. In the simulations we simulate the effects of both phenomena.

IV. Simulation Results

In this section we present simulation results for the above techniques. We distinguish among different types of pilot signals and discuss their impact on the system performance. We use three types of cells [11], which are shown in table I. For each technique, we only show results in the environment

Cell type	**AOD** (deg)	**AS** (deg)
Macro	15	10
Micro	30	45
Pico	0	120

TABLE I
CHANNEL TYPES USED IN THE SIMULATIONS

where it yields the best performance (i.e. beamforming techniques in the macro cell, diversity techniques in the pico cell etc.), so that the only performance degradation is due to pilot signal effects. Also, the modulation is BPSK, the channel is flat fading, the symbol period is $T_{\mathrm{s}} = 14.2\mu sec$ and the maximum Doppler frequency shift $f_{\mathrm{D}} = 110$Hz.

A. Pilot signals for channel estimation at the MS receiver

First we discuss the effects of pilot signals used for channel coefficient estimation at the MS receiver: the BS transmits pilot signals which are used by the MS receiver to estimate the downlink channel and demodulate the received signals.

Fig. 1 shows simulation results (bit error ratio (BER) versus SNR) with both perfect channel knowledge and noisy channel estimates at the MS receiver for STS and $M = 2, 4, 8$. The downlink carrier frequency is $f_{\mathrm{c}} = 2$GHz, the spacing is $D = \lambda/2$ and the environment is a pico cell. The BS trans-

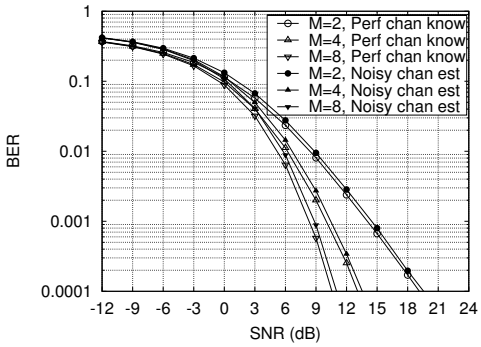

Fig. 1. Effect of noisy channel estimates in STS in the pico cell.

mits a pilot signal from each antenna so that the MS can estimate each channel coefficient. The ratio of each antenna's pilot signal power to the total power of each data symbol across all M antennas is $A = 10$dB. As it is expected, the performance with noisy channel estimates is worse than the performance with perfect channel estimates for the same M. The amount by which the performance deteriorates depends on A: the larger the A the better the channel estimates and the smaller the performance degradation. Also, the performance degradation is almost the same for all values of M and equal to about 0.5dB. This is in contrast with the results in [6], where the degradation increases with M. However, in [6] the *total* power allocated to pilot signals is 10dB higher than the total data signal power across all M antennas, so the ratio of *each* antenna's pilot signal power to the total data signal power is $A = 10 - 10\log_{10}(M)$dB. Hence, each antenna's pilot signal power decreases as M increases, yielding worse channel coefficient estimates and worse performance. This behaviour is characteristic to STS because the MS needs to estimate all M channel coefficients. The other techniques do not exhibit this behaviour as the MS does not need to estimate all M channel coefficients to demodulate the received signal. Consequently, their performance degradation due to this type of pilot signals is the same for all values of M, without requiring more pilot power as M increases. Nevertheless, selection diversity and fixed beams need more pilot power as M increases for the best antenna or beam selection, respectively, as the MS needs to estimate the SNR of all antennas or beams.

B. Pilot signals for CCM estimation at BS

Next, we move on to the effects of pilot signals used for the uplink CCM $\mathbf{R}^{\mathrm{UL}}$ estimation at the BS. Fig. 2 shows simulation results for both perfect knowledge of $\mathbf{R}^{\mathrm{UL}}$ and noisy estimates of $\mathbf{R}^{\mathrm{UL}}$ for MAX SNR and $M = 2, 4, 8$ in the macro cell. The downlink and uplink carrier frequencies are $f_{\mathrm{c}}^{\mathrm{DL}} = 1.95$GHz and $f_{\mathrm{c}}^{\mathrm{UL}} = 2.14$GHz respectively, while the spacing is $D = \lambda^{\mathrm{MID}}/2$, where λ^{MID} is the wavelength of the carrier frequency $f_{\mathrm{c}}^{\mathrm{MID}} = (f_{\mathrm{c}}^{\mathrm{DL}} + f_{\mathrm{c}}^{\mathrm{UL}})/2$. The BS uses the principal eigenvector $\mathbf{u}_{\mathrm{max}}^{\mathrm{UL}}$ of the uplink CCM $\mathbf{R}^{\mathrm{UL}}$ as beamformer to transmit signals on the downlink. In the case of perfect $\mathbf{R}^{\mathrm{UL}}$ knowledge, $\mathbf{R}^{\mathrm{UL}}$ is calculated theoretically as described in [12]. In the case of noisy $\mathbf{R}^{\mathrm{UL}}$ estimates, the BS estimates the uplink channel vector $\mathbf{h}_i^{\mathrm{UL}}(t+iT_{\mathrm{s}})$, $i = 0, 1, \cdots, N_{\mathrm{p}} - 1$ of N_{p} consecutive pilot symbols transmitted by the MS, and then calculates $\mathbf{R}^{\mathrm{UL}}$ as the expectation of the instantaneous CCMs of the N_{p} channel vectors $\mathbf{R}^{\mathrm{UL}} = \frac{1}{N_{\mathrm{p}}}\sum_{i=0}^{N_{\mathrm{p}}-1}\mathbf{h}_i^{\mathrm{UL}}(t+iT_{\mathrm{s}})\mathbf{h}_i^{\mathrm{UL}}(t+iT_{\mathrm{s}})^{\mathrm{H}}$. After the estimation of $\mathbf{R}^{\mathrm{UL}}$, its principal eigenvector $\mathbf{u}_{\mathrm{max}}^{\mathrm{UL}}$ is calculated and used as beamformer to transmit N_{d} data symbols on the downlink. In the simulation we use $N_{\mathrm{p}} = 4$ and $N_{\mathrm{d}} = 20$, i.e. the ratio of pilot symbols to data symbols is $\gamma = N_{\mathrm{p}}/N_{\mathrm{d}} = 0.2$. The ratio of the pilot symbol power to the data symbol power is $A = 10$dB.

Fig. 2 shows that the performance with $\mathbf{R}^{\mathrm{UL}}$ estimated from pilot symbols is worse than the performance with perfect $\mathbf{R}^{\mathrm{UL}}$ knowledge for the same M. This is partly because of the noise that is present in the channel vector estimates and partly because of the small number of pilot symbols over which $\mathbf{R}^{\mathrm{UL}}$ is averaged. Nevertheless, the noise is much less significant than the number of pilot symbols, since it does not affect much the principal component of the eigendecomposition of $\mathbf{R}^{\mathrm{UL}}$ which is used as beamformer but the components with smaller amplitude (i.e. the eigenvectors that correspond to eigenvalues with smaller amplitude). On the other hand, the small number of $\mathbf{h}_i^{\mathrm{UL}}$ samples cannot yield the direction that maximises the expected SNR of the decision signal (in the form of $\mathbf{u}_{\mathrm{max}}^{\mathrm{UL}}$) with high accuracy. Consequently, the main beam of the array is not steered exactly in the direction that maximises the average SNR.

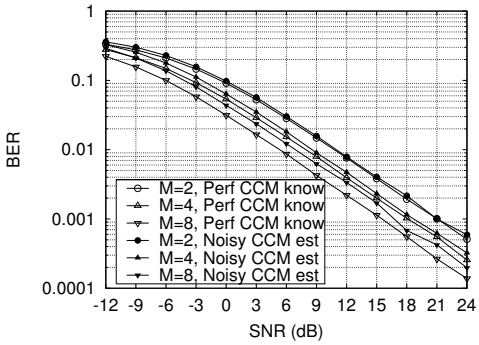

Fig. 2. Effect of noisy uplink CCM estimates in MAX SNR in the macro cell.

Also, the performance loss is greater for higher values of M (about 2dB for $M = 2$ and about 4dB for $M = 4, 8$ at BER $= 10^{-3}$). This is due to the fact that the beamwidth of the array with $M = 2$ is so broad that even if the main beam is steered slightly off the correct direction, it still 'illuminates' a large part of the AS. On the other hand, the array beamwidth is much narrower with $M = 4, 8$ and even small fluctuations of the main beam around the correct direction cause it to 'illuminate' a much smaller part of the AS.

C. Pilot signals for best antenna or beam selection at MS

Next we discuss the effects of pilot signals used for selecting the best antenna or the best beam for data signal transmission on the downlink of selection diversity or fixed beams, respectively. In this scenario, the BS transmits pilot signals which are used by the MS to select the antenna or beam that provides the highest SNR, and this antenna or beam is then used for transmission on the downlink. Here we only simulate

the effects of selecting the best antenna or beam from noisy pilot signals, while we assume that the feedback of the index to the best antenna or beam from MS to BS is performed noiselessly. Also, we assume that the MS has perfect knowledge of the downlink channel coefficients during the transmission of the data signals and after the selection of the best antenna or beam. These assumptions eliminate all other sources of performance degradation due to pilot signals except for the noisy selection of the best antenna or beam, so we can discuss their impact on the performance separately.

Fig. 3 shows simulation results for selection diversity with both noiseless and noisy selection of the best antenna by the MS, for $M = 2, 4, 8$ in the pico cell. For the noiseless antenna selection we assume that the BS knows which antenna yields the highest instantaneous SNR over each data symbol and uses this antenna for transmission to the MS. Although this assumption is unrealistic, it yields reference results which can be compared to the results from the noisy antenna selection to reveal its effects. For the noisy antenna selection the MS averages the SNR of the M antennas over $N_{\mathrm{p}} = 4$ pilot symbols which are transmitted by the BS, and determines which gives the highest SNR. Then an index to this antenna is fed back to the BS (noiselessly), which uses it for the transmission of $N_{\mathrm{d}} = 20$ data symbols ($\gamma = N_{\mathrm{p}}/N_{\mathrm{d}} = 0.2$). The ratio of the pilot symbol power *per antenna* to the total data symbol power is $A = 6$dB. The downlink carrier frequency is $f_{\mathrm{c}}^{\mathrm{DL}} = 2$GHz, and the spacing is $D = \lambda/2$, where λ is the wavelength of $f_{\mathrm{c}}^{\mathrm{DL}}$.

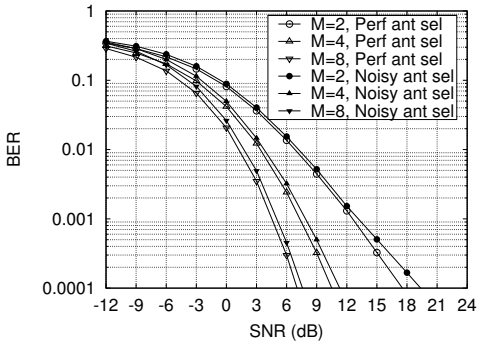

Fig. 3. Effect of noisy antenna selection in selection diversity in the pico cell.

The results of Fig. 3 show that the performance with noisy antenna selection is about 0.5dB worse than the performance with noiseless antenna selection. Also, the degradation is constant for all values of M, as the total power allocated to pilot signals increases with M (i.e. the pilot signal of each antenna has a power 6dB higher than the data signal, regardless of the total number of antennas in the BS). This is the same as the assumption used in STS for downlink channel estimation at the MS using pilot signals.

Next, Fig. 4 shows simulation results for fixed beams with both noiseless and noisy selection of the best beam by the MS, for $M = 2, 4, 8$ in the micro cell. The number of beams formed in the 120^{o} cell sector is equal to the number of antennas in the BS, $N_{\mathrm{B}} = M$ [4]. For the noiseless beam selection we assume that the BS knows which beam yields the highest instantaneous SNR over each data symbol and uses this beam for transmission to the MS, for the same reason as in selection diversity. For the noisy beam selection the MS averages the SNR of the N_{B} beams over $N_{\mathrm{p}} = 4$ pilot symbols which are transmitted by the BS, and determines which gives the highest SNR. Then an index to this beam is fed back to the BS (noiselessly), which uses it for the transmission of $N_{\mathrm{d}} = 20$ data symbols ($\gamma = N_{\mathrm{p}}/N_{\mathrm{d}} = 0.2$). The ratio of the pilot symbol power *per beam* to the total data symbol power is $A = 6$dB. The downlink carrier frequency is $f_{\mathrm{c}}^{\mathrm{DL}} = 2$GHz, and the spacing is $D = \lambda/2$ where λ is the wavelength of $f_{\mathrm{c}}^{\mathrm{DL}}$.

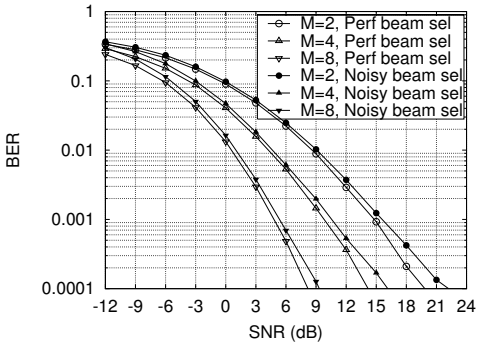

Fig. 4. Effect of noisy beam selection in fixed beams in the micro cell.

The results are similar to those of selection diversity. That is, the performance with noisy beam selection is about 0.5dB worse than the performance with noiseless beam selection. Also, this performance degradation is the same for all values of M, as the total power allocated to pilot signals increases with M.

D. Pilot signals for best antenna or beam feedback from MS to BS

Finally, the simulations in this section study the effects of errors due to noise in the feedback path used to feed an index to the best antenna or beam in selection diversity or fixed beams, respectively. We assume that the best antenna or beam is selected by the MS from noiseless pilot signals (i.e. the MS has perfect knowledge of which antenna or beam yields the highest average SNR over the $N_{\mathrm{p}} = 4$ pilot symbols), and transform the index to the best antenna or beam from decimal into binary form. Then, we alter the value of each binary digit of the index with probability BER $= 10^{-2}$ and transform the resulting binary number back into decimal. Finally, the BS uses the antenna or beam that the resulting decimal number points to for transmission of $N_{\mathrm{d}} = 20$ data symbols to MS. All other assumptions and parameters are the same as in the previous subsection. Also, we simulate the two techniques using an error probability of BER $= 0$ for the feedback path (i.e. no errors on the feedback path), and compare the results with the noisy feedback results.

Fig. 5 shows simulation results for selection diversity in the pico cell and for $M = 2, 4, 8$. For small SNR values, the BER of the data signals is larger than the BER of the feedback signals, making the noise in the received data signals the dominant source of errors. Therefore, the noise in the received data

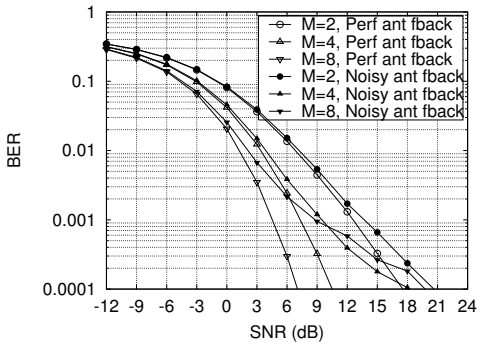

Fig. 5. Effect of noisy antenna feedback in selection diversity in the pico cell.

signals dominates the performance, while the effect of the noise in the feedback signals is small, and the curves overlap. As the SNR increases, the noise in the received data signals becomes smaller and the noise in the feedback signals starts to dominate. Thus, the performance with noisy feedback signals becomes increasingly worse as the SNR increases.

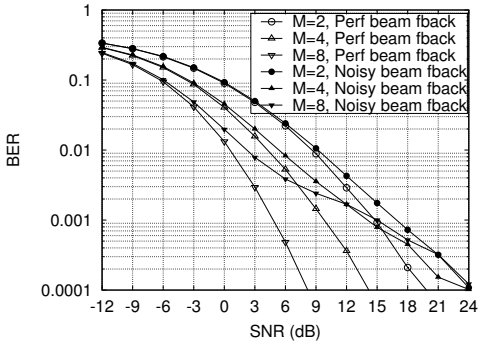

Fig. 6. Effect of noisy beam feedback in fixed beams in the micro cell.

Fig. 6 shows simulation results for fixed beams in the micro cell and for $M = 2, 4, 8$. Although the results of Fig. 6 show the same trend as those of Fig. 5 (for the same reasons), fixed beams is affected more by the noisy feedback signals than selection diversity. The antenna elements of the ULA in the BS are omnidirectional and even if the wrong element is used for transmission, a certain amount of power will eventually be transmitted in the direction of the MS, so the performance is not affected too much. However, if the wrong beam is used for transmission, there may be very little or even not at all transmitted power in the direction of the MS (depending on the particular beam and the central AOD of the channel), and the performance is affected dramatically. Consequently, fixed beams is more sensitive to feedback noise than selection diversity.

V. Conclusions

In this paper we described different types of pilot signals used in adaptive antenna arrays which operate on the downlink of FDD wideband CDMA mobile communication systems. We also simulated a number of antenna array techniques using these pilot signals, and discussed the impact of each type of pilot signals on their performance. Differences of the impact of the pilot signals on the performance of different antenna array algorithms were also discussed.

Simulation results show that the performance loss is approximately 0.5dB, when the MS estimates the downlink channel coefficients from pilot signals which have 10dB higher power than the data signals. STS requires that the total power allocated to this type of pilot signals increases with M so that the loss does not increase with M, while the other techniques do not have this requirement. Furthermore, when the BS estimates the uplink CCM from pilot signals in MAX SNR, the performance loss increases with M, as the array beamwidth decreases with M. Also, there is a performance loss of about 0.5dB in both selection diversity and fixed beams, when the MS selects the best antenna or beam, respectively, from pilot signals that have 6dB higher power than the data signals. In addition, when errors on the feedback path occur with a constant probability, both selection diversity and fixed beams yield increasingly worse performance with SNR. Finally, fixed beams is more sensitive to feedback path noise than selection diversity, as choosing the wrong beam usually has a greater effect on the final system performance than choosing the wrong antenna.

References

[1] IEEE Personal Communications Magazine, Special Issue on Smart Antennas, February 1998. Vol. 5, No. 1.

[2] A. J. Paulraj and C. B. Papadias. Space-time processing for wireless communications. *IEEE Signal Processing Magazine*, 14(6):49–83, November 1997.

[3] J. S. Thompson, P. M. Grant, and B. Mulgrew. Smart antenna arrays for CDMA systems. *IEEE Personal Communications Magazine*, 3(5):16–25, October 1996.

[4] A. C. Koutalos, J. S. Thompson, and P. M. Grant. Downlink adaptive antenna techniques for WCDMA. In *IEEE Vehicular Technology Conference*, May 6-10 2002. Birmingham, Al, USA.

[5] J. S. Thompson, J. E Hudson, P. M. Grant, and B. Mulgrew. CDMA downlink beamforming for frequency selective channels. In *PIMRC'99*, pages 233–237, 1999.

[6] B. Hochwald, T. L. Marzetta, and C. B. Papadias. A transmitter diversity scheme for wideband CDMA systems based on space-time spreading. *IEEE Journal on Selected Areas in Communications*, 19(1):48–60, January 2001.

[7] V. Tarokh, H. Jafarkhani, and A. R. Calderbank. Space-Time block codes from orthogonal designs. *IEEE Transactions on Information Theory*, 45(5):1456–1467, July 1999.

[8] G. G. Raleigh, S. N. Diggavi, V. K. Jones, and A. Paulraj. A blind adaptive transmit antenna algorithm for wireless communication. In *IEEE International Conference on Communications*, volume 3, pages 1494–1499, June 1995.

[9] A. Annamalai and V. K. Bhargava. Performance of selection diversity for DS/CDMA communications over Rayleigh fading channels. *IEE Electronics Letters*, 32(21):1966–1968, October 1996.

[10] E. Tiirola and J. Ylitalo. Performance evaluation of fixed-beam beamforming in WCDMA downlink. In *IEEE Vehicular Technology Conference*, volume 2, May 15-18 2000. Tokyo, Japan.

[11] Siemens. Channel model for TX diversity simulations using correlated antennas. Available: http://www.3gpp.org/ftp/tsg_ran/WG1_RL1/TSGR1_15/Docs/PDFs/, Document: R1-00-1067.pdf, 22-25 August 2000. Berlin, Germany.

[12] J. Salz and J. Winters. Effect of fading correlation on adaptive arrays in digital mobile radio. *IEEE Transactions on Vehicular Technology*, 43(4):1049–1057, November 1994.

Effect of Frequency Division Duplex on Open Loop Downlink Beamforming in WCDMA Systems

Antonis C Koutalos[†], John S Thompson
Signals and Systems Group, Department of Electronics and Electrical Engineering,
The University of Edinburgh, Edinburgh, EH9 3JL, UK.
Email: Antonis.Koutalos@ee.ed.ac.uk, John.Thompson@ee.ed.ac.uk

Abstract— **We investigate the effect of the frequency division duplex (FDD) gap on the performance of open loop adaptive beamforming antenna arrays for wideband code division multiple access (WCDMA) communication systems. We show that the system performance worsens with increasing FDD gap. Also, a simple technique that mitigates the FDD effect is presented. It is easily implemented and compensates for most of the performance loss even for relatively large FDD gap values. Finally, we compare this technique with a more complex one and show that the two compensation techniques yield very similar results in the studied channel environment.**

Keywords—**Frequency transformation downlink beamforming, open loop downlink beamforming.**

I. Introduction

Adaptive antenna arrays are used in base stations of WCDMA communication systems, as they offer desirable advantages over single antenna systems. These include mitigation of the received signal amplitude fading and spatially selective reception and transmission. Typically, they are exploited on the uplink (mobile-to-base station link) [1], but recently there has been increasing interest in applying them also to the downlink (base-to-mobile station link) [2], [3], [4]. In this work we will focus on beamforming adaptive antennas which can be used to transmit power only in the direction of the intended user, thus enhancing the signal-to-noise ratio (SNR) of this user and minimising interference to non-intended users.

In order to calculate the beamforming vector, the base station typically needs information about the downlink channel vector of the intended mobile user. In time division duplex (TDD) systems the uplink and downlink channels use the same carrier frequency and the base station can obtain downlink channel information by measuring the uplink channel vector. In frequency division duplex (FDD) systems, however, the two channels use different carrier frequencies and the instantaneous channels are not the same. Nevertheless, when the separation of their carrier frequencies due to FDD, f_{FDD} (FDD gap), is not large, there is a strong relationship between their *average* statistical properties [2]. Therefore, techniques that calculate the beamforming vector by taking into account the average statistical properties of the downlink channel (such as the one introduced in [2]), may be able to obtain this information from the uplink channel. We note that in this case there will be some performance loss, as the average statistical properties of the two channels are similar but not *exactly* the same. This paper studies the effect of the FDD gap f_{FDD} on the correlation of the two channels and the system performance. Also, a simple technique is introduced to compensate most of this performance loss. In [2] the authors provide theoretical results about the performance loss due to FDD. However, these results only provide the approximate *maximum* performance loss and are valid for small f_{FDD} values. Here, we will express the loss as a function of f_{FDD} and provide results for larger f_{FDD} values.

The paper is organised as follows. The next section introduces the system model assumed herein, while section III briefly describes the open loop beamforming technique to be examined. Next, section IV studies the impact of FDD on the performance of the beamforming technique and section V introduces the compensating algorithm. Finally, section VI provides our conclusions.

[†]Antonis C Koutalos wishes to acknowledge the financial support of his studies by the Electronics and Electrical Engineering Department, University of Edinburgh, Edinburgh, Scotland, UK.

II. System Model

For the purpose of this work, we assume that the base station serves a 120^{o} sector of a cell and is equipped with a uniform linear array (ULA) containing M omnidirectional elements, while the mobile stations use a single-element omnidirectional antenna. The signal of the i-th element is multiplied by the weight w_i^* before being transmitted. A simple schematic diagram of such a base station is shown in Figure 1. The distance between adjacent elements is denoted by D, θ is the central angle of departure (AOD), while δ is the angular spread (AS) which arises from the fact that the signal is reflected/scattered by objects in the channel before being received by the mobile station.

The downlink channel vector $\mathbf{h}_{\text{DL}}(t) \in \mathbb{C}^{M\times 1}$ is modeled as follows:

$$\mathbf{h}_{\text{DL}}(t) = \sqrt{\frac{P}{Q}} \sum_{q=1}^{Q} e^{j(\phi_q + 2\pi f_q t)} \underbrace{\begin{bmatrix} 1 \\ e^{j\frac{2\pi D}{\lambda}\sin(\theta_q)} \\ \vdots \\ e^{j\frac{2\pi D}{\lambda}(M-1)\sin(\theta_q)} \end{bmatrix}}_{\mathbf{a}(\theta_q)} \tag{1}$$

where P is the channel power, Q the number of scattered signals (components) contributing to the channel, ϕ_q the random phase of the q-th component uniformly distributed over $[0, 2\pi)$, f_q the Doppler frequency shift of the q-th component and θ_q the AOD of the q-th component uniformly distributed over $[\theta - \delta/2, \theta + \delta/2]$. Also, λ is the wavelength of the carrier frequency f_c, and $\mathbf{a}(\theta_q)$ the array steering vector.

The mean downlink channel correlation matrix (CCM) $\mathbf{R}_{\text{DL}} \in \mathbb{C}^{M\times M}$ is obtained as

$$\mathbf{R}_{\text{DL}} = \text{E}\left[\mathbf{h}_{\text{DL}}(t)\mathbf{h}_{\text{DL}}(t)^{\text{H}}\right], \tag{2}$$

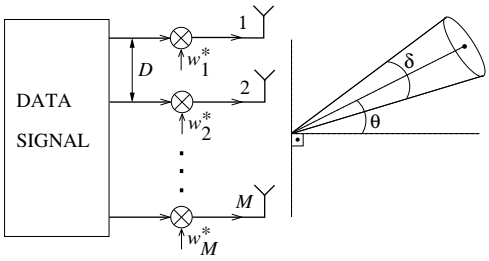

Figure 1. Schematic diagram of a base station using a uniform linear array to form beams.

where E[•] denotes expectation and the H superscript complex conjugate transpose, and expresses the second order statistics of the downlink channel. When the distribution of the angles of departure θ_q, $q = 1..Q$, is uniform over the angular spread δ, the mean correlation matrix can be expressed analytically as shown in [5]. In the rest of the paper we use the expressions of [5] whenever we need to calculate the downlink or uplink theoretical correlation matrix.

III. Open Loop Downlink Beamforming

In this paper we will study the effects of the FDD gap on the SNR performance of the open loop beamforming algorithm introduced in [2]. This algorithm maximises the average SNR of the decision signal at the mobile receiver and hereafter we call it MAX SNR. If $\mathbf{w}^{\mathrm{H}} \in \mathbb{C}^{1\times M}$ is the beamforming vector used by the base station, the average SNR of the decision signal at the mobile receiver is expressed as

$$\mathrm{SNR} = \frac{\mathbf{w}^{\mathrm{H}}\mathbf{R}_{\mathrm{DL}}\mathbf{w}}{\sigma_n^2}, \tag{3}$$

where σ_n^2 denotes the power spectral density of the additive white Gaussian noise. In order to maximise this SNR, the base station must use as beamforming vector the unit-norm principal eigenvector $\mathbf{u}_{\mathrm{DL,max}}$ of $\mathbf{R}_{\mathrm{DL}}$: $\mathbf{w}^{\mathrm{H}} = \mathbf{u}_{\mathrm{DL,max}}^{\mathrm{H}}$ ($\mathbf{u}_{\mathrm{DL,max}} \in \mathbb{C}^{M\times 1}$ is the eigenvector that corresponds to the maximum eigenvalue $e_{\mathrm{DL,max}}$ of $\mathbf{R}_{\mathrm{DL}}$). The SNR in this case is given as

$$\mathrm{SNR} = \frac{\mathbf{u}_{\mathrm{DL,max}}^{\mathrm{H}}\mathbf{R}_{\mathrm{DL}}\mathbf{u}_{\mathrm{DL,max}}}{\sigma_n^2} = \frac{e_{\mathrm{DL,max}}}{\sigma_n^2}. \tag{4}$$

In order to calculate $\mathbf{u}_{\mathrm{DL,max}}$, the base station needs information about the downlink channel and its correlation matrix. To this end, the mobile station can estimate the downlink channel vector and feed it back to the base station by means of feedback signals. However, these feedback signals affect the overall system capacity negatively, and the system would be more efficient if it could function without them. We have already noted that when the FDD gap is not large, there is a strong relationship between the average statistical properties of the uplink and downlink channels [2] (which are expressed by the correlation matrix of each channel). Therefore, the base station can operate the beamforming array 'blindly' by calculating the uplink correlation matrix $\mathbf{R}_{\mathrm{UL}}$ and using its principal eigenvector $\mathbf{u}_{\mathrm{UL,max}}$ as beamformer. The feedback signals are now avoided but the performance may worsen because $\mathbf{u}_{\mathrm{UL,max}}$ is not an exact estimate of $\mathbf{u}_{\mathrm{DL,max}}$, as the uplink and downlink carrier frequencies differ. The less correlated the two principal eigenvectors are, the larger the performance loss becomes. The next section shows that the correlation between the two principal eigenvectors and, consequently, the performance loss, depends on the FDD gap f_{FDD} and the number of transmit antennas M.

IV. Effects of the Carrier Frequency Separation due to FDD

This section studies the impact of the FDD gap on the correlation of the two principal eigenvectors and on the SNR performance of MAX SNR. Beamforming algorithms such as MAX SNR are usually employed in environments with small angular spread values where they are able to yield the maximum beamforming gain [2], [4]. Therefore, we consider such an environment only, which is represented by a macro cell with an angle of departure $\theta = 15^{\mathrm{o}}$ and an angular spread $\delta = 10^{\mathrm{o}}$ [6]. Practical use of MAX SNR in environments with larger δ values is highly unlikely, as diversity techniques may be more efficient in these scenarios, and will not be considered here.

To facilitate our analysis we assume that $f_c = 2$ GHz is the 'central' carrier frequency, while $f_{\mathrm{UL}} = f_c - f_{\mathrm{FDD}}/2$ and $f_{\mathrm{DL}} = f_c + f_{\mathrm{FDD}}/2$ are the uplink and downlink carrier frequencies, respectively. Thus, the separation between the carrier frequencies of the uplink and downlink channels is equal to the FDD gap f_{FDD}. We use the 'duplex array' approach of [2], where the same antenna array is used by the base station for reception of signals from the uplink and transmission of signals on the downlink. Therefore, the antenna element spacing of this single array is $D = \lambda_c/2$, where λ_c is the wavelength that corresponds to the central carrier frequency ($\lambda_c = u_l/f_c$, where $u_l = 3\times 10^8$ m/sec is the speed of light).

A. Correlation between uplink and downlink principal eigenvectors

Since the uplink principal eigenvector $\mathbf{u}_{\mathrm{UL,max}}$ is used as beamformer instead of the downlink principal eigenvector $\mathbf{u}_{\mathrm{DL,max}}$, its correlation with the downlink principal eigenvector is expected to be the main factor affecting the performance. To calculate this correlation as a function of the FDD gap, we vary the value of f_{FDD} from 0 to 1 GHz (i.e. up to 50% of the central carrier frequency) with a step of 100 GHz, obtain the two carrier frequencies f_{UL} and f_{DL}, and calculate the two correlation matrices $\mathbf{R}_{\mathrm{UL}}$ and $\mathbf{R}_{\mathrm{DL}}$ using the expressions of [5] for each f_{FDD} value. The correlation matrices depend on AOD, AS, antenna element spacing and carrier wavelength. The values of AOD and AS are those of a macro cell ($\theta = 15^{\mathrm{o}}$ and $\delta = 10^{\mathrm{o}}$ respectively), the spacing is $D = \lambda_c/2$ and the uplink and downlink carrier wavelengths are $\lambda_{\mathrm{UL}} = u_l/f_{\mathrm{UL}}$ and $\lambda_{\mathrm{DL}} = u_l/f_{\mathrm{DL}}$ respectively. Next, we obtain the two principal eigenvectors by performing the eigendecomposition of the two correlation matrices and calculate their correlation as

$$\rho = \Re\left\{\mathbf{u}_{\mathrm{DL,max}}^{\mathrm{H}}\mathbf{u}_{\mathrm{UL,max}}\right\}, \tag{5}$$

where $\Re\{\bullet\}$ denotes the real part of a complex number. The correlation is plotted as a function of the FDD gap and for

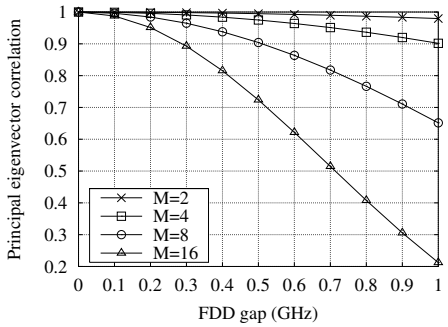

Figure 2. Correlation between the uplink and downlink principal eigenvectors as a function of the FDD gap for $M = 2, 4, 8, 16$ in a macro cell.

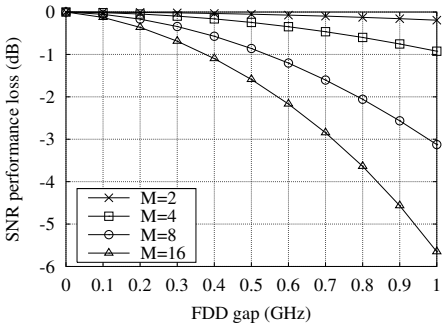

Figure 3. SNR performance loss as a function of the FDD gap for $M = 2, 4, 8, 16$ in a macro cell.

various numbers of elements M in the antenna array, in Figure 2.

The results show that the correlation is a decreasing function of f_{FDD} and M. Also, when $M = 2$ and $M = 4$ the two eigenvectors are highly correlated ($\rho \geq 0.9$) for all shown f_{FDD} values. In this case $\mathbf{u}_{\text{UL,max}}$ is a good estimate of $\mathbf{u}_{\text{DL,max}}$ and the SNR performance is not expected to deteriorate by a large amount as f_{FDD} increases up to 50% of the central carrier frequency (1 GHz). When $M = 8$ the two eigenvectors become less correlated and ρ becomes smaller than 0.7 when f_{FDD} is larger than about 45% of the central carrier frequency (0.9 GHz). When $M = 16$ the eigenvectors become even less correlated and ρ becomes smaller than 0.7 when f_{FDD} is larger than about 25% of the central carrier frequency (0.5 GHz) (also, now $\rho < 0.5$ when f_{FDD} is larger than about 35% of f_c, which is 0.7 GHz). In the last two cases the uplink principal eigenvector becomes an increasingly poor estimate of the downlink one, and the SNR performance loss is expected to be larger than previously as f_{FDD} increases. This performance loss is studied in the next section.

B. Performance loss

We follow the same procedure as in the previous section to calculate the SNR performance loss due to f_{FDD}. First we calculate the SNR without FDD, i.e. when the base station has access to the exact downlink channel correlation matrix. For this purpose, we assume $f_{\text{FDD}} = 0$ (i.e. $f_{\text{UL}} = f_{\text{DL}} = f_c$) and obtain the downlink correlation matrix and its principal eigenvector $\mathbf{u}_{\text{DL,max}}$. Then, we calculate the SNR without FDD as

$$\text{SNR}_{\text{withoutFDD}} = \frac{\mathbf{u}_{\text{DL,max}}^{\text{H}} \mathbf{R}_{\text{DL}} \mathbf{u}_{\text{DL,max}}}{\sigma_n^2}. \quad (6)$$

Next, in order to calculate the SNR with FDD, we assume $f_{\text{FDD}} \neq 0$ (i.e. $f_{\text{UL}} \neq f_{\text{DL}}$) and obtain the uplink and downlink carrier frequencies. We also calculate the uplink and downlink correlation matrices, and the uplink principal eigenvector $\mathbf{u}_{\text{UL,max}}$ by eigendecomposition of the uplink correlation matrix. Finally, we calculate the SNR with FDD as

$$\text{SNR}_{\text{withFDD}} = \frac{\mathbf{u}_{\text{UL,max}}^{\text{H}} \mathbf{R}_{\text{DL}} \mathbf{u}_{\text{UL,max}}}{\sigma_n^2}. \quad (7)$$

We define the performance loss due to FDD as

$$L = 10 \log_{10}\left(\frac{\text{SNR}_{\text{withFDD}}}{\text{SNR}_{\text{withoutFDD}}}\right). \quad (8)$$

The value of f_{FDD} is varied from 0 to 1 GHz with a step of 100 MHz, and the performance loss is plotted as a function of the FDD gap and for various numbers of elements M in the antenna array, in Figure 3.

The results show that the performance loss is an increasing function of f_{FDD} and M. This is expected, as the correlation between the two principal eigenvectors is a decreasing function of f_{FDD} and M, making $\mathbf{u}_{\text{UL,max}}$ an increasingly poor estimate of $\mathbf{u}_{\text{DL,max}}$ which results in larger performance loss values. When f_{FDD} is smaller than 10% of f_c (0.2 GHz) the loss is smaller than 0.5 dB for all M values. Therefore, in this case $\mathbf{u}_{\text{UL,max}}$ is a good estimate of $\mathbf{u}_{\text{DL,max}}$ and can be used as beamformer on the downlink with small performance overhead. Also, the performance loss is small for $M = 2, 4$ ($L < 1$ dB) over all shown f_{FDD} values, since the two principal eigenvectors in these two cases are highly correlated. Finally, L becomes 3 dB when f_{FDD} approaches 50% of f_c (1 GHz) for $M = 8$, and when f_{FDD} is just above 35% of f_c (0.7 GHz) for $M = 16$.

The next section introduces a simple technique which effectively compensates for most of the performance loss, even for large M and f_{FDD} values.

V. Compensating for the FDD Effect

In this section we introduce a simple technique that compensates for most of the performance loss due to FDD. The idea behind it is that, instead of using directly the principal eigenvector of the uplink correlation matrix as beamformer on the downlink, the base station can estimate the uplink correlation matrix, transform it from the uplink to the downlink carrier frequency using a *simple* algorithm, and use the principal eigenvector of the transformed correlation matrix as beamformer. To this end, it estimates the uplink correlation matrix and calculates its spatial power spectrum over the azimuth as

$$S(\theta, f_{\text{UL}}) = \mathbf{v}(\theta, f_{\text{UL}})^{\text{H}} \mathbf{R}_{\text{UL}} \mathbf{v}(\theta, f_{\text{UL}}). \quad (9)$$

The vector

$$\mathbf{v}(\theta, f_{\text{UL}}) = \left[1 \;\; e^{j\frac{2\pi D}{\lambda_{\text{UL}}}\sin(\theta)} \;\; \cdots \;\; e^{j\frac{2\pi D}{\lambda_{\text{UL}}}(M-1)\sin(\theta)}\right]^{\text{T}} \tag{10}$$

is a conventional beamformer at the uplink carrier frequency with the main beam pointing in the direction of θ, and the T superscript denotes transposition. Next, it uses the calculated uplink power spectrum to construct an estimated downlink correlation matrix as

$$\hat{\mathbf{R}}_{\text{DL}} = \sum_{i=1}^{N} P_i \left[\mathbf{v}(\theta_i, f_{\text{DL}})\mathbf{v}(\theta_i, f_{\text{DL}})^{\text{H}}\right], \tag{11}$$

where θ_i are the directions where the main peaks of $S(\theta, f_{\text{UL}})$ occur and P_i are the corresponding amplitudes of these peaks, normalised so that

$$\sum_{i=1}^{N} P_i = 1. \tag{12}$$

In order for a power spectrum peak to be included in the summation that yields $\hat{\mathbf{R}}_{\text{DL}}$, it must satisfy the relationship $P^{\text{dB}} \geq P^{\text{dB}}_{\text{max}} - 10$, where P^{dB} is the peak's amplitude and $P^{\text{dB}}_{\text{max}}$ is the amplitude of the maximum peak, both in dB. Finally, the base station uses the principal eigenvector of the estimated downlink correlation matrix $\hat{\mathbf{u}}_{\text{DL,max}}$ as beamformer on the downlink. We call this technique the conventional beamformer FDD compensation technique (CBF).

A similar technique was proposed in [7]. According to this technique, the uplink spatial power spectrum is calculated using the minimum variance distortionless response filter as

$$S(\theta, f_{\text{UL}}) = \frac{1}{\mathbf{v}(\theta, f_{\text{UL}})^{\text{H}}\mathbf{R}_{\text{UL}}^{-1}\mathbf{v}(\theta, f_{\text{UL}})}. \tag{13}$$

Next, the spatial power spectrum is modified to avoid beam-pointing problems and the modified $S_{\text{mod}}(\theta, f_{\text{UL}})$ is obtained. Then, the downlink correlation matrix is constructed as

$$\hat{\mathbf{R}}_{\text{DL}} = \int_{\theta} S_{\text{mod}}(\theta, f_{\text{UL}})\mathbf{v}(\theta, f_{\text{DL}})\mathbf{v}(\theta, f_{\text{DL}})^{\text{H}}. \tag{14}$$

Note that the CBF method is (much) simpler than the minimum variance method, as it does not involve matrix inversion or integration.

Figure 4 shows the spatial power spectrum that the CBF technique yields, while Figure 5 shows the spatial power spectrum of the minimum variance algorithm, both under the macro cell scenario. The CBF technique for a particular M yields a power spectrum that resembles the radiation pattern of a ULA with the same M. That is, the power spectrum contains the main peak in the azimuthal area where the uplink power is concentrated but is not particularly suppressed over other azimuthal areas. The minimum variance algorithm, on the other hand, yields a power spectrum with a shape that is similar for all M values. This spectrum is almost flat over the azimuthal area where the uplink power is concentrated, and is also suppressed over other azimuthal areas. Therefore, the minimum variance power spectrum looks more accurate and is expected to yield a better estimate of the real downlink correlation matrix. However, it is (much) more complex than the CBF method.

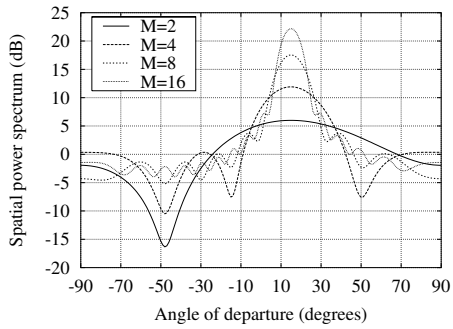

Figure 4. Uplink spatial power spectrum of the CBF algorithm in a macro cell as a function of angle of departure for $M = 2, 4, 8, 16$.

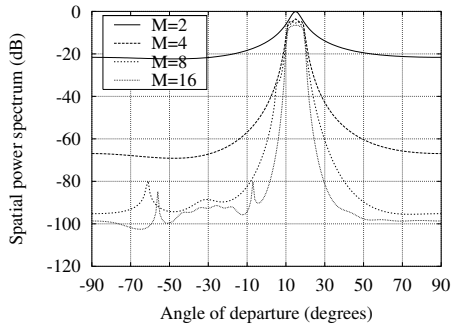

Figure 5. Uplink spatial power spectrum of the minimum variance algorithm in a macro cell as a function of angle of departure for $M = 2, 4, 8, 16$.

Now we move on to apply the CBF technique to compensate for the FDD impact on the performance of open loop MAX SNR, and calculate the SNR improvement that it yields. As we have done above, to calculate the SNR without FDD we assume $f_{\text{FDD}} = 0$ (i.e. $f_{\text{UL}} = f_{\text{DL}} = f_{\text{c}}$) and obtain the downlink correlation matrix and its principal eigenvector $\mathbf{u}_{\text{DL,max}}$. We then calculate the SNR without FDD as

$$\text{SNR}_{\text{withoutFDD}} = \frac{\mathbf{u}^{\text{H}}_{\text{DL,max}}\mathbf{R}_{\text{DL}}\mathbf{u}_{\text{DL,max}}}{\sigma_n^2}. \tag{15}$$

For the calculation of the SNR with FDD, we obtain the uplink correlation matrix and its CBF spatial power spectrum. Then we construct the estimated downlink correlation matrix as described above and calculate its principal eigenvector $\hat{\mathbf{u}}_{\text{DL,max}}$ by eigendecomposition. Finally, we calculate the SNR with FDD as

$$\text{SNR}_{\text{withFDD}} = \frac{\hat{\mathbf{u}}^{\text{H}}_{\text{DL,max}}\mathbf{R}_{\text{DL}}\hat{\mathbf{u}}_{\text{DL,max}}}{\sigma_n^2}, \tag{16}$$

where $\mathbf{R}_{\text{DL}}$ is the *real* downlink correlation matrix. The performance loss is again calculated as

$$L = 10\log_{10}\left(\frac{\text{SNR}_{\text{withFDD}}}{\text{SNR}_{\text{withoutFDD}}}\right). \tag{17}$$

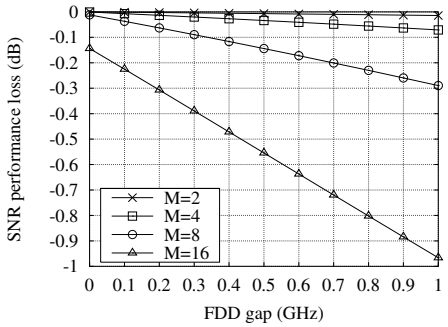

Figure 6. SNR performance loss after CBF compensation as a function of the FDD gap for $M = 2, 4, 8, 16$ in a macro cell.

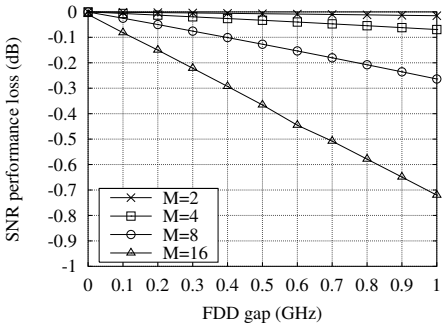

Figure 7. SNR performance loss after minimum variance compensation as a function of the FDD gap for $M = 2, 4, 8, 16$ in a macro cell.

The value of f_{FDD} is varied from 0 to 1 GHz with a step of 100 MHz, and the performance loss L is plotted as a function of f_{FDD} and for various numbers of elements M in the antenna array, in Figure 6.

Comparison of the results of Figure 6 with those of Figure 3 shows that the CBF compensation technique can lower the performance loss by a large amount. For instance, after the application of the CBF technique, the performance loss for $M = 2$ is very close to 0 dB, while for $M = 4$ it is smaller than 0.1 dB over all shown f_{FDD} values. Also, while the maximum loss without compensation for $M = 8$ and $M = 16$ is about 3.1 dB and 5.7 dB respectively, the maximum loss with CBF compensation for $M = 8$ and $M = 16$ is smaller than 0.3 dB and 0.97 dB respectively.

Next, in order to compare the CBF and minimum variance techniques, we estimate the downlink principal eigenvector $\hat{\mathbf{u}}_{\text{DL,max}}$ according to the minimum variance technique and use it to calculate the performance loss in this case. We plot the results in Figure 7. Comparison between Figures 7 and 6 shows that when $M = 2$ and $M = 4$ the two techniques yield very similar performance loss reduction, although minimum variance yields a spatial power spectrum (and, consequently, a $\mathbf{u}_{\text{DL,max}}$ estimate) which is theoretically better. This may be attributed to the fact that when $M = 2$ and $M = 4$ the beamwidth of the base station ULA is wide and able to cover the entire angular spread of the macro cell, even when the downlink beamformer (in the form of $\hat{\mathbf{u}}_{\text{DL,max}}$) is not estimated with very high accuracy. When $M = 8$ and $M = 16$, however, the beamwidth becomes narrower and even small shifts in the direction of the main beam may impact the system performance. In this case, the fact that minimum variance yields a more accurate downlink beamformer estimate enables it to perform slightly better than CBF. Nevertheless, it does so at the cost of (much) higher computational complexity and the resulting gain is very small (smaller than 0.25 dB over all shown f_{FDD} values).

Figure 4 shows that the CBF spatial power spectrum of the macro cell has essentially only one main peak. Therefore, the estimated downlink correlation matrix $\hat{\mathbf{R}}_{\text{DL}}$ is constructed by the CBF algorithm taking into account only one conventional beamformer at the downlink carrier frequency. Although this seems to neglect a lot of information included in the uplink spatial power spectrum, Figures 6 and 7 show that CBF yields results similar to minimum variance which uses much more information about the uplink spatial power spectrum. Thus, highly detailed information about the uplink spatial power spectrum does not appear to be very important to the construction of the downlink correlation matrix (especially when M is relatively small). What seems to be of great importance is the transformation of the bulk directional information that is included in the uplink spatial power spectrum from the uplink to the downlink carrier frequency.

VI. Conclusions

In this paper we studied the effect of frequency division duplex on the performance of open loop adaptive beamforming under a macro cell scenario. The performance loss was shown to increase with the FDD gap and the number of transmit antennas. Also, a simple method of combating for the FDD effect was introduced, which improves the performance by a large amount in the studied macro cell environment, even for large M and f_{FDD} values. The proposed technique was compared with the (much) more complex FDD compensation technique proposed in [7], and was shown to yield very similar performance loss reduction in the macro cell.

References

[1] IEEE Personal Communications Magazine, Special Issue on Smart Antennas, February 1998. Vol. 5, No. 1.

[2] G. G. Raleigh, S. N. Diggavi, V. K. Jones, and A. Paulraj. A blind adaptive transmit antenna algorithm for wireless communication. In *IEEE International Conference on Communications*, volume 3, pages 1494–1499, June 1995. Seattle.

[3] J. S. Thompson, J. E Hudson, P. M. Grant, and B. Mulgrew. CDMA downlink beamforming for frequency selective channels. In *PIMRC'99*, pages 233–237, 1999.

[4] A. C. Koutalos, J. S. Thompson, and P. M. Grant. Downlink adaptive antenna techniques for WCDMA. In *IEEE Vehicular Technology Conference*, May 6-10 2002. Birmingham, Al, USA.

[5] J. Salz and J. Winters. Effect of fading correlation on adaptive arrays in digital mobile radio. *IEEE Transactions on Vehicular Technology*, 43(4):1049–1057, November 1994.

[6] Siemens TSGR1#16 R1-00-1180. Simulation parameters for TX diversity simulations using correlated antennas. In *3GPP TSG RAN WG1*, 10-13 October 2000. Pusan, Korea.

[7] K. Hugl, J. Laurila, and E. Bonek. Downlink beamforming for frequency division duplex systems. In *Proc. IEEE Globecom*, volume 4, pages 2097–2101, 5-9 December 1999. Rio de Janeiro, Brasil.

References

[1] B. W. Kernighan and D. M. Ritchie, *The C programming language*, Prentice Hall, New Jersey, USA, 2nd edition, 1988.

[2] W. H. Press, S. A. Teukolsky, W. T. Vetterling and B. P. Flannery, *Numerical recipes in C, The art of scientific computing*, Cambridge University Press, USA, 2nd edition, 1992.

[3] H. Kopka and P. W. Daly, *A guide to LaTeX*, Addison-Wesley, England, 3rd edition, 1999.

[4] D. E. Knuth, *The TeX book*, Addison-Wesley, 1st edition, 1984.

[5] The FreeBSD Documentation Project, *FreeBSD handbook*, Freely available, 2002 version used, Available from ftp://ftp1.freebsd.org/pub/FreeBSD/doc/en/books/handbook.

[6] M. Welsh, M. K. Dalheimer, L. Kaufman and M. Welsh, *Running Linux*, O'Reilly & Associates, 3rd edition, 1999.

[7] The Linux Documentation Project, *Various Linux guides*, Freely available, 2002 versions used, Available from http://www.tldp.org.

[8] 3rd Generation Partnership Project (3GPP), "Documents and specificatons at the web site http://www.3gpp.org", Note: The documents are updated regularly.

[9] 3rd Generation Partnership Project (3GPP) Document TS 25.211, "Physical channels and mapping of transport channels onto physical channels (FDD)", Release 5, Version 5.2.0 (2002-09) at time of writing.

[10] 3rd Generation Partnership Project (3GPP) Document TS 25.213, "Spreading and modulation (FDD)", Release 5, Version 5.2.0 (2002-09) at time of writing.

[11] 3rd Generation Partnership Project (3GPP) Document TS 25.214, "Physical layer procedures (FDD)", Release 5, Version 5.2.0 (2002-09) at time of writing.

[12] EURASIP Journal on Applied Signal Processing, "Special Issue on Space-Time Coding and its Applications—Part I", , March 2002, vol 2002, no 3.

[13] IEEE Personal Communications Magazine, "Special Issue on Smart Antennas", , February 1998, vol 5, no 1.

[14] European Transactions on Telecommunications, "Special Issue on Smart Antennas", , September-October 2001, vol 12, no 5.

[15] F. Adachi, M. Sawahashi and H. Suda, "Wideband DS-CDMA for next-generation mobile communications systems", *IEEE Communications Magazine*, vol. 36, no. 9, September 1998, pages 56–69.

[16] S. M. Alamouti, "A simple transmit diversity technique for wireless communications", *IEEE Journal on Selected Areas in Communications*, vol. 16, no. 8, October 1998, pages 1451–1458.

[17] A. Alexiou, "Comparison of multiple antenna techniques for UMTS downlink capacity enhancemcnt", in proceedings of the *IEEE Vehicular Technology Conference (VTC)*, vol. 1, Rhodes, Hellas, 6–9 May 2001, pages 3–7.

[18] A. Alexiou and R.-H. Yan, "Downlink capacity enhancement by employing SDMA in GSM", in proceedings of the *IEEE Sensor Array and Multichannel Signal Processing Workshop*, Cambridge, MA, USA, 16–17 March 2000, pages 413–417.

[19] B. Allen, J. Webber, P. Karlsson and M. Beach, "UMTS spatio-temporal propagation trial results", in proceedings of the *11th International Conference on Antennas and Propagation*, vol. 2, Manchester, UK, 17–20 April 2001, pages 497–501.

[20] B. Allen, M. Beach and P. Karlsson, "Spatial de-correlation of the UTRA-FDD radio channel", in proceedings of the *8th COST260 MCM*, Rennes, France, 1–3 October 2000.

[21] F. Amoroso, "Use of DS/SS signaling to mitigate Rayleigh fading in a dense scatterer environment", *IEEE Personal Communications*, vol. 3, no. 2, April 1996, pages 52–61.

[22] F. Amoroso, "The bandwidth of digital data signals", *IEEE Communications Magazine*, vol. 18, no. 6, November 1980, pages 13–24.

[23] J. B. Andersen, "Antenna arrays in mobile communications: Gain, diversity, and channel capacity", *IEEE Antennas and Propagation Magazine*, vol. 42, no. 2, April 2000, pages 12–16.

[24] J. B. Andersen, T. S. Rappaport and S. Yoshida, "Propagation measurements and models for wireless communications channels", *IEEE Communications Magazine*, vol. 33, no. 1, January 1995, pages 42–49.

[25] S. Anderson, M. Millnert, M. Viberg and B. Wahlberg, "An adaptive array for mobile communication systems", *IEEE Transactions on Vehicular Technology*, vol. 40, no. 1, February 1991, pages 230–236.

[26] S. Anderson, B. Hangerman, H. Dam, U. Forssén, J. Karlsson, F. Kronestedt and S. Mazur, "Adaptive antennas for GSM and TDMA systems", *IEEE Personal Communications*, vol. 6, no. 3, June 1999, pages 74–86.

[27] A. Annamalai Jr. and V. K. Bhargava, "Performance of selection diversity for DS/CDMA communications over Rayleigh fading channels", *IEE Electronics Letters*, vol. 32, no. 21, 10th October 1996, pages 1966–1968.

[28] A. Annamalai Jr., "Analysis of selection diversity on Nakagami fading channels", *IEE Electronics Letters*, vol. 33, no. 7, 27th March 1997, pages 548–549.

[29] A. Annamalai Jr., "Unified analysis of practical selection diversity system in different fading environments", *IEE Electronics Letters*, vol. 34, no. 3, 5th February 1998, pages 243–244.

[30] A. Annamalai, C. Tellambura and V. Bhargava, "Equal-gain diversity receiver performance in wireless channels", *IEEE Transactions on Communications*, vol. 48, no. 10, October 2000, pages 1732–1745.

[31] S. Ariyavisitakul and L. Fung, "Signal and interference statistics of a CDMA system with feedback power control", *IEEE Transactions on Communications*, vol. 41, no. 11, November 1993, pages 1626–1634.

[32] S. Ariyavisitakul, "Signal and interference statistics of a CDMA system with feedback power control - Part II", *IEEE Transactions on Communications*, vol. 42, no. 2/3/4, February/March/April 1994, pages 597–605.

[33] A. Baier, U.-C. Fiebig, W. Granzow, W. Koch, P. Teder and J. Thielecke, "Design study for a CDMA-based third-generation mobile radio system", *IEEE Journal on Selected Areas in Communications*, vol. 12, no. 4, May 1994, pages 733–743.

[34] P. Balaban and J. Salz, "Dual diversity combining and equalization in digital cellular mobile radio", *IEEE Transactions on Vehicular Technology*, vol. 40, no. 2, May 1991, pages 342–354.

[35] M. Barrett and R. Arnott, "Adaptive antennas for mobile communications", *Electronics and Communication Engineering Journal*, August 1994, pages 203–214.

[36] H. L. Bertoni, P. Pongsilamanee, C. Cheon and G. Liang, "Sources and statistics of multipath arrival at elevated base station antenna", in proceedings of the *IEEE Vehicular Technology Conference (VTC)*, vol. 1, Houston, TX, USA, 16–20 May 1999, pages 581–585.

[37] M. Beach, B. Allen and P. Karlsson, "Spatial decorrelation of frequency division duplex links", *IEE Electronics Letters*, vol. 36, no. 22, 26th October 2000, pages 1884–1885.

[38] M. Beach, P. Guémas and A. R. Nix, "Capacity and service extension for wireless networks using adaptive antennas", *IEE Electronics Letters*, vol. 30, no. 22, 27 October 1994, pages 1813–1814.

[39] N. C. Beaulieu and M. L. Merani, "Efficient simulation of correlated diversity channels", in proceedings of the *IEEE Wireless Communications and Networking Conference (WCNC)*, vol. 1, Chicago, IL, USA, 23–28 September 2000, pages 207–210.

[40] S. E. Bensley and B. Aazhang, "Subspace-based channel estimation for code division multiple access communications systems", *IEEE Transactions on Communications*, vol. 44, no. 8, August 1996, pages 1009–1020.

[41] D. D. Bevan, V. T. Ermolayev and A. G. Flaksman, "Analysis of weight error loss with a multichannel beamformer processor", *IEE Proceedings Radar, Sonar and Navigation*, vol. 145, no. 1, February 1998, pages 63–72.

[42] B. A. Bjerke, J. G. Proakis and Z. Zvonar, "Antenna diversity combining schemes for WCDMA systems in fading multipath channels", in proceedings of the *IEEE Vehicular Technology Conference (VTC)*, vol. 1, 2000, pages 421–428.

[43] B. A. Bjerke and J. G. Proakis, "Equalization and decoding for multiple-input multiple-output wireless channels", *EURASIP Journal on Applied Signal Processing*, vol. 2002, no. 3, March 2002, pages 249–266.

[44] H. Boche and M. Schubert, "Theoretical and experimental comparison of optimisation criteria for downlink beamforming", *European Transactions on Telecommunications*, vol. 12, no. 5, September-October 2001, pages 417–426.

[45] W. R. Braun and U. Dersch, "A physical mobile radio channel model", *IEEE Transactions on Vehicular Technology*, vol. 40, no. 2, May 1991, pages 472–482.

[46] C. Brunner, J. S. Hammerschmidt and J. A. Nossek, "Downlink eigenbeamforming in WCDMA", in proceedings of the *European Wireless*, Dresden, Germany, 12–14 September 2000, pages 195–200.

[47] C. Brunner, J. S. Hammerschmidt, A. Seeger and J. A. Nossek, "Space-time eigenrake and downlink eigenbeamformer: exploiting long-term and short-term channel properties in in WCDMA", in proceedings of the *Global Telecommunications Conference (GLOBECOM)*, San Fransisco, CA, USA, November 2000, pages 138–142.

[48] C. Brunner, W. Utschick and J. A. Nossek, "Exploiting the short-term and long-term channel properties in space and time: eigenbeamforming concepts for the BS in WCDMA", *European Transactions on Telecommunications*, vol. 12, no. 5, September-October 2001, pages 365–378.

[49] M. R. G. Butler, A. R. Nix, D. R. Bull and P. Karlsson, "The performance of HIPERLAN/2 systems with multiple antennas", in proceedings of the *IEEE Vehicular Technology Conference (VTC)*, vol. 3, Rhodes, Greece, 6–9 May 2001, pages 2123–2127.

[50] J. K. Cavers, "Single-user and multiuser adaptive maximal ratio transmission for Rayleigh channels", *IEEE Transactions on Vehicular Technology*, vol. 49, no. 6, November 2000, pages 2043–2050.

[51] Y. A. Chau and S.-H. Yu, "Transmission diversity with limited feedback information in fading channels", in proceedings of the *IEEE Vehicular Technology Conference (VTC)*, vol. 2, Tokyo, Japan, 15–18 May 2000, pages 874–878.

[52] J. Choi, "Performance analysis for transmit antenna diversity with/without channel information", *IEEE Transactions on Vehicular Technology*, vol. 51, no. 1, January 2002, pages 101–113.

[53] G.-T. Chyi, J. G. Proakis and C. M. Keller, "On the symbol error probability of maximum-selection diversity reception schemes over a Rayleigh fading channel", *IEEE Transactions on Communications*, vol. 37, no. 1, January 1989, pages 79–83.

[54] R. T. Compton, "An adaptive array in a spread-spectrum communication system", *Proceedings of the IEEE*, vol. 66, no. 3, March 1978, pages 289–298.

[55] C. E. Cook and H. S. Marsh, "An introduction to spread spectrum", *IEEE Communications Magazine*, March 1983, pages 8–16.

[56] A. Czylwik and T. Matsumoto, "Downlink beamforming for frequency-duplex systems in frequency-selective fading", in proceedings of the *IEEE Vehicular Technology Conference (VTC)*, vol. 2, Tokyo, Japan, 15–18 May 2000, pages 695–699.

[57] A. G. Dadak, S. Hosur, T. Schmidl and C. Sengupta, "A comparison of the open loop transmit diversity schemes for third generation wireless systems", in proceedings of the *IEEE Wireless Communications and Networking Conference (WCNC)*, vol. 1, Chicago, IL, USA, 23–28 September 2000, pages 437–442.

[58] E. Dahlman, B. Gudmundson, M. Nilsson and J. Sköld, "UMTS/IMT-2000 based on wideband CDMA", *IEEE Communications Magazine*, vol. 36, no. 9, September 1998, pages 70–80.

[59] E. H. Dinan and B. Jabbari, "Spreading codes for direct sequence CDMA and wideband CDMA cellular networks", *IEEE Communications Magazine*, vol. 36, no. 9, September 1998, page 1998.

[60] R. C. Dixon, "Why spread spectrum?", *IEEE Communications Society Magazine*, vol. 13, July 1975, pages 21–25.

[61] A. Edelman, *Eigenvalues and condition numbers of random matrices*, Ph.D. thesis, Massachusetts Institute of Technology, Department of Mathematics, May 1989.

[62] E. Erez and M. Feder, "A novel decoder for unknown diversity channels employing space-time codes", *EURASIP Journal on Applied Signal Processing*, vol. 2002, no. 3, March 2002, pages 267–274.

[63] R. B. Ertel, P. Cardieri, K. W. Sowerby, T. S. Rappaport and J. H. Reed, "Overview of spatial channel models for antenna array communication systems", *IEEE Personal Communications*, vol. 5, no. 1, February 1998, pages 10–22.

[64] R. Esmailzadeh, M. Nakagawa and E. A. Sourour, "Time-division duplex CDMA communications", *IEEE Personal Communications*, April 1997, pages 51–56.

[65] D. D. Falconer, M. Abdulrahman, N. W. K. Lo, B. R. Petersen and A. U. H. Sheikh, "Advances in equalization and diversity for portable wireless systems", *Digital Signal Processing*, vol. 3, 1993, pages 148–162.

[66] C. Farsakh and J. A. Nossek, "Spatial covariance based downlink beamforming in an SDMA mobile radio system", *IEEE Transactions on Communications*, vol. 46, no. 11, November 1998, pages 1497–1506.

[67] J. R. Fonollosa, J. Goldberg and G. Vásquez, "Downlink beamforming for cellular mobile communications in frequency selective channels", in proceedings of the *IEEE SPAWC Workshop*, Paris, France, April 1997, pages 197–200.

[68] G. D. Forney, "The Viterbi algorithm", *Proceedings of the IEEE*, vol. 61, no. 3, March 1973, pages 268–277.

[69] G. J. Foschini and M. J. Gans, "On limits of wireless communications in a fading environment when using multiple antennas", *Wireless Personal Communications*, vol. 6, 1998, pages 311–335, ©1998 Kluwer Academic Publishers. Printed in the Netherlands.

[70] G. J. Foschini and J. Salz, "Digital communications over fading radio channels", *Bell System Technical Journal*, vol. 62, no. 2, January 1983, pages 429–456.

[71] R. C. French, "The effect of fading and shadowing on channel reuse in mobile radio", *IEEE Transactions on Vehicular Technology*, vol. VT-28, no. 3, August 1979, pages 171–181.

[72] V. K. Garg and J. E. Wilkes, *Wireless and personal communications systems*, Prentice Hall, New Jersey, 1st edition, 1996.

[73] D. Gerlach and A. Paulraj, "Adaptive transmitting antenna arrays with feedback", *IEEE Signal Processing Letters*, vol. 1, no. 10, October 1994, pages 150–152.

[74] D. Gerlach and A. Paulraj, "Base station transmitting antenna arrays for multipath environments", *ELSEVIER Signal Processing*, vol. Signal Processing 54, 1996, pages 59–73.

[75] A. J. Giger and W. T. Barnett, "Effects of multipath propagation on digital radio", *IEEE Transactions on Communications*, vol. COM-29, no. 9, September 1981, pages 1345–1352.

[76] K. S. Gilhousen, I. M. Jacobs, R. Padovani, A. J. Viterbi, L. A. Weaver Jr. and C. E. Wheatley, "On the capacity of a cellular CDMA system", *IEEE Transactions on Vehicular Technology*, vol. 40, no. 2, May 1991, pages 303–312.

[77] L. C. Godara, "Applications of antenna arrays to mobile communications Part I: performance improvement, feasibility, and system considerations", *Proceedings of the IEEE*, vol. 85, no. 7, July 1997, pages 1031–1060.

[78] L. C. Godara, "Application of antenna arrays to mobile communications, Part II: beamforming and direction-of-arrival considerations", *Proceedings of the IEEE*, vol. 85, no. 8, August 1997, pages 1195–1245.

[79] J. M. Goldberg and J. R. Fonollosa, "Downlink beamforming for spatially distributed sources in cellular mobile communications", *ELSEVIER Signal Processing*, vol. Signal Processing 65, 1998, pages 181–197.

[80] M. Goldburg and R. H. Roy, "The impacts of SDMA on PCS systems design", in proceedings of the *3rd Annual International Conference on Universal Personal Communications*, San Diego, CA, USA, 27 September–1 October 1994, pages 242–246.

[81] D. J. Goodman, *Wireless personal communications systems*, Prentice Hall, New Jersey, 1st edition, 1997.

[82] B. Göransson, B. Hagerman and J. Barta, "Adaptive antennas in WCDMA systems—link level simulation results based on typical user scenarios", in proceedings of the *IEEE Vehicular Technology Conference (VTC)*, vol. 1, Boston, MA, USA, 24–28 September 2000, pages 157–164.

[83] F. Goulam and A. J. Levy, "A statistical model for the simulation of multipath mobile propagation channel", in proceedings of the *IEEE Vehicular Technology Conference (VTC)*, vol. 1, Denver, CO, USA, 10–13 May 1992, pages 135–138.

[84] A. Grant, "Rayleigh fading multi-antenna channels", *EURASIP Journal on Applied Signal Processing*, vol. 2002, no. 3, March 2002, pages 316–329.

[85] J.-C. Guesy, M. P. Fitz, M. R. Bell and W.-Y. Kuo, "Signal design for transmitter diversity wireless communication systems over Rayleigh fading channels", in proceedings of the *IEEE Vehicular Technology Conference (VTC)*, vol. 1, Atlanta, GA, USA, 28 April–1 May 1996, pages 136–140.

[86] J.-C. Guesy, M. P. Fitz, M. R. Bell and W.-Y. Kuo, "Signal design for transmitter diversity wireless communication systems over Rayleigh fading channels", *IEEE Transactions on Communications*, vol. 47, no. 4, April 199, pages 527–537.

[87] S. Gurunathan and K. Feher, "Multipath simulation models for mobile radio channels", in proceedings of the *IEEE Vehicular Technology Conference (VTC)*, vol. 1, Denver, CO, USA, 10–13 May 1992, pages 131–134.

[88] M. Haardt, C. F. Mecklenbräuker, M. Vollmer and P. Slanina, "Smart antennas for UTRA TDD", *European Transactions on Telecommunications*, vol. 12, no. 5, September-October 2001, pages 393–406.

[89] J. S. Hammerschmidt, C. Brunner and C. Drewes, "Eigenbeamforming: a novel concept in space and space-time processing", in proceedings of the *European Wireless*, Dresden, Germany, September 2000.

[90] J. S. Hammerschmidt and C. Brunner, "A unified approach to diversity, beamforming, and interference suppression", in proceedings of the *European Wireless*, Dresden, Germany, September 2000.

[91] J. S. Hammerschmidt and C. Brunner, "The implications of array and multipath geometries in spatial processing", in proceedings of the *International Conference on Telecommunications (ICT)*, Acapulco, Mexico, May 2000.

[92] S. Haykin, *Adaptive filter theory*, Prentice Hall, New Jersey, 3rd edition, 1996.

[93] R. W. Health and A. Paulraj, "Multiple antenna arrays for transmitter diversity and space-time coding", in proceedings of the *IEEE International Conference on Communications (ICC)*, Vancouver, BC, Canada, 6–10 June 1999, pages 36–40.

[94] A. Hiroike, F. Adachi and N. Nakajima, "Combined effects of phase sweeping transmitter diversity and channel coding", *IEEE Transactions on Vehicular Technology*, vol. 41, no. 2, May 1992, pages 170–176.

[95] M.-J. Ho, G. L. Stüber and M. D. Austin, "Performance of switched-beam smart antennas for cellular radio systems", *IEEE Transactions on Vehicular Technology*, vol. 47, no. 1, February 1998, pages 10–19.

[96] H. Holma and A. Toskala, editors, *WCDMA for UMTS*, John Wiley, 2nd edition, 2002.

[97] J. M. Holtzman, "A simple, accurate method to calculate spread-spectrum mulitple-access error probabilities", *IEEE Transactions on Communications*, vol. 40, no. 3, March 1992, pages 461–464.

[98] R. A. Horn and C. R. Johnson, *Matrix analysis*, Cambridge University Press, New York, 1999 reprint.

[99] A. Hottinen and R. wichman, "Transmit diversity by antenna selection in CDMA downlink", in proceedings of the *IEEE International Symposium on Spread Spectrum Techniques and Applications (ISSSTA)*, Sun City, South Africa, 2–4 September 1998, pages 767–770.

[100] K. Hugl, "Frequency transformation based downlink beamforming", in proceedings of the *COST259/260 Joint Workshop on Spatial Channel Models and Adaptive Antennas*, Vienna, Austria, April 1999, pages 111–118.

[101] K. Hugl, J. Laurila and E. Bonek, "Downlink beamforming for frequency division duplex systems", in proceedings of the *Global Telecommunications Conference (GLOBECOM)*, vol. 4, Rio De Janeiro, Brazil, 5–9 December 1999, pages 2097–2101.

[102] K. Hugl, J. Laurila and E. Bonek, "Smart antenna downlink beamforming for uncorrelated communication links", in proceedings of the *Conference on Antennas and Propagation*, Davos, Switcherland, 9–14 April 2000.

[103] K. Hugl, J. Laurila and E. Bonek, "Transformation based downlink beamforming techniques for frequency division duplex systems", in proceedings of the *Interim Symposium on Antennas and Propagation*, vol. 4, Fukuoka, Japan, 21–25 August 2000, pages 1529–1532.

[104] W. C. Jakes, editor, *Microwave mobile communications*, John Wiley, New York, 1974.

[105] A. Jalali and P. Mermelstein, "Effects of diversity, power control, and bandwidth on the capacity of microcellular CDMA systems", *IEEE Journal on Selected Areas in Communications*, vol. 12, no. 5, June 1994, pages 952–961.

[106] L. M. A. Jalloul, K. Rohani, K. Kuchi and J. J. Chen, "Performance analysis of CDMA transmit diversity methods", in proceedings of the *IEEE Vehicular Technology Conference (VTC)*, vol. 3, Amsterdam, Netherlands, 19–22 September 1999, pages 1326–1330.

[107] A. Jarosch and D. Dahlhaus, "Linear space-time diversity receivers for the downlink of UMTS with WCDMA", *European Transactions on Telecommunications*, vol. 12, no. 5, September-October 2001, pages 379–391.

[108] C. A. Jötten, M. Meurer and H. H. R. Tröger, "Transmit array processing for CDMA downlinks operating in mixed service environments", in proceedings of the *IEEE International Symposium on Spread Spectrum Techniques and Applications (ISSSTA)*, vol. 2, Prague, Czech Republic, 2–5 September 2002, pages 555–560.

[109] G. Jöngren, M. Skoglund and B. Ottersen, "Combining beamforming and orthogonal space-time block coding", *IEEE Transactions on Information Theory*, vol. 48, no. 3, March 2002, pages 611–627.

[110] M. Katz and J. Ylitalo, "Extension of space-time coding to beamforming WCDMA base stations", in proceedings of the *IEEE Vehicular Technology Conference (VTC)*, vol. 2, Tokyo, Japan, 15–18 May 2000, pages 1230–1234.

[111] C. Kchao and G. L. Stüber, "Analysis of a direct-sequence spread-spectrum cellular radio system", *IEEE Transactions on Communications*, vol. 41, no. 10, October 1993, pages 1507–1516.

[112] J. Kennedy and M. C. Sullivan, "Direction finding and "smart antennas" using software radio architectures", *IEEE Communications Magazine*, vol. 33, no. 5, May 1995, pages 62–68.

[113] B. H. Khalaj, A. Paulraj and T. Kailath, "Antenna arrays for CDMA systems with multipath", in proceedings of the *IEEE Military Communications Conference*, vol. 2, Boston, MA, USA, 11–14 October 1993, pages 624–628.

[114] K. S. Kim, I. Song, S. C. Bang and T.-J. Kim, "Performance analysis of forward link beamforming techniques for DS/CDMA systems using base station antenna arrays", *IEEE Transactions on Signal Processing*, vol. 48, no. 3, March 2000, pages 862–865.

[115] D. N. Knisely, S. Kumar, S. Laha and S. Nanda, "Evolution of wireless data services: IS-95 to CDMA2000", *IEEE Communications Magazine*, vol. 36, no. 10, October 1998, pages 140–149.

[116] R. Kohno, R. Meidan and L. B. Milstein, "Spread spectrum access methods for wireless communications", *IEEE Communications Magazine*, vol. 33, no. 1, January 1995, pages 58–67.

[117] R. Kohno, "Spatial and temporal communication theory using adaptive antenna array", *IEEE Personal Communications*, vol. 5, no. 1, February 1998, pages 28–35.

[118] S. S. Kouris, *Elements of antenna theory and propagation of electromagnetic waves*, Zitis, Thessaloniki, GREECE, 1994, Book is written in Greek.

[119] A. C. Koutalos, J. S. Thompson and P. M. Grant, "Downlink adaptive antenna techniques for WCDMA", in proceedings of the *IEEE Vehicular Technology Conference (VTC)*, vol. 3, Birmingham, AL, USA, 6–9 May 2002, pages 1135–1139.

[120] A. C. Koutalos and J. S. Thompson, "Pilot signal effects on adaptive antenna arrays in FDD wideband CDMA", in proceedings of the *IEEE International Symposium on Spread Spectrum Techniques and Applications (ISSSTA)*, vol. 2, Prague, Czech Republic, 2–5 September 2002, pages 531–535.

[121] A. C. Koutalos and J. S. Thompson, "Effect of frequency division duplex on open loop downlink beamforming in WCDMA systems", in proceedings of the *IEEE Vehicular Technology Conference (VTC)*, vol. 2, Vancouver, BC, Canada, 24–28 September 2002, pages 686–690.

[122] W. C. Y. Lee, *Mobile cellular telecommunications systems*, McGraw-Hill, New York, 1989.

[123] W. C. Y. Lee, *Mobile communications engineering: theory and applications*, McGraw-Hill, New York, 2nd edition, 1997.

[124] W. C. Y. Lee, "Effects on correlation between two mobile radio base-station antennas", *IEEE Transactions on Communications*, vol. COM-21, no. 11, November 1973, pages 1214–1224.

[125] W. C. Y. Lee, "Overview of cellular CDMA", *IEEE Transactions on Vehicular Technology*, vol. 40, no. 2, May 1991, pages 291–302.

[126] W. C. Y. Lee, "Spectrum efficiency in cellular", *IEEE Transactions on Vehicular Technology*, vol. 38, no. 2, May 1989, pages 69–75.

[127] W. C. Y. Lee, "Spectrum and technology of a wireless local loop system", *IEEE Personal Communications*, vol. 5, no. 1, February 1998, pages 49–54.

[128] W. C. Y. Lee, "Antenna spacing requirement for a mobile radio base-station diversity", *Bell System Technical Journal*, vol. 50, no. 6, July-August 1971, pages 1859–1876.

[129] W. C. Y. Lee, "Estimate of local average power of a mobile radio signal", *IEEE Transactions on Vehicular Technology*, vol. VT-34, no. 1, February 1985, pages 22–27.

[130] W. C. Y. Lee, "Elements of cellular mobile radio systems", *IEEE Transactions on Vehicular Technology*, vol. VT-35, no. 2, May 1986, pages 48–56.

[131] J. S. Lee and L. E. Miller, *CDMA systems engineering handbook*, Artech House, Boston, 1998.

[132] Y. Li, M. J. Feuerstein and D. O. Reudink, "Performance evaluation of a cellular base station multibeam antenna", *IEEE Transactions on Vehicular Technology*, vol. 46, no. 1, February 1997, pages 1–9.

[133] Y. G. Li, J. C. Chuang and N. R. Sollenberger, "Transmitter diversity for OFDM systems and its impact on high-rate data wireless networks", *IEEE Journal on Selected Areas in Communications*, vol. 17, no. 7, july 1999, pages 1233–1243.

[134] Y.-C. Liang and F. P. S. Chin, "Downlink channel covariance matrix (DCCM) estimation and its applications in wireless DS-CDMA systems", *IEEE Journal on Selected Areas in Communications*, vol. 19, no. 2, February 2001, pages 222–232.

[135] J. C. Liberti and T. S. Rappaport, "Analytical results for capacity improvements in CDMA", *IEEE Transactions on Vehicular Technology*, vol. 43, no. 3, August 1994, pages 680–690.

[136] H. Liu and M. D. Zoltowski, "Blind equalization in antenna array CDMA systems", *IEEE Transactions on Signal Processing*, vol. 45, no. 1, January 1997, pages 161–172.

[137] T. K. Y. Lo, "Maximum ratio transmission", *IEEE Transactions on Communications*, vol. 47, no. 10, October 1999, pages 1458–1461.

[138] T. Lo and V. Tarokh, "Space-time block coding — from a physical perspective", in proceedings of the *IEEE Wireless Communications and Networking Conference (WCNC)*, vol. 1, 1999, pages 150–153.

[139] H.-L. Lou, "Implementing the Viterbi algorithm", *IEEE Signal Processing Magazine*, vol. 12, no. 5, September 1995, pages 42–52.

[140] R. Lupas and S. Verdú, "Linear multiuser detectors for asynchronous code-division multiple-access channels", *IEEE Transactions on Information Theory*, vol. 35, no. 1, January 1989, pages 123–136.

[141] R. Martínez, D. Trosa, L. de Haro and M. Calvo, "Smart antennas performance evaluation and capacity increase for WCDMA UMTS", in proceedings of the *IEEE Vehicular Technology Conference (VTC)*, vol. 1, Rhodes, Hellas, 6–9 May 2001, pages 147–151.

[142] L. B. Milstein, "Interference rejection techniques in spread spectrum communications", *Proceedings of the IEEE*, vol. 76, no. 6, June 1988, pages 657–671.

[143] S. Moshavi, "Multi-user detection for DS-CDMA communications", *IEEE Communications Magazine*, vol. 34, no. 10, October 1996, pages 124–136.

[144] T. Moorti, A. Paulraj and R. Stützle, "Performance of a fixed-beam system in the IS-95 CDMA forward link", *European Transactions on Telecommunications*, vol. 9, no. 4, 1998, pages 361–370.

[145] A. F. Naguib, *Adaptive antennas for CDMA wireless networks*, Ph.D. thesis, Stanford University, August 1996.

[146] A. F. Naguib, A. Paulraj and T. Kailath, "Capacity improvement with base-station antenna arrays in cellular CDMA", *IEEE Transactions on Vehicular Technology*, vol. 43, no. 3, August 1994, pages 691–698.

[147] A. F. Naguib and A. Paulraj, "Performance enhancements and trade-offs of smart antennas in CDMA cellular networks", in proceedings of the *IEEE Vehicular Technology Conference (VTC)*, vol. 1, Chicago, IL, USA, 25–28 July 1995, pages 40–44.

[148] A. F. Naguib, "Space-time receivers for CDMA multipath signals", in proceedings of the *IEEE International Conference on Communications (ICC)*, vol. 1, Montreal, Quebeq, Canada, 8–12 June 1997, pages 304–308.

[149] A. Narula, M. J. Lopez, M. D. Trott and G. W. Wornell, "Efficient use of side information in multiple-antenna data transmission over fading channels", *IEEE Journal on Selected Areas in Communications*, vol. 16, no. 8, October 1998, pages 1423–1436.

[150] A. Narula, M. D. Trott and G. W. Wornell, "Performance limits of coded diversity methods for transmitter antenna arrays", *IEEE Transactions on Information Theory*, vol. 45, no. 7, November 1999, pages 2418–2433.

[151] R. Negi, A. M. Tehran and J. Gioffi, "Adaptive antennas for space-time coding over block-time invariant multi-path fading channels", in proceedings of the *IEEE Vehicular Technology Conference (VTC)*, vol. 1, Houston, TX, USA, 16–20 May 1999, pages 70–74.

[152] E. Nikula, A. Toskala, E. Dahlman, L. Girard and A. Klein, "FRAMES multiple access for UMTS and IMT-2000", *IEEE Personal Communications*, vol. 5, no. 2, April 1998, pages 16–24.

[153] Nokia, "Recommended simulation parameters for TX diversity simulations", Available at: http://www.3gpp.org/ftp/tsg_ran/WG1_RL1/TSGR1_14/Docs, Document: R1-00-0867.pdf, 4–7 July 2000.

[154] D. M. Novakovic, M. J. Juntti and M. L. Dukic, "An algorithm for generalized transmit diversity", in proceedings of the *Global Telecommunications Conference (GLOBECOM)*, vol. 6, San Antonio, TX, USA, 25–29 November 2001, pages 3380–3384.

[155] T. Ojanperä and R. Prasad, editors, *WCDMA: towards IP mobility and mobile Internet*, Artech House, USA, 2001.

[156] T. Ojanperä and R. Prasad, "An overview of third-generation wireless personal communications: a European perspective", *IEEE Personal Communications*, vol. 5, no. 6, December 1998, pages 59–65.

[157] R. Padovani, "The application of spread spectrum to PCS has become a reality: Reverse link performance of IS-95 based cellular systems", *IEEE Personal Communications*, vol. 1, no. 3, 3rd Quarter 1994, pages 28–34.

[158] S. M. Panas, *Analysis of stochastic signals*, Publishing Department of Aristotle University of Thessaloniki, Thessaloniki, GREECE, 1993, Book is written in Greek.

[159] A. J. Paulraj and C. B. Papadias, "Space-time processing for wireless communications", *IEEE Signal Processing Magazine*, vol. 14, no. 6, November 1997, pages 49–83.

[160] B. Hochwald, T. L. Marzetta and C. B. Papadias, "A transmitter diversity scheme for wideband CDMA systems based on space-time spreading", *IEEE Journal on Selected Areas in Communications*, vol. 19, no. 1, January 2001, pages 48–60.

[161] C. Papadias, "On the spectral efficiency of space-time spreading schemes for multiple antenna CDMA systems", in proceedings of the *Asilomar Conference on Signals, Systems, and Computers*, Pacific Grove, CA, USA, 24–27 October 1999, pages 639–643.

[162] A. Papoulis, *Probability, random variables and stochastic processes*, McGraw-Hill, Singapore, 3rd edition, 1991.

[163] S. Parkvall, M. Karlsson, M. Samuelsson, L. Hedlund and B. Göransson, "Transmit diversity in WCDMA: link and system level results", in proceedings of the *IEEE Vehicular Technology Conference (VTC)*, vol. 2, Tokyo, Japan, 15–18 May 2000, pages 864–868.

[164] M. Pätzold, U. Killat, F. Laue and Y. Li, "On the statistical properties of deterministic simulation models for mobile fading channels", *IEEE Transactions on Vehicular Technology*, vol. 47, no. 1, February 1998, pages 254–269.

[165] A. J. Paulraj and B. C. Ng, "Space-time modems for wireless personal communications", *IEEE Personal Communications*, vol. 5, no. 1, February 1998, pages 36–48.

[166] K. I. Pedersen, P. E. Mogensen and F. Frederiksen, "Joint directional properties of uplink and downlink channel in mobile communications", *IEE Electronics Letters*, vol. 35, no. 16, 5th August 1999, pages 1311–1312.

[167] G. F. Pedersen, K. Olesen and S. L. Larsen, "Bodyloss for handheld phones", in proceedings of the *IEEE Vehicular Technology Conference (VTC)*, vol. 2, Houston, TX, USA, 16-20 May 1999, pages 1580–1584.

[168] G. F. Pedersen, M. Tartiere and M. B. Knudsen, "Radiation efficiency of handheld phones", in proceedings of the *IEEE Vehicular Technology Conference (VTC)*, vol. 2, Tokyo, Japan, 15-18 May 2000, pages 1381–1385.

[169] K. I. Pedersen and P. E. Mogensen, "A simple downlink antenna array algorithm based on a hybrid scheme of transmit diversity and conventional beamforming", in proceedings of the *IEEE Vehicular Technology Conference (VTC)*, vol. 1, Rhodes, Hellas, 6–9 May 2001, pages 58–62.

[170] R. L. Pickholtz, L. B. Milstein and D. L. Schilling, "Spread spectrum for mobile communications", *IEEE Transactions on Vehicular Technology*, vol. 40, no. 2, May 1991, pages 313–322.

[171] S. Ponnekanti and S. Sali, "Effective adaptive antenna scheme for mobile communications", *IEE Electronics Letters*, vol. 32, no. 5, 29 February 1996, pages 417–418.

[172] R. Prasad, *Universal wireless personal communications*, Artech House, Boston, 1st edition, 1998.

[173] R. Prasad, W. Mohr and W. Konhauser, editors, *Third generation mobile communication systems*, Artech House, Boston, 1st edition, 2000.

[174] R. Price and P. E. Green Jr., "A communication technique for multipath channels", *Proceedings of the IRE*, vol. 46, March 1958, pages 555–570.

[175] R. Price, "Further notes and anecdotes on spread-spectrum origins", *IEEE Transactions on Communications*, vol. COM-31, no. 1, January 1983, pages 85–97.

[176] J. G. Proakis, *Digital communications*, McGraw-Hill, Malaysia, 3rd edition, 1995.

[177] J. G. Proakis and M. Salehi, *Communication systems engineering*, Prentice Hall, New Jersey, USA, 2nd edition, 2001.

[178] J. G. Proakis and M. Salehi, *Contemporary communication systems using MATLAB®*, Brooks/Cole, 1st edition, 1999.

[179] J. G. Proakis and D. G. Manolakis, *Digital signal processing. Principles, algorithms and applications*, Prentice Hall, New Jersey, USA, 3rd edition, 1996.

[180] M. Raitola, A. Hottinen and R. Wichman, "Transmission diversity in wideband CDMA", in proceedings of the *IEEE Vehicular Technology Conference (VTC)*, vol. 2, Houston, TX, USA, 16-20 May 1999, pages 1545–1549.

[181] D. Rajan and S. D. Gray, "Transmit diversity schemes for CDMA-2000", in proceedings of the *IEEE Wireless Communications and Networking Conference (WCNC)*, vol. 2, New Orleans, LA, USA, 21–24 September 1999, pages 669–673.

[182] G. G. Raleigh, S. N. Diggavi, V. K. Jones and A. Paulraj, "A blind adaptive transmit antenna algorithm for wireless communication", in proceedings of the *IEEE International Conference on Communications (ICC)*, vol. 3, June 1995, pages 1494–1499.

[183] G. G. Raleigh and J. M. Gioffi, "Spatio-temporal coding for wireless communication", *IEEE Transactions on Communications*, vol. 46, no. 3, March 1998, pages 357–366.

[184] T. S. Rappaport and L. B. Milstein, "Effects of propagation path loss on DS-CDMA cellular frequency reuse efficiency for the reverse channel", *IEEE Transactions on Vehicular Technology*, vol. 41, no. 3, August 1992, pages 231–242.

[185] T. S. Rappaport, *Wireless communications: principles and practice*, Prentice Hall, New Jersey, 2nd edition, 2001.

[186] J. Razavilar, F. Rashid-Farrokhi and K. J. R. Liu, "Software radio architecture with smart antennas: a tutorial on algorithms and complexity", *IEEE Journal on Selected Areas in Communications*, vol. 17, no. 4, April 1999, pages 662–676.

[187] K. Rohani, M. Harrison and K. Kuchi, "A comparison of base station transmit diversity methods for third generation cellular standards", in proceedings of the *IEEE Vehicular Technology Conference (VTC)*, 16–20 May 1999, pages 351–355.

[188] R. Roy and T. Kailath, "ESPRIT—Estimation of signal parameters via rotational invariance techniques", *IEEE Transactions on Acoustics, Speech, and Signal Processing*, vol. 37, no. 7, July 1989, pages 984–995.

[189] Z. Safar and K. J. R. Liu, "Systematic design of space-time trellis codes for diversity and coding advantages", *EURASIP Journal on Applied Signal Processing*, vol. 2002, no. 3, March 2002, pages 221–235.

[190] J. Salz and J. Winters, "Effect of fading correlation on adaptive arrays in digital mobile radio", *IEEE Transactions on Vehicular Technology*, vol. 43, no. 4, November 1994, pages 1049–1057.

[191] J. Salz, "Optimum mean-square decision feedback equalization", *Bell System Technical Journal*, vol. 52, no. 8, October 1973, pages 1341–1373.

[192] M. Sanders, "Analytical analysis of transmit diversity in WCDMA on fading multipath channels", in proceedings of the *IEEE International Symposium on Personal, Indoor and Mobile Radio Comunications (PIMRC)*, Osaka, JAPAN, 12–15 September 1999, pages 946–950.

[193] A. Sathyendran, K. W. Sowerby and M. Shafi, "A statistical approach to the analysis of DS/CDMA cellular systems employing RAKE receivers and sectorised antennas", *IEEE Transactions on Vehicular Technology*, vol. 48, no. 1, January 1999, pages 8–19.

[194] S. R. Saunders, *Antennas and propagation for wireless communication systems*, John Wiley, Great Britain, 1999 reprint.

[195] D. L. Schilling, "Wireless communications going into the 21st century", *IEEE Transactions on Vehicular Technology*, vol. 43, no. 3, August 1994, pages 645–652.

[196] D. L. Schilling, L. B. Milstein, R. L. Pickholtz, F. Bruno, E. Kanterakis, M. Kullback, V. Erceg, W. Biederman, D. Fishman and D. Salerno, "Broadband CDMA for personal communications systems", *IEEE Communications Magazine*, vol. 29, no. 11, November 1991, pages 86–93.

[197] R. O. Schmidt, "Multiple emitter location and signal parameter estimation", *IEEE Transactions on Antennas and Propagation*, vol. AP-34, no. 3, March 1986, pages 276–280.

[198] R. A. Scholtz, "The spread spectrum concept", *IEEE Transactions on Communications*, vol. COM-25, no. 8, August 1977, pages 748–755.

[199] R. A. Scholtz, "The origins of spread-spectrum communications", *IEEE Transactions on Communications*, vol. COM-30, no. 5, May 1982, pages 822–854.

[200] R. A. Scholtz, "The evolution of spread-spectrum multiple-access communications", in proceedings of the *IEEE International Symposium on Spread Spectrum Techniques and Applications (ISSSTA)*, Oulu, Finland, July 1994, pages 4–13.

[201] C. Sengupta, J. R. Cavallaro and B. Aazhang, "Subspace-based tracking of multipath channel parameters for CDMA systems", *European Transactions on Telecommunications*, vol. 9, no. 5, September-October 1998, pages 439–447.

[202] N. Seshadri and J. H. Winters, "Two signalling schemes for improving the error performance of frequency division duplex (FDD) transmission systems using transmitter antenna diversity", *International Journal of Wireless Information Networks*, vol. 1, no. 1, 1994, pages 49–60.

[203] C. E. Shannon, "A mathematical theory of communication", *Bell System Technical Journal*, vol. 27, October 1948, pages 623–656.

[204] Siemens, "Channel model for TX diversity simulations using correlated antennas", Available at: http://www.3gpp.org/ftp/tsg_ran/WG1_RL1/TSGR1_15/Docs/PDFs/, Document: R1-00-1067.pdf, 22–25 August 2000.

[205] Siemens, "Simulation parameters for TX diversity simulations using correlated antennas", Available at: http://www.3gpp.org/ftp/tsg_ran/WG1_RL1/TSGR1_16/Docs/PDFs/, Document: R1-00-1180.pdf, 10–13 October 2000.

[206] Siemens, "Description of the eigenbeamformer concept (update) and performance evaluation", Available at: http://www.3gpp.org/ftp/tsg_ran/WG1_RL1/TSGR1_19/-Docs/PDFs/, Document: R1-01-0203.pdf, 27 February–2 March 2001.

[207] Siemens, "Advanced closed loop TX diversity concept (eigenbeamformer)", Available at: http://www.3gpp.org/ftp/tsg_ran/WG1_RL1/TSGR1_14/Docs/PDFs, Document: R1-00-0949.pdf, 4–7 July 2000.

[208] M. K. Simon and M.-S. Alouini, *Digital communication over fading channels*, John Wiley, New York, 1st edition, 2000.

[209] K. Siwiak, *Radiowave propagation and antennas for personal communications*, Artech House, Boston, 2 edition, 1999.

[210] B. Sklar, "Rayleigh fading channels in mobile digital communication systems Part I: Characterization", *IEEE Communications Magazine*, vol. 35, no. 9, September 1997, pages 136–146.

[211] B. Sklar, "Rayleigh fading channels in mobile digital communication systems Part II: Mitigation", *IEEE Communications Magazine*, vol. 35, no. 9, September 1997, pages 148–155.

[212] Y. S. Song and H. M. Kwon, "Analysis of a simple smart antenna for CDMA wireless communications", in proceedings of the *IEEE Vehicular Technology Conference (VTC)*, vol. 1, Houston, TX, USA, 16–20 May 1999, pages 254–258.

[213] G. L. Stüber, C. Kchao, N. C. Hightower and M. D. Frerking, "Capacity of direct-sequence CDMA for cellular radio", in proceedings of the *IEEE International Conference on Selected Topics in Wireless Communications*, Vancouver, BC, Canada, 25–26 June 1992, pages 199–202.

[214] P. Suvikunnas, P. Vainikainen and K. Hugl, "The comparison methods of different geometric configurations of adaptive antenna arrays", in proceedings of the *European Personal Mobile Communications Conference (EPMCC)*, Vienna, Austria, 20–22 February 2001.

[215] S. C. Swales, M. A. Beach, D. J. Edwards and J. P. McGeehan, "The performance enhancements of multibeam adaptive base-station antennas for cellular land mobile radio systems", *IEEE Transactions on Vehicular Technology*, vol. 39, no. 1, February 1990, pages 56–67.

[216] Y. Takatori, K. Cho, K. Nishimori and T. Hori, "Adaptive array employing eigenvector beam of maximum eigenvalue and fractionally-spaced TDL with real tap", *IEICE Transactions on Communications*, vol. E83-B, no. 8, August 2000, pages 1678–1687.

[217] V. Tarokh, H. Jafarkhani and A. R. Calderbank, "Space-time block codes from orthogonal designs", *IEEE Transactions on Information Theory*, vol. 45, no. 5, July 1999, pages 1456–1467.

[218] V. Tarokh, N. Seshadri and A. R. Calderbank, "Space-time codes for high data rate wireless communication: performance criterion and code construction", *IEEE Transactions on Information Theory*, vol. 44, no. 2, March 1998, pages 744–765.

[219] A. M. Tehrani, R. Negi and J. Cioffi, "Space-time coding over a code division multiple access system", in proceedings of the *IEEE Wireless Communications and Networking Conference (WCNC)*, New Orleans, LA, USA, 21–24 September 1999, pages 134–138.

[220] J. S. Thompson, P. M. Grant and B. Mulgrew, "Smart antenna arrays for CDMA systems", *IEEE Personal Communications*, vol. 3, no. 5, October 1996, pages 16–25.

[221] J. S. Thompson, J. E. Hudson, P. M. Grant and B. Mulgrew, "CDMA downlink beamforming for frequency selective channels", in proceedings of the *IEEE International Symposium on Personal, Indoor and Mobile Radio Comunications (PIMRC)*, 1999, pages 233–237.

[222] J. S. Thompson, R. Tanner and D. Bevan, "Weight error loss for wireless systems with antenna arrays", in proceedings of the *International Zurich Seminar on Broadband Communications*, Zurich, Switzerland, 19–21 February 2002, pages 4–1 – 4–6.

[223] E. Tiirola and J. Ylitalo, "Performance evaluation of fixed-beam beamforming in WCDMA downlink", in proceedings of the *IEEE Vehicular Technology Conference (VTC)*, vol. 2, May 15–18 2000.

[224] H. Tröger, T. Weber, M. Meurer and P. W. Baier, "Performance assessment of joint transmission (JT) multi-user downlinks with multi-element transmit antennas", *European Transactions on Telecommunications*, vol. 12, no. 5, September-October 2001, pages 407–415.

[225] T. D. Tsimpoukis, *Introduction to the fundamental theory of electromagnetic field*, vol. I, II and III, University Studio Press, Thessaloniki, GREECE, 1991, Book is written in Greek.

[226] G. V. Tsoulos, "Smart antennas for mobile communication systems: benefits and challenges", *Electronics and Communication Engineering Journal*, April 1999, pages 84–94.

[227] G. V. Tsoulos, M. Beach and J. McGeehan, "Wireless personal communications for the 21st century: European advances in adaptive antennas", *IEEE Communications Magazine*, vol. 35, no. 9, September 1997, pages 102–109.

[228] G. V. Tsoulos, M. A. Beach and S. C. Swales, "DS-CDMA capacity enhancement with adaptive antennas", *IEE Electronics Letters*, vol. 31, no. 16, 3 August 1995, pages 1319–1320.

[229] G. L. Turin, "Introduction to spread-spectrum antimultipath techniques and their applications to urban digital radio", *Proceedings of the IEEE*, vol. 68, no. 3, March 1980, pages 328–353.

[230] G. L. Turin, "The effects of multipath and fading on the performance of direct-sequence CDMA systems", *IEEE Journal on Selected Areas in Communications*, vol. SAC-2, no. 4, July 1984, pages 597–603.

[231] W. Utschick and J. A. Nossek, "Downlink beamforming for FDD mobile radio systems based on spatial covariances", in proceedings of the *European Wireless and ITG Mobile Communications*, Munich, Germany, 1999, pages 65–67.

[232] W. Utschick and C. Brunner, "Efficient tracking and feedback of DL-eigenbeams in WCDMA", in proceedings of the *European Personal Mobile Communications Conference (EPMCC)*, Vienna, Austria, 20–22 February 2001.

[233] S. Verdú, *Multiuser detection*, Cambridge university press, USA, 1st edition, September 1998.

[234] S. Verdú, "Minimum probability of error for asynchronous Gaussian multiple-access channels", *IEEE Transactions on Information Theory*, vol. IT-32, no. 1, January 1986, pages 85–96.

[235] M. Viberg and B. Ottersten, "Sensor array processing based on subspace fitting", *IEEE Transactions on Signal Processing*, vol. 39, no. 5, May 1991, pages 1110–1121.

[236] A. J. Viterbi, *CDMA: Principles of spread spectrum communication*, Prentice-Hall, 1st edition, June 1995.

[237] A. J. Viterbi, A. M. Viterbi, K. S. Gilhousen and E. Zehavi, "Soft handoff extends CDMA cell coverage and increases reverse link capacity", *IEEE Journal on Selected Areas in Communications*, vol. 12, no. 8, October 1994, pages 1281–1288.

[238] A. J. Viterbi, A. M. Viterbi and E. Zehavi, "Other-cell interference in cellular power-controlled CDMA", *IEEE Transactions on Communications*, vol. 42, no. 2/3/4, February/March/April 1994, pages 1501–1504.

[239] A. J. Viterbi, A. M. Viterbi and E. Zehavi, "Performance of power-controlled wideband terrestrial digital communication", *IEEE Transactions on Communications*, vol. 41, no. 4, April 1993, pages 559–569.

[240] A. J. Viterbi and R. Padovani, "Implications of mobile cellular CDMA", *IEEE Communications Magazine*, vol. 30, no. 2, December 1992, pages 38–41.

[241] A. J. Viterbi, "The orthogonal-random waveform dichotomy for digital mobile personal communication", *IEEE Personal Communications*, vol. 1, no. 1, 1st Quarter 1994, pages 18–24.

[242] S. Vembu and A. J. Viterbi, "Two different philosophies in CDMA—a comparison", in proceedings of the *IEEE Vehicular Technology Conference (VTC)*, vol. 2, Atlanta, GA, USA, 28 April–1 May 1996, pages 869–873.

[243] A. M. Viterbi and A. J. Viterbi, "Erlang capacity of a power controlled CDMA system", *IEEE Journal on Selected Areas in Communications*, vol. 11, no. 6, August 1993, pages 892–900.

[244] A. J. Viterbi, "The evolution of digital wireless technology from space exploration to personal communication services", *IEEE Transactions on Vehicular Technology*, vol. 43, no. 3, August 1994, pages 638–644.

[245] A. J. Viterbi, "When not to spread spectrum—a sequel", *IEEE Communications Magazine*, vol. 23, no. 4, April 1985, pages 12–17.

[246] K. Watanabe, S. Sampei and N. Morinaga, "Beam pattern selection diversity technique for DS/CDMA reverse link", *IEE Electronics Letters*, vol. 36, no. 16, 3rd August 2000, pages 1419–1420.

[247] V. Weerackody, "Diversity for the direct-sequence spread spectrum system using multiple transmit antennas", in proceedings of the *IEEE International Conference on Communications (ICC)*, vol. 3, Geneva, Switzerland, 23–26 May 1993, pages 1775–1779.

[248] D. P. Whipple, "North American cellular CDMA", *Hwelett-Packard Journal*, December 1993, pages 90–97.

[249] R. Wichman and A. Hottinen, "IMT-2000 transmit diversity concepts", in proceedings of the *IEEE International Symposium on Personal, Indoor and Mobile Radio Comunications (PIMRC)*, Osaka, JAPAN, 12–15 September 1999, pages 238–242.

[250] J. H. Winters, "The diversity gain of transmit diversity in wireless systems with Rayleigh fading", *IEEE Transactions on Vehicular Technology*, vol. 47, no. 1, February 1998, pages 119–123.

[251] J. H. Winters, "Optimum combining in digital mobile radio with cochannel interference", *IEEE Transactions on Vehicular Technology*, vol. VT-33, no. 3, August 1984, pages 144–155.

[252] J. H. Winters, J. Salz and R. D. Gitlin, "The impact of antenna diversity on the capacity of wireless communication systems", *IEEE Transactions on Communications*, vol. 42, no. 2/3/4, February/March/April 1994, pages 1740–1751.

[253] J. H. Winters, "On the capacity of radio communication systems with diversity in a Rayleigh fading environment", *IEEE Journal on Selected Areas in Communications*, vol. SAC-5, no. 5, June 1987, pages 871–878.

[254] J. H. Winters, "Smart antennas for wireless systems", *IEEE Personal Communications*, vol. 5, no. 1, February 1998, pages 23–27.

[255] G. W. Wornell and M. D. Trott, "Efficient signal processing techniques for exploiting transmit antenna diversity on fading channels", *IEEE Transactions on Signal Processing*, vol. 45, no. 1, January 1997, pages 191–205.

[256] J. Ylitalo and M. Katz, "An adaptive antenna method for improving downlink performance of CDMA base stations", in proceedings of the *IEEE International Symposium on Spread Spectrum Techniques and Applications (ISSSTA)*, vol. 2, Sun City, South Africa, 2–4 September 1998, pages 599–603.

[257] P. Zetterberg and B. Ottersten, "The spectrum efficiency of a base station antenna array system for spatially selective transmission", *IEEE Transactions on Vehicular Technology*, vol. 44, no. 3, August 1995, pages 651–660.